

Degradable Vinyl Copolymers via  
Photocontrolled Radical Ring-Opening  
Cascade Copolymerization

Wenqi Wang

A dissertation  
submitted to the Faculty of  
the department of Chemistry  
in partial fulfillment  
of the requirements for the degree of  
Doctor of Philosophy

Boston College  
Morrissey College of Arts and Sciences  
Graduate School

October 2023



# Degradable Vinyl Copolymers via Photocontrolled Radical Ring-Opening Cascade Copolymerization

Wenqi Wang

Advisor: Prof. Jia Niu

**Abstract:** This dissertation discusses two main projects focusing on synthesizing degradable vinyl copolymers. The first project describes the development of a general approach to synthesizing degradable vinyl random copolymers through photocontrolled radical ring-opening cascade copolymerization (rROCCP). The rROCCP of a macrocyclic allylic sulfone with acrylates or acrylamides mediated by visible light at ambient temperature achieved near-unity comonomer reactivity ratios over the entire range of feed compositions. Such a powerful approach provides degradable vinyl random copolymers with comparable material properties to their non-degradable counterparts. Experimental and computational evidence also revealed an unusual reversible inhibition of chain propagation by *in situ* generated sulfur dioxide (SO<sub>2</sub>), which was successfully overcome by reducing the solubility of SO<sub>2</sub> during polymerization. The second project depicts a general method for organocatalyzed photocontrolled radical copolymerization of a macrocyclic allylic sulfone and various types of vinyl monomers, including acrylates, acrylamides, styrene, and methacrylate. Catalyzed by Eosin Y under visible light irradiation, copolymerization of the macrocyclic allylic sulfone and acrylic monomers displayed near unity comonomer reactivity ratios by fitting the copolymer composition to the Beckingham-Sanoya-Lynd integrated model. The macrocyclic allylic sulfone was also successfully copolymerized with styrene or methyl methacrylate to generate degradable polystyrene and poly(methyl methacrylate). These degradable vinyl copolymers exhibited tunable

thermal properties correlated with the incorporation of degradable main-chain diester motif.

## Table of Contents

<b>Chapter 1. Degradable Polymers from Radical Ring-Opening Polymerization.....</b>	<b>1</b>
1.1 Introduction.....	2
1.2 Radical ring-opening polymerization of cyclic ketene acetals.....	3
1.3 Radical ring-opening polymerization of vinyl cyclopropanes.....	4
1.4 Radical ring-opening polymerization of sulfide cyclic methacrylates.....	6
1.5 Radical ring-opening polymerization of thionolactones.....	7
References.....	8
<b>Chapter 2. Degradable Vinyl Random Copolymers through Photocontrolled Radical Ring-Opening Cascade Copolymerization.....</b>	<b>13</b>
2.1 Introduction.....	14
2.2 PET-RAFT homopolymerization of macrocyclic allylic sulfones.....	16
2.3 Copolymerization of macrocyclic allylic sulfone with acrylates or acrylamides .....	28
2.4 Degradable nanostructures through polymerization-induced self-assembly.	50
2.5 Understanding the unusual kinetic behavior.....	54
2.6 Overcoming the propagation inhibition by SO <sub>2</sub> .....	62
2.7 Conclusion.....	69
Experimental section.....	70
References.....	185
<b>Chapter 3. Organocatalyzed Photocontrolled Radical Copolymerization of Macrocyclic Allylic Sulfone with Vinyl Monomers.....</b>	<b>195</b>
3.1 Introduction.....	196

3.2 Organocatalyzed photocontrolled homopolymerization of macrocyclic allylic sulfone.....	198
3.3 Copolymerization of macrocyclic allylic sulfone with acrylic monomers...	202
3.4 Copolymerization of macrocyclic allylic sulfone with styrene.....	223
3.5 Copolymerization of macrocyclic allylic sulfone with methacrylate.....	227
3.6 Thermal properties of the degradable vinyl copolymers.....	233
3.7 Conclusion.....	235
Experimental section.....	237
References.....	248

## List of Abbreviations

AIBN	azobisisobutyronitrile
Ar	argon
atm	standard atmosphere
BMDO	5,6-benzo-2-methylene-1,3-dioxepane
BnA	benzyl acrylate
BSL	Beckingham-Sanoja-Lynd
°C	degree Celsius
CAS	cyclic allylic sulfide
CDCl <sub>3</sub>	deuterated chloroform
CKA	cyclic ketene acetal
Conv.	total conversion of two comonomers
CTA	chain transfer agent
CVS	cyclic vinyl sulfone
<i>D</i>	dispersity
DCM	dichloromethane
DEA	<i>N,N</i> -diethylacrylamide
DFT	Density Functional Theory
DMA	<i>N,N</i> -dimethylacrylamide
DMF	<i>N,N</i> -dimethylformamide
DMSO	dimethyl sulfoxide
DOT	dibenzo[ <i>c,e</i> ]oxepane-5-thione
DP	degree of polymerization
DSC	differential scanning calorimetry

EA	ethyl acetate
ECVCP	1,1-bis(ethoxycarbonyl)-2-vinylcyclopropane
EosinY	2',4',5',7'-Tetrabromofluorescein
EPR	electron paramagnetic resonance
$f_1^0$	molar fraction of <b>1</b> in the initial comonomer mixture
$F_1$	molar fraction of <b>1</b> incorporated into the copolymer
<i>fac</i> -Ir(ppy) <sub>3</sub>	Tris[2-phenylpyridinato- <i>C</i> <sup>2</sup> , <i>N</i> ]iridium(III)
g	gram
$g_0$	<i>g</i> -value/factor
$G'$	storage modulus
$G''$	loss modulus
GPC	gel permeation chromatography
h	hour
HCl	hydrochloric acid
HPLC	high-performance liquid chromatography
Hz	Hertz
Ir(dFppy) <sub>3</sub>	Tris[3,5-difluoro-2-(2-pyridinyl)phenyl]iridium(III)
[Ir(dtbbpy)(ppy) <sub>2</sub> ] <sup>+</sup> PF <sub>6</sub> <sup>-</sup>	[4,4'-Bis(1,1-dimethylethyl)-2,2'-bipyridine- <i>N</i> 1, <i>N</i> 1']bis[2-(2-pyridinyl- <i>N</i> )phenyl- <i>C</i> ]iridium(III) hexafluorophosphate
Ir( <i>p</i> -CF <sub>3</sub> -ppy) <sub>3</sub>	Tris[(2-(2-pyridinyl- <i>N</i> ')-5-(trifluoromethyl)phenyl- <i>C</i> ')]iridium(III)
Ir( <i>p</i> -F-ppy) <sub>3</sub>	Tris[5-fluoro-2-(2-pyridinyl- <i>N</i> ')phenyl- <i>C</i> ']iridium(III)
K	Kelvin
L	liter

LED	light-emitting diode
m	meter
M	molarity
MA	methyl acrylate
MALDI-TOF	matrix-assisted laser desorption/ionization time-of-flight
MAS	macrocyclic allylic sulfide
<i>m</i> CPBA	<i>meta</i> -chloroperoxybenzoic acid
MDO	2-methylene-1,3-dioxepane
MMA	methyl methacrylate
$M_n$	number average molecular weight
MPDL	2-methylenephanyl-1,3-dioxolane
mPEG <sub>100</sub> -TTC	trithiocarbonate-terminated poly(ethylene glycol)
	monomethyl ether
mol	mole
$[M]_0$	initial monomer concentration
$[M]_0/[I]_0$	feeding monomer/initiator ratio
$[M]_t$	monomer concentration at a given time $t$
N	normality
NAM	<i>N</i> -acryloylmorpholine
Na <sub>2</sub> SO <sub>4</sub>	sodium sulfate
NMR	nuclear magnetic resonance
NaOH	sodium hydroxide
NaOMe	sodium methoxide
Pa	pascal
PEG	poly(ethylene glycol)

PET-RAFT	photoinduced electron/energy transfer-reversible addition/fragmentation chain transfer
PISA	polymerization-induced self-assembly
PMA	poly(methyl acrylate)
PMMA	poly(methyl methacrylate)
ppm	parts per million
PtBA	poly( <i>tert</i> -butyl acrylate)
PTFE	polytetrafluoroethylene
$r_1$	reactivity ratio of <b>1</b>
$r_B$	reactivity ratio of comonomer B
rad/s	radian per second
RDRP	reversible deactivation radical polymerization
rROCCP	radical ring-opening cascade copolymerization
rROP	radical ring-opening polymerization
Ru(bpy) <sub>3</sub> Cl <sub>2</sub>	Tris(2,2'-bipyridyl)dichlororuthenium(II)
SCM	sulfide cyclic methacrylate
SMD	Solvation Model based on Density
SEC	size-exclusion chromatogram
SO <sub>2</sub>	sulfur dioxide
SOC	spiro-ortho-carbonate
St	styrene
tan( $\delta$ )	loss/damping factor = $G''/G'$
<i>t</i> BA	<i>tert</i> -butyl acrylate
$T_d$	5% weight loss decomposition temperature
TEM	transmission electron microscopy

$T_g$	glass transition temperature
TGA	thermogravimetry analysis
THF	tetrahydrofuran
TLC	thin-layer chromatography
VCB	vinylcyclobutane
VCH	vinylcyclohexadiene
VCP	vinyl cyclopropane
VO	vinylloxirane
W	Watt
wt%	percent by weight
ZnTPP	5,10,15,20-Tetraphenyl-21 <i>H</i> ,23 <i>H</i> -porphine zinc(II)
$\delta$	chemical shift
$\lambda_{\max}$	wavelength with strongest photon absorption/emission

## Acknowledgment

As I approach the end of my graduate study at Boston College, I would like to express my profound appreciation and gratitude to everyone who helped me complete my Ph.D. at Boston College.

Firstly, I am grateful to my Ph.D. advisor, Prof. Jia Niu, for his continuous support and guidance throughout my graduate study. He is always willing to leave his students enough space to think critically, write independently, and work smartly. I would also like to thank Prof. Amir H. Hoveyda, Prof. Jeffery A. Byers, and Prof. James P. Morken for being my committee members, whose rigorous comments and hard questions provoked me to widen my knowledge from various perspectives. I also appreciate the characterization assistance and professional discussion from Prof. Junpeng Wang and his lab members, Zeyu Wang and Devavrat Sathe, at the University of Akron.

I am lucky to work as a member of Niu research group, and I would like to thank all the past and present members of our group for creating a supportive environment for each other. I also want to thank Dr. Hanchu Huang, Dr. Cangjie Yang, Dr. Jingsong Yuan, and Dr. Lianqian Wu as my mentors. I have learned considerable knowledge, techniques, and the logic behind experiments from our discussions. I am grateful to collaborate with Dr. Jing Jin, Dr. Fredrik Haeffner, Zefeng Zhou, Brayan Rondon, Xuanting Tang, and Stephanie Moran. I enjoy working with all of them.

I am glad to be part of polymer subgroup and grateful for having many intelligent colleagues, Dr. Zhensheng Zhao, Dr. Xiaonan Li, Gavin Giardino, and Nachuan Jiang. I also thank my dear friends, Dr. Mi Zhou, Chao Liu, Qiwen Su, and Yu Deng, who have stood by me during my highs and lows. I want to express my heartfelt thanks to all those who have been helpful but have not been mentioned here.

Lastly, I thank my family for their never-ending love and support. I am eternally grateful to my parents, Hongtu Wang and Chunhong Yang, who have supported me financially and emotionally throughout my studies. Their unconditional love and help encourage me to keep pursuing my dreams.

## Chapter 1

### Degradable Polymers from Radical Ring-Opening Polymerization

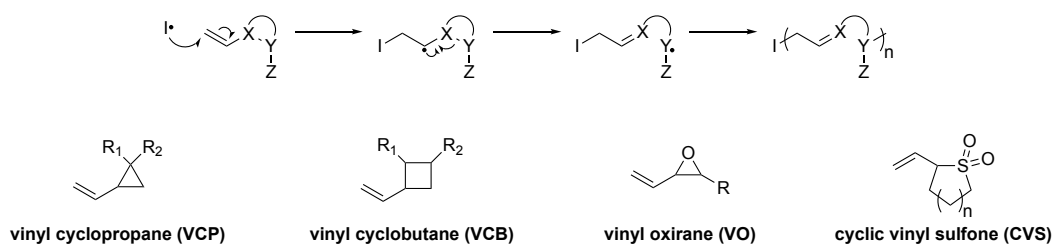
A significant portion of the work described in this chapter has been published in:

Yuan, J.; Wang, W.; Zhou, Z.; Niu, J. Cascade Reactions in Chain-Growth Polymerization. *Macromolecules* **2020**, *53*, 5655-5673.

## 1.1 Introduction

Radical polymerization is best known for constructing all-carbon polymer backbones. While an all-carbon backbone demonstrates high chemical and mechanical stability, it becomes a liability when the degradability of a polymer is a property of interest. With the ever-growing need for degradable polymers in biomedical applications and our society's increasing awareness of sustainability and carbon neutrality, polymers with bio-based or degradable main-chain functionalities have recently attracted significant attention.<sup>1-2</sup> Therefore, radical ring-opening polymerization (rROP) approaches capable of facilely incorporating degradable main-chain functionalities into polymer backbones hold great potential. In general, monomers capable of rROP often contain a cyclic structure bearing a vinyl or *exo*-methylene group, as shown in Figure 1.1. During polymerization, radical addition to the terminal double bond is followed by a ring-opening process to release ring strain and yield thermodynamically favored open-chain intermediates capable of propagation.<sup>3</sup> Since the first report in the 1960s,<sup>4</sup> numerous *exo*-methylene-type monomers for rROP have been reported. Examples of vinyl-type monomers include vinyl cyclopropane (VCP),<sup>5</sup> vinylcyclobutane (VCB),<sup>6</sup> vinyl oxirane (VO),<sup>7</sup> and cyclic vinyl sulfone (CVS)<sup>8-9</sup> (Figure 1.1A). Examples of *exo*-methylene-type monomers include sulfide cyclic methacrylate (SCM),<sup>10</sup> cyclic allylic sulfide (CAS),<sup>11-12</sup> cyclic ketene acetal (CKA),<sup>13</sup> spiro-ortho-carbonate (SOC),<sup>14</sup> and vinyl cyclohexadiene (VCH)<sup>15-16</sup> (Figure 1.1B). Extensive work has been devoted to implementing these rROP techniques to fabricate functional materials for applications such as low-shrinkage materials,<sup>17</sup> degradable polymers,<sup>18</sup> and drug delivery.<sup>19</sup>

### A Vinyl-Type Cyclic Monomers



### B Exo-Methylene-Type Cyclic Monomers

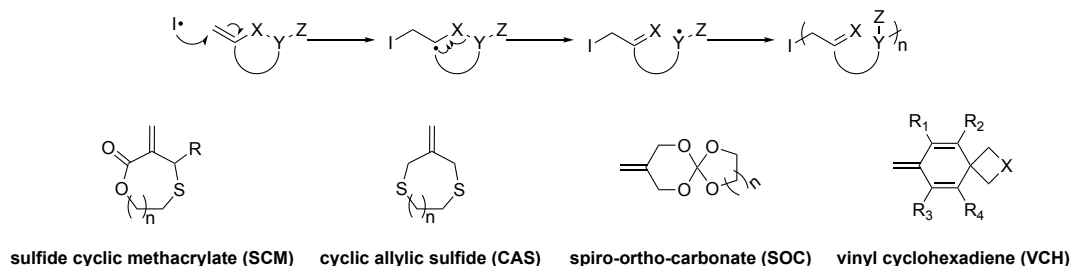


**Figure 1.1.** Structures of two types of cyclic monomers capable of rROP. (A) Vinyl-type cyclic monomers (B) *Exo*-methylene-type cyclic monomers.

## 1.2 Radical ring-opening polymerization of cyclic ketene acetals

Among rROP monomers, cyclic ketene acetals (CKAs) were comprehensively studied over several decades. The popularity of CKAs can be primarily attributed to their ability to readily generate aliphatic polyesters by rROP, which are well-known for their excellent biodegradability. As depicted in Figure 1.2A, the mechanism of CKA rROP includes the radical addition of an *exo*-methylene group and a subsequent ring-opening process to form an ester group in the main chain. A main side reaction in the polymerization of CKAs is a 1,2-addition pathway that generates an all-carbon main chain structure, resulting in heterogeneous backbone composition and nondegradable segments. Although great efforts have been made in studying how ring size, steric hindrance, solvent, and temperature influence the reactivity of CKAs, a general monomer design principle remains elusive. To date, only 2-methylene-1,3-dioxepane (MDO), 5,6-benzo-2-methylene-1,3-dioxepane (BMDO), and 2-methylenephényl-1,3-

dioxolane (MPDL) (Figure 1.2B) are known to undergo quantitative ring-opening polymerization under a broad range of conditions.<sup>20</sup>

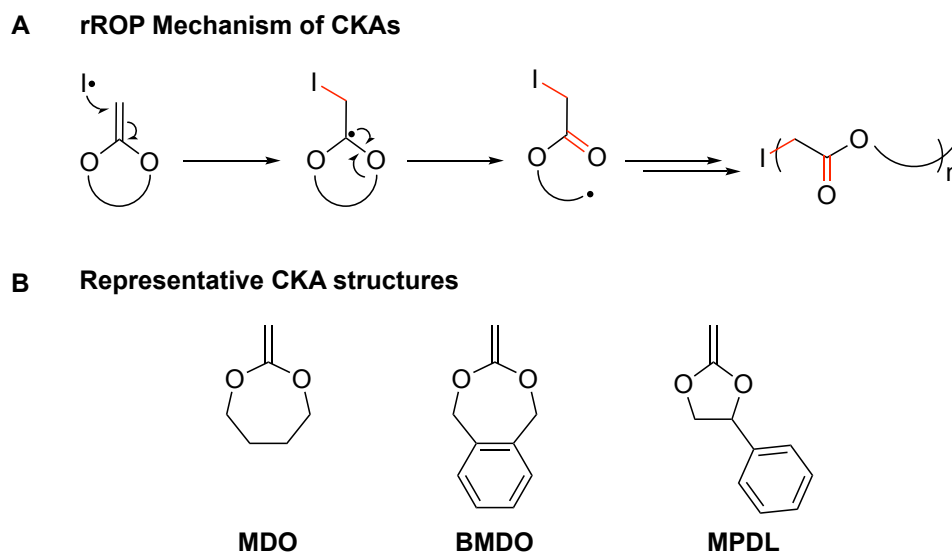


**Figure 1.2.** (A) rROP mechanism of CKAs. (B) Representative CKA structures.

As the main interest of CKA rROP lies within the incorporation of degradable functionality into the polymer backbone, copolymerization of CKA monomers with traditional acyclic monomers (e.g., styrene and acrylates) provides a promising solution, as it combines the degradability from CKAs with the low cost and predictable reactivity of styrene and acrylates. Moreover, copolymerization allows the regulation of polymer degradability by simply varying comonomer ratios. However, the low reactivity of CKAs compared to styrene and acrylates makes it a great challenge to achieve a high ratio of degradable units.<sup>21-22</sup>

### 1.3 Radical ring-opening polymerization of vinyl cyclopropanes

The rROP of vinyl cyclopropanes (VCPs), a vinyl-type cyclic monomer, has been studied extensively.<sup>5</sup> The original interest in this monomer class stems from their ability

to undergo a unique 1,5-ring-opening pathway to form an internal double bond (denoted as *l*) in the polymer main chain (Figure 1.3A). However, a competing intramolecular cyclization to form cyclobutane (denoted as *c*) often occurred with uncontrollable frequencies (Figure 1.3B). The first rROP of VCP that led to predominant 1,5-ring-opening products was the atom transfer radical polymerization (ATRP) of 1,1-bis(ethoxycarbonyl)-2-vinylcyclopropane (ECVCP) reported by Rimmer et al. (*l* content > 98%).<sup>23</sup> However, under these conditions, polymers were generated with only modest conversion and low  $M_n$ , perhaps caused by catalyst deactivation due to the coordination with ECVCP. In 2019, this challenge was overcome by Miyake et al. using organocatalyzed ATRP (O-ATRP), where highly reducing organic photoredox catalysts enabled a fast chain end activation/deactivation cycle and eliminated the unfavorable monomer coordination.<sup>24-25</sup> High-molecular-weight polyVCPs with well-defined linear structures were readily prepared. The excellent polymerization control was further demonstrated by elaborately designed control experiments, kinetic characterizations, chain-end group analysis, and block copolymerization. The temporal control of the polymerization was successfully achieved by using pulsed irradiation. Interestingly, polyVCPs with high *c* content could also be prepared when reactions were conducted at a low initial monomer concentration and high temperature. A highlight of this study is that the *l/c* contents of well-defined high-molecular-weight polyVCPs can be readily controlled by tuning the reaction conditions.

**A Formation of Inner Double Bond (*l* content)**



**B Formation of Cyclobutane (*c* content)**

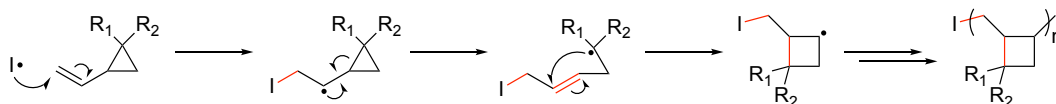


**Figure 1.3.** rROP of VCPs (A) Formation of the inner double bond (*l* content). (B) Formation of cyclobutane (*c* content)

#### 1.4 Radical ring-opening polymerization of sulfide cyclic methacrylates

In 1994, Rizzardo et al. reported sulfide cyclic methacrylates (SCMs) as an *exo*-methylene-type monomer for rROP.<sup>10</sup> The mechanism of this polymerization consists of an initial radical addition to the terminal vinyl group, followed by  $\beta$ -elimination of a thiyl radical for chain propagation (Scheme 1.4A). It is noteworthy that the severe cross-linking observed in the homopolymerization of monomer 4a could be effectively suppressed by incorporating a methyl group at the  $\beta$ -position (4b), as a trisubstituted alkene formed after the  $\beta$ -elimination of a thiyl radical is less susceptible to further radical attack compared to the terminal alkene formed in the reaction of 4a. Hawker et al. further introduced ester, thioester, and disulfide groups into SCM monomers to build up main-chain degradable polymers (Scheme 1.4B, 4c-e).<sup>26</sup> This seminal work highlighted the utility of rROP in overcoming the non-degradability challenge associated with polyacrylates. However, a prominent shortcoming is the high dispersity ( $D > 1.8$ ) in the homo- and copolymerization of SCMs, which is attributed to the incompatibility of thiyl radical and RAFT process.

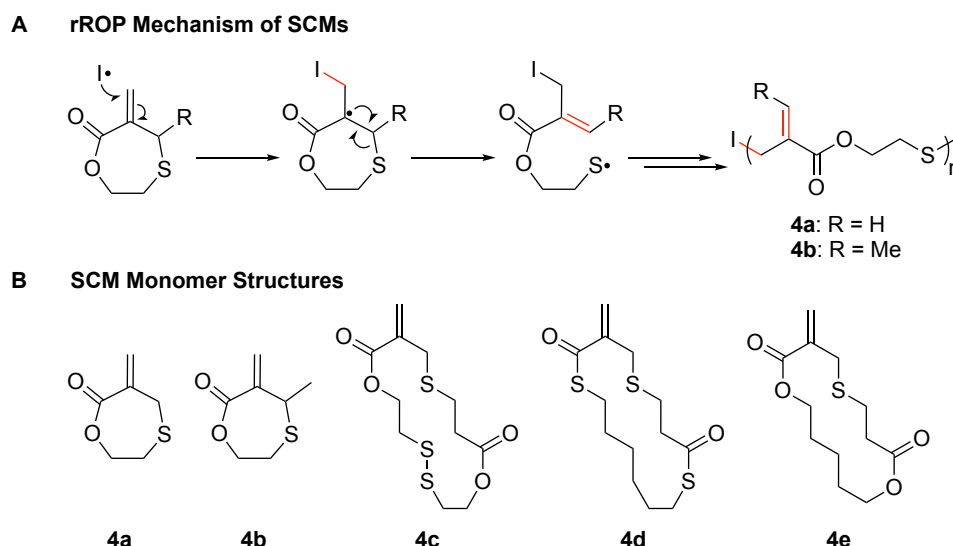


**Figure 1.4.** (A) rROP of SCMs and (B) Examples of SCM monomers.

## 1.5 Radical ring-opening polymerization of thionolactones

Besides ester groups, incorporating thioester groups into the polymer main chain also affords an efficient way of introducing degradability. Among different potential structures to incorporate thioesters, thionolactones have recently emerged as an impressive candidate to prepare degradable polymers by rROP. In 2019, Roth<sup>27</sup> and Gutekunst<sup>28</sup> independently reported dibenzo[*c,e*]oxepane-5-thione (DOT) as a new cyclic monomer for the radical copolymerization with acrylic monomers (Figure 1.5). The synthesis of DOT only involves two major steps (Figure 1.5A): reduction of diphenic anhydride and subsequent vulcanization of the resulting lactone with Lawesson's reagent. The mechanism of DOT rROP is depicted in Figure 1.5B: the radical of an initiator/polymer chain end attacks the C=S double bond. Subsequent rearrangement and fragmentation generate a thermodynamically more stable thioester as well as a benzylic radical which can undergo reversible deactivation/reactivation for controlled radical polymerization. In 2022, Johnson<sup>29</sup> and Guillaneuf<sup>30</sup> expanded the comonomer scope of DOT by incorporating thioesters as cleavage points into originally

non-degradable polystyrene and realized excellent vinyl polymer circularity. Recently, Guillaneuf et al. further exemplified the usage of DOT in 3D-printed polymer networks, such as poly(pentaerythritol triacrylate)<sup>31</sup> and poly(styrene-*co*-divinylbenzene)<sup>30</sup>, both of which were able to undergo efficient degradation. Roth and coworkers further reported fully degradable polyacrylate networks<sup>32</sup> and degradable linear and bottlebrush thioester-functional copolymers<sup>33</sup> enabled by DOT. However, the homopolymerization of DOT remains elusive.

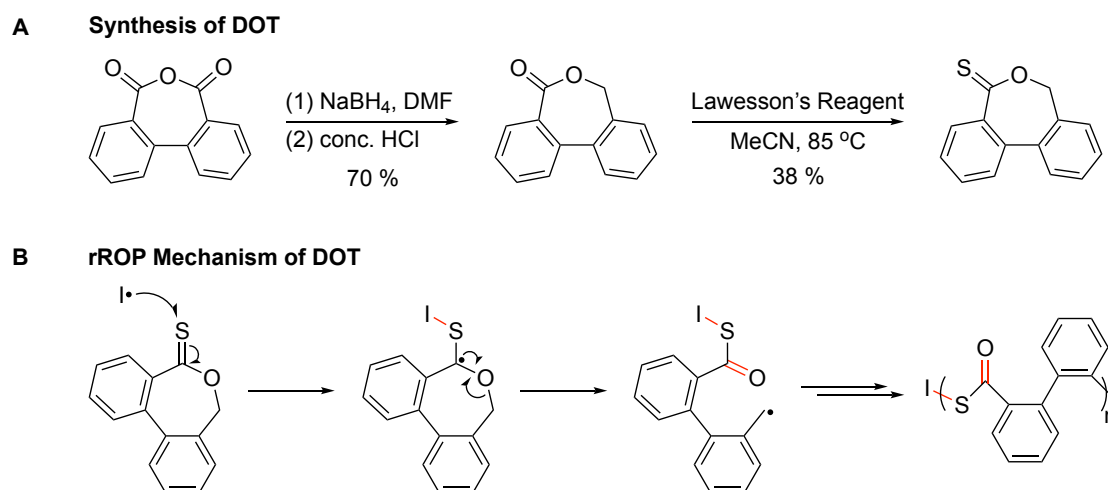


**Figure 1.5.** (A) Synthesis of DOT. (B) rROP of DOT.

## Reference

- (1) Schneiderman, D. K.; Hillmyer, M. A. 50th Anniversary Perspective: There Is a Great Future in Sustainable Polymers. *Macromolecules* **2017**, *50*, 3733-3749.
- (2) Zhu, Y.; Romain, C.; Williams, C. K. Sustainable Polymers from Renewable Resources. *Nature* **2016**, *540*, 354-362.
- (3) For some rROP systems (e.g., 3- or 4-membered ring system), ring strain is the main driving force. While for some other systems, formation of thermodynamically

more stable bonds can also be a driving force (e.g., production of C=O double bond in CKA polymerization).

(4) Errede, L. A. Chemistry of Xylylenes. 10. Some Polymers and Telomers of Spiro-Di-O-Xylylene. *J. Polym. Sci.* **1961**, *49*, 253-265.

(5) Moszner, N.; Zeuner, F.; Volkel, T.; Rheinberger, V. Synthesis and polymerization of vinylcyclopropanes. *Macromol. Chem. Phys.* **1999**, *200*, 2173-2187.

(6) Hiraguri, Y.; Endo, T. Synthesis and Radical Ring-Opening Polymerization of 1,2-Dicarbomethoxy-3-Vinylcyclobutane. *J. Polym. Sci., Part C: Polym. Lett.* **1989**, *27*, 333-337.

(7) Murata, K. Polymerization of 1,2-Epoxy-3-Butene and Its Graft Copolymerization to Polyethylene by Gamma-Radiation. *J. Polym. Sci., Part A-1: Polym. Chem.* **1972**, *10*, 3673-3677.

(8) Tanaka, S.; Furusho, Y.; Endo, T. Radical Ring-Opening Polymerization of Five-Membered Cyclic Vinyl Sulfone Using *p*-Toluenesulfonyl Halides. *J. Polym. Sci., Part A: Polym. Chem.* **2013**, *51*, 222-227.

(9) Cho, I. New Ring-Opening Polymerizations for Copolymers Having Controlled Microstructures. *Prog. Polym. Sci.* **2000**, *25*, 1043-1087.

(10) Evans, R. A.; Moad, G.; Rizzardo, E.; Thang, S. H. New Free-Radical Ring-Opening Acrylate Monomers. *Macromolecules* **1994**, *27*, 7935-7937.

(11) Evans, R. A.; Rizzardo, E. Free-Radical Ring-Opening Polymerization of Cyclic Allylic Sulfides. *Macromolecules* **1996**, *29*, 6983-6989.

(12) Choi, K.; Chon, J. W. M.; Gu, M.; Malic, N.; Evans, R. A. Low-Distortion Holographic Data Storage Media Using Free-Radical Ring-Opening Polymerization. *Adv. Funct. Mater.* **2009**, *19*, 3560-3566.

- (13) Agarwal, S. Chemistry, Chances and Limitations of the Radical Ring-Opening Polymerization of Cyclic Ketene Acetals for the Synthesis of Degradable Polyesters. *Polym. Chem.* **2010**, *1*, 953-964.
- (14) Endo, T.; Bailey, W. J. Radical Ring-Opening Polymerization of 3,9-Dimethylene-1,5,7,11-Tetraoxaspiro-[5,5]Undecane. *J. Polym. Sci., Polym. Lett. Ed.* **1975**, *13*, 193-195.
- (15) Mori, H.; Masuda, S.; Endo, T. Ring-Opening RAFT Polymerization Based on Aromatization as Driving Force: Synthesis of Well-Defined Polymers Containing Anthracene Units in the Main Chain. *Macromolecules* **2006**, *39*, 5976-5978.
- (16) Mori, H.; Tando, I.; Tanaka, H. Synthesis and Optoelectronic Properties of Alternating Copolymers Containing Anthracene Unit in the Main Chain by Radical Ring-Opening Polymerization. *Macromolecules* **2010**, *43*, 7011-7020.
- (17) Moszner, N. New Monomers for Dental Application. *Macromol. Symp.* **2004**, *217*, 63-76.
- (18) Seema, A.; Liqun, R. Polycaprolactone-Based Novel Degradable Ionomers by Radical Ring-Opening Polymerization of 2-Methylene-1,3-dioxepane. *Macromolecules* **2009**, *42*, 1574-1579.
- (19) Delplace, V.; Nicolas, J. Degradable vinyl polymers for biomedical applications. *Nat. Chem.* **2015**, *7*, 771-784.
- (20) Tardy, A.; Nicolas, J.; Gigmes, D.; Lefay, C.; Guillaeneuf, Y. Radical Ring-Opening Polymerization: Scope, Limitations, and Application to (Bio)Degradable Materials. *Chem. Rev.* **2017**, *117*, 1319-1406.
- (21) Yuan, J.-Y.; Pan, C.-Y. "Living" free radical ring-opening copolymerization of 4,7-dimethyl-2-methylene-1,3-dioxepane and conventional vinyl monomers. *Eur. Polym. J.* **2002**, *38*, 2069-2076.

- (22) Wickel, H.; Agarwal, S. Synthesis and Characterization of Copolymers of 5,6-Benzo-2-methylene-1,3-dioxepane and Styrene. *Macromolecules* **2003**, *36*, 6152-6159.
- (23) Singha, N. K.; Kavitha, A.; Sarker, P.; Rimmer, S. Copper-Mediated Controlled Radical Ring-Opening Polymerization (RROP) of A Vinylcycloalkane. *Chem. Commun.* **2008**, 3049-3051.
- (24) Chen, D. F.; Boyle, B. M.; McCarthy, B. G.; Lim, C. H.; Miyake, G. M. Controlling Polymer Composition in Organocatalyzed Photoredox Radical Ring-Opening Polymerization of Vinylcyclopropanes. *J. Am. Chem. Soc.* **2019**, *141*, 13268-13277.
- (25) Theriot, J. C.; Lim, C. H.; Yang, H.; Ryan, M. D.; Musgrave, C. B.; Miyake, G. M. Organocatalyzed Atom Transfer Radical Polymerization Driven by Visible Light. *Science* **2016**, *352*, 1082-1086.
- (26) Paulusse, J. M. J.; Amir, R. J.; Evans, R. A.; Hawker, C. J. Free Radical Polymers with Tunable and Selective Bio- and Chemical Degradability. *J. Am. Chem. Soc.* **2009**, *131*, 9805-9812.
- (27) Bingham, N. M.; Roth, P. J. Degradable vinyl copolymers through thiocarbonyl addition-ring-opening (TARO) polymerization. *Chem. Commun.* **2019**, *55*, 55-58.
- (28) Smith, R. A.; Fu, G.; McAteer, O.; Xu, M.; Gutekunst, W. R. Radical Approach to Thioester-Containing Polymers. *J. Am. Chem. Soc.* **2019**, *141*, 1446-1451.
- (29) Kiel, G. R.; Lundberg, D. J.; Prince, E.; Husted, K. E. L.; Johnson, A. M.; Lensch, V.; Li, S.; Shieh, P.; Johnson, J. A. Cleavable Comonomers for Chemically Recyclable Polystyrene: A General Approach to Vinyl Polymer Circularity. *J. Am. Chem. Soc.* **2022**, *144*, 12979-12988.
- (30) Gil, N.; Caron, B.; Siri, D.; Roche, J.; Hadiouch, S.; Khedaioui, D.; Ranque, S.; Cassagne, C.; Montarnal, D.; Gigmes, D.; Lefay, C.; Guillaneuf, Y. Degradable

Polystyrene via the Cleavable Comonomer Approach. *Macromolecules* **2022**, *55*, 6680-6694.

(31) Gil, N.; Thomas, C.; Mhanna, R.; Mauriello, J.; Maury, R.; Leuschel, B.; Malval, J.-P.; Clément, J.-L.; Gimes, D.; Lefay, C.; Soppera, O.; Guillaneuf, Y. Thionolactone as a Resin Additive to Prepare (Bio)degradable 3D Objects via VAT Photopolymerization. *Angew. Chem., Int. Ed.* **2022**, *61*, No. e202117700.

(32) Elliss, H.; Dawson, F.; Nisa, Q. u.; Bingham, N. M.; Roth, P. J.; Kopeć, M. Fully Degradable Polyacrylate Networks from Conventional Radical Polymerization Enabled by Thionolactone Addition. *Macromolecules*, **2022**, *55*, 6695-6702.

(33) Nisa, Q. u.; Theobald, W.; Hepburn, K. S.; Riddlestone, I.; Bingham, N. M.; Kopeć, M.; Roth, P. J. Degradable Linear and Bottlebrush Thioester-Functional Copolymers through Atom-Transfer Radical Ring-Opening Copolymerization of a Thionolactone. *Macromolecules* **2022**, *55*, 7392-7400.

## Chapter 2

### Degradable Vinyl Random Copolymers through Photocontrolled Radical Ring-Opening Cascade Copolymerization

A significant portion of the work described in this chapter has been published in:

Wang, W.; Zhou, Z.; Sathe, D.; Tang, X.; Moran, S.; Jin, J.; Haeffner, F.; Wang, J.; Niu, J. Degradable Vinyl Random Copolymers via Photocontrolled Radical Ring-Opening Cascade Copolymerization. *Angew. Chem., Int. Ed.* **2022**, *61*, No. e202113302.

## 2.1 Introduction

Vinyl polymers have been widely used in an array of applications, including packaging, structural materials, synthetic fibers, coating, absorbents, and many others. While an all-carbon backbone makes vinyl polymers highly robust materials, it has also created significant challenges in their degradation, leading to critical environmental issues, including plastic accumulation in landfills and the ocean.<sup>1-2</sup> Therefore, significant efforts have been made in recent years to develop innovative synthetic polymers that possess thermal and mechanical properties comparable to the original nondegradable vinyl polymers but can undergo facile degradation at the end of their life cycle.<sup>3-4</sup> Among various approaches to degradable vinyl polymers, radical ring-opening polymerization (rROP) is of great interest. Attractive features of rROP include its ability to incorporate labile functional groups (e.g., esters, thioesters, disulfide, etc.) into the main chain<sup>5-7</sup> of polymers and the ability to interface with reversible deactivation radical polymerization (RDRP) techniques for the synthesis of polymers with complex and defined macromolecular architectures.<sup>8</sup>

Since the advent of rROP, various cyclic monomers have been successfully developed for the synthesis of degradable vinyl (co)polymers.<sup>6</sup> As a representative class of rROP monomer, cyclic ketene acetals (CKAs) (Figure 2.1A) have been extensively investigated since the 1980s.<sup>9</sup> Despite the recent progress made by Dove,<sup>10-14</sup> Nicolas,<sup>15-20</sup> and Sumerlin,<sup>21-22</sup> unfavorable reactivity ratios in the copolymerization of CKAs with other vinyl monomers often led to gradient or tapered compositions of the resultant copolymer.<sup>23</sup> Gradient composition, in turn, resulted in highly dispersed degradation products and large non-degradable fragments, as part of the copolymer lacked main-chain degradable units. Although new cyclic monomer classes, including macrocyclic allylic sulfides (MASSs)<sup>24-27</sup> and dibenzo[*c,e*]oxepane-5-thiones (DOTs),<sup>28-30</sup> (Figure

2.1A) have demonstrated promising properties, ideal random copolymers of these cyclic monomers with acrylates or acrylamides, which require both comonomer reactivity ratios to equal one in copolymerization, remain challenging.

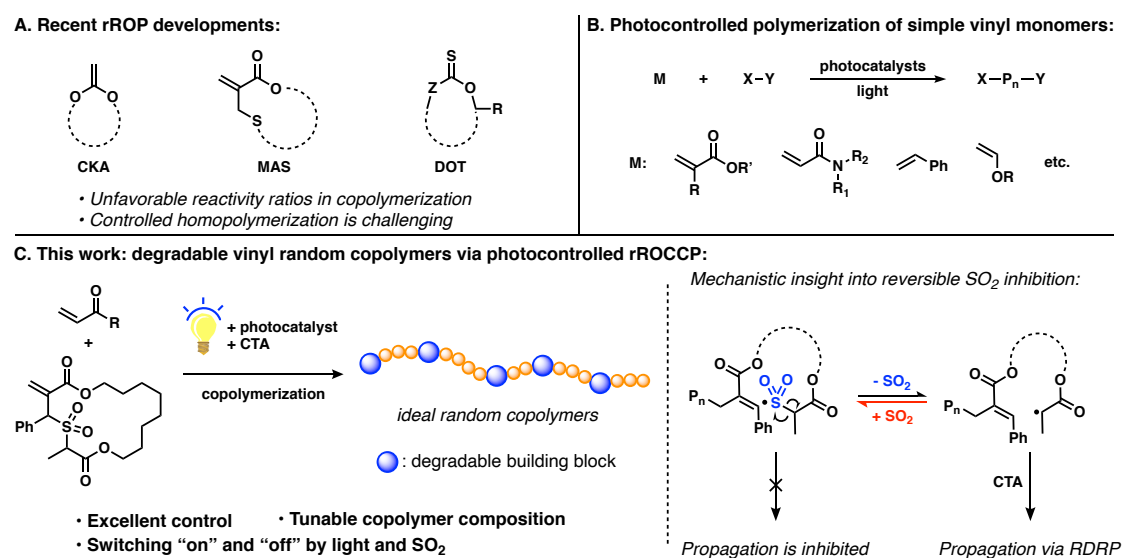


**Figure 2.1.** Degradable vinyl random copolymers through photocontrolled radical ring-opening cascade copolymerization (rROCCP).

In 2018, we reported an approach to thermally initiated radical ring-opening cascade polymerization of allylic sulfone macrocyclic monomers.<sup>31</sup> The radical cascade reaction of the macrocyclic allylic sulfone could extrude sulfur dioxide (SO<sub>2</sub>) and generate a secondary alkyl radical capable of controlled chain propagation.<sup>32</sup> However, the macrocyclic allylic sulfone exhibited a significantly faster rate of incorporation than acrylates in the thermally initiated copolymerization, resulting in unfavorable comonomer reactivity ratios. Therefore, it is essential to develop a method that provides access to ideal random copolymers with tunable compositions and evenly distributed main-chain functional groups.

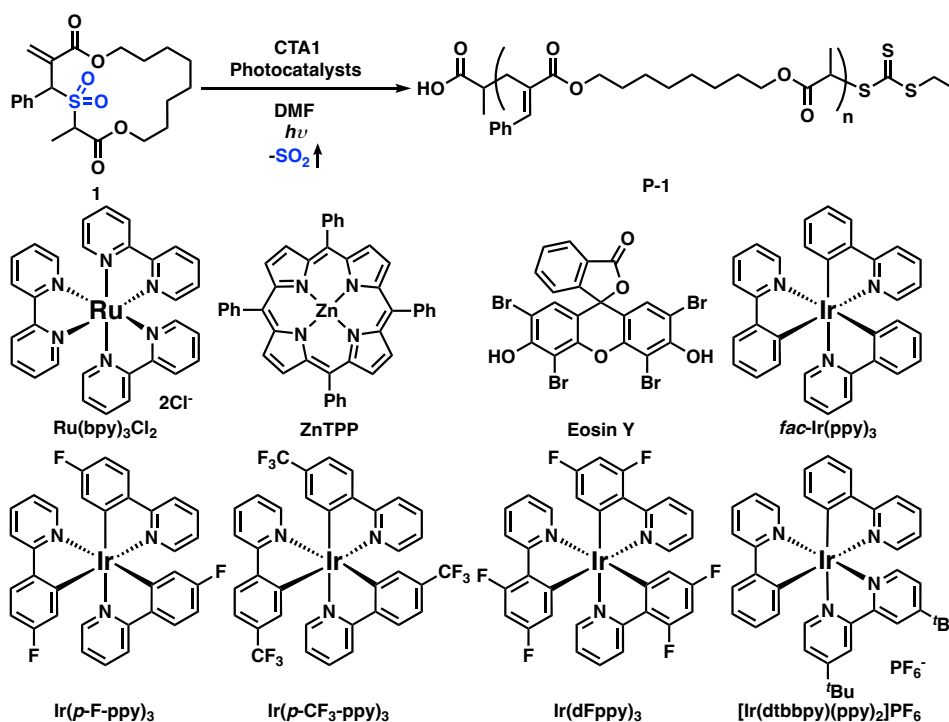
Previous studies have suggested that temperature has a strong influence on the reactivity ratios of cyclic and acyclic vinyl comonomers during radical copolymerization.<sup>6,33</sup> We reasoned that performing the copolymerization at lower temperatures would provide a key opportunity to modulate the reactivity ratios of vinyl comonomers. Therefore, we turned our attention to light-mediated polymerization techniques, as recent works have demonstrated that they are versatile tools to mediate controlled polymerization following radical,<sup>34-42</sup> cationic,<sup>43-47</sup> and metathesis pathways<sup>48-50</sup> at ambient temperature (Figure 2.1B).<sup>51</sup> In particular, we envisioned that photoinduced electron/energy transfer-reversible addition/fragmentation chain transfer (PET-RAFT) polymerization developed by Boyer and coworkers<sup>52-56</sup> could be employed to mediate radical ring-opening cascade copolymerization (rROCCP)<sup>57-58</sup> of the macrocyclic allylic sulfone with acrylates or acrylamides (Figure 2.1C). Unlike the polymerization that is thermally initiated by azobisisobutyronitrile (AIBN), which requires high temperatures (80-100 °C) to maintain a sufficiently high rate of propagation, PET-RAFT can be performed at mild temperatures, thereby enabling favorable comonomer reactivity ratios in copolymerization.<sup>59</sup> To the best of our knowledge, photocontrolled rROCCP represents the first general approach to nearly ideal random copolymers of cyclic and acrylic monomers over an entire range of comonomer feed compositions.

## 2.2 PET-RAFT homopolymerization of macrocyclic allylic sulfones

Our investigation began by screening various well-established photocatalysts to mediate photocontrolled homopolymerization of allylic sulfone macrocyclic monomer **1** under visible light irradiation (Table 2.1).<sup>52-56</sup> We screened an array of photocatalysts, including *fac*-[Ir(ppy)<sub>3</sub>], Ru(bpy)<sub>3</sub>Cl<sub>2</sub>, ZnTPP, and Eosin Y (Table 2.1). We identified

*fac*-[Ir(ppy)<sub>3</sub>] as a promising photocatalyst for the reaction due to the excellent control over polymerization when combined with a chain transfer agent (CTA).

**Table 2.1.** Screening of photocatalysts for PET-RAFT polymerization of **1**.

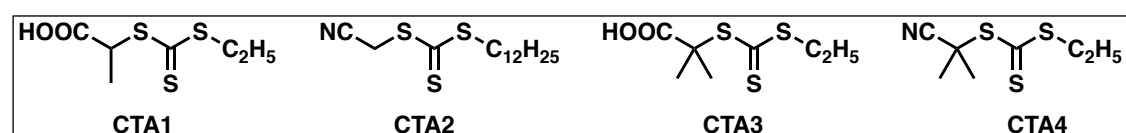
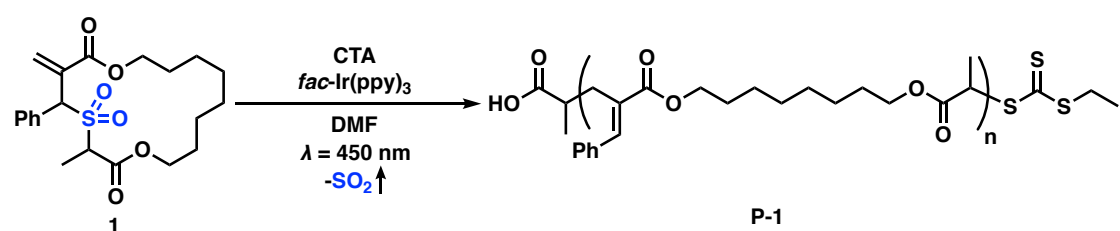


Entry <sup>a</sup>	Photocatalysts	Light	$\lambda$ (nm)	Conv. <sup>b</sup>	$M_n^{(\text{theo})}$ ( $\text{g mol}^{-1}$ ) <sup>c</sup>	$M_n^{(\text{SEC})}$ ( $\text{g mol}^{-1}$ ) <sup>d</sup>	$\mathcal{D}$ <sup>d</sup>
1	$\text{Ru}(\text{bpy})_3\text{Cl}_2$	blue	450	0	-	-	-
2	$\text{ZnTPP}$	blue	450	0	-	-	-
3	$\text{ZnTPP}$	green	525	0	-	-	-
4	$\text{ZnTPP}$	red	660	0	-	-	-
5	Eosin Y	blue	450	20%	3650	5300	1.08
6	$\text{fac-Ir}(\text{ppy})_3$	blue	450	67%	11700	9800	1.11
7	$\text{Ir}(p\text{-F-ppy})_3$	blue	450	44%	7800	8100	1.08
8	$\text{Ir}(p\text{-CF}_3\text{-ppy})_3$	blue	450	39%	6900	7700	1.08
9	$\text{Ir}(\text{dFppy})_3$	blue	450	35%	6200	7400	1.08
10	$[\text{Ir}(\text{dtbbpy})(\text{ppy})_2]\text{PF}_6$	blue	450	28%	5000	7000	1.07

<sup>a</sup>Experimental conditions: 25 °C under argon in a sealed vial for 10 h with  $[\text{M}]_0:[\text{CTA}]_0:[\text{PC}] = 50:1:0.01$ ,  $[\text{M}]_0 = 0.2 \text{ M}$ ,  $[\text{PC}]/[\text{M}]_0 = 200 \text{ ppm}$ . <sup>b</sup>Monomer conversion was determined by  $^1\text{H}$  NMR spectroscopy. <sup>c</sup>Theoretical  $M_n$  was calculated based on  $[\text{M}]_0/[\text{CTA}]_0$  and conversion. <sup>d</sup> $M_n$  and  $\mathcal{D}$  were determined by SEC analysis calibrated to polystyrene standards.

At a monomer/CTA ratio of 50:1, our initial attempt at polymerization of macrocyclic allylic sulfone **1** mediated by *fac*-[Ir(ppy)<sub>3</sub>] and **CTA1** under 450 nm light irradiation yielded **P-1** with number average molecular weight ( $M_n^{(SEC)}$ ) of 9.8 kg/mol and dispersity ( $D$ ) of 1.11 (Table 2.2).

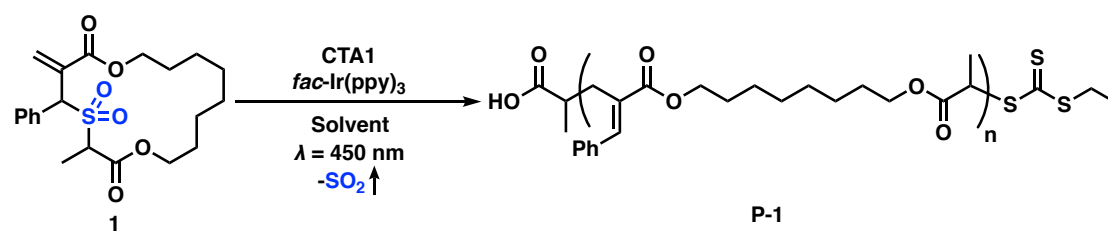
**Table 2.2.** Effect of CTA on PET-RAFT polymerization of **1**.



Entry <sup>a</sup>	CTAs	Conv. <sup>b</sup>	$M_n^{(theo)}$ (g mol <sup>-1</sup> ) <sup>c</sup>	$M_n^{(SEC)}$ (g mol <sup>-1</sup> ) <sup>d</sup>	$D^d$
1	CTA1	67%	11700	9800	1.11
2	CTA2	66%	11600	10600	1.11
3	CTA3	43%	7400	7700	1.12
4	CTA4	26%	4700	3700	1.07

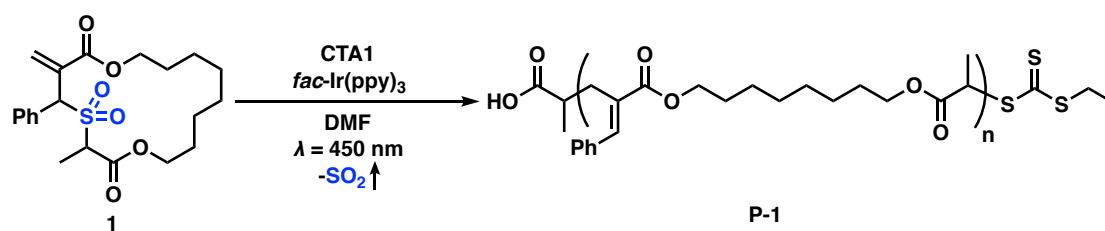
<sup>a</sup>Experimental conditions: 25 °C under argon in a sealed vial for 10 h with  $[M]_0:[CTA]_0:[Ir] = 50:1:0.01$ ,  $[M]_0 = 0.2$  M,  $[PC]/[M]_0 = 200$  ppm. <sup>b</sup>Monomer conversion was determined by <sup>1</sup>H NMR spectroscopy. <sup>c</sup>Theoretical  $M_n$  was calculated based on  $[M]_0/[CTA]_0$  and conversion. <sup>d</sup> $M_n$  and  $D$  were determined by SEC analysis calibrated to polystyrene standards.

Further examination of reaction conditions revealed that the optimal polymerization was achieved when the monomer concentration was 0.2 M in *N,N*-dimethylformamide (DMF), and the catalyst loading was 200 ppm (Table 2.3-2.5).

**Table 2.3.** Influence of solvent on PET-RAFT polymerization of **1**.

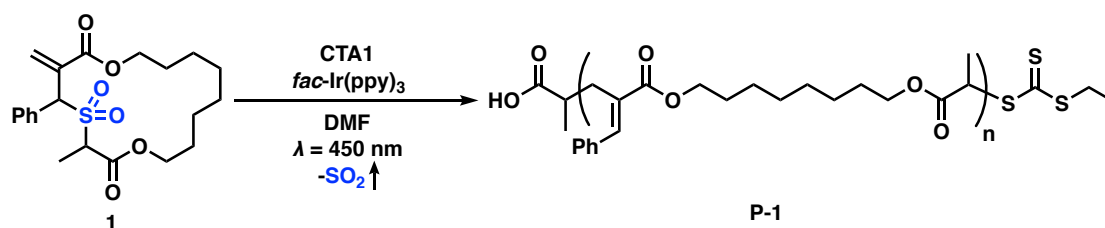
Entry <sup>a</sup>	Solvents	Conv. <sup>b</sup>	$M_n^{\text{(theo)}}$ (g mol <sup>-1</sup> ) <sup>c</sup>	$M_n^{\text{(SEC)}}$ (g mol <sup>-1</sup> ) <sup>d</sup>	$D^d$
1	DMF	67%	11700	9800	1.11
2	Dioxane	67%	11700	10000	1.14
3	Toluene	53%	9300	8800	1.10
4	THF	41%	7300	7100	1.11
5	DMSO	48%	8500	9600	1.26

<sup>a</sup>Experimental conditions: 25 °C under argon in a sealed vial for 10 h with  $[\text{M}]_0:[\text{CTA}]_0:[\text{Ir}] = 50:1:0.01$ ,  $[\text{M}]_0 = 0.2 \text{ M}$ ,  $[\text{PC}]/[\text{M}]_0 = 200 \text{ ppm}$ . <sup>b</sup>Monomer conversion was determined by <sup>1</sup>H NMR spectroscopy. <sup>c</sup>Theoretical  $M_n$  was calculated based on  $[\text{M}]_0/[\text{CTA}]_0$  and conversion. <sup>d</sup> $M_n$  and  $D$  were determined by SEC analysis calibrated to polystyrene standards.

**Table 2.4.** Effect of initial monomer concentration on PET-RAFT polymerization of **1**.

Entry <sup>a</sup>	[M] <sub>0</sub>	Conv. <sup>b</sup>	$M_n^{\text{(theo)}}$ (g mol <sup>-1</sup> ) <sup>c</sup>	$M_n^{\text{(SEC)}}$ (g mol <sup>-1</sup> ) <sup>d</sup>	$D^d$
1	0.1 M	47%	8300	7700	1.08
2	0.2 M	67%	11700	9800	1.11
3	0.4 M	76%	13300	10600	1.14

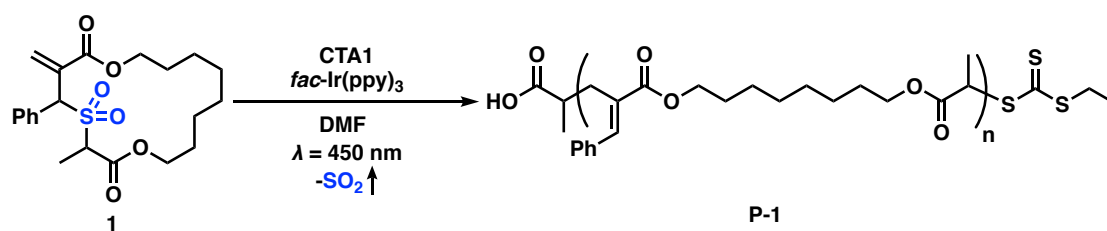
<sup>a</sup>Experimental conditions: 25 °C under argon in a sealed vial for 10 h with [M]<sub>0</sub>:[CTA]<sub>0</sub>:[Ir] = 50:1:0.01, [PC]/[M]<sub>0</sub> = 200 ppm. <sup>b</sup>Monomer conversion was determined by <sup>1</sup>H NMR spectroscopy. <sup>c</sup>Theoretical  $M_n$  was calculated based on [M]<sub>0</sub>/[CTA]<sub>0</sub> and conversion. <sup>d</sup> $M_n$  and  $D$  were determined by SEC analysis calibrated to polystyrene standards.

**Table 2.5.** Influence of catalyst loading on PET-RAFT polymerization of **1**.

Entry <sup>a</sup>	Cat. loading	Conv. <sup>b</sup>	$M_n^{(\text{theo})}$ (g mol <sup>-1</sup> ) <sup>c</sup>	$M_n^{(\text{SEC})}$ (g mol <sup>-1</sup> ) <sup>d</sup>	$D^d$
1	100 ppm	53%	9300	8600	1.11
2	200 ppm	67%	11700	9800	1.11
3	400 ppm	72%	12600	10300	1.18

<sup>a</sup>Experimental conditions: 25 °C under argon in a sealed vial for 10 h with  $[\text{M}]_0:[\text{CTA}]_0:[\text{Ir}] = 50:1:0.01$ ,  $[\text{M}]_0 = 0.2$  M. <sup>b</sup>Monomer conversion was determined by <sup>1</sup>H NMR spectroscopy. <sup>c</sup>Theoretical  $M_n$  was calculated based on  $[\text{M}]_0/[\text{CTA}]_0$  and conversion. <sup>d</sup> $M_n$  and  $D$  were determined by SEC analysis calibrated to polystyrene standards.

Polymerization of **1** at other monomer/CTA ratios of 25:1, 100:1, and 200:1 successfully yielded polymers with predictable  $M_n$  and low  $D$ , demonstrating excellent control over the polymerization (Table 2.6).

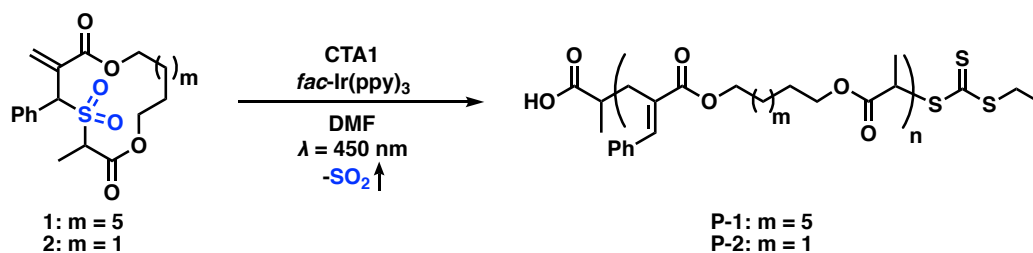
**Table 2.6.** PET-RAFT polymerization of **1** with different monomer/CTA ratios.

Entry <sup>a</sup>	[M] <sub>0</sub> /[CTA] <sub>0</sub>	Conv. <sup>b</sup>	$M_n^{(\text{theo})}$ (g mol <sup>-1</sup> ) <sup>c</sup>	$M_n^{(\text{SEC})}$ (g mol <sup>-1</sup> ) <sup>d</sup>	$\bar{D}$ <sup>d</sup>
1	25/1	68%	6100	6900	1.09
2	50/1	67%	11700	9800	1.11
3	100/1	62%	21500	23000	1.14
4	200/1	57%	39100	39100	1.14

<sup>a</sup>Experimental conditions: 25 °C under argon in a sealed vial for 10 h with  $[\text{M}]_0 = 0.2$  M and  $[\text{PC}]/[\text{M}]_0 = 200$  ppm. <sup>b</sup>Monomer conversion was determined by <sup>1</sup>H NMR spectroscopy. <sup>c</sup>Theoretical  $M_n$  was calculated based on  $[\text{M}]_0/[\text{CTA}]_0$  and conversion. <sup>d</sup> $M_n$  and  $\bar{D}$  were determined by SEC analysis calibrated to polystyrene standards.

Similarly, macrocyclic allylic sulfone **2**, which is a smaller ring, was also polymerized with good control under the same conditions (Table 2.7). It is noteworthy that no ring-retaining propagation of both allylic sulfone macrocyclic monomers **1** and **2** was observed.

**Table 2.7.** Effect of monomer ring strain on PET-RAFT polymerization of macrocyclic allylic sulfones.



Entry <sup>a</sup>	$m$	Conv. <sup>b</sup>	$M_n^{(\text{theo})}$ ( $\text{g mol}^{-1}$ ) <sup>c</sup>	$M_n^{(\text{SEC})}$ ( $\text{g mol}^{-1}$ ) <sup>d</sup>	$D^d$
1	5	67%	11700	9800	1.11
2	1	69%	10100	7500	1.09

<sup>a</sup>Experimental conditions: 25 °C under argon in a sealed vial for 10 h with  $[M]_0:[CTA]_0:[Ir] = 50:1:0.01$ ,  $[M]_0 = 0.2$  M, and  $[PC]/[M]_0 = 200$  ppm. <sup>b</sup>Monomer conversion was determined by <sup>1</sup>H NMR spectroscopy. <sup>c</sup>Theoretical  $M_n$  was calculated based on  $[M]_0/[CTA]_0$  and conversion. <sup>d</sup> $M_n$  and  $D$  were determined by SEC analysis calibrated to polystyrene standards.

Following the exploration of reaction conditions, we examined the living characteristics of the polymerization. First, kinetic analysis revealed that the polymerization of **1** deviated from first-order kinetics in the late stage (Figure 2.2).

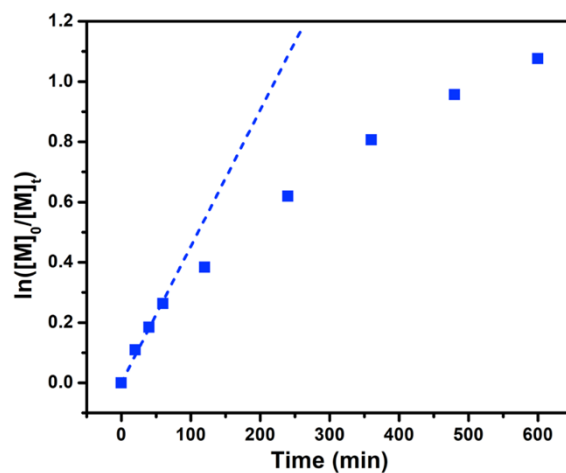


**Figure 2.2.** Kinetic plot of  $\ln([M]_0/[M]_t)$  versus reaction time, where  $[M]_0$  is the initial monomer concentration and  $[M]_t$  is the monomer concentration at a given time  $t$ .

This observation was consistent with our previous results when cascade polymerization of the macrocyclic allylic sulfone was thermally initiated.<sup>31,60</sup> Despite the kinetic anomaly, the polymerization of **1** still exhibited a linear increase of  $M_n$  with respect to monomer conversion and retained low  $\mathcal{D}$  throughout the reaction, suggesting that control over the polymerization was well maintained even after the rate decreased in the late stage (Figure 2.3A).

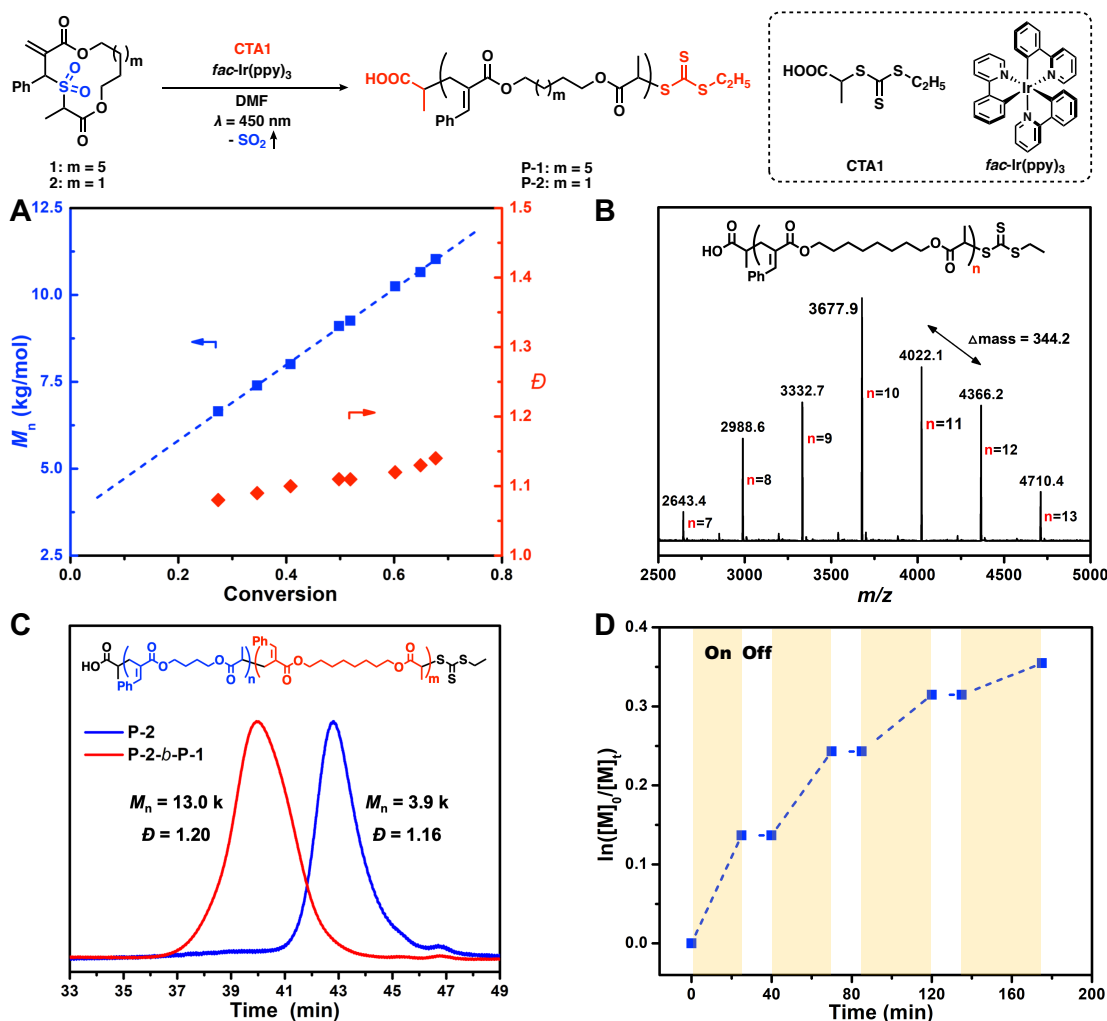


**Figure 2.3.** Analysis of PET-RAFT polymerization of macrocyclic allylic sulfones. (A) Plots of  $M_n$  and  $D$  as a function of monomer conversion. (B) MALDI-TOF analysis of P-1-5k. The spacing between these discrete oligomers was consistent with the expected mass of the repeating unit (344 g/mol). Each peak corresponds to a discrete oligomer that consists of an  $\alpha$ - and  $\omega$ -chain end, the number of repeating units multiplied by its molar mass, and a sodium cation. (C) SEC analysis of block copolymer P-2-*b*-P-1. (D)  $\ln([M]_0/[M]_t)$  vs. reaction time with intermittent light exposure.

$^1\text{H}$  NMR analysis of P-1-6k ( $M_n^{\text{(SEC)}} = 6.4$  kg/mol,  $D = 1.07$ ) confirmed the fidelity of the chain end groups (2.46 and 1.21 ppm for  $\alpha$ -chain end and 4.81 and 3.36 ppm for  $\omega$ -chain end, Figure 2.4), an important indicator of controlled polymerization.

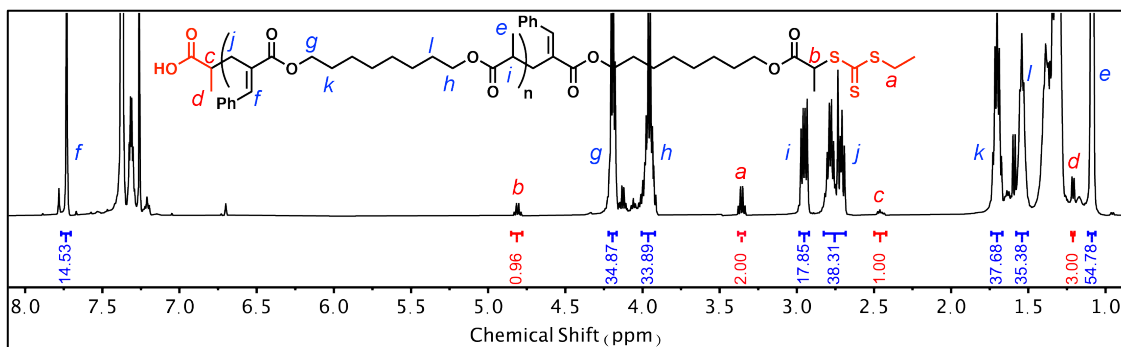
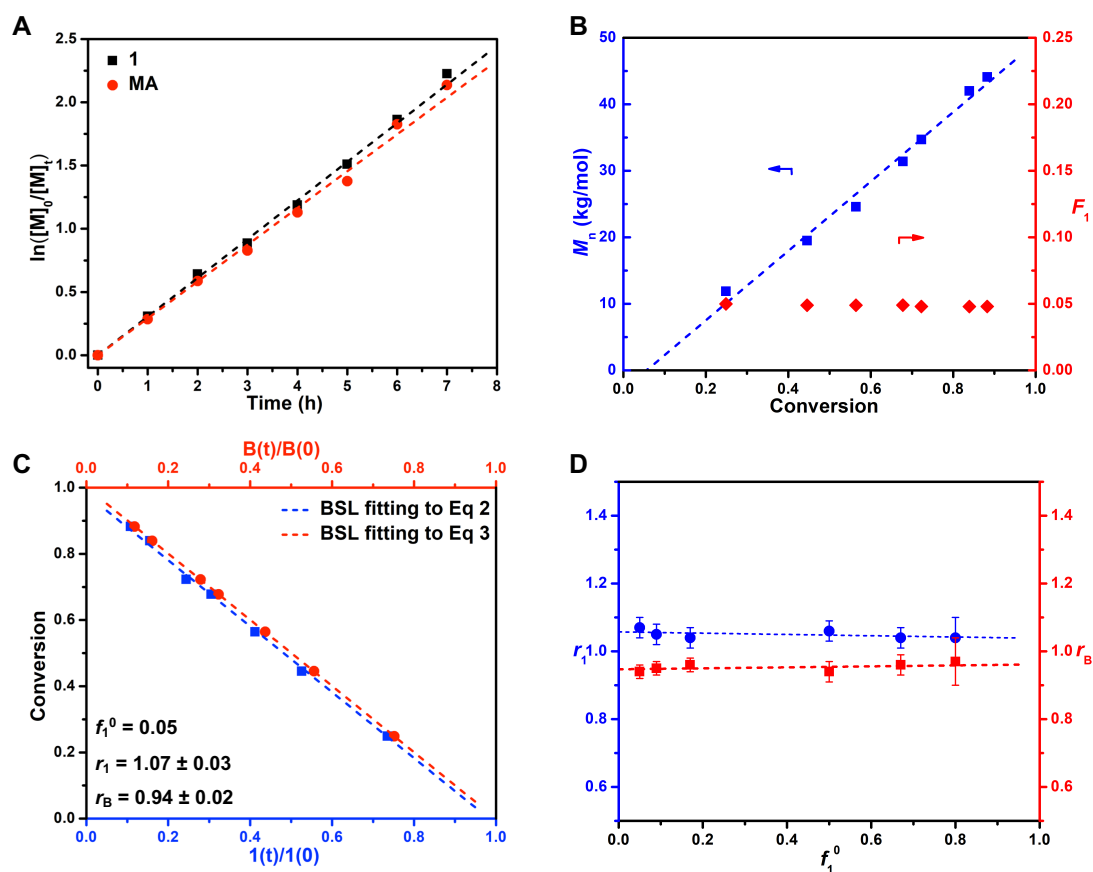


**Figure 2.4.**  $^1\text{H}$  NMR spectroscopy of **P-1-6k**.

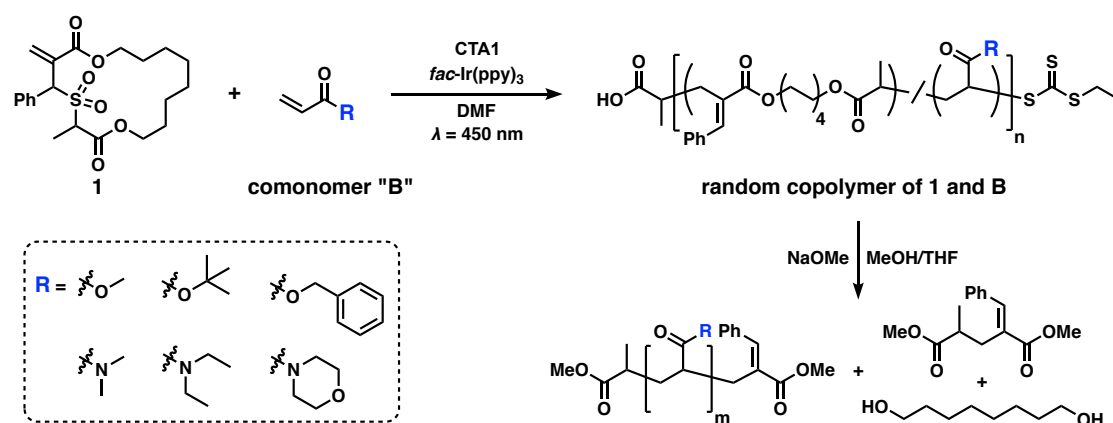
Besides, the discrete oligomers of **P-1-5k** ( $M_n^{\text{(SEC)}} = 5.5 \text{ kg/mol}$ ,  $D = 1.10$ ) observed by matrix-assisted laser desorption/ionization time-of-flight (MALDI-TOF) mass spectrometry showed masses consistent with the predicted values of these oligomers with intact chain ends (Figure 2.3B). Furthermore, chain extension of the macroinitiator **P-2-4k** ( $M_n^{\text{(SEC)}} = 3.9 \text{ kg/mol}$ ,  $D = 1.16$ ) by **1** exhibited a clear shift to the higher molecular weight region on size-exclusion chromatogram (SEC), suggesting the formation of a diblock copolymer **P-2-b-P-1** ( $M_n^{\text{(SEC)}} = 13.0 \text{ kg/mol}$ ,  $D = 1.20$ , Figure 2.3C). Finally, the reaction exhibited excellent temporal control: chain propagation completely halted when the light was switched “off”; polymerization resumed efficiently after the light was switched back “on” (Figure 2.3D). Taken together, these results unambiguously supported that PET-RAFT polymerization of the macrocyclic allylic sulfone maintained excellent control throughout the reaction despite deviating from first-order kinetics at the late stage.

### 2.3 Copolymerization of macrocyclic allylic sulfone with acrylates or acrylamides

Building upon the results of photocontrolled homopolymerization of macrocyclic allylic sulfones, we then investigated the copolymerization of **1** and various acrylic monomers (denoted hereafter as comonomer B). First, **1** was copolymerized with methyl acrylate (MA) at a feed composition of  $f_1^0 = 0.05$ , where  $f_1^0$  is the molar fraction of **1** in the initial comonomer mixture, yielding copolymer **P-1-co-MA** with  $M_n^{(SEC)}$  of 44.0 kg/mol and  $D$  of 1.28 (Table 2.8, entry 1). The propagation of both comonomers demonstrated first-order kinetics throughout copolymerization (Figure 2.5A).



**Figure 2.5.** Photocontrolled rROCCP of the macrocyclic allylic sulfone with various acrylates or acrylamides generates nearly ideal random copolymers. (A) Kinetic plots of  $\ln([M]_0/[M]_t)$  versus reaction time of both comonomers. (B) Plots of  $M_n$  and incorporation of **1** ( $F_1$ ) as a function of total conversion. (C) Plot of total conversion with respect to  $[1(t)]/[1(0)]$  or  $[B(t)]/[B(0)]$  is fitted to Equations (2) and (3) of the BSL model independently to derive the reactivity ratios. (D) The reactivity ratios of **1** and MA in photocontrolled rROCCP remained close to unity in a broad range of monomer feed compositions. The error bars indicate a 95% confidence interval of the reactivity ratios.

**Table 2.8.** Photocontrolled rROCCP of **1** with various acrylates or acrylamides.

Entry <sup>a</sup>	B	$f_1^0$	$r_1^b$	$r_B^b$	Conv. <sup>c</sup>	$M_n^{(\text{SEC})}$ (kg/mol) <sup>d</sup>	$\bar{D}^d$	$F_1^{(\text{end})c}$	Degraded $M_n^{(\text{SEC})}$ (kg/mol) <sup>d</sup>	Degraded $\bar{D}^d$
1	MA	0.05	1.07±0.03	0.94±0.02	88%	44.0	1.28	0.05	2.8	1.58
2	MA	0.09	1.05±0.03	0.95±0.02	82%	21.7	1.27	0.10	1.3	1.33
3	MA	0.17	1.04±0.03	0.96±0.02	76%	14.8	1.15	0.17	0.7	1.30
4	MA	0.50	1.06±0.03	0.94±0.03	70%	9.3	1.12	0.51	0.6	1.12
5	MA	0.67	1.04±0.03	0.96±0.03	75%	7.7	1.18	0.68	0.5	1.07
6	MA	0.80	1.04±0.06	0.97±0.07	61%	6.8	1.17	0.80	0.5	1.06
7	<i>t</i> BA	0.09	1.04±0.04	0.96±0.03	85%	39.0	1.29	0.09	2.6	1.34
8	BnA	0.09	0.84±0.03	1.19±0.04	89%	22.1	1.38	0.08	2.9	1.35
9	DMA	0.09	1.03±0.03	0.97±0.03	75%	16.1	1.21	0.09	1.8	1.42
10	DEA	0.09	0.89±0.06	1.16±0.08	79%	20.1	1.14	0.07	2.2	1.38
11	NAM	0.09	0.94±0.05	1.07±0.06	82%	20.9	1.34	0.09	2.8	1.32

<sup>a</sup>Experimental conditions: 18 W blue LED light ( $\lambda_{\text{max}} = 450$  nm), 25 °C under argon in a sealed vial for 8 h; light intensity at the reaction vial = 34 mW/cm<sup>2</sup>, [PC]/[M]<sub>0</sub> = 200 ppm. <sup>b</sup>The reactivity ratios were obtained by fitting the comonomer conversion and composition of copolymers to the BSL integrated model. The mean and 95% confidence interval of the reactivity ratios were calculated based on five to seven independent fitting results. <sup>c</sup>Monomer conversion and  $F_1^{(\text{end})}$  were determined by <sup>1</sup>H NMR spectroscopy. <sup>d</sup> $M_n$  and  $\bar{D}$  were determined by SEC analysis calibrated to polystyrene standards.

The molecular weight also increased linearly with respect to the overall monomer conversion, which is defined by Equation (1):

$$conv. = 1 - \frac{[1(t)]+[B(t)]}{[1(0)]+[B(0)]} \quad (1)$$

where  $[1(t)]$  and  $[B(t)]$  are the respective instantaneous concentrations of **1** and comonomer B at time  $t$ , and  $[1(0)]$  and  $[B(0)]$  are the respective initial concentrations of **1** and comonomer B (Figure 2.5B). Importantly, the instantaneous molar fraction of **1** incorporated into the copolymer (denoted hereafter as  $F_1$ ) remained identical to  $f_1^0$  throughout the copolymerization (Figure 2.6).

#### P-1-co-MA with $f_1^0 = 0.05$

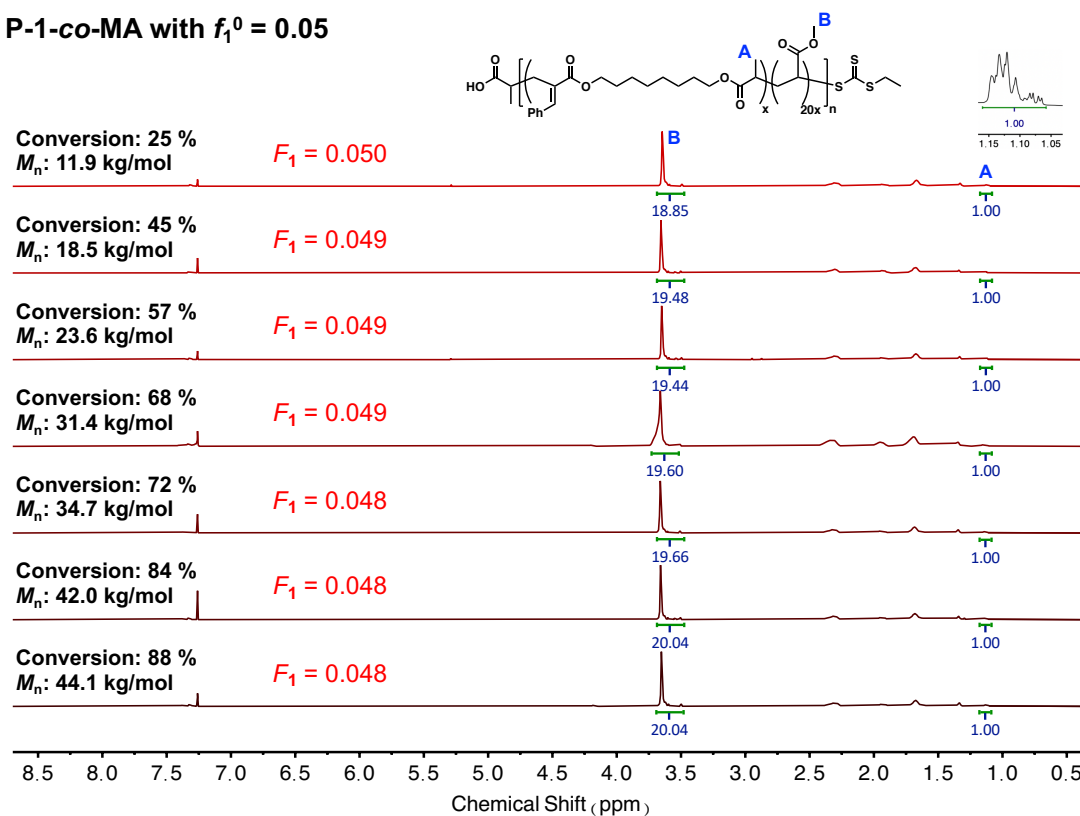


**Figure 2.6.** Compositional analysis of copolymers **P-1-co-MA** at  $f_1^0 = 0.05$  at different time points of the reaction by  $^1\text{H}$  NMR spectroscopy.

Correspondingly, the final copolymer composition,  $F_1^{(\text{end})}$ , when the reaction reached the end point, was also identical to  $f_1^0$  (Table 2.8, entry 1). These results suggested that the reactivities of the two comonomers are highly similar in chain propagation. To determine the reactivity ratios of the copolymerization, the compositional data of **1** and B throughout copolymerization was fitted to the Beckingham-Sanoja-Lynd (BSL) integrated model reported by Lynd et al.<sup>61</sup> [Equations (2) and (3)]

$$\text{conv.} = 1 - f_1^0 \left[ \frac{\mathbf{1}(t)}{\mathbf{1}(0)} \right] - (1 - f_1^0) \left[ \frac{\mathbf{1}(t)}{\mathbf{1}(0)} \right]^{r_B} \quad (2)$$

$$\text{conv.} = 1 - f_1^0 \left[ \frac{\mathbf{B}(t)}{\mathbf{B}(0)} \right]^{r_1} - (1 - f_1^0) \left[ \frac{\mathbf{B}(t)}{\mathbf{B}(0)} \right] \quad (3)$$

where  $r_1$  and  $r_B$  are the reactivity ratios of **1** and comonomer B. It is noteworthy that although the BSL model is derived for ideal copolymerization where the product of comonomer reactivity ratios equals unity, such as ionic or metal-catalyzed copolymerization systems, we reasoned that copolymerization of the macrocyclic allylic sulfone and acrylic monomers is a close approximation of ideal copolymerization, because the allylic sulfone motif was designed such that the propagating secondary alkyl radical formed after the radical cascade process is structurally similar to the propagating radical of polyacrylates.<sup>62</sup> Independent fitting of the polymer compositional data to Equations (2) and (3) supported this rationale, as the derived reactivity ratios of comonomers were  $r_1 = 1.07 \pm 0.03$  and  $r_B = 0.94 \pm 0.02$ , with  $r_1 \times r_B = 1.01 \pm 0.05$  (Figure 2.5C). These results suggested that the copolymerization reaction is indeed highly analogous to an ideal copolymerization and that the copolymer generated from the reaction is very close to an ideal random copolymer. The reactivity ratios of **1** and MA in the entire range of monomer feed compositions ( $f_1^0 = 0-1$ ) remained close to unity (Table 2.8, entries 1-6 & Figure 2.5D & Figure 2.7-2.16).

**P-1-co-MA with  $f_1^0 = 0.09$**

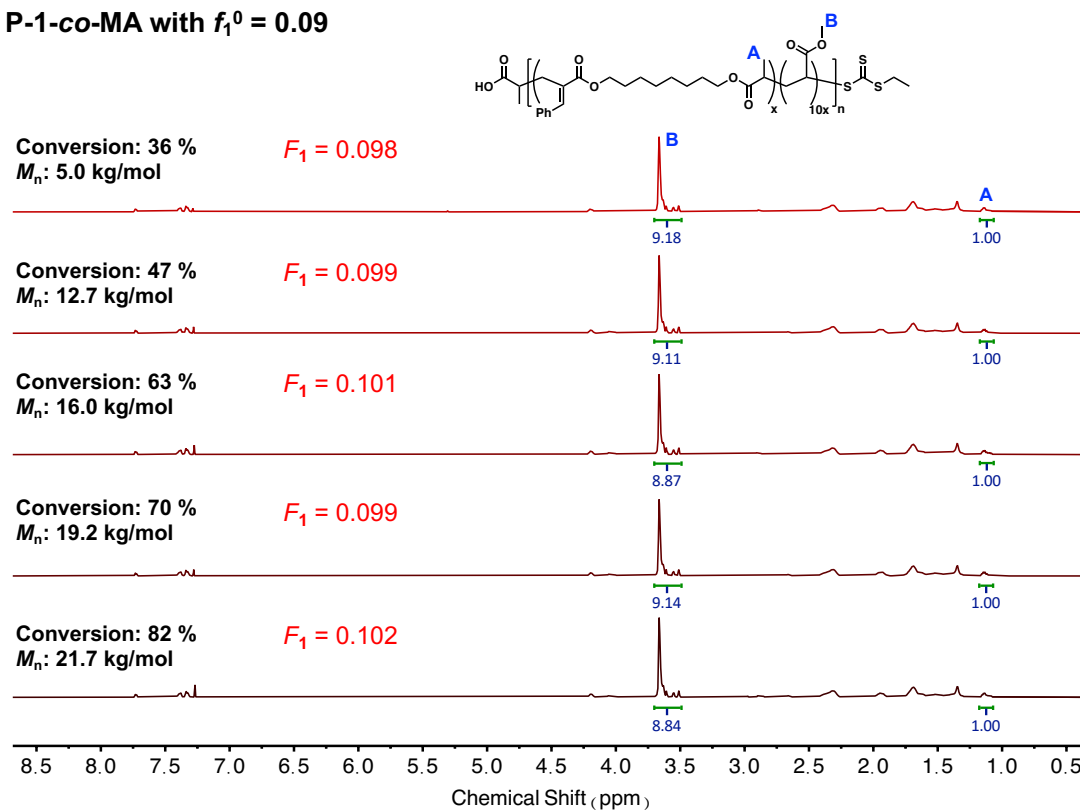


**Figure 2.7.** Compositional analysis of copolymers **P-1-co-MA** at  $f_1^0 = 0.09$  at different time points of the reaction by <sup>1</sup>H NMR spectroscopy.

**P-1-co-MA with  $f_1^0 = 0.17$**

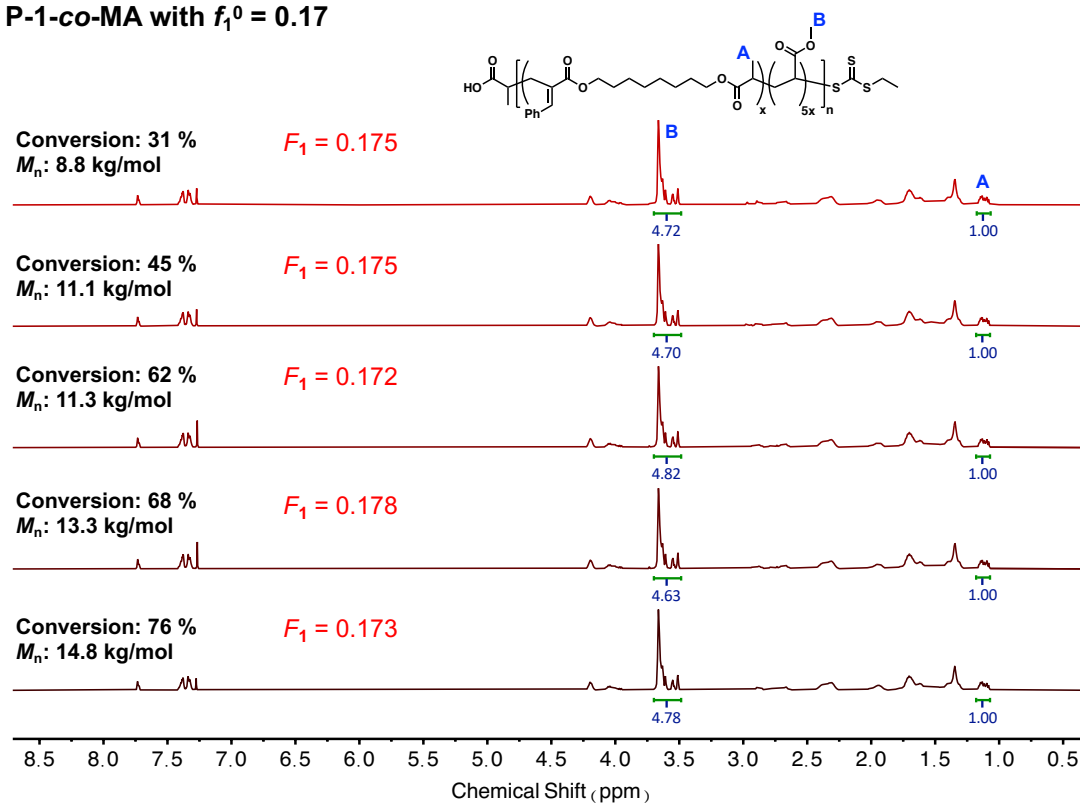


**Figure 2.8.** Compositional analysis of copolymers **P-1-co-MA** at  $f_1^0 = 0.17$  at different time points of the reaction by <sup>1</sup>H NMR spectroscopy.

**P-1-co-MA with  $f_1^0 = 0.50$**

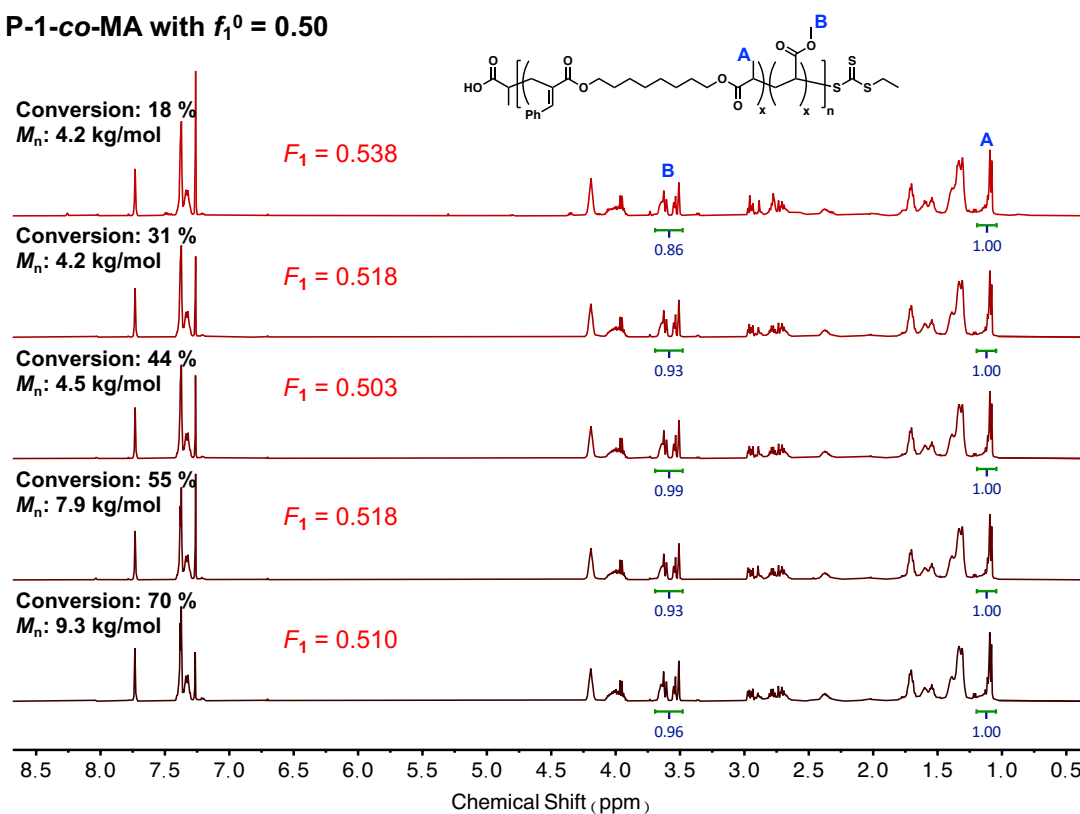


**Figure 2.9.** Compositional analysis of copolymers **P-1-co-MA** at  $f_1^0 = 0.50$  at different time points of the reaction by  $^1\text{H}$  NMR spectroscopy.



**P-1-co-MA with  $f_1^0 = 0.80$**

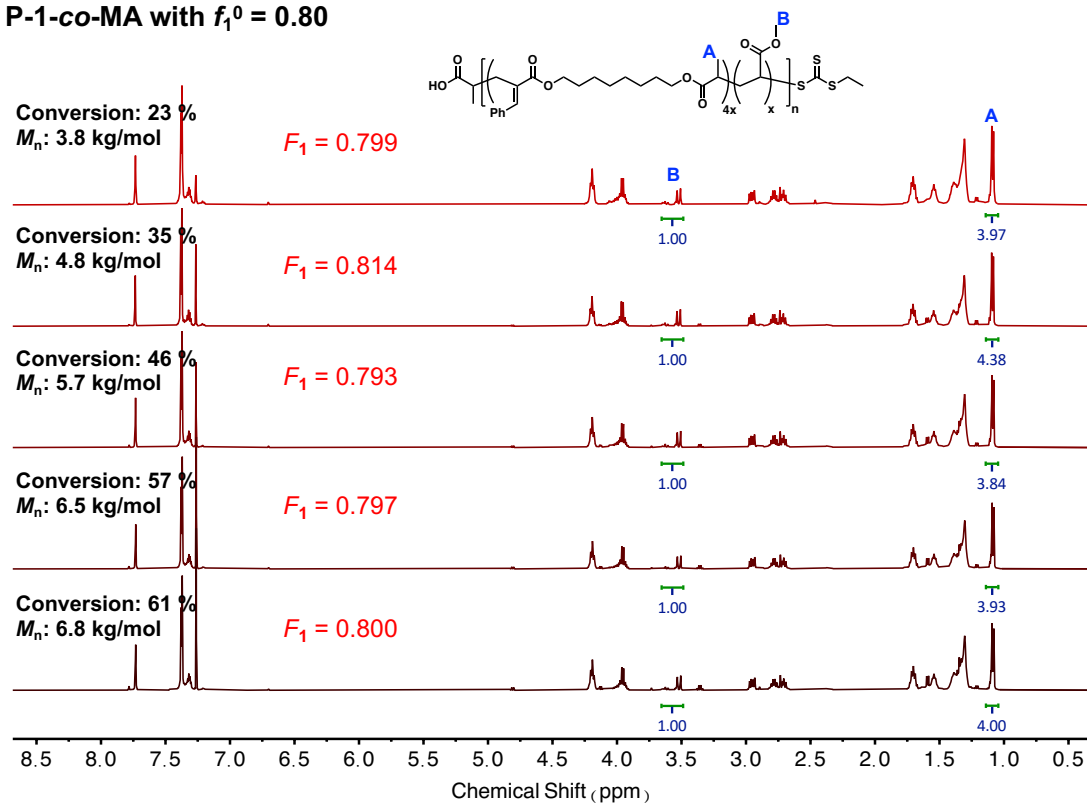


**Figure 2.11.** Compositional analysis of copolymers **P-1-co-MA** at  $f_1^0 = 0.80$  at different time points of the reaction by  $^1\text{H}$  NMR spectroscopy.

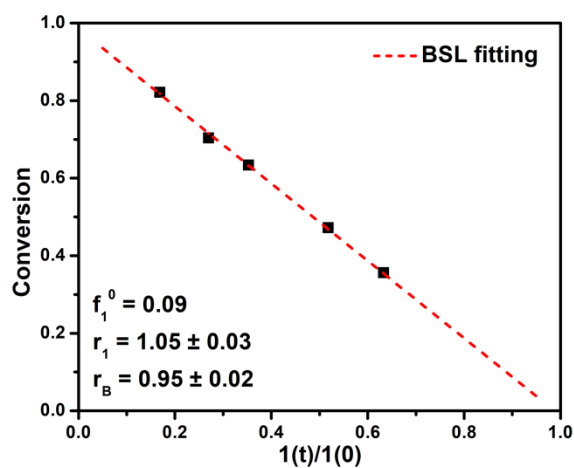


**Figure 2.12.** Plot of total conversion with respect to  $[1(t)]/[1(0)]$  is fitted to the BSL model to derive the comonomer reactivity ratios for copolymerization of **1** and MA at  $f_1^0 = 0.09$  at 25 °C.

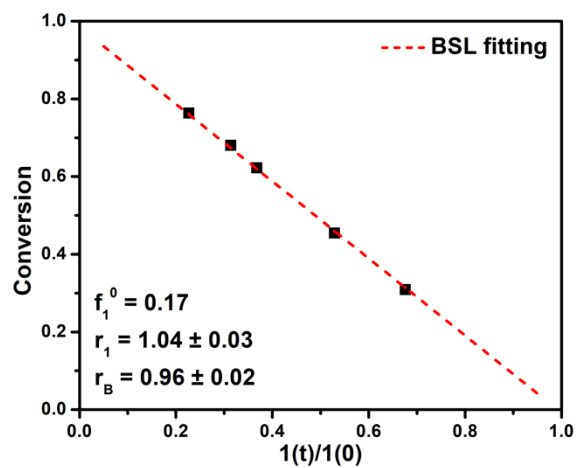


**Figure 2.13.** Plot of total conversion with respect to  $[1(t)]/[1(0)]$  is fitted to the BSL model to derive the comonomer reactivity ratios for copolymerization of **1** and MA at  $f_1^0 = 0.17$  at 25 °C.

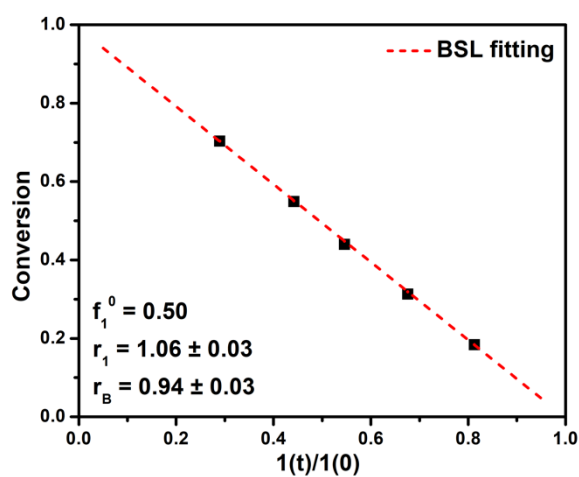


**Figure 2.14.** Plot of total conversion with respect to  $[1(t)]/[1(0)]$  is fitted to the BSL model to derive the comonomer reactivity ratios for copolymerization of **1** and MA at  $f_1^0 = 0.50$  at 25 °C.

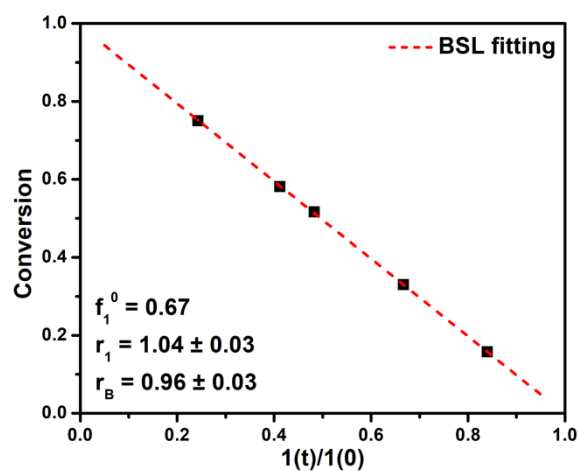


**Figure 2.15.** Plot of total conversion with respect to  $[1(t)]/[1(0)]$  is fitted to the BSL model to derive the comonomer reactivity ratios for copolymerization of **1** and MA at  $f_1^0 = 0.67$  at 25 °C.

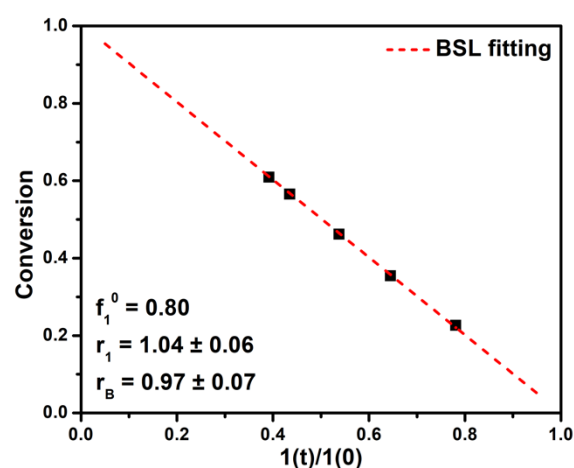


**Figure 2.16.** Plot of total conversion with respect to  $[1(t)]/[1(0)]$  is fitted to the BSL model to derive the comonomer reactivity ratios for copolymerization of **1** and MA at  $f_1^0 = 0.80$  at 25 °C.

Furthermore, copolymerization of **1** with other acrylic comonomers, including *tert*-butyl acrylate (*t*BA), benzyl acrylate (BnA), *N,N*-dimethylacrylamide (DMA), *N,N*-diethylacrylamide (DEA), and *N*-Acryloylmorpholine (NAM), at  $f_1^0 = 0.09$  all exhibited excellent control over polymerization and near-unity reactivity ratios,

suggesting that this method is generally applicable to a wide range of acrylates and acrylamides (Table 2.8, entries 7-11 & Figure 2.17-2.26).

**P-1-co-tBA with  $f_1^0 = 0.09$**

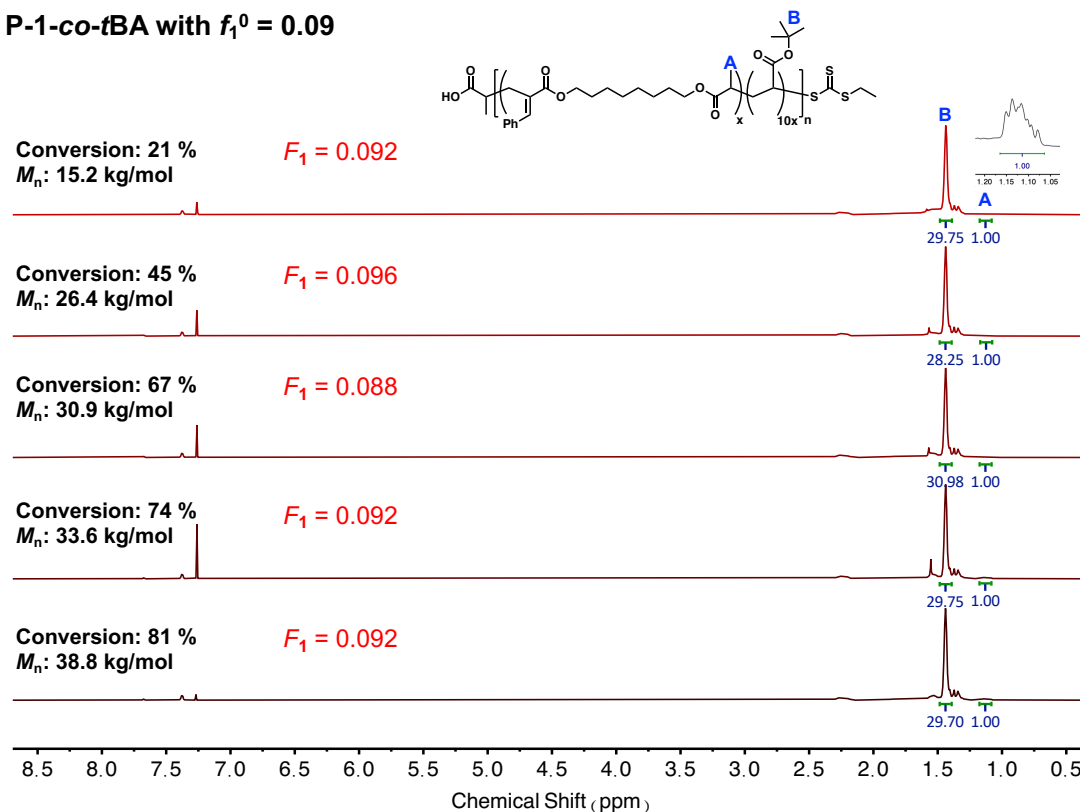


**Figure 2.17.** Compositional analysis of copolymers **P-1-co-tBA** at  $f_1^0 = 0.09$  at different time points of the reaction by  $^1\text{H}$  NMR spectroscopy.

**P-1-co-BnA with  $f_1^0 = 0.09$**

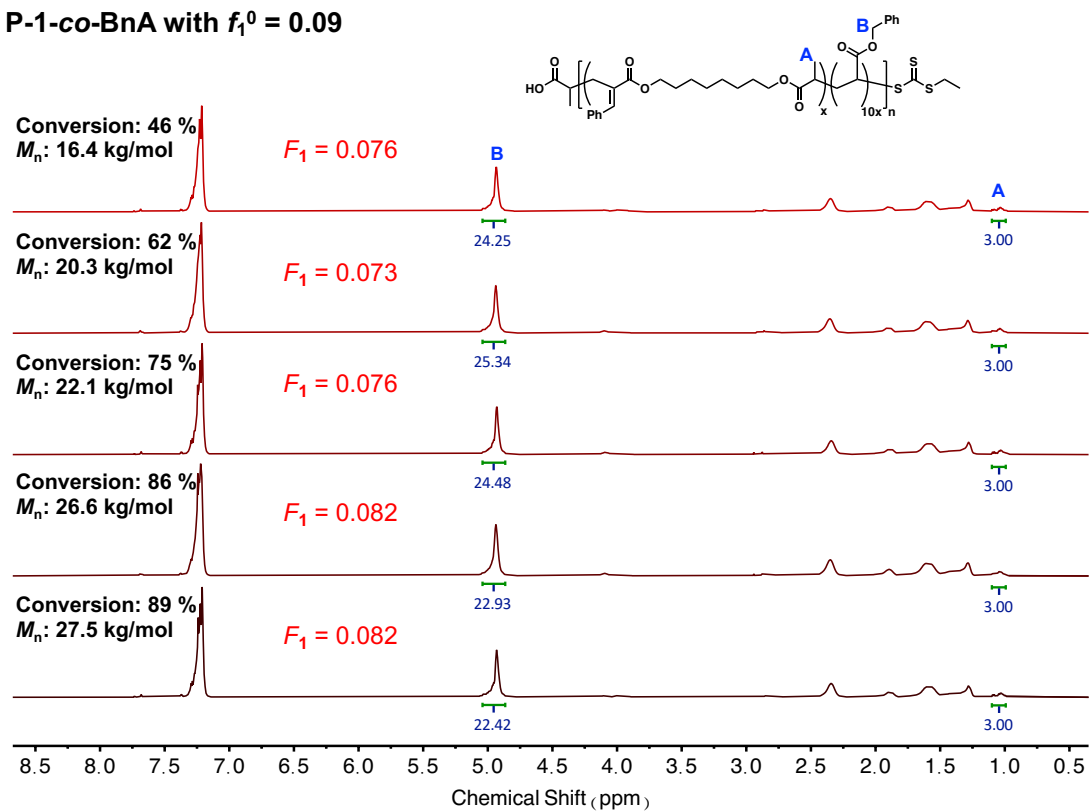


**Figure 2.18.** Compositional analysis of copolymers **P-1-co-BnA** at  $f_1^0 = 0.09$  at different time points of the reaction by  $^1\text{H}$  NMR spectroscopy.

**P-1-co-DMA with  $f_1^0 = 0.09$**

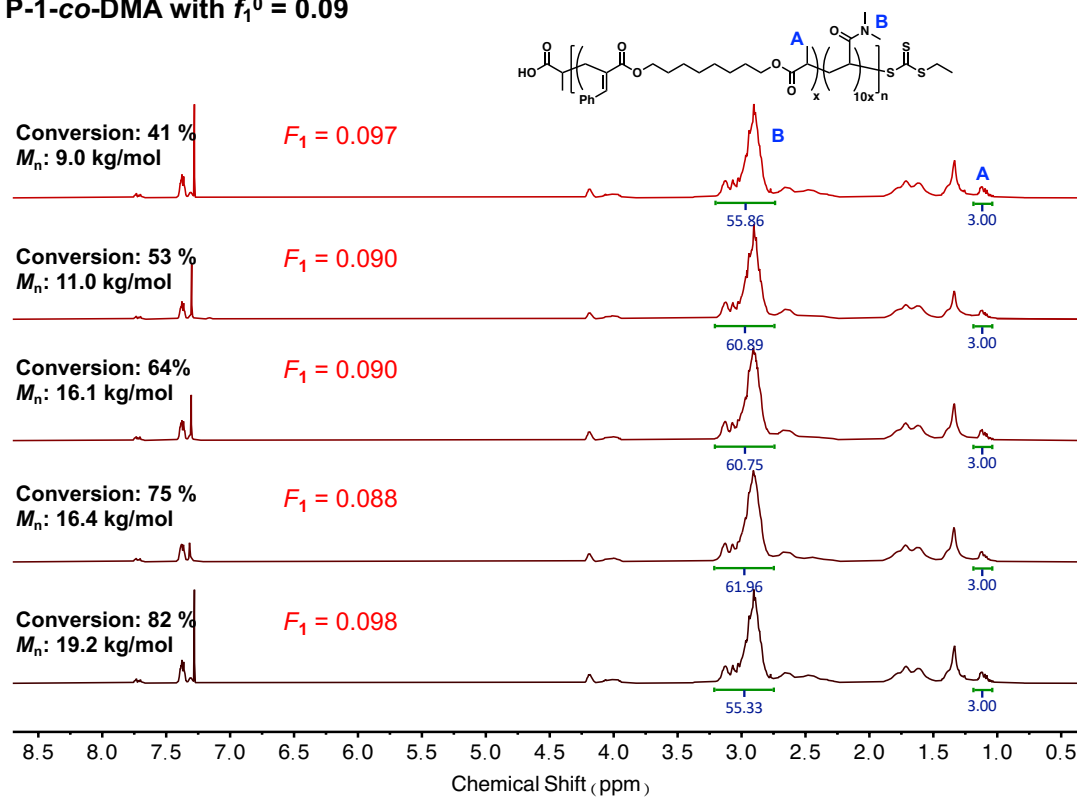


**Figure 2.19.** Compositional analysis of copolymers **P-1-co-DMA** at  $f_1^0 = 0.09$  at different time points of the reaction by <sup>1</sup>H NMR spectroscopy.



**P-1-co-NAM with  $f_1^0 = 0.09$**

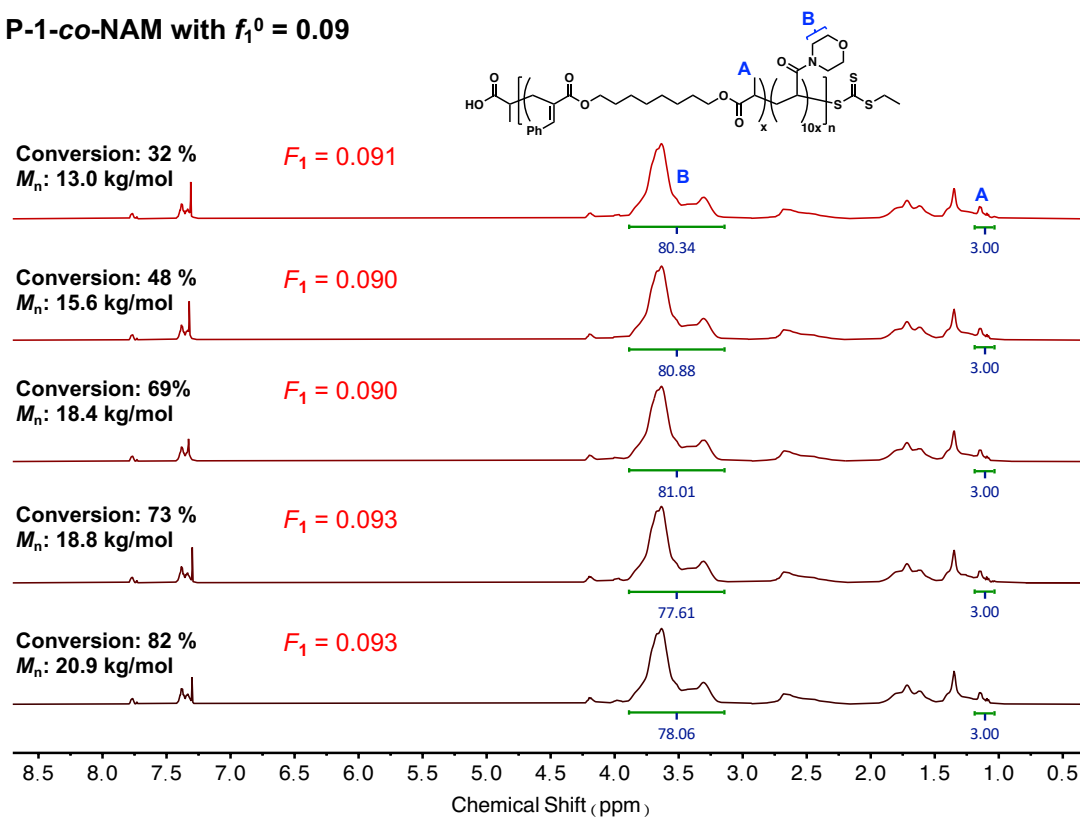


**Figure 2.21.** Compositional analysis of copolymers **P-1-co-NAM** at  $f_1^0 = 0.09$  at different time points of the reaction by  $^1\text{H}$  NMR spectroscopy.

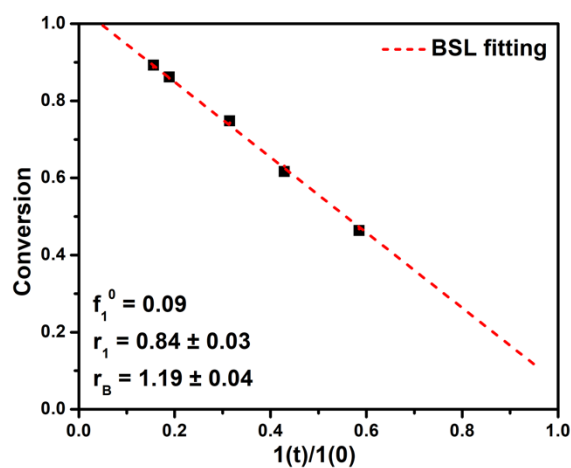


**Figure 2.22.** Plot of total conversion with respect to  $[\mathbf{1}(t)]/[\mathbf{1}(0)]$  is fitted to the BSL model to derive the comonomer reactivity ratios for copolymerization of **1** and BnA at  $f_1^0 = 0.09$  at 25 °C.

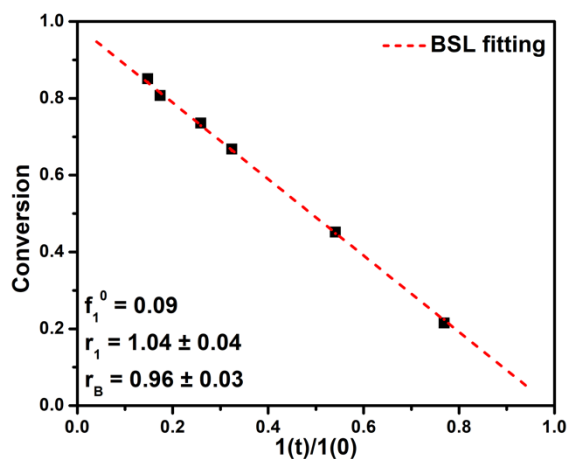


**Figure 2.23.** Plot of total conversion with respect to  $[1(t)]/[1(0)]$  is fitted to the BSL model to derive the comonomer reactivity ratios for copolymerization of **1** and *t*BA at  $f_1^0 = 0.09$  at 25 °C.

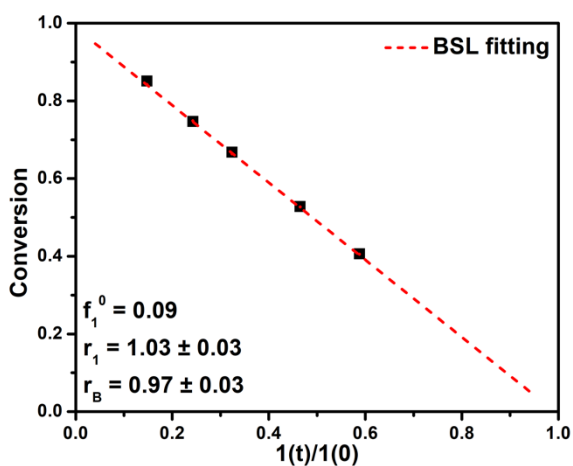


**Figure 2.24.** Plot of total conversion with respect to  $[1(t)]/[1(0)]$  is fitted to the BSL model to derive the comonomer reactivity ratios for copolymerization of **1** and DMA at  $f_1^0 = 0.09$  at 25 °C.

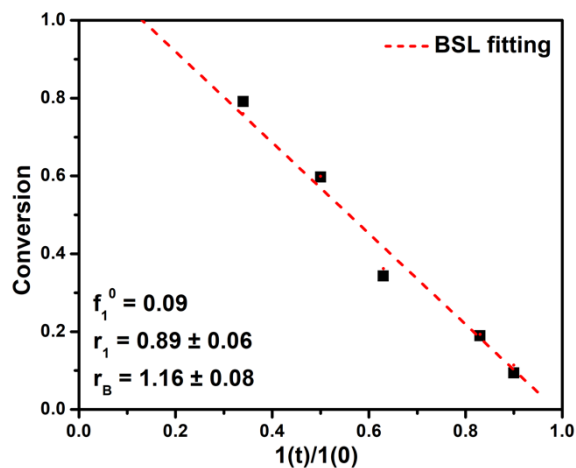


**Figure 2.25.** Plot of total conversion with respect to  $[1(t)]/[1(0)]$  is fitted to the BSL model to derive the comonomer reactivity ratios for copolymerization of **1** and DEA at  $f_1^0 = 0.09$  at 25 °C.

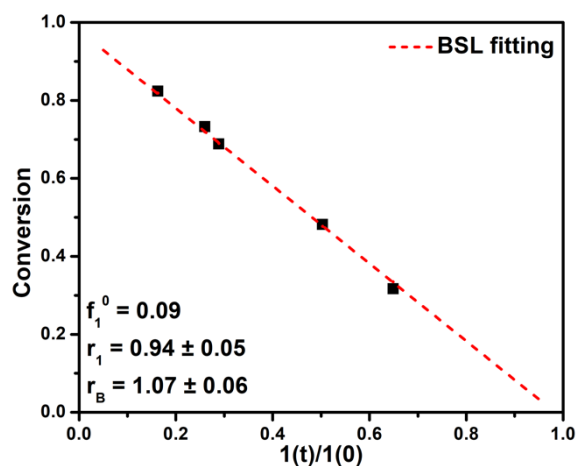


**Figure 2.26.** Plot of total conversion with respect to  $[1(t)]/[1(0)]$  is fitted to the BSL model to derive the comonomer reactivity ratios for copolymerization of **1** and NAM at  $f_1^0 = 0.09$  at 25 °C.

As acrylates and *N,N*-dialkylacrylamides have been shown to exhibit similar reactivities in radical copolymerization,<sup>63-64</sup> our results further indicate that the

macrocyclic allylic sulfone, which is designed to resemble acrylates in radical propagation, also possesses a similar reactivity to these two monomer classes.

To investigate how degradability is influenced by the composition and distribution of degradable building blocks in the copolymers, the copolymers were treated with sodium methoxide to cleave the main-chain esters. SEC analysis of degradation of copolymer **P-1-co-MA** prepared by photocontrolled rROCCP ( $F_1^{(\text{end})} = 0.10$ ,  $M_n^{(\text{SEC})} = 19.2$  kg/mol, and  $D = 1.27$ ) exhibited a dramatic molecular weight reduction, resulting in oligomers with  $M_n^{(\text{SEC})}$  of 1.3 kg/mol and  $D$  of 1.33 (Table 2.8, entry 2 & Figure 2.27A). In contrast, degradation of the copolymer with a similar overall composition ( $F_1^{(\text{end})} = 0.08$ ,  $M_n^{(\text{SEC})} = 16.4$  kg/mol, and  $D = 1.52$ ) generated by thermally initiated copolymerization produced fragments with higher  $M_n$  and  $D$  ( $M_n^{(\text{SEC})} = 7.3$  kg/mol,  $D = 1.98$ ) (Figure 2.27A).

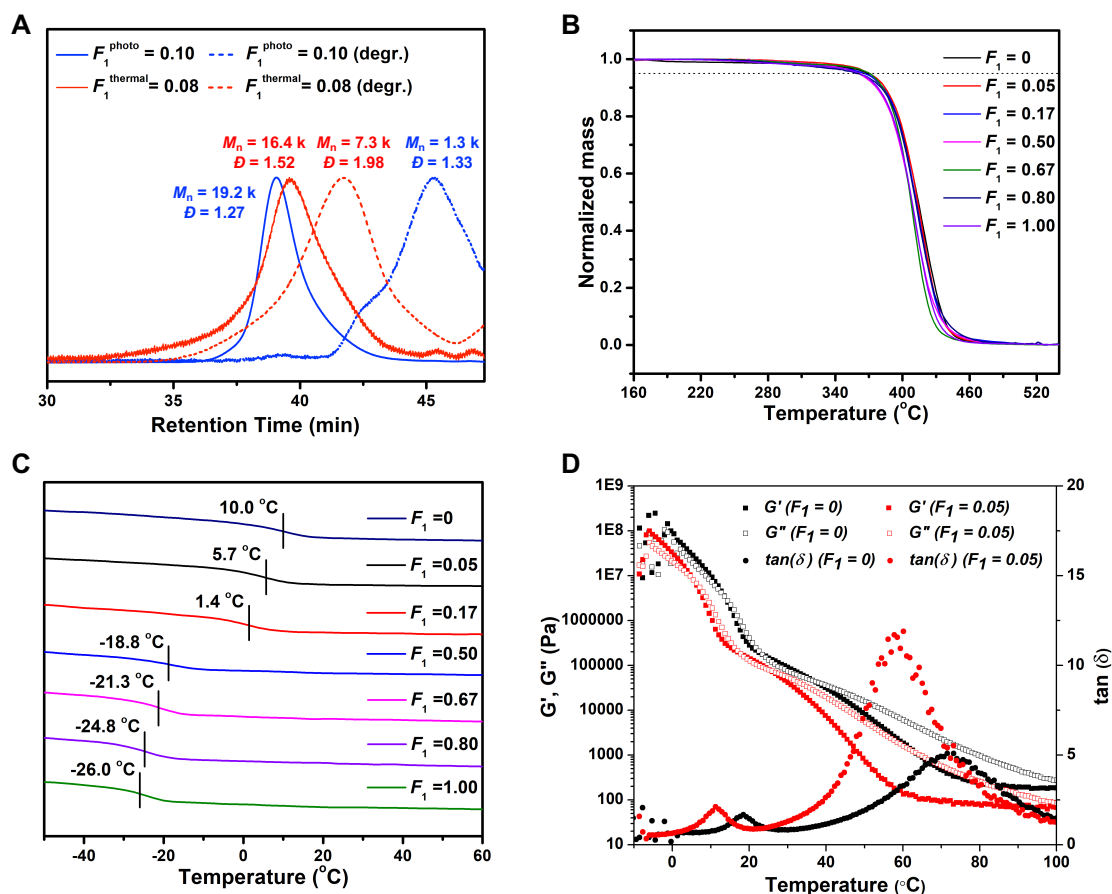


**Figure 2.27.** Material properties of degradable vinyl random copolymers prepared by photocontrolled rROCCP. (A) Degradation of **P-1-co-MA** generated by photocontrolled copolymerization ( $F_1^{\text{(end)}} = 0.10$ ) and thermally initiated radical copolymerization ( $F_1^{\text{(end)}} = 0.08$ ) respectively. (B)  $T_d$  of copolymers **P-1-co-MA** with different compositions demonstrated similar thermal stability with PMA. (C)  $T_g$  of copolymers **P-1-co-MA** could be fine-tuned by the initial comonomer feed composition. (D) Storage moduli, loss moduli, and  $\tan(\delta)$  for PMA and **P-1-co-MA** ( $F_1^{\text{(end)}} = 0.05$ ) were obtained from rheological measurements.

Furthermore, the degradation of copolymers with different comonomer compositions generated by photocontrolled rROCCP consistently produced fragments with low  $M_n$  and narrow molecular weight distributions (Table 2.8). These results indicated that while the thermally initiated copolymerization yielded a gradient copolymer that could only be partially degraded, copolymers generated by photocontrolled rROCCP possessed even and tunable distributions of the main-chain degradable functionalities that could be degraded efficiently into low molecular weight fragments.

The thermal properties of the copolymers were evaluated by thermogravimetry (TGA) and differential scanning calorimetry (DSC) analyses. Copolymers **P-1-co-MA** with main-chain degradable functionalities at different copolymer compositions exhibited a thermal stability comparable to that of poly(methyl acrylate) (PMA) with a 5% weight loss decomposition temperature ( $T_d$ ) between 363-368 °C (Figure 2.27B). Furthermore, the glass transition temperature ( $T_g$ ) of **P-1-co-MA** can be fine-tuned by the initial comonomer feed composition in the copolymerization, highlighting the potential utility of this method in generating degradable vinyl polymers with tailor-made material properties (Figure 2.27C). The thermomechanical properties of **P-1-co-MA** ( $F_1^{(end)} = 0.05$ ) and PMA were further studied using temperature sweep measurements with a parallel plate rheometer. The  $T_g$ s measured from the storage moduli ( $G'$ ) for **P-1-co-MA** and PMA were 4.6 °C and 13 °C (Figure 2.27 D), respectively, which agree well with the DSC analyses. Furthermore, the onset of the terminal region for **P-1-co-MA** was 31.5 °C, while the value for PMA was 41.2 °C. Similar to the effect on  $T_g$ , the incorporation of 5% of **1** only resulted in minimal impacts on the mechanical properties of the polymer; the  $G'$  at the onset of the rubbery plateau was ~0.4 MPa for PMA and 0.3 MPa for **P-1-co-MA**. Compared to PMA, the

slightly larger  $\tan(\delta)$  peaks for **P-1-co-MA** during the glass transition and the transition to the terminal region indicate slightly higher viscous responses to deformation.

## 2.4 Degradable nanostructures through polymerization-induced self-assembly

Degradable nanostructures are of great interest for their potential applications in drug delivery and self-healing materials.<sup>65</sup> The excellent control over PET-RAFT homopolymerization of the macrocyclic allylic sulfone and its ability to undergo chain extension created a unique opportunity to generate block copolymer nanostructures. In particular, we are interested in exploring the formation of degradable nanostructures via polymerization-induced self-assembly (PISA), an emerging approach to complex nanostructures without the requirement for post-polymerization processing.<sup>66</sup> In 2016, Zhang et al. reported a **mPEG<sub>100</sub>-b-PtBA** diblock copolymer that could undergo PISA in a thermally initiated RAFT polymerization.<sup>67</sup> Inspired by this work, we envisioned that a triblock copolymer **mPEG<sub>100</sub>-b-P-1-b-PtBA**, in which a short degradable **P-1** middle block was inserted into the previously reported **mPEG<sub>100</sub>-b-PtBA** diblock copolymer, could lead to the formation of degradable nanostructures via PISA, as the short degradable middle block would likely not affect the strong phase separation between the mPEG block and the PtBA block (Figure 2.28A).

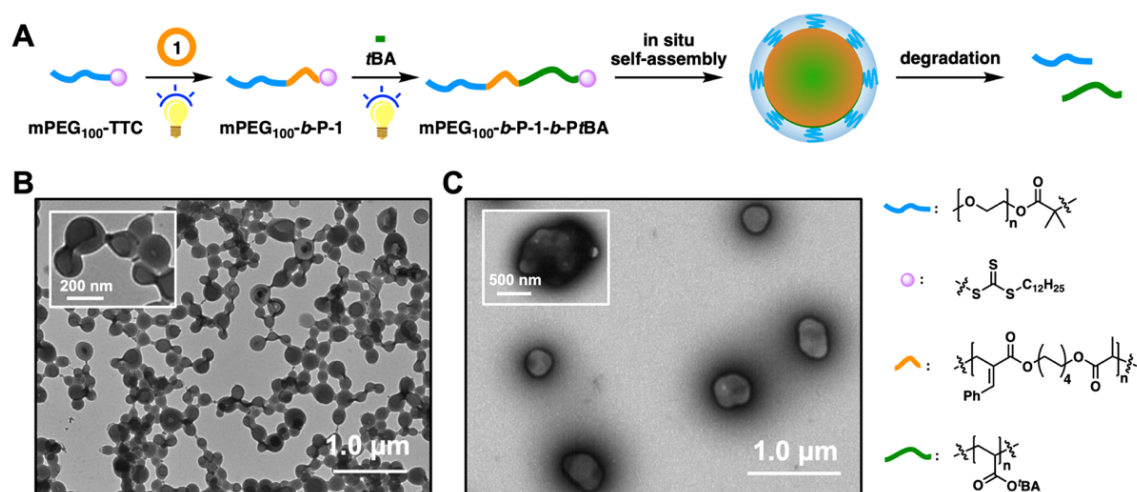


**Figure 2.28.** Generation of degradable nanoparticles via PISA. (A) Scheme of the triblock copolymer nanoparticle synthesis and degradation. (B) TEM image of the nanoparticles formed via PISA. (C) TEM image of the nanoparticles after NaOH treatment at 50 °C. The large aggregates are the insoluble  $Pt\text{BA}$  fragments after nanoparticle degradation.

To this end, a macroCTA, trithiocarbonate-terminated poly(ethylene glycol) monomethyl ether ( $m\text{PEG}_{100}\text{-TTC}$ ,  $M_n^{(\text{SEC})} = 4.7 \text{ kg/mol}$ ,  $D = 1.14$ ), was first extended by macrocyclic monomer **1** at a monomer/CTA ratio of 10:1, to generate a soluble diblock  $m\text{PEG}_{100}\text{-}b\text{-P-1}$  copolymer with a short **P-1** block ( $M_n^{(\text{SEC})} = 10.4 \text{ kg/mol}$ ,  $D = 1.16$ ). The diblock copolymer was further extended by  $t\text{BA}$  at a ratio of  $t\text{BA}/\text{CTA} = 500:1$  using PEG400 as a solvent to induce PISA. SEC analysis of the triblock copolymer clearly showed a shift to the higher molecular weight region after each chain extension (Figure 2.29-2.30).

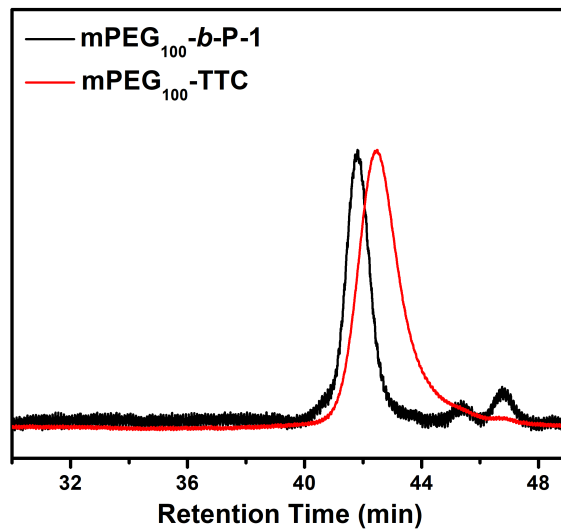


**Figure 2.29.** SEC analysis of diblock copolymer  $\text{mPEG}_{100}\text{-}b\text{-P-1}$ .

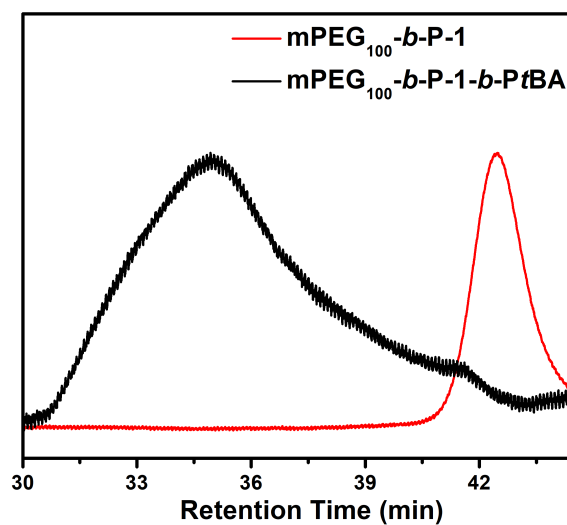


**Figure 2.30.** SEC analysis of nanoparticle  $\text{mPEG}_{100}\text{-}b\text{-P-1-}b\text{-PtBA}$ . The broad dispersity of the final *PtBA* block is likely caused by the aggregation of the triblock copolymer as it was being formed.

Well-defined nanoparticles with diameters ranging from 100 to 200 nm were observed by transmission electron microscopy (TEM) (Figure 2.28B). Interestingly, these nanoparticles

were found to be resistant to hydrolytic degradation in a 2.5 M sodium hydroxide (NaOH) aqueous solution at room temperature. We reasoned that the short base-labile **P-1** block was buried within the hydrophobic *Pt*BA core due to its hydrophobicity and, consequently, was protected from the base. We hypothesized that elevating the temperature could facilitate the degradation due to the increased permeability of the hydrophilic shell. Indeed, the nanoparticle disintegrated after exposure to 2.5 M NaOH at 50 °C (Figure 2.28C). SEC analysis also confirmed the degradation of the **P-1** middle block and the formation of two independent fragments after treatment with NaOH at 50 °C (Figure 2.31).

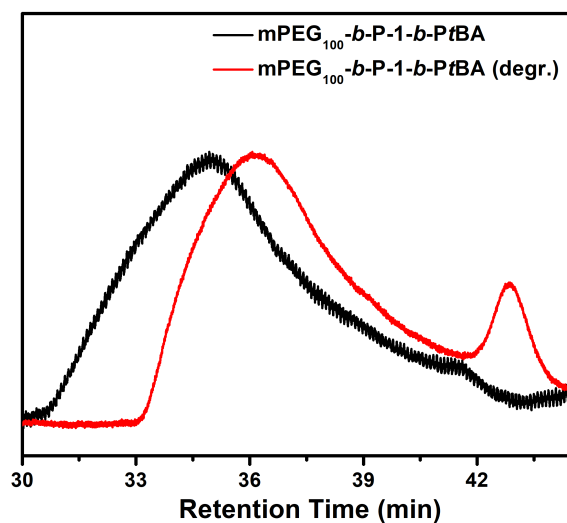


**Figure 2.31.** Degradation of nanoparticle  $m\text{PEG}_{100}\text{-}b\text{-P-1-}b\text{-PtBA}$ . The two peaks in the SEC trace of the degraded copolymer correspond to the *Pt*BA and mPEG fragments, respectively.

## 2.5 Understanding the unusual kinetic behavior

Our studies have shown that while PET-RAFT homopolymerization and copolymerization (Figure 2.2 & Figure 2.32-2.39) involving macrocyclic allylic sulfones deviated from first-order kinetics, the polymerization remained well-controlled.

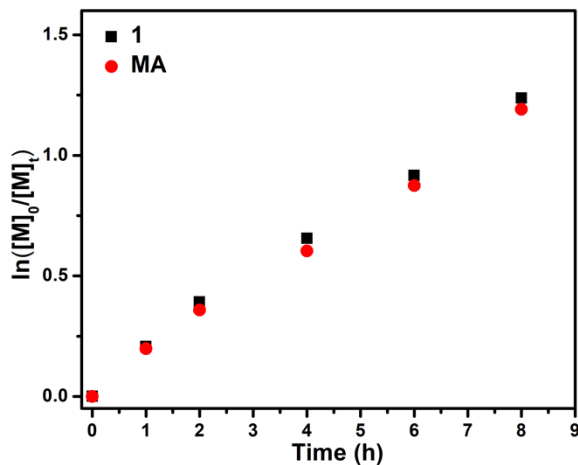


**Figure 2.32.** Kinetics of photocontrolled rROCCP of **1** and MA at  $f_1^0 = 0.09$  at 25 °C.

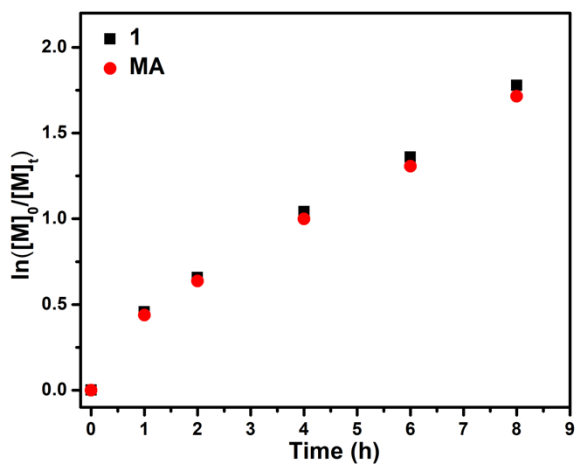


**Figure 2.33.** Kinetics of photocontrolled rROCCP of **1** and MA at  $f_1^0 = 0.17$  at 25 °C.

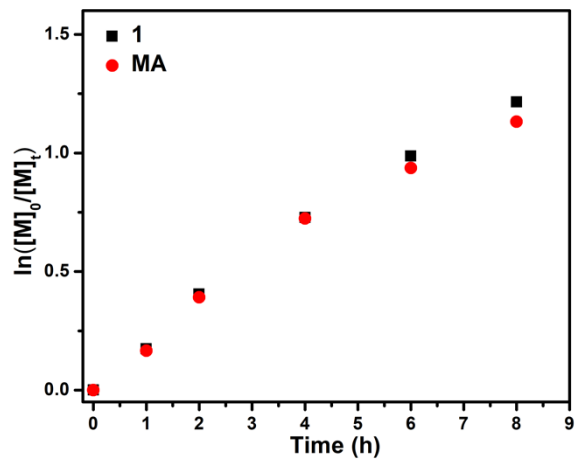


**Figure 2.34.** Kinetics of photocontrolled rROCCP of **1** and MA at  $f_1^0 = 0.50$  at 25 °C.

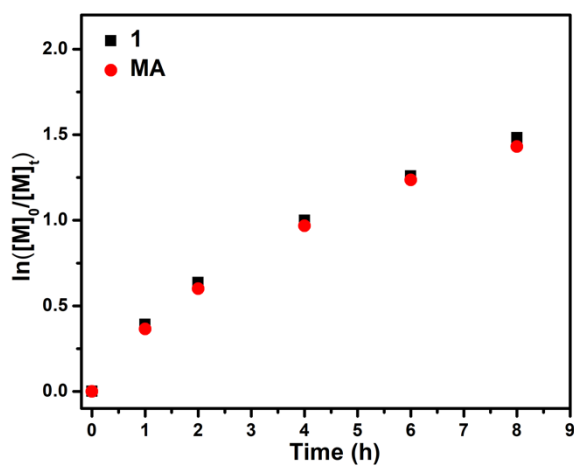


**Figure 2.35.** Kinetics of photocontrolled rROCCP of **1** and MA at  $f_1^0 = 0.67$  at 25 °C.

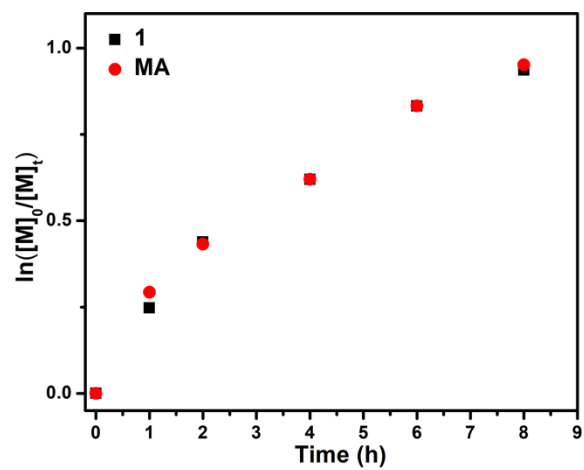


**Figure 2.36.** Kinetics of photocontrolled rROCCP of **1** and MA at  $f_1^0 = 0.80$  at 25 °C.

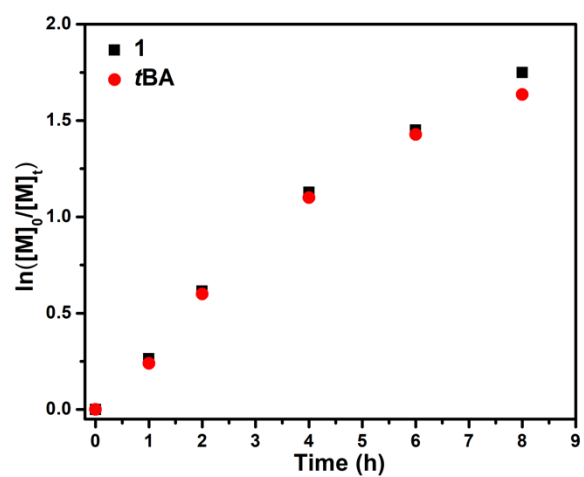


**Figure 2.37.** Kinetics of photocontrolled rROCCP of **1** and *t*BA at  $f_1^0 = 0.09$  at 25 °C.

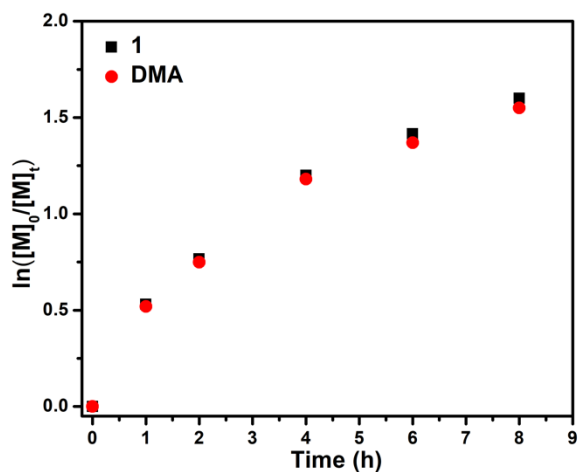


**Figure 2.38.** Kinetics of photocontrolled rROCCP of **1** and DMA at  $f_1^0 = 0.09$  at 25 °C.

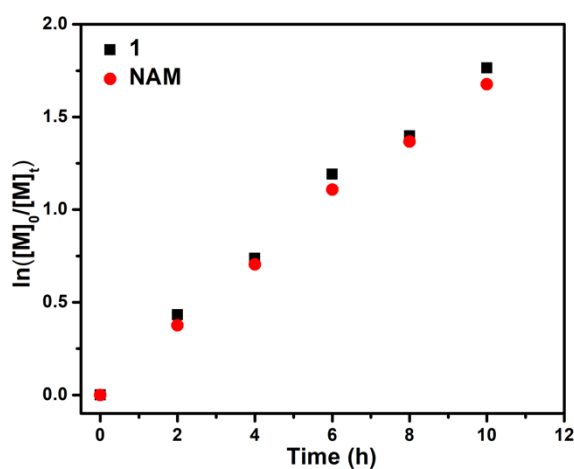


**Figure 2.39.** Kinetics of photocontrolled rROCCP of **1** and NAM at  $f_1^0 = 0.09$  at 25 °C.

This phenomenon was in stark contrast to traditional controlled polymerization in which the deviation from first-order kinetics is usually a sign of loss of control, suggesting an unusual kinetic behavior that warranted further investigation. Furthermore, the near-unity reactivity ratios of the comonomers during photocontrolled rROCCP at lower temperatures also differ from some conventional radical copolymerization systems, in which comonomer reactivity ratios move further away from unity when temperature decreases.<sup>33</sup>

We suspected that the *in situ* generated SO<sub>2</sub> during the radical cascade process affected the reaction kinetics and comonomer reactivities in the copolymerization (Figure 2.40A).<sup>68-70</sup>

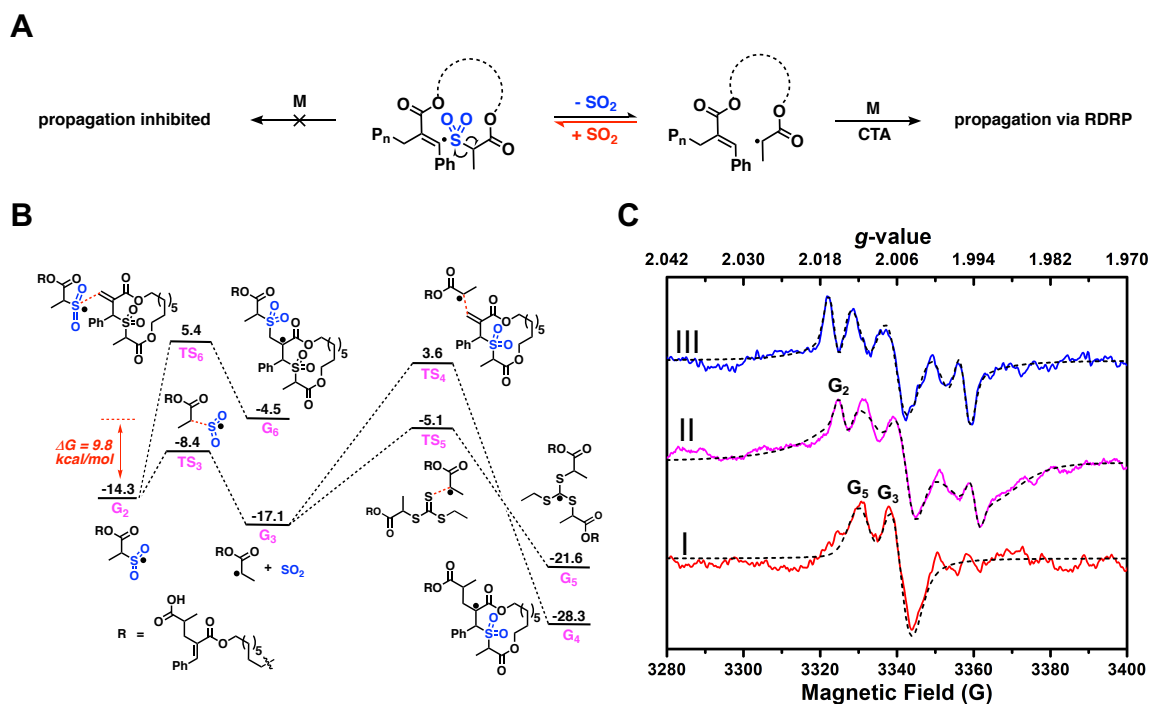


**Figure 2.40.** Mechanistic investigation of the cascade process of the polymerization of the macrocyclic allylic sulfone. (A) SO<sub>2</sub> is hypothesized to inhibit chain propagation by recombining with the propagating radical. **M** denotes monomers. (B) DFT calculations. All geometry optimizations and frequency calculations were carried out employing the B3LYP/6-31G(d) method and the SMD solvation model in DMF. Single-point energies were calculated using the M06-2X/6-311++G(d,p) method and the SMD solvation model in DMF. (C) EPR studies of the polymerization of the macrocyclic allylic sulfone. The experimental results are shown as solid lines. The simulated EPR spectra based on the hypothesized composition of the reaction mixture at different stages of the reaction are shown as dotted lines. The experimental EPR spectra are well aligned with the simulated

ones. Spectrum I: Early stage of polymerization (first two hours). Spectrum II: Late stage of polymerization (after five hours). Spectrum III: Injection of exogenous SO<sub>2</sub> at the early stage of polymerization.

To investigate the aforementioned hypothesis, Density Functional Theory (DFT) calculations were carried out by the use of the M06-2X/6-311++G(d,p)//B3LYP/6-31G(d) method in conjunction with the Solvation Model based on Density (SMD) simulating the effect from DMF to compute a plausible potential energy surface of the cascade process in the polymerization of the macrocyclic allylic sulfone (Figure 2.40B).<sup>71</sup> Our calculations showed that the  $\alpha$ -scission/SO<sub>2</sub> extrusion step (G<sub>2</sub> to G<sub>3</sub>) has a low energy barrier of 5.9 kcal/mol and that the transformation is exergonic by 2.8 kcal/mol. The low activation energy and relatively small change in Gibbs free energy indicate that this step is likely reversible. The DFT calculations also suggest that G<sub>3</sub>, with the lowest energy in the whole cascade process, exists at a high enough concentration during steady-state conditions, making it a plausible intermediate for chain propagation (Figure 2.41).

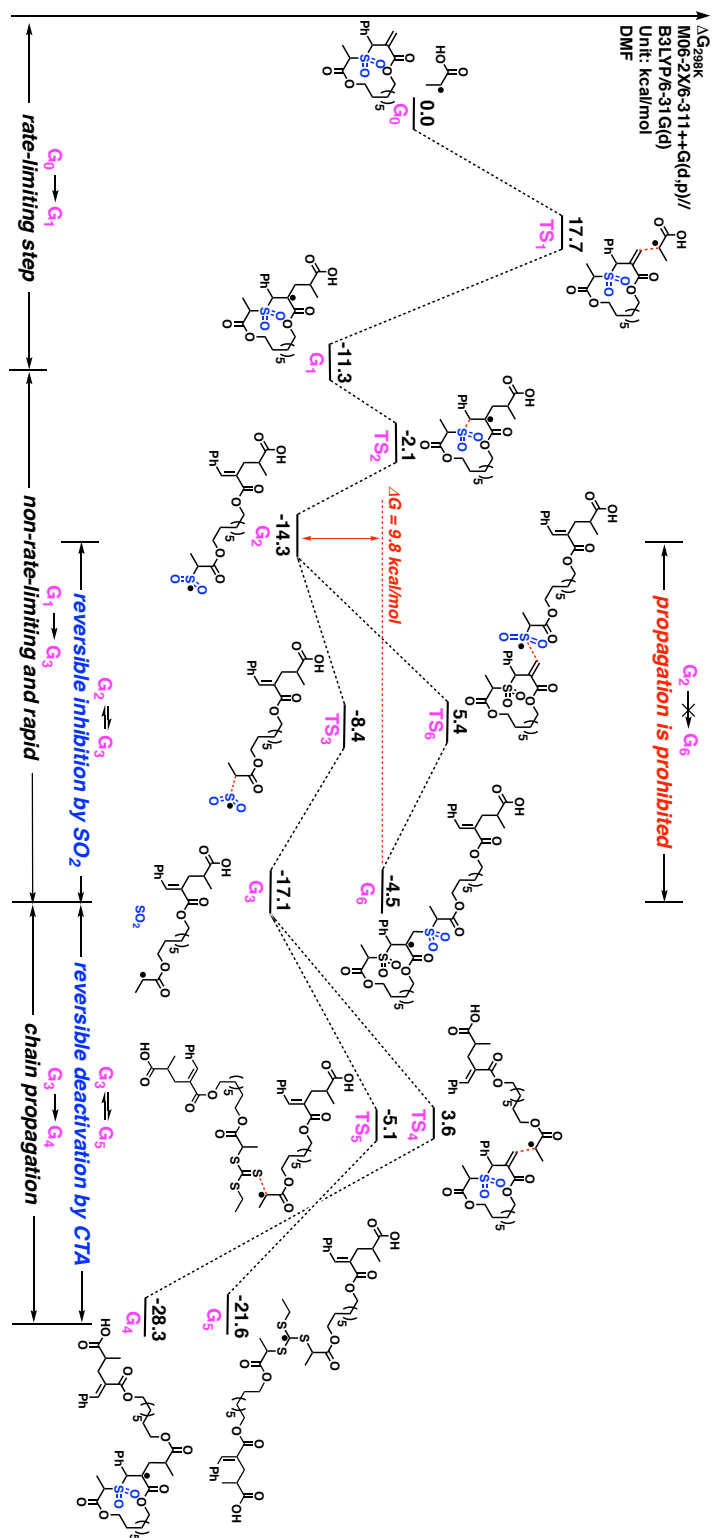


**Figure 2.41.** Mechanistic investigation of the cascade process of the polymerization of the macrocyclic allylic sulfone by DFT calculations.

Compared to chain propagation ( $G_3$ -TS<sub>4</sub>- $G_4$ , with an energy barrier of 20.7 kcal/mol), two alternative reaction pathways of  $G_3$  with lower energy barriers are the reversible addition by the CTA ( $G_3$ -TS<sub>5</sub>- $G_5$ , with an energy barrier of 12.0 kcal/mol) or  $SO_2$  ( $G_3$ -TS<sub>3</sub>- $G_2$ , with an energy barrier of 8.7 kcal/mol). While the former serves as the reversible deactivation of chain propagation to achieve controlled polymerization, the latter is a reverse reaction of the  $\alpha$ -scission/ $SO_2$  extrusion step and regenerates the sulfonyl radical  $G_2$ . Because of a high energy barrier of 19.7 kcal/mol and being endergonic by 9.8 kcal/mol, chain propagation of  $G_2$  by the monomer ( $G_2$ -TS<sub>6</sub>- $G_6$ ) is prohibited thermodynamically and kinetically. These results indicate that excess  $SO_2$  in the reaction could indeed recombine with the propagating alkyl radical to regenerate the sulfonyl radical and inhibit chain propagation.

To provide further evidence of the presence and accumulation of the sulfonyl radical over the course of the reaction, we employed electron paramagnetic resonance (EPR) to monitor the evolution of radical species in the reaction *in situ* (Figure 2.40C). In the early stage (initial two hours) of the reaction, the EPR spectrum only consisted of signals corresponding to the alkyl radical  $G_3$  ( $g_0 = 2.004$ ) and the degenerative intermediate  $G_5$  ( $g_0 = 2.009$ ) (Spectrum I, Figure 2.40C). The  $g$ -values of the peaks and patterns of the spectrum are both consistent with the radical species generated in the radical polymerization of MA. The EPR spectrum gradually evolved as the polymerization proceeded. In the late stage (after five hours) of the reaction, a new peak with a  $g$ -value of 2.014 appeared in the EPR spectrum (Spectrum II, Figure 2.40C), which is consistent with the  $g$ -value of the sulfonyl radical  $G_2$  reported in the literature.<sup>72</sup> Furthermore, the simulated EPR spectra (dotted lines) based on the absence and presence of the sulfonyl radical in the reaction perfectly fit the

experimental data as shown in Spectrum I and II, respectively, confirming the proposed assignments. Notably, Spectrum II is also consistent with Spectrum III obtained after the exogenous SO<sub>2</sub> gas was introduced to the system at the early stage of the reaction (Figure 2.40C). Collectively, the DFT calculations and EPR analyses are consistent with the observed kinetic results, confirming that G<sub>2</sub>, G<sub>3</sub>, and G<sub>5</sub> (Figure 2.40B & 2.40C) are long-lived radical intermediates in the polymerization of the macrocyclic allylic sulfone and that the concentration of SO<sub>2</sub> could have a significant effect on the direction of the reaction. The inhibition of chain propagation by SO<sub>2</sub> also explains the favorable comonomer reactivity ratios in photocontrolled rROCCP at lower temperatures, as SO<sub>2</sub> likely retards the rate of incorporation of the macrocyclic allylic sulfone more than that of acrylates/acrylamides when the temperature decreases.

## 2.6 Overcoming the propagation inhibition by SO<sub>2</sub>

Based on the DFT calculations, we reasoned that the propagation inhibition by the *in situ* generated SO<sub>2</sub> may be reversible, given the low energy barrier of the process. This reversibility implies that the extrusion of SO<sub>2</sub> and the formation of the alkyl radical are favored at low SO<sub>2</sub> concentrations, whereas the recombination of SO<sub>2</sub> and the formation of the sulfonyl radical are favored at high SO<sub>2</sub> concentrations. Therefore, the propagation inhibition could be alleviated by removing SO<sub>2</sub> from the reaction. Indeed, we found that sparging the reaction mixture with argon (Ar) steadily increased the rate of PET-RAFT homopolymerization of **1** in the late stage of the reaction at 25 °C (Figure 2.42).

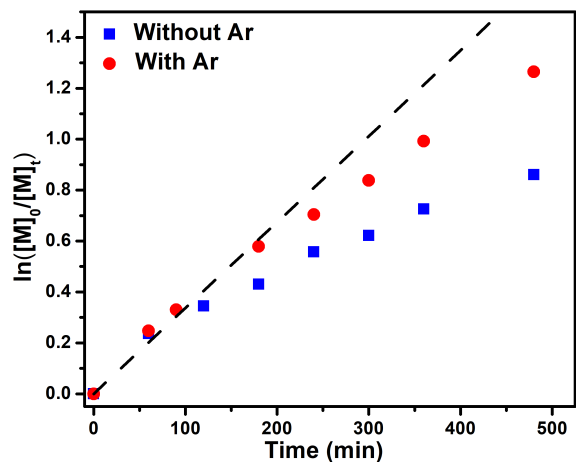


**Figure 2.42.** Kinetics of PET-RAFT homopolymerization of **1** at 25 °C with and without Ar.

In fact, both the SO<sub>2</sub> inhibition and reactivation of chain propagation by argon sparging were reversible, and the polymerization could be switched “on”/“off” by alternating the exogenous SO<sub>2</sub> and Ar introduced into the reaction vessel (Figure 2.43-2.44).

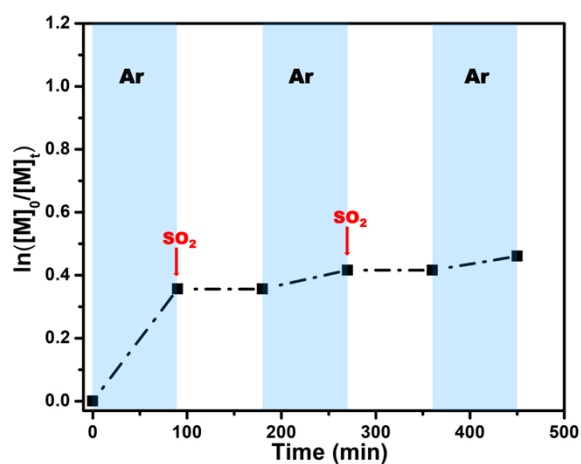


**Figure 2.43.** Alternating introduction of Ar and SO<sub>2</sub> gas to PET-RAFT homopolymerization of **1** at 25 °C.

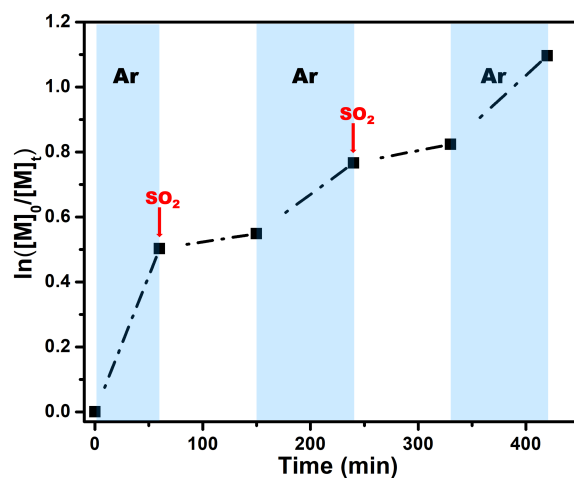


**Figure 2.44.** Alternating introduction of Ar and SO<sub>2</sub> gas to PET-RAFT homopolymerization of **1** at 50 °C.

Similarly, the propagation inhibition was also alleviated in the copolymerization of **1** and BnA ( $f_1^0 = 0.09$ ) by argon sparging at 25 °C (Figure 2.45).

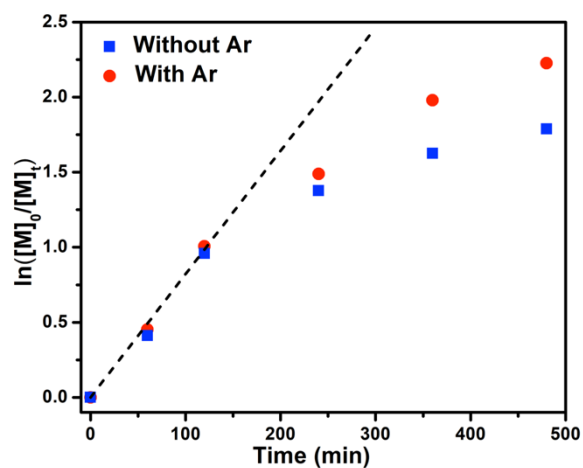


**Figure 2.45.** Kinetics of photocontrolled rROCCP of **1** and BnA at  $f_1^0 = 0.09$  at 25 °C with and without Ar.

Additionally, increasing the reaction temperature to 50 °C was also found to improve the rate of PET-RAFT homopolymerization of **1** in the late stage (Figure 2.46).

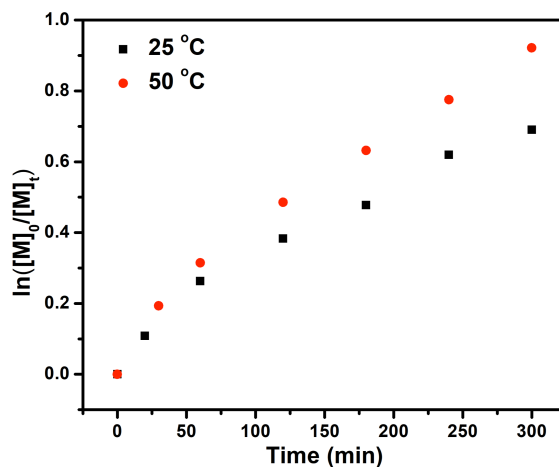


**Figure 2.46.** Kinetics of PET-RAFT homopolymerization of **1** at 25 °C and 50 °C in a sealed vial.

Combining Ar sparging and temperature elevation to 50 °C further improved the reaction kinetics of PET-RAFT homopolymerization of **1**, allowing it to remain pseudo-first order throughout the reaction (Figure 2.47-2.48).

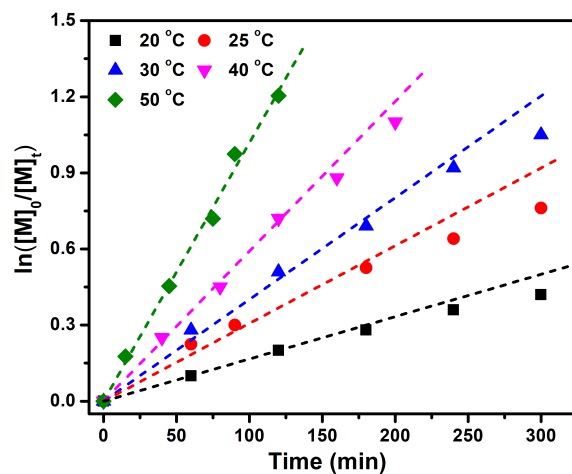


**Figure 2.47.** Kinetics of PET-RAFT homopolymerization of **1** under different temperatures with Ar bubbling.

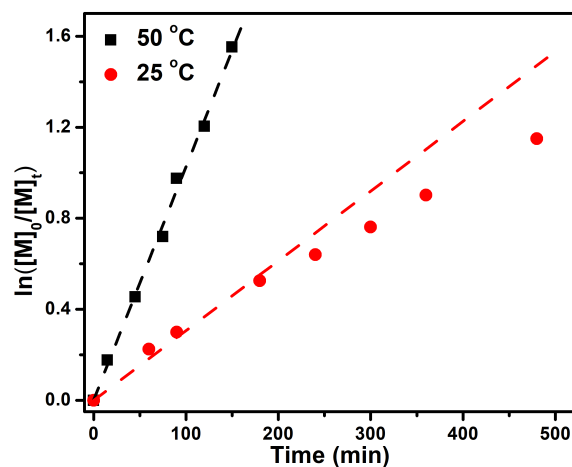


**Figure 2.48.** Pseudo-first-order kinetics were achieved in PET-RAFT homopolymerization of **1** by elevating the temperature to 50 °C plus argon sparging.

The rate of the copolymerization of **1** and MA was also improved when the reaction temperature was elevated to 50 °C (Figure 2.49), but a modest deviation of the comonomer reactivity ratios from unity was observed (Figure 2.50).

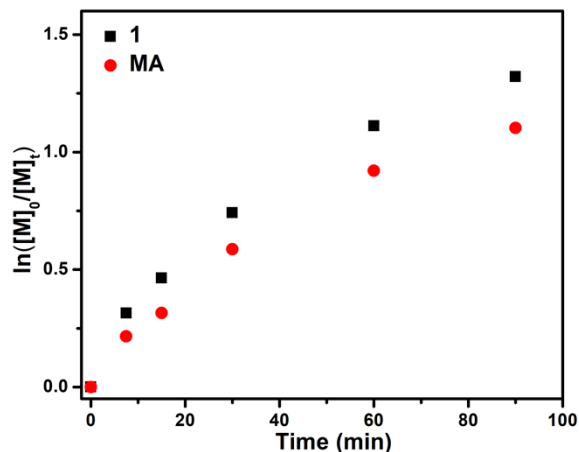


**Figure 2.49.** Kinetics of photocontrolled rROCCP of **1** with MA at  $f_1^0 = 0.09$  at 50 °C.

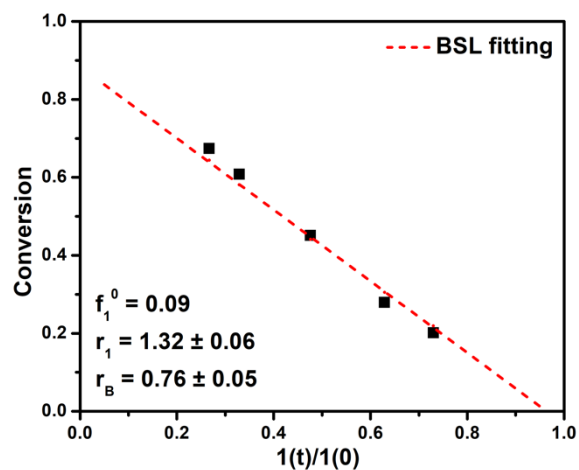


**Figure 2.50.** Plot of total conversion with respect to  $[1(t)]/[1(0)]$  is fitted to the BSL model to derive the comonomer reactivity ratios for copolymerization of **1** and MA at  $f_1^0 = 0.09$  at 50 °C. The result,  $r_1 = 1.32$  and  $r_B = 0.76$ , suggests that the resulting copolymer may have a gradient composition.

We reasoned that an alternative strategy to reduce the propagation inhibition by  $\text{SO}_2$  was to switch the solvent from DMF to dioxane, in which  $\text{SO}_2$  has lower solubility (Figure 2.51).

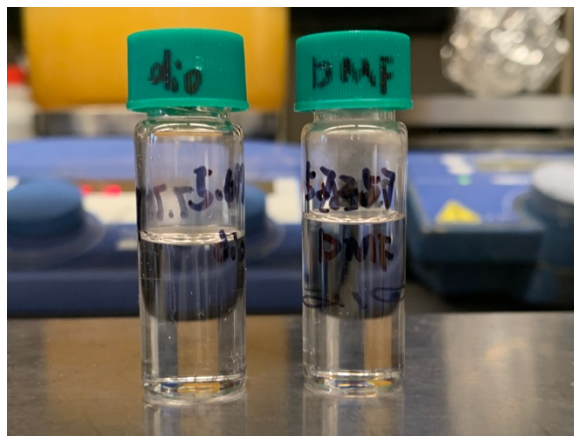


**Figure 2.51.** The solubility of SO<sub>2</sub> in DMF and dioxane was determined to be 0.69 g/mL and 0.43 g/mL, respectively. The solubility of SO<sub>2</sub> in each solvent was measured through mass difference before and after vigorously purging the solvent with SO<sub>2</sub> gas for 5 min.

Encouragingly, we found that the kinetics of the copolymerization of **1** and BnA at 25 °C remained pseudo-first order throughout the reaction when dioxane was used as the solvent (Figure 2.52).

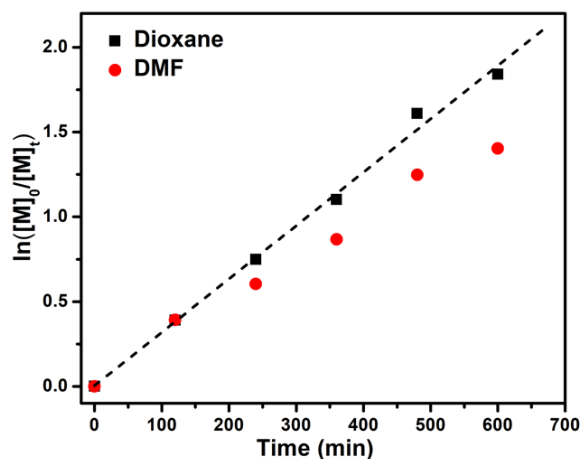


**Figure 2.52.** Photocontrolled rROCCP of **1** and BnA at  $f_1^0 = 0.09$  in dioxane remained pseudo-first order throughout the reaction.

## 2.7 Conclusion

A general approach to degradable vinyl random copolymers with tunable main-chain compositions through photocontrolled radical ring-opening cascade copolymerization (rROCCP) is presented in this article. Compared to existing rROP systems, photocontrolled rROCCP enabled the synthesis of degradable vinyl random copolymers with evenly distributed, tunable composition of main-chain labile groups at ambient temperature. These copolymers demonstrated readily tunable  $T_g$ s based on the composition and possess thermal and mechanical properties comparable to the corresponding nondegradable homopolymers when the composition of main-chain labile groups was kept low (e.g.,  $F_1^{(\text{end})} = 0.05$ ). Computational and EPR analyses revealed that the reversible inhibition of chain propagation by the *in situ* generated  $\text{SO}_2$  caused an unusual kinetic behavior that showed a deviation from first-order kinetics in the late stage of the reaction. Removal of  $\text{SO}_2$  was found to reverse the inhibition of chain propagation and improve the reaction kinetics in both the homopolymerization and the copolymerization involving the macrocyclic allylic sulfone. Taken together, excellent control and favorable comonomer reactivity ratios make photocontrolled rROCCP a powerful strategy for the preparation of degradable vinyl random copolymers with tunable main-chain compositions for a wide range of applications. In addition, the mechanistic insights into the reversible inhibition of chain propagation by  $\text{SO}_2$  shed light on using chemical cues to control radical chain-growth cascade polymerization systems.

## Experimental section

### Materials

Organic solvents, such as tetrahydrofuran (THF), dichloromethane (DCM), DMF, toluene, and dioxane, were purchased from Fisher Scientific and used after purification by a dry solvent system (Pure Process Technology). Dimethyl sulfoxide (DMSO) was purchased from Acros and used as received. Chain transfer agents were prepared according to the reported procedures.<sup>73</sup> Chemicals were purchased from Alfa Aesar, Sigma-Aldrich, Acros, Fisher Scientific, or TCI chemical companies and used as received without further purification. SO<sub>2</sub> gas was purchased from Sigma-Aldrich (>99.9%, #295698). Thin layer chromatography was performed on Merck TLC plates (silica gel 60 F254).

### Instrumentation and characterization

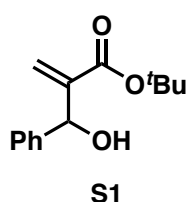
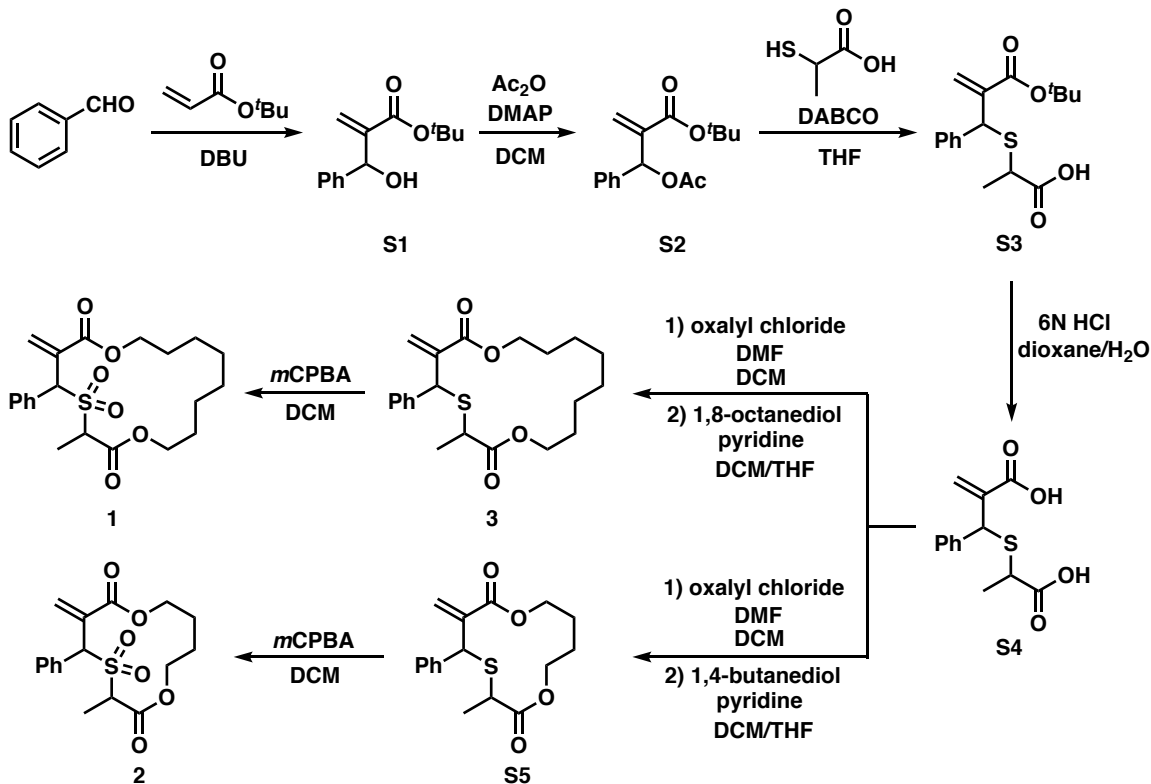
Photocontrolled polymerization was performed in a HepatoChem EvoluChem PhotoRedOx Box TC with EvoluChem LED spotlights (P201-18-2, 450 nm, 18W, light intensity = 34W/cm<sup>2</sup>) and circulated water heating/cooling (Figure 2.53). Silica gel chromatography was carried out using automated flash chromatography (Biotage). <sup>1</sup>H and <sup>13</sup>C NMR spectra were recorded in CDCl<sub>3</sub> on either a Varian Gemini-600 (600 MHz) or Varian Inova-500 (500 MHz) NMR spectrometer using residual chloroform ( $\delta = 7.26$  for <sup>1</sup>H NMR and  $\delta = 77.16$  for <sup>13</sup>C NMR) as internal standard. High-resolution mass spectrometry was performed on JEOL AccuTOF DART Micromass LCT ESI-MS. SEC measurements were performed on Tosoh's high-performance SEC system HLC-8320GPC with TSKgel Alpha-M columns at 50 °C and a flow rate of 0.6 mL/min. HPLC grade DMF with 0.01 M LiBr (anhydrous, purchased from Sigma-Aldrich) was used as the eluent.

Polystyrene standards (ReadyCal Kit, Sigma-Aldrich #81434) were used to determine the molecular weight and molecular weight distribution of polymers. The polymers were dissolved in the DMF solution with 0.01 M LiBr and filtered through a 0.20  $\mu\text{m}$  PTFE filter before being injected into the SEC system. Gel permeation chromatography (multi-angle light scattering detector) was performed on an Agilent GPC220 in THF at 40  $^{\circ}\text{C}$  with three PL gel columns (10  $\mu\text{m}$ ) in series. DSC measurements were performed on a Netzsch instrument DSC 214 Polyma for three heating cycles from -100  $^{\circ}\text{C}$  to 200  $^{\circ}\text{C}$  at a ramp of 10  $^{\circ}\text{C}/\text{min}$ . TGA measurements were performed on a Netzsch instrument STA 449 F1 Jupiter from room temperature to 600  $^{\circ}\text{C}$  at a ramp of 10  $^{\circ}\text{C}/\text{min}$ .



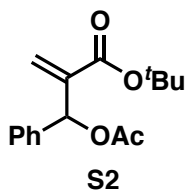
**Figure 2.53.** Experimental setup for photocontrolled polymerization.

**Scheme 2.1.** Synthesis of allylic sulfone macrocyclic monomer **1-2**.



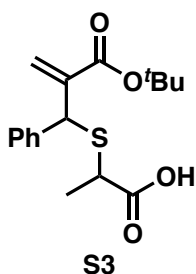
A slightly modified procedure was followed.<sup>31</sup> A mixture of benzaldehyde (53.1 g, 0.5 mol), *tert*-butyl acrylate (64.1 g, 0.5 mol), and 1,8-diazabicyclo[5.4.0]undec-7-ene (45.7 g, 0.3 mol) was allowed to stir at 25

°C for 100 hours. The mixture was then diluted with ethyl acetate (EA) (100.0 mL). The organic phase was washed with 3M HCl aqueous solution (3 x 100.0 mL), brine (50.0 mL), dried over Na<sub>2</sub>SO<sub>4</sub>, and concentrated *in vacuo*. The residue benzaldehyde and *tert*-butyl acrylate were distilled away under reduced pressure to give a yellow liquid **S1** (75.5 g, 322.2 mmol, 64.4% yield). <sup>1</sup>H NMR (500 MHz, CDCl<sub>3</sub>): δ 7.35-7.18 (m, 5H), 6.20 (s, 1H), 5.74 (s, 1H), 5.42 (d, *J* = 4.3 Hz, 1H), 3.58 (d, *J* = 4.7 Hz, 1H), 1.34 (s, 9H); <sup>13</sup>C NMR (125 MHz, CDCl<sub>3</sub>): δ 165.7, 143.8, 141.9, 128.4, 127.7, 126.9, 124.8, 81.5, 73.2, 28.0.



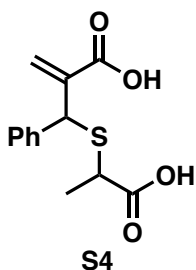
Acetic anhydride (31.9 g, 312.1 mmol) and *N,N*-dimethylaminopyridine (6.4 g, 52.0 mmol) were added to an ice-cooled solution of **S1** (60.9 g, 260.0 mmol) in DCM (100.0 mL). The reaction mixture was brought back

to 25 °C and stirred for 16 hours. The reaction mixture was washed with 1M HCl aqueous solution (3 x 50.0 mL), brine (50.0 mL), dried over Na<sub>2</sub>SO<sub>4</sub>, and concentrated *in vacuo*. The resulting residue was purified by silica gel chromatography to give a yellow liquid **S2** (71.9 g, 254.8 mmol, 98.0% yield). <sup>1</sup>H NMR (500 MHz, CDCl<sub>3</sub>): δ 7.38-7.27 (m, 5H), 6.64 (s, 1H), 6.32 (t, *J* = 1.1 Hz, 1H), 5.72 (t, *J* = 1.4 Hz, 1H), 2.10 (s, 3H), 1.37 (s, 9H); <sup>13</sup>C NMR (125 MHz, CDCl<sub>3</sub>): δ 169.5, 164.3, 141.2, 138.1, 128.4, 128.4, 127.9, 124.8, 81.5, 73.5, 28.0, 21.2.

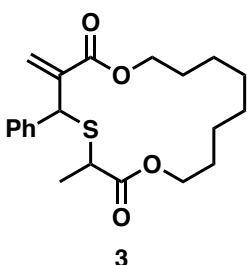


1,4-diazabicyclo[2.2.2]octane (36.7 g, 327.0 mmol) was added to a well-stirred solution of **S2** (75.3 g, 272.5 mmol) in THF (150.0 mL) at 25 °C for 60 minutes, followed by addition of 100.0 mL 2-mercaptopropionic acid (28.9 g, 272.5 mmol) and 1,4-diazabicyclo[2.2.2]octane (30.6 g,

272.5 mmol) THF solution. After stirring for 1 hour at 25 °C, the solvent was removed. It was then diluted with EA (100.0 mL), washed with 3M HCl aqueous solution (3 x 100.0 mL), brine (30.0 mL), dried by Na<sub>2</sub>SO<sub>4</sub>, and concentrated *in vacuo*. The resulting residue was purified by silica gel chromatography to afford a colorless oil **S3** (87.9 g, 245.3 mmol, 90.0% yield). <sup>1</sup>H NMR (500 MHz, CDCl<sub>3</sub>): δ 7.41 (d, *J* = 7.5 Hz, 2H), 7.28 (m, 3H), 6.33 (s, 1H), 5.85 (s, 1H), 5.27 (s, 1H), 3.14 (q, *J* = 7.2 Hz, 1H), 1.39 (s, 9H), 1.36 (d, *J* = 7.2 Hz, 3H); <sup>13</sup>C NMR (125 MHz, CDCl<sub>3</sub>): δ 179.1, 164.9, 141.9, 139.6, 128.7, 128.6, 127.6, 126.3, 81.6, 49.3, 40.9, 28.0, 16.8.

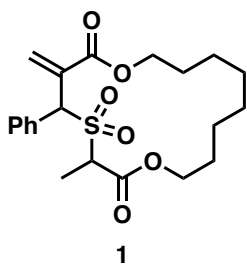


To a solution of **S3** (30.1 g, 93.4 mmol) in 1,4-dioxane (30.0 mL), 6N HCl aqueous solution (30.0 mL) was added. The reaction mixture was refluxed at 90 °C for 2 hours. After completion, the reaction mixture was cooled to 25 °C, diluted with water (100.0 mL), and extracted with EA (2 × 100.0 mL). The organic layer was washed with brine (3 x 100.0 mL), dried by Na<sub>2</sub>SO<sub>4</sub>, and concentrated *in vacuo* to give a white solid **S4** (22.5 g, 84.5 mmol, 90.5% yield). <sup>1</sup>H NMR (500 MHz, CDCl<sub>3</sub>): δ 7.48 (d, *J* = 7.7 Hz, 2H), 7.33 (m, 3H), 6.50 (s, 1H), 5.84 (s, 1H), 5.41 (s, 1H), 3.18 (q, *J* = 7.2 Hz, 1H), 1.35 (d, *J* = 7.2 Hz, 3H); <sup>13</sup>C NMR (125 MHz, CDCl<sub>3</sub>): δ 179.9, 171.5, 140.2, 139.1, 129.7, 128.8, 128.7, 127.9, 48.7, 41.3, 16.5.

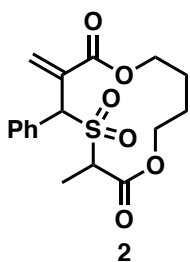


To the ice-cooled solution of **S4** (8.3 g, 31.0 mmol) in dry DCM (80.0 mL), oxalyl chloride (15.7 g, 123.9 mmol) was added dropwise, followed by the addition of five drops of DMF. The solution was left stirring at 25 °C for 2 hours. The solvent was then removed, and the remaining oil was immediately dissolved in dry DCM (40.0 mL) and transferred into a syringe. Then, 1,8-octanediol (4.5 g, 31.0 mmol) was dissolved in dry THF (30.0 mL) and dry DCM (10.0 mL) and transferred into another syringe. Both solutions were added via a syringe pump to a solution of pyridine (12.3 g, 154.9 mmol) in dry DCM (400.0 mL) over 120 minutes. After completion, the reaction mixture was left to stir for another 60 minutes, which was then concentrated, yielding brown pyridinium chloride salts. The residue was filtered, and the supernatant was diluted with DCM (50.0 mL) and washed with 1M HCl aqueous solution (3 x 100.0 mL). Subsequent concentration *in vacuo* and purification via

silica gel chromatography yielded a colorless oil **3** (2.8 g, 7.4 mmol, 23.9% yield).  $^1\text{H}$  NMR (500 MHz,  $\text{CDCl}_3$ ):  $\delta$  7.40 (d,  $J = 7.4$  Hz, 2H), 7.33 (t,  $J = 7.5$  Hz, 2H), 7.26 (t,  $J = 7.3$  Hz, 1H), 6.46 (s, 1H), 5.97 (s, 1H), 5.27 (s, 1H), 4.27-4.06 (m, 4H), 3.05 (q,  $J = 7.3$  Hz, 1H), 1.74-1.41 (m, 12H), 1.29 (d,  $J = 7.3$  Hz, 3H);  $^{13}\text{C}$  NMR (125 MHz,  $\text{CDCl}_3$ ):  $\delta$  173.9, 165.8, 140.9, 139.8, 128.7, 128.6, 127.8, 127.2, 65.8, 64.7, 49.4, 40.9, 28.3, 27.5, 26.9, 26.4, 24.6, 23.7, 17.2.



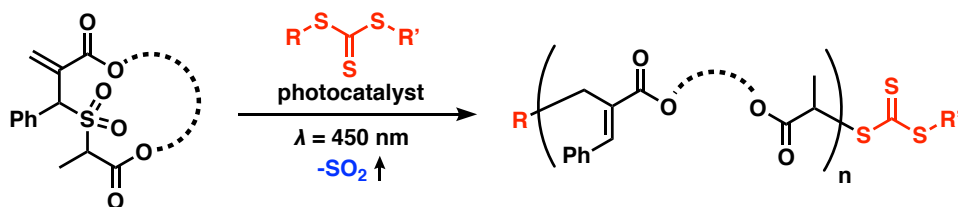
To the solution of **3** (2.8 g, 7.4 mmol) in DCM (50.0 mL) at 0 °C, 77 wt% *m*CPBA (5.0 g, 22.3 mmol) was added. The reaction mixture was brought back to 25 °C and stirred for 2 hours. After completion, the reaction mixture was filtered. The supernatant was collected, concentrated, and purified by silica gel chromatography to give a colorless oil (2.6 g, 6.4 mmol, 86.5% yield).  $^1\text{H}$  NMR (500 MHz,  $\text{CDCl}_3$ ):  $\delta$  7.65 (d,  $J = 7.8$  Hz, 2H), 7.46-7.36 (m, 3H), 6.76 (s, 1H), 6.55 (s, 1H), 6.11 (s, 1H), 4.44 (dt,  $J = 11.3, 5.8$  Hz, 1H), 4.32-4.20 (m, 3H), 3.88 (q,  $J = 7.4$  Hz, 1H), 1.81-1.35 (m, 15H);  $^{13}\text{C}$  NMR (125 MHz,  $\text{CDCl}_3$ ):  $\delta$  166.3, 165.4, 132.6, 132.5, 131.8, 130.3, 129.5, 129.3, 67.1, 66.0, 65.0, 59.5, 28.5, 28.2, 27.3, 26.5, 24.3, 23.7, 9.3.



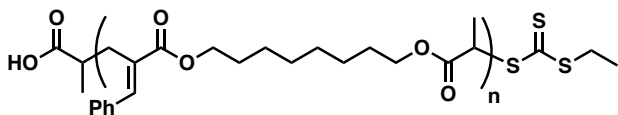
To the ice-cooled solution of **S4** (10.6 g, 39.7 mmol) in dry DCM (80.0 mL), oxalyl chloride (20.2 g, 158.9 mmol) was added dropwise, followed by the addition of five drops of DMF. The solution was left stirring at 25 °C for 2 hours. The solvent was then removed, and the remaining oil was immediately dissolved in dry DCM (40.0 mL) and transferred into a syringe. Then,

1,4-butanediol (3.6 g, 39.7 mmol) was dissolved in dry THF (30.0 mL) and dry DCM (10.0 mL) and transferred into another syringe. Both solutions were added via a syringe pump to a solution of pyridine (15.7 g, 198.6 mmol) in dry DCM (400.0 mL) over 120 minutes. After completion, the solution was left to stir for another 60 minutes, which was then concentrated, yielding brown pyridinium chloride salts. The residue was filtered, and the supernatant was diluted with DCM (50.0 mL) and washed with 1M HCl aqueous solution (3 x 100.0 mL). Subsequent concentration *in vacuo* and purification via silica gel chromatography yielded a colorless oil **S5**, which was directly subjected to oxidation. To the solution of **S5** (2.4 g, 7.4 mmol) in DCM (50.0 mL) at 0 °C, 77 wt% *m*CPBA (4.9 g, 22.1 mmol) was added. The reaction mixture was brought back to 25 °C and stirred for 2 hours. After completion, the reaction mixture was filtered. The supernatant was collected, concentrated, and purified by silica gel column chromatography to give a white solid **2** (2.2 g, 6.2 mmol, 15.6% total yield). <sup>1</sup>H NMR (500 MHz, CDCl<sub>3</sub>): δ 7.67-7.59 (m, 2H), 7.46-7.37 (m, 3H), 6.70 (s, 1H), 6.31 (s, 1H), 6.19 (s, 1H), 4.49-4.27 (m, 4H), 3.85 (q, *J* = 8.4, 7.8 Hz, 1H), 2.19-1.79 (m, 4H), 1.57 (d, *J* = 7.3 Hz, 3H); <sup>13</sup>C NMR (125 MHz, CDCl<sub>3</sub>): δ 166.8, 165.3, 132.9, 132.8, 131.1, 130.7, 129.5, 129.1, 67.0, 66.7, 66.0, 61.3, 25.8, 25.1, 10.2.

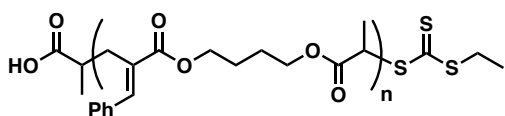
**Scheme 2.2.** General procedure of PET-RAFT homopolymerization of macrocyclic allylic sulfones and NMR data of their polymers.



All polymerization reactions were performed under argon in 4 mL glass vials equipped with TFE lined silicone SURE-LINK septa (Chemglass CG-4909-04) using a HepatoChem EvoluChem PhotoRedOx Box TC with EvoluChem LED spotlights (P201-18-2, 450 nm, 18W, light intensity = 34 W/cm<sup>2</sup>) and circulated water heating/cooling. The stock solution of allylic sulfone macrocyclic monomers **1** and **2**, CTAs, and photocatalysts was prepared and stored in a freezer. A typical procedure for PET-RAFT homopolymerization of macrocyclic allylic sulfones is given as follows. A 4 mL glass vial equipped with a stir bar was charged with allylic sulfone macrocyclic monomer (0.1 mmol), CTA (2.0 μmol), photocatalyst (20.0 nmol), and solvent (0.5 mL). The mixture was covered in aluminum foil and degassed with argon for 20 minutes. The mixture was then irradiated by a blue LED lamp (18 W,  $\lambda_{\text{max}} = 450 \text{ nm}$ , light intensity = 34 W/cm<sup>2</sup>) at 25 °C. The vial was exposed to air to stop the polymerization. The reaction mixture was diluted with DCM and precipitated in hexane three times. The resulting polymers were analyzed by <sup>1</sup>H NMR spectroscopy, <sup>13</sup>C NMR spectroscopy, and SEC.

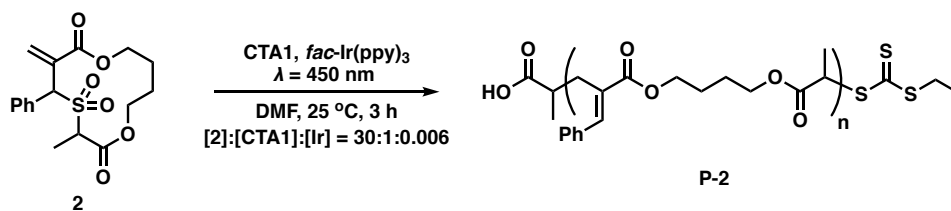


$^1\text{H}$  NMR (500 MHz,  $\text{CDCl}_3$ ):  $\delta$  7.73 (s, 1H), 7.40-7.28 (m, 5H), 4.19 (t,  $J = 6.7$  Hz, 2H), 4.02-3.89 (m, 2H), 2.95 (dd,  $J = 13.3, 6.6$  Hz, 1H), 2.83-2.67 (m, 2H), 1.70 (p,  $J = 6.8$  Hz, 2H), 1.60-1.48 (m, 2H), 1.44-1.24 (m, 8H), 1.08 (d,  $J = 6.8$  Hz, 3H).  $^{13}\text{C}$  NMR (125 MHz,  $\text{CDCl}_3$ ):  $\delta$  176.0, 168.2, 140.7, 135.6, 131.1, 129.3, 128.7, 128.6, 65.2, 64.6, 38.8, 31.0, 29.3, 29.3, 28.8, 28.7, 26.1, 26.0, 16.8.

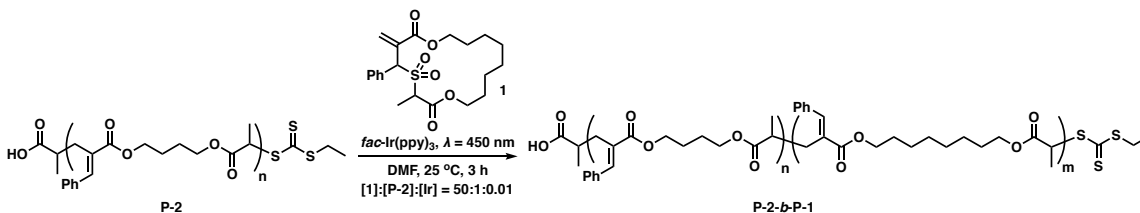


$^1\text{H}$  NMR (500 MHz,  $\text{CDCl}_3$ ):  $\delta$  7.72 (s, 1H), 7.40-7.28 (m, 5H), 4.24-4.15 (m, 2H), 4.06-3.96 (m, 2H), 2.96 (dt,  $J = 13.2, 5.8$  Hz, 1H), 2.82-2.67 (m, 2H), 1.82-1.62 (m, 4H), 1.08 (d,  $J = 6.8$  Hz, 3H).  $^{13}\text{C}$  NMR (125 MHz,  $\text{CDCl}_3$ ):  $\delta$  175.8, 168.0, 141.0, 135.5, 130.9, 129.3, 128.7, 128.7, 64.6, 64.0, 38.9, 31.0, 25.5, 25.5, 16.8.

**Scheme 2.3.** Procedure for synthesis of diblock copolymers **P-2-b-P-1** through photocontrolled cascade polymerization.



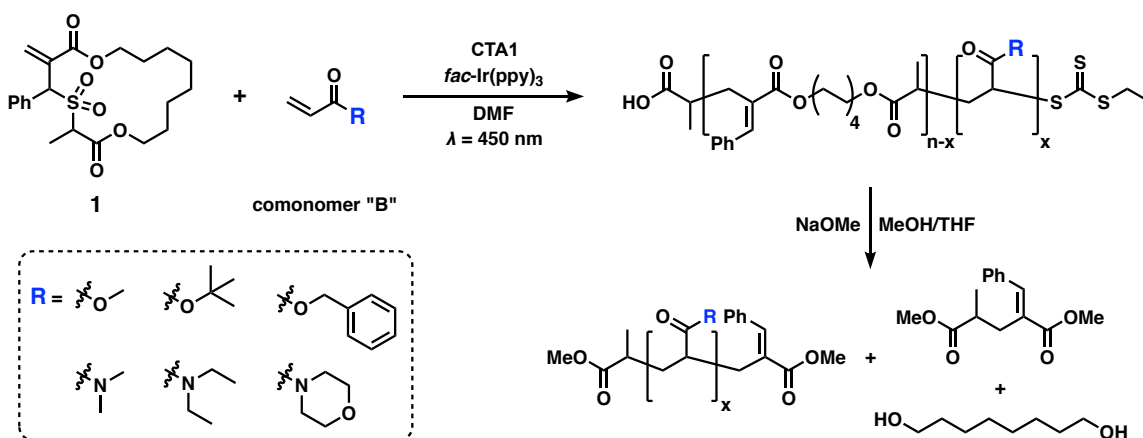
Following a general polymerization procedure, a 4 mL glass vial equipped with a stir bar was charged with allylic sulfone macrocyclic monomer **2** (0.1 mmol), **CTA1** (3.3  $\mu\text{mol}$ ), *fac*-[Ir(ppy)<sub>3</sub>] (20.0 nmol), and DMF (0.5 mL). The mixture was covered in aluminum foil and degassed with argon for 20 minutes. The mixture was then irradiated by a blue LED lamp (18 W,  $\lambda_{\text{max}} = 450 \text{ nm}$ , light intensity = 34 W/cm<sup>2</sup>) at 25 °C for 3 hours. The monomer conversion was monitored by <sup>1</sup>H NMR spectroscopy (46% monomer conversion). The vial was then exposed to air to stop the polymerization. The reaction mixture was diluted with DCM and precipitated in hexane three times. The resulting polymers were analyzed by <sup>1</sup>H NMR spectroscopy, <sup>13</sup>C NMR spectroscopy, and SEC.



A 4 mL glass vial equipped with a stir bar was charged with allylic sulfone macrocyclic monomer **1** (0.1 mmol), macroinitiator **P-2** (2.0  $\mu\text{mol}$ ), *fac*-[Ir(ppy)<sub>3</sub>] (20.0 nmol), and DMF (0.5 mL). The mixture was covered in aluminum foil and degassed with argon for 20 minutes. The mixture was then irradiated by a blue LED lamp (18 W,  $\lambda_{\text{max}} = 450 \text{ nm}$ , light

intensity = 34 W/cm<sup>2</sup>) at 25 °C for 5 hours. The monomer conversion was monitored by <sup>1</sup>H NMR spectroscopy (64% monomer conversion). The vial was then exposed to air to stop the polymerization. The reaction mixture was diluted with DCM and precipitated in hexane three times. The resulting polymers were analyzed by <sup>1</sup>H NMR spectroscopy, <sup>13</sup>C NMR spectroscopy, and SEC.

**Scheme 2.4.** Procedure for synthesis and degradation of random copolymers from photocontrolled rROCCP.



### Synthesis of degradable vinyl random copolymers

A typical procedure for photocontrolled rROCCP of the allylic sulfone macrocyclic monomer with acrylic comonomer is given as follows. A 4 mL glass vial equipped with a stir bar was charged with allylic sulfone macrocyclic monomer **1** (0.1 mmol), acrylic comonomer (1.0 mmol), CTA (2.0  $\mu$ mol), photocatalyst (20.0 nmol), and solvent (0.5 mL). The mixture was covered in aluminum foil and degassed with argon at 0 °C for 20 minutes. The mixture was then irradiated by a blue LED lamp (18 W,  $\lambda_{\text{max}} = 450 \text{ nm}$ , light intensity = 34 W/cm<sup>2</sup>) at 25 °C. The vial was exposed to air to stop the polymerization. The reaction

mixture was diluted with DCM and precipitated in hexane (80% MeOH/H<sub>2</sub>O (v/v) mixture for **P-1-co-tBA**) three times. The resulting polymers were analyzed by <sup>1</sup>H NMR spectroscopy and SEC.

### **Degradation of degradable vinyl random copolymers**

In a 4 mL glass vial equipped with a stir bar, 10.0 mg random copolymers were dissolved in 1.0 mL THF. A solution of sodium methoxide (20.0  $\mu$ L of a 25 wt% solution in methanol) was added, and the vial was capped. After 20 minutes, the reaction was stopped by the addition of a 1 M aqueous HCl solution (0.1 mL). To collect the degraded products for NMR and GPC analyses, the mixture was extracted with DCM (2 x 2.0 mL). The organic phase was dried with Na<sub>2</sub>SO<sub>4</sub> and concentrated *in vacuo*.

### **Determination of monomer conversion by <sup>1</sup>H NMR spectroscopy**

The monomer conversion for the polymerization of allylic sulfone macrocyclic monomer **1** was determined based on the assignment that the integral of the doublet at  $\delta = 1.09$  ppm (Peak *a*, Figure 2.54) corresponds to the methyl group of polymer **P-1** (3H), and the integral of the singlet at  $\delta = 6.53$  ppm (Peak *b*, Figure 2.54) corresponds to the terminal alkene of unreacted monomer **1** (1H). When the integral of Peak *a* is normalized, the monomer conversion  $\theta$  is calculated based on the following equation, where  $I_b$  is the integral of Peak *b*.

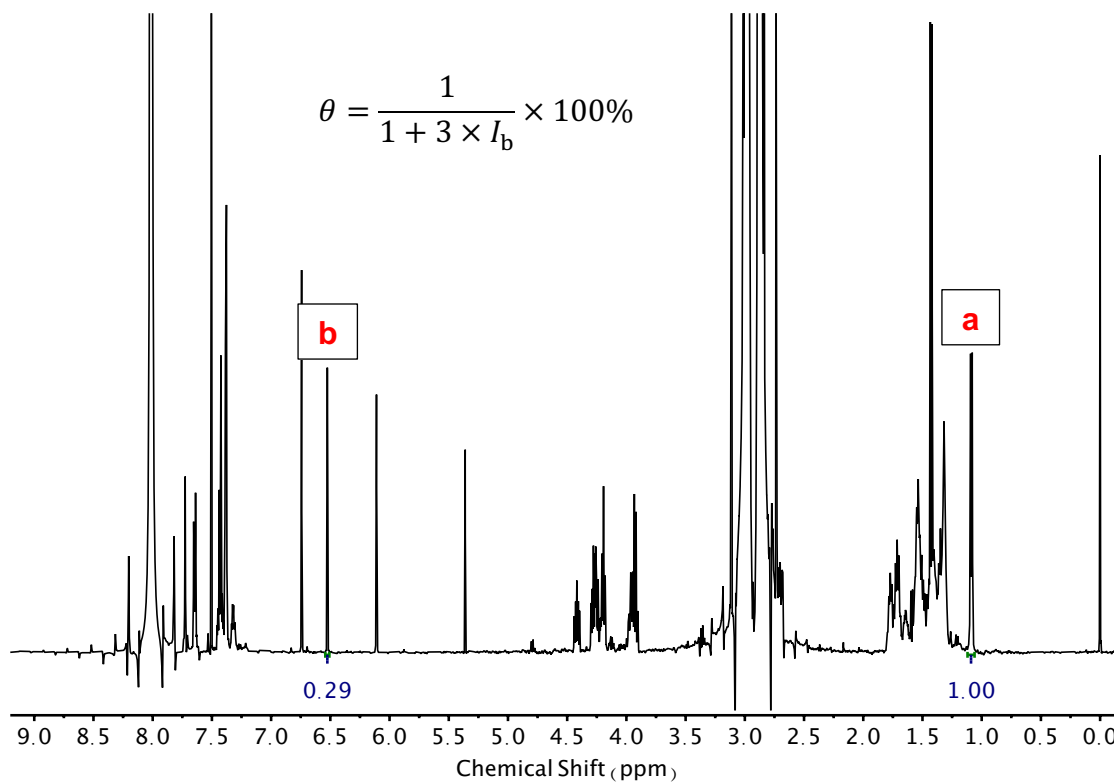


**Figure 2.54.**  $^1\text{H}$  NMR determination of monomer conversion for the polymerization of allylic sulfone macrocyclic monomer **1**.

### Determination of degree of polymerization by monomer conversion

The degree of polymerization of **P-1** could be determined based on the following equation, where  $[M]_0$  is the initial concentration of monomer **1**,  $[\text{CTA}]_0$  is the initial concentration of **CTA1**, and  $\theta$  is the conversion of allylic sulfone macrocyclic monomer **1**.

$$DP = \frac{[M]_0}{[\text{CTA}]_0} \times \theta$$

### Determination of theoretical $M_n$ of P-1

After the degree of polymerization was obtained by monomer conversion, the theoretical  $M_n$  of P-1 was determined based on the following equation, where  $MW^{RU}$  is the molecular weight of the repeating unit, and  $MW^{CTA}$  is the molecular weight of the CTA.

$$M_n^{theo} = MW^{RU} \times DP + MW^{CTA}$$

### Determination of degree of polymerization by chain end analysis

The degree of polymerization of P-1 could also be determined based on the assignment that the integral of a doublet of doublet at  $\delta = 2.95$  ppm (Peak *c*, Figure 2.55) corresponds to the  $\alpha$  position of the carbonyl group in the backbone of polymer P-1 (1H), and the integral of the quartet at  $\delta = 4.81$  ppm (Peak *d*, Figure 2.55) corresponds to the  $\alpha$  position of the carbonyl group linked with a trithiocarbonate chain end (1H). The degree of polymerization ( $DP$ ) is calculated based on the following equation, where  $I_c$  is the integral of Peak *c*, and  $I_d$  is the integral of Peak *d*:

$$DP = \frac{I_c}{I_d}$$

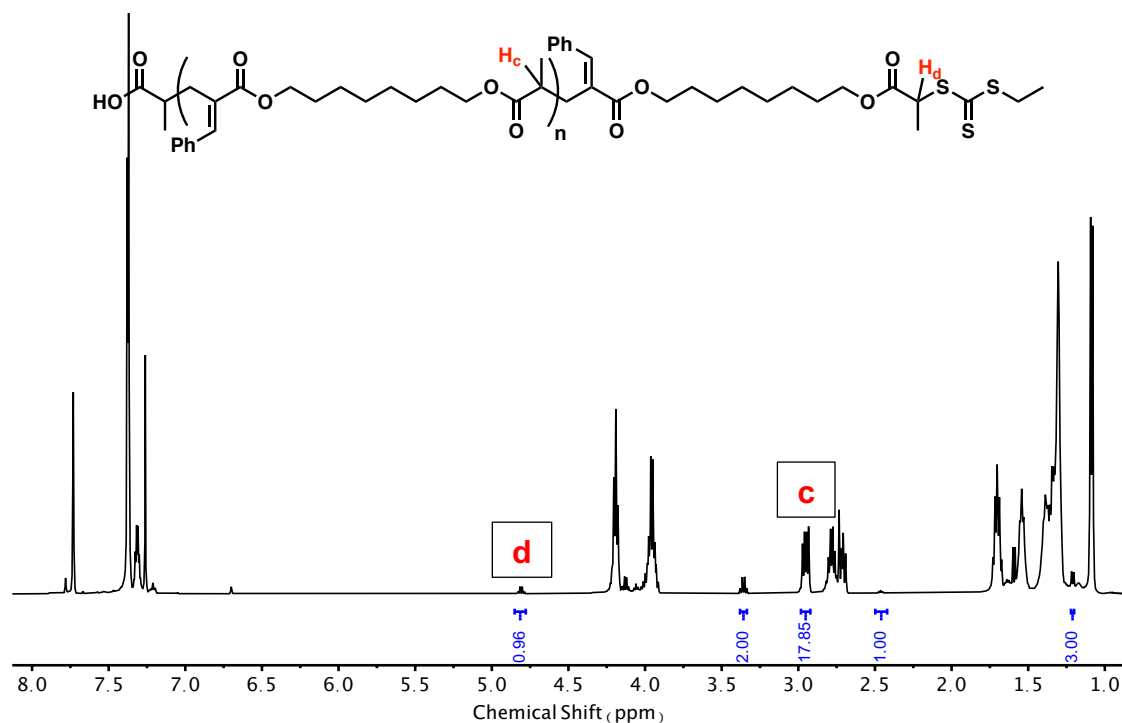


**Figure 2.55.**  $^1\text{H}$  NMR determination of degree of polymerization of purified **P-1**.

### Determination of monomer conversion for random copolymerization of **1** and MA

The monomer conversion for random copolymerization of **1** and MA was determined based on the assignment that the integral of the multiplet at  $\delta = 1.13$  ppm (Peak *a*, Figure 2.56) corresponds to the methyl group of **P-1** unit (3H); the integral of the singlet at  $\delta = 6.51$  ppm (Peak *b*, Figure 2.56) corresponds to the terminal alkene of unreacted allylic sulfone macrocyclic monomer **1** (1H); the integral of the singlet at  $\delta = 3.67$  ppm (Peak *c*, Figure 2.56) corresponds to the methyl group of PMA unit (3H); and the integral of the singlet at  $\delta = 3.75$  ppm (Peak *d*, Figure 2.56) corresponds to the methyl group of unreacted MA (3H). The monomer conversion  $\theta$  of **1** and MA is calculated based on the following

equation, where  $I_a$  is the integral of Peak  $a$ ,  $I_b$  is the integral of Peak  $b$ ,  $I_c$  is the integral of Peak  $c$ , and  $I_d$  is the integral of Peak  $d$ .

$$\theta_1 = \frac{I_a}{I_a + 3 \times I_b} \times 100\%$$

$$\theta_{MA} = \frac{I_c}{I_c + I_d} \times 100\%$$

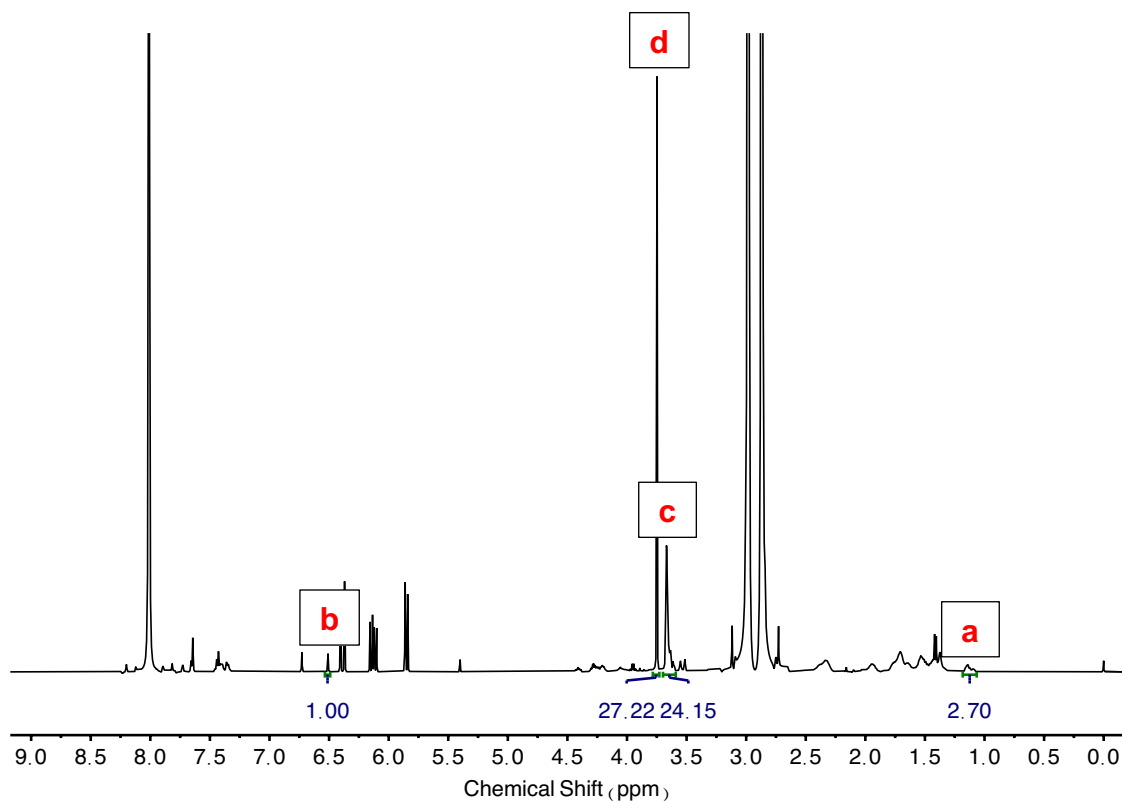


**Figure 2.56.** <sup>1</sup>H NMR analysis of random copolymerization of allylic sulfone macrocyclic monomer **1** and MA.

### Determination of mean and 95% confidence interval of reactivity ratios

The reactivity ratios were obtained by fitting the comonomer conversion and composition of copolymers to the Beckingham-Sanoja-Lynd integrated model. The mean values of reactivity ratios were calculated based on five to seven independent fitting results.

The 95% confidence interval of reactivity ratios was calculated based on the equation below:

$$\bar{x} \pm \frac{ts}{\sqrt{n}}$$

where  $t$  is the “student t factor”,  $s = \sqrt{\frac{\sum(x_i - \bar{x})^2}{n-1}}$ ,  $n$  is the number of data points.

### **MALDI-TOF analysis**

The mass spectrum was obtained using a Bruker Auto Flex Max instrument (positive mode).  $\alpha$ -Cyano-4-hydroxycinnamic acid (10.0 mg/mL in THF) was used as the matrix, with NaI (1.0 mg/mL in THF) added as the cation source for all the polymers.

### **Thermomechanical property analysis**

Oscillatory temperature sweeps were performed on a TA DHR-2 rheometer with an 8 mm parallel plate geometry. The sample thickness was controlled to be approximately 900  $\mu\text{m}$ . Strain sweep experiments were done to identify the appropriate strains. The angular strains used for PMA and **P-1-co-MA** ( $F_1^{\text{end}} = 0.05$ ) were 0.2% and 1.0%, respectively. An angular frequency of 0.5  $\text{rad s}^{-1}$  was used for both samples. The temperature was ramped at a rate of 3  $^\circ\text{C min}^{-1}$  from -10  $^\circ\text{C}$  to 100  $^\circ\text{C}$ .

### **EPR studies**

#### **Sample preparation**

The stock solution of allylic sulfone macrocyclic monomer **1**, **CTA1**, and *fac*-[Ir(ppy)<sub>3</sub>] was prepared in the glove box. **1** (75.0  $\mu\text{mol}$ ), **CTA1** (1.5  $\mu\text{mol}$ ), *fac*-[Ir(ppy)<sub>3</sub>] (15.0 nmol),

and dioxane (0.4 mL) were mixed in a vial and transferred to an EPR tube in the glove box. The mixture was then irradiated by a blue LED lamp (18 W,  $\lambda_{\text{max}} = 450$  nm) during the EPR measurement at 25 °C. The exogenous SO<sub>2</sub> was injected through the rubber septum of the EPR tube for 10 seconds and sealed with wax after completion.

### **EPR measurement and simulation**

X-band continue wave electron paramagnetic resonance (CW-EPR) spectra were recorded on a Bruker EMX-Plus spectrometer at 300 K. The microwave bridge frequency of the CW-EPR measurements was at 9.4 GHz; microwave power was set at 20.0 mW. The modulation amplitude and modulation frequency were adjusted at 2.0 G and 100.0 kHz. The simulation was carried out by the Xenon SpinFit software package (Bruker BioSpin).

### **DFT calculations**

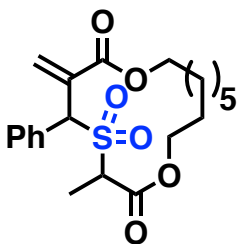
All geometry optimizations and frequency calculations were carried out employing the B3LYP/6-31G(d) method and the SMD solvation model in DMF. Single-point energies were calculated using the M06-2X/6-311++G(d,p) method and the SMD solvation model in DMF. Gibbs free energies (298.15 K and 1.0 atm) were computed as the sum of single-point energies and the Gibbs free energy corrections using unscaled normal mode frequencies. All quantum chemical calculations were carried out with the Gaussian 09 computer program.<sup>74</sup>

### Gibbs free energies

<b>Method</b>	M06-2X/6-311++G(d,p)//B3LYP/6-31G(d)	
<b>Unit</b>	Hartree	kcal/mol
<b>G<sub>0</sub> (S<sub>1</sub>+Initiator)</b>	-1933.707434	0.0
<b>TS<sub>1</sub></b>	-1933.679279	17.7
<b>G<sub>1</sub></b>	-1933.725471	-11.3
<b>TS<sub>2</sub></b>	-1933.710842	-2.1
<b>G<sub>2</sub></b>	-1933.730277	-14.3
<b>TS<sub>3</sub></b>	-1933.720772	-8.4
<b>G<sub>3</sub>+SO<sub>2</sub></b>	-1933.734664	-17.1
<b>TS<sub>4</sub></b>	-3051.140600	3.6
<b>G<sub>4</sub></b>	-3051.191546	-28.3
<b>TS<sub>5</sub></b>	-4082.103486	-5.1
<b>G<sub>5</sub></b>	-4082.129667	-21.6
<b>TS<sub>6</sub></b>	-3599.730839	5.4
<b>G<sub>6</sub></b>	-3599.746706	-4.5
<b>S<sub>1</sub></b>	-1666.032045	
<b>Initiator</b>	-267.675389	
<b>G<sub>3</sub></b>	-1385.141584	
<b>SO<sub>2</sub></b>	-548.593079	
<b>G<sub>5</sub>_CTA</b>	-2696.980961	

## Cartesian coordinates for intermediates and transition states

S<sub>1</sub>



56

S	-0.590	-2.591	0.560
O	-0.910	-2.112	1.920
O	-1.462	-3.622	-0.040
O	0.607	0.325	-2.656
O	1.590	1.770	-1.210
O	3.216	-2.292	0.300
O	2.199	-2.112	2.316
C	-0.580	-1.175	-0.654
H	-0.200	-1.653	-1.560
C	0.342	-0.022	-0.300
C	0.855	0.692	-1.520
C	2.125	2.599	-2.282
H	1.900	3.623	-1.973
H	1.587	2.377	-3.206
C	3.627	2.389	-2.418

H	4.029	3.241	-2.983
H	4.070	2.448	-1.415
C	5.574	-1.998	-0.105
H	5.641	-3.091	-0.166
H	6.497	-1.657	0.385
C	4.419	-1.650	0.822
H	4.593	-2.018	1.835
H	4.227	-0.574	0.874
C	2.205	-2.479	1.160
C	1.115	-3.329	0.511
H	1.321	-3.453	-0.555
C	-2.024	-0.762	-0.896
C	-2.695	0.098	-0.017
H	-2.179	0.506	0.847
C	-4.026	0.449	-0.253
H	-4.535	1.118	0.436
C	-4.698	-0.052	-1.370
H	-5.732	0.226	-1.555
C	-4.033	-0.909	-2.251
H	-4.547	-1.300	-3.126
C	-2.706	-1.265	-2.013
H	-2.191	-1.932	-2.700
C	0.636	0.407	0.935

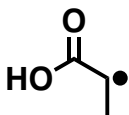
H	1.280	1.266	1.080
H	0.256	-0.089	1.820
C	1.052	-4.695	1.211
H	2.030	-5.179	1.127
H	0.306	-5.336	0.736
H	0.811	-4.580	2.272
C	4.031	1.080	-3.116
C	5.523	0.742	-2.944
C	5.475	-1.393	-1.516
C	5.856	0.095	-1.586
H	3.787	1.165	-4.184
H	3.424	0.250	-2.734
H	6.114	1.660	-3.071
H	5.842	0.064	-3.747
H	4.457	-1.545	-1.895
H	6.136	-1.954	-2.189
H	6.932	0.188	-1.387
H	5.351	0.652	-0.784

	1	2	3
Frequencies --	20.0325	26.1259	36.2334
Red. masses --	4.7728	5.6356	4.0722
Zero-point correction=			0.468455 (Hartree/Particle)

Thermal correction to Energy=	0.496283
Thermal correction to Enthalpy=	0.497227
Thermal correction to Gibbs Free Energy=	0.408784
Sum of electronic and zero-point Energies=	-1666.142687
Sum of electronic and thermal Energies=	-1666.114859
Sum of electronic and thermal Enthalpies=	-1666.113915
Sum of electronic and thermal Free Energies=	-1666.202358

	Item	Value	Threshold	Converged?
Maximum	Force	0.000019	0.000450	YES
RMS	Force	0.000003	0.000300	YES

### Initiator



10

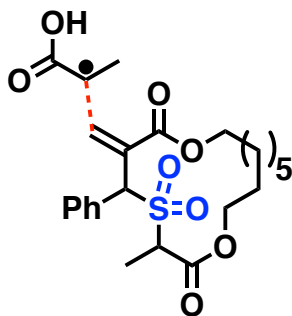
C	-2.767	1.713	0.143
C	-1.645	2.618	0.062
C	-4.193	2.076	-0.046
O	-0.474	2.283	0.227
O	-1.987	3.907	-0.218
H	-1.149	4.410	-0.244

H	-2.506	0.681	0.360
H	-4.333	3.142	-0.234
H	-4.784	1.794	0.839
H	-4.627	1.512	-0.886

	1	2	3
Frequencies --	84.8260	123.8148	261.8526
Red. masses --	1.1179	2.6550	3.6235
Zero-point correction=			0.076689 (Hartree/Particle)
Thermal correction to Energy=			0.082489
Thermal correction to Enthalpy=			0.083433
Thermal correction to Gibbs Free Energy=			0.046875
Sum of electronic and zero-point Energies=			-267.672892
Sum of electronic and thermal Energies=			-267.667092
Sum of electronic and thermal Enthalpies=			-267.666147
Sum of electronic and thermal Free Energies=			-267.702706

	Item	Value	Threshold	Converged?
Maximum	Force	0.000093	0.000450	YES
RMS	Force	0.000029	0.000300	YES

TS<sub>1</sub>



66

C	-0.444	2.582	1.368
C	0.177	0.052	-0.383
C	0.425	0.542	0.881
H	-0.218	3.758	3.134
H	1.018	2.510	2.945
C	-0.046	2.722	2.800
H	-0.637	2.070	3.449
O	-2.756	2.244	1.854
C	-1.865	2.472	1.045
S	-0.720	-2.533	0.452
O	-1.060	-2.078	1.816
O	-1.558	-3.582	-0.165
O	0.657	0.263	-2.718
O	1.547	1.760	-1.262
O	3.123	-2.223	0.274
O	2.011	-1.948	2.227

C	-0.730	-1.110	-0.749
H	-0.292	-1.569	-1.640
C	0.813	0.676	-1.577
C	2.147	2.545	-2.332
H	1.940	3.582	-2.054
H	1.636	2.317	-3.269
C	3.648	2.300	-2.418
H	4.084	3.140	-2.976
H	4.061	2.360	-1.402
C	5.508	-2.014	-0.014
H	5.551	-3.111	-0.033
H	6.414	-1.677	0.508
C	4.319	-1.607	0.842
H	4.429	-1.956	1.872
H	4.160	-0.524	0.860
C	2.067	-2.360	1.088
C	1.004	-3.224	0.416
H	1.228	-3.336	-0.648
C	-2.179	-0.775	-1.083
C	-3.097	-0.363	-0.108
H	-2.790	-0.278	0.928
C	-4.414	-0.062	-0.461
H	-5.115	0.254	0.306

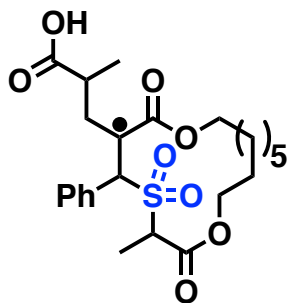
C	-4.828	-0.163	-1.792
H	-5.852	0.076	-2.065
C	-3.918	-0.575	-2.769
H	-4.230	-0.661	-3.806
C	-2.604	-0.886	-2.415
H	-1.901	-1.207	-3.177
H	1.330	1.116	1.034
H	0.012	0.044	1.749
C	0.966	-4.599	1.104
H	1.959	-5.055	1.034
H	0.248	-5.256	0.610
H	0.701	-4.501	2.160
C	4.048	0.981	-3.095
C	5.541	0.644	-2.921
C	5.488	-1.459	-1.448
C	5.875	0.026	-1.550
H	3.802	1.049	-4.163
H	3.440	0.159	-2.698
H	6.133	1.558	-3.070
H	5.855	-0.053	-3.710
H	4.491	-1.623	-1.875
H	6.181	-2.045	-2.066
H	6.951	0.121	-1.352

H	5.372	0.603	-0.761
H	0.173	3.059	0.613
O	-2.112	2.651	-0.277
H	-3.063	2.466	-0.410

	1	2	3
Frequencies --	-425.2710	14.8751	24.0335
Red. masses --	8.4249	4.3283	5.1185
Zero-point correction=			0.547186 (Hartree/Particle)
Thermal correction to Energy=			0.581312
Thermal correction to Enthalpy=			0.582256
Thermal correction to Gibbs Free Energy=			0.478593
Sum of electronic and zero-point Energies=			-1933.802884
Sum of electronic and thermal Energies=			-1933.768757
Sum of electronic and thermal Enthalpies=			-1933.767813
Sum of electronic and thermal Free Energies=			-1933.871476

	Item	Value	Threshold	Converged?
Maximum	Force	0.000004	0.000450	YES
RMS	Force	0.000001	0.000300	YES

G<sub>1</sub>



66

H	-0.913	4.434	1.803
H	0.395	3.336	2.282
C	-0.629	3.380	1.894
C	-0.709	2.672	0.540
H	-1.296	2.914	2.626
O	-3.129	2.970	0.592
C	-2.111	2.757	-0.033
S	-0.290	-2.407	0.076
O	-0.086	-2.157	1.521
O	-1.155	-3.534	-0.332
O	0.826	0.062	-2.713
O	1.468	1.807	-1.406
O	3.322	-2.807	0.662
O	2.464	-0.757	0.232
C	-1.000	-0.865	-0.785
H	-0.897	-1.157	-1.832

C	-0.180	0.365	-0.572
C	0.743	0.704	-1.668
C	2.350	2.343	-2.429
H	2.173	3.421	-2.390
H	2.035	1.967	-3.405
C	3.818	2.037	-2.141
H	4.410	2.816	-2.642
H	3.993	2.165	-1.065
C	5.736	-2.472	0.511
H	5.862	-3.553	0.373
H	6.590	-2.133	1.114
C	4.482	-2.243	1.348
H	4.540	-2.784	2.296
H	4.292	-1.188	1.548
C	2.442	-1.968	0.116
C	1.385	-2.693	-0.715
H	1.328	-2.166	-1.674
C	-2.481	-0.768	-0.451
C	-2.998	-0.856	0.851
H	-2.336	-1.034	1.692
C	-4.372	-0.749	1.074
H	-4.757	-0.829	2.087
C	-5.247	-0.540	0.006

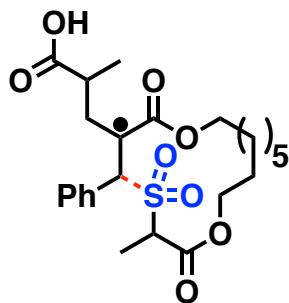
H	-6.316	-0.455	0.184
C	-4.741	-0.448	-1.293
H	-5.413	-0.292	-2.132
C	-3.369	-0.568	-1.519
H	-2.981	-0.504	-2.533
C	-0.242	1.184	0.681
H	0.768	1.225	1.109
H	-0.882	0.694	1.419
C	1.600	-4.187	-0.936
H	2.565	-4.332	-1.431
H	0.818	-4.589	-1.583
H	1.608	-4.748	0.002
C	4.315	0.663	-2.618
C	5.781	0.392	-2.218
C	5.748	-1.777	-0.861
C	5.946	-0.253	-0.827
H	4.212	0.623	-3.710
H	3.667	-0.126	-2.218
H	6.339	1.338	-2.257
H	6.253	-0.263	-2.964
H	4.822	-2.023	-1.399
H	6.559	-2.216	-1.458
H	6.951	-0.042	-0.436

H 5.239 0.209 -0.125  
H -0.041 3.160 -0.174  
O -2.115 2.568 -1.375  
H -3.052 2.563 -1.659

	1	2	3
Frequencies --	23.0009	26.6247	36.0278
Red. masses --	4.8990	5.3319	4.9737
Zero-point correction=			0.550740 (Hartree/Particle)
Thermal correction to Energy=			0.584493
Thermal correction to Enthalpy=			0.585437
Thermal correction to Gibbs Free Energy=			0.483694
Sum of electronic and zero-point Energies=			-1933.843075
Sum of electronic and thermal Energies=			-1933.809322
Sum of electronic and thermal Enthalpies=			-1933.808378
Sum of electronic and thermal Free Energies=			-1933.910120

	Item	Value	Threshold	Converged?
Maximum	Force	0.000018	0.000450	YES
RMS	Force	0.000004	0.000300	YES

TS<sub>2</sub>



66

H	0.212	0.120	0.096
H	0.227	-0.034	2.565
O	1.431	0.208	-4.198
C	1.070	-0.310	0.606
C	1.079	-0.396	1.997
H	1.064	-0.472	-1.983
C	2.513	0.563	-3.740
C	2.085	-0.612	-1.633
C	2.167	-0.759	-0.151
C	2.178	-0.955	2.656
O	0.486	-3.038	-2.038
H	2.185	-1.027	3.740
C	3.016	0.145	-2.410
H	1.761	-2.147	-4.550
S	1.933	-2.772	-2.247
C	3.259	-1.335	0.522

C	3.262	-1.430	1.913
C	2.239	-3.017	-4.088
C	4.379	0.583	-1.957
C	3.735	-2.897	-4.324
H	4.695	0.006	-1.088
H	5.101	0.389	-2.757
H	4.094	-1.738	-0.041
H	4.112	-1.881	2.418
O	2.909	-3.641	-1.537
O	4.408	-2.025	-3.803
H	5.946	-4.809	-5.503
H	6.141	-3.200	-4.765
C	5.613	-3.770	-5.531
H	2.001	-5.186	-4.046
H	6.891	-3.081	-7.061
O	4.198	-3.825	-5.165
C	5.805	-3.158	-6.914
C	1.566	-4.311	-4.538
O	3.352	1.396	-4.388
H	1.695	-4.422	-5.618
H	5.434	-3.848	-7.682
H	3.337	2.967	-5.665
C	2.868	1.980	-5.633

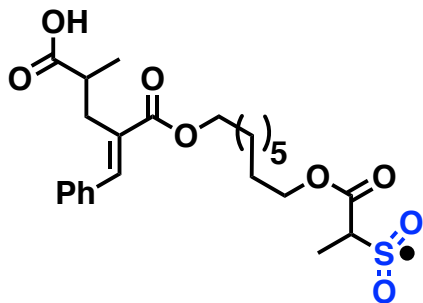
H	0.497	-4.273	-4.319
H	1.786	2.101	-5.550
O	2.339	2.880	-0.838
C	3.461	2.493	-0.572
H	4.235	2.672	-2.504
C	4.500	2.106	-1.609
H	6.040	3.509	-0.965
C	5.937	2.443	-1.196
H	6.251	1.872	-0.316
H	6.623	2.208	-2.018
O	3.887	2.341	0.700
H	3.130	2.561	1.280
C	5.148	-1.777	-7.083
C	5.771	-0.939	-8.206
C	3.233	1.147	-6.857
C	4.694	1.273	-7.318
C	5.024	0.368	-8.531
H	5.228	-1.223	-6.142
H	4.074	-1.914	-7.271
H	5.839	-1.540	-9.124
H	6.807	-0.701	-7.922
H	2.580	1.481	-7.675
H	2.969	0.101	-6.665

H 5.374 1.053 -6.484  
H 4.874 2.324 -7.583  
H 5.631 0.929 -9.252  
H 4.088 0.125 -9.056

	1	2	3
Frequencies --	-223.9178	18.9871	30.4432
Red. masses --	10.3213	6.1531	5.6791
Zero-point correction=			0.549221 (Hartree/Particle)
Thermal correction to Energy=			0.583048
Thermal correction to Enthalpy=			0.583992
Thermal correction to Gibbs Free Energy=			0.481029
Sum of electronic and zero-point Energies=			-1933.835040
Sum of electronic and thermal Energies=			-1933.801212
Sum of electronic and thermal Enthalpies=			-1933.800268
Sum of electronic and thermal Free Energies=			-1933.903232

	Item	Value	Threshold	Converged?
Maximum	Force	0.000009	0.000450	YES
RMS	Force	0.000002	0.000300	YES

G<sub>2</sub>



66

H	-0.763	6.615	-5.234
H	0.856	6.234	-5.850
C	0.295	6.896	-5.181
C	0.828	6.770	-3.747
H	0.394	7.923	-5.547
O	-0.183	8.862	-3.021
C	0.045	7.685	-2.821
S	7.800	-7.988	-1.733
O	6.411	-7.547	-1.415
O	8.203	-9.404	-1.485
O	3.235	5.469	-0.477
O	2.801	4.679	-2.552
O	8.933	-4.594	-0.284
O	8.694	-5.289	-2.430
C	3.454	8.034	-1.570
H	3.753	7.767	-0.557

C	2.954	7.020	-2.313
C	3.007	5.671	-1.659
C	2.874	3.314	-2.060
H	2.261	2.742	-2.762
H	2.415	3.272	-1.069
C	4.309	2.801	-2.035
H	4.749	2.931	-3.032
H	4.895	3.413	-1.339
C	7.420	-2.705	-0.745
H	6.945	-2.879	0.229
H	6.869	-3.297	-1.486
C	8.862	-3.190	-0.687
H	9.369	-3.079	-1.648
H	9.431	-2.668	0.085
C	8.833	-5.513	-1.243
C	8.962	-6.927	-0.684
H	9.952	-7.307	-0.958
C	3.645	9.454	-1.905
C	4.089	9.904	-3.163
H	4.322	9.187	-3.944
C	4.281	11.265	-3.406
H	4.632	11.591	-4.381
C	4.036	12.203	-2.400

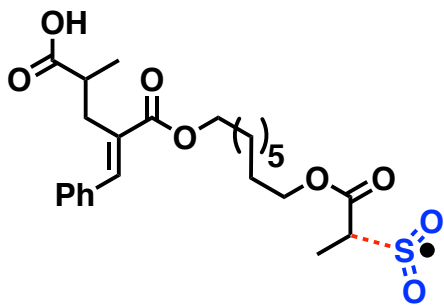
H	4.185	13.262	-2.593
C	3.617	11.770	-1.139
H	3.439	12.491	-0.345
C	3.439	10.410	-0.891
H	3.124	10.077	0.095
C	2.338	7.140	-3.690
H	2.860	6.488	-4.399
H	2.442	8.163	-4.054
C	8.674	-7.135	0.797
H	9.423	-6.589	1.379
H	8.751	-8.195	1.055
H	7.682	-6.768	1.072
C	4.382	1.325	-1.621
C	5.819	0.792	-1.563
C	7.343	-1.216	-1.109
C	5.904	-0.690	-1.175
H	3.796	0.719	-2.328
H	3.906	1.197	-0.637
H	6.398	1.390	-0.844
H	6.300	0.938	-2.541
H	7.834	-1.054	-2.079
H	7.912	-0.630	-0.372
H	5.417	-0.841	-0.200

H 5.333 -1.288 -1.900  
H 0.698 5.744 -3.398  
O -0.381 7.047 -1.707  
H -0.851 7.710 -1.161

	1	2	3
Frequencies --	8.4356	13.7888	17.9054
Red. masses --	6.3981	6.5825	7.8203
Zero-point correction=			0.548147 (Hartree/Particle)
Thermal correction to Energy=			0.584070
Thermal correction to Enthalpy=			0.585014
Thermal correction to Gibbs Free Energy=			0.471120
Sum of electronic and zero-point Energies=			-1933.863960
Sum of electronic and thermal Energies=			-1933.828037
Sum of electronic and thermal Enthalpies=			-1933.827092
Sum of electronic and thermal Free Energies=			-1933.940987

	Item	Value	Threshold	Converged?
Maximum	Force	0.000004	0.000450	YES
RMS	Force	0.000001	0.000300	YES

TS<sub>3</sub>



66

O 6.878 -2.288 -8.871

S 7.933 -2.546 -9.871

O 7.693 -3.632 -10.841

H 0.647 7.987 -0.146

H 2.334 7.583 0.220

C 1.303 7.491 0.579

C 0.930 6.012 0.739

H 1.220 8.023 1.533

O -0.989 6.510 2.151

C -0.500 5.881 1.233

O 1.389 1.739 0.783

O 2.409 3.483 -0.234

O 9.032 -3.461 -6.286

O 10.055 -1.624 -7.160

C 1.209 3.264 3.113

H 0.964 2.205 3.043

C	1.618	3.841	1.960
C	1.769	2.899	0.801
C	2.640	2.678	-1.420
H	2.689	3.406	-2.233
H	1.777	2.025	-1.577
C	3.934	1.880	-1.318
H	4.759	2.567	-1.091
H	3.858	1.175	-0.481
C	7.453	-1.968	-5.124
H	6.638	-2.658	-5.379
H	7.522	-1.235	-5.937
C	8.759	-2.750	-5.047
H	9.606	-2.096	-4.824
H	8.707	-3.539	-4.292
C	9.677	-2.784	-7.252
C	9.894	-3.597	-8.462
H	10.602	-3.161	-9.162
C	1.014	3.845	4.452
C	1.882	4.794	5.026
H	2.761	5.125	4.481
C	1.653	5.281	6.313
H	2.341	6.006	6.741
C	0.556	4.834	7.053

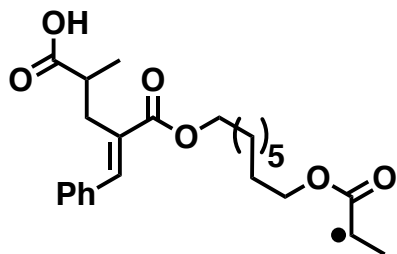
H	0.379	5.218	8.055
C	-0.303	3.877	6.505
H	-1.151	3.512	7.078
C	-0.067	3.378	5.226
H	-0.730	2.624	4.808
C	1.890	5.314	1.747
H	2.912	5.461	1.378
H	1.809	5.845	2.697
C	9.596	-5.047	-8.553
H	10.413	-5.606	-8.066
H	9.559	-5.380	-9.594
H	8.670	-5.320	-8.040
C	4.232	1.119	-2.618
C	5.529	0.302	-2.553
C	7.142	-1.252	-3.803
C	5.841	-0.441	-3.858
H	4.295	1.835	-3.450
H	3.392	0.449	-2.849
H	5.462	-0.422	-1.728
H	6.367	0.971	-2.308
H	7.976	-0.583	-3.547
H	7.078	-1.992	-2.992
H	5.005	-1.112	-4.104

H	5.904	0.286	-4.682
H	1.002	5.510	-0.228
O	-1.198	4.953	0.541
H	-2.090	4.909	0.944

	1	2	3
Frequencies --	-42.4387	8.4801	12.8712
Red. masses --	12.4905	6.5019	6.3392
Zero-point correction=			0.545222 (Hartree/Particle)
Thermal correction to Energy=			0.581544
Thermal correction to Enthalpy=			0.582488
Thermal correction to Gibbs Free Energy=			0.467348
Sum of electronic and zero-point Energies=			-1933.857757
Sum of electronic and thermal Energies=			-1933.821436
Sum of electronic and thermal Enthalpies=			-1933.820492
Sum of electronic and thermal Free Energies=			-1933.935631

	Item	Value	Threshold	Converged?
Maximum	Force	0.000003	0.000450	YES
RMS	Force	0.000001	0.000300	YES

G<sub>3</sub>



63

H	2.314	4.408	-7.446
H	2.747	4.211	-5.727
H	-4.302	7.072	-3.223
C	2.232	3.744	-6.571
O	0.840	4.321	-4.035
H	2.764	2.821	-6.845
H	-1.473	5.864	-3.724
H	-5.320	6.496	-0.996
C	-3.671	6.893	-2.340
H	-2.831	7.599	-2.414
C	0.234	3.795	-4.966
C	0.813	3.463	-6.252
H	-3.847	7.017	-0.188
C	-4.477	7.199	-1.071
H	-2.502	5.278	-1.502
C	-2.317	5.166	-3.655

C	-3.130	5.458	-2.387
H	-1.112	3.554	-2.828
H	0.172	2.998	-6.995
H	-2.941	5.323	-4.544
O	-1.079	3.443	-4.905
C	-1.781	3.738	-3.674
H	-5.163	8.778	1.137
C	-5.012	8.636	-1.022
H	-3.969	4.750	-2.319
H	-6.652	8.251	0.344
C	-5.802	8.939	0.258
H	-4.170	9.340	-1.105
H	-2.598	3.011	-3.646
H	-5.652	8.816	-1.898
C	-6.317	10.373	0.282
H	-7.022	10.561	-0.532
H	-5.494	11.089	0.214
H	-6.753	14.911	3.947
H	-5.954	13.433	4.511
C	-6.928	13.904	4.344
C	-7.761	13.062	3.369
H	-7.435	14.003	5.309
O	-9.858	14.118	4.011

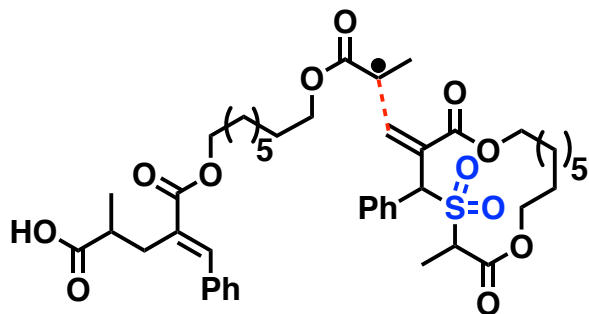
C	-9.116	13.710	3.140
O	-8.922	9.861	0.779
O	-6.961	10.689	1.544
C	-9.993	10.185	3.339
H	-10.482	9.647	2.528
C	-8.787	10.717	3.037
C	-8.269	10.378	1.670
C	-10.766	10.232	4.590
C	-10.186	10.116	5.868
H	-9.115	9.973	5.964
C	-10.979	10.138	7.015
H	-10.511	10.039	7.991
C	-12.366	10.275	6.913
H	-12.980	10.294	7.809
C	-12.959	10.368	5.651
H	-14.038	10.460	5.560
C	-12.169	10.331	4.503
H	-12.636	10.393	3.523
C	-7.965	11.624	3.928
H	-6.970	11.196	4.094
H	-8.444	11.716	4.904
H	-7.248	13.001	2.407
O	-9.437	13.777	1.828

H -10.330 14.175 1.773

	1	2	3
Frequencies --	-16.6910	6.4817	13.7645
Red. masses --	2.0345	4.9614	5.0457
Zero-point correction=			0.536176 (Hartree/Particle)
Thermal correction to Energy=			0.568107
Thermal correction to Enthalpy=			0.569051
Thermal correction to Gibbs Free Energy=			0.465160
Sum of electronic and zero-point Energies=			-1385.268964
Sum of electronic and thermal Energies=			-1385.237033
Sum of electronic and thermal Enthalpies=			-1385.236089
Sum of electronic and thermal Free Energies=			-1385.339980

	Item	Value	Threshold	Converged?
Maximum	Force	0.000008	0.000450	YES
RMS	Force	0.000001	0.000300	YES

TS<sub>4</sub>



119

C	-0.713	-0.307	-3.572
C	-1.032	1.129	-3.602
O	-1.485	1.756	-2.653
O	-0.765	1.685	-4.809
C	-0.998	3.111	-4.939
H	-1.883	3.380	-4.357
H	-1.209	3.260	-6.001
C	0.221	3.916	-4.503
C	-0.001	5.426	-4.664
H	-0.859	5.734	-4.049
H	-0.272	5.650	-5.706
C	1.229	6.256	-4.271
C	0.998	7.769	-4.361
H	0.169	8.050	-3.695
H	0.677	8.031	-5.380
C	2.241	8.593	-3.997

C	1.989	10.107	-4.030
H	1.198	10.368	-3.315
H	1.640	10.408	-5.025
C	3.246	10.896	-3.683
O	2.977	12.320	-3.594
C	3.026	13.033	-4.741
C	2.705	14.480	-4.513
C	2.571	14.976	-3.091
H	2.144	15.981	-3.087
H	1.861	14.330	-2.561
C	3.873	14.973	-2.233
C	3.592	15.525	-0.831
H	3.261	16.568	-0.878
H	2.808	14.935	-0.345
H	4.489	15.482	-0.203
C	4.970	15.774	-2.909
O	5.115	16.980	-2.842
O	5.801	14.991	-3.631
H	6.452	15.584	-4.061
H	4.221	13.940	-2.158
C	2.475	15.189	-5.644
C	2.084	16.590	-5.860
C	1.297	16.863	-6.999

C	0.867	18.156	-7.288
C	1.237	19.217	-6.457
H	0.912	20.229	-6.684
C	2.044	18.971	-5.344
H	2.358	19.794	-4.707
H	0.252	18.336	-8.166
H	1.015	16.042	-7.654
C	2.466	17.675	-5.046
H	3.128	17.521	-4.201
H	2.532	14.609	-6.563
O	3.289	12.535	-5.823
H	3.616	10.630	-2.689
H	4.040	10.731	-4.415
H	2.586	8.305	-2.993
H	3.058	8.342	-4.689
H	1.526	5.997	-3.244
H	2.075	5.975	-4.915
H	0.446	3.686	-3.454
H	1.088	3.599	-5.097
C	-0.381	-0.906	-2.244
H	-1.091	-0.596	-1.471
H	0.614	-0.558	-1.922
H	-0.341	-1.995	-2.301

H	-0.240	-0.722	-4.453
C	-2.801	-1.181	-3.982
H	-3.207	-0.178	-3.987
H	-2.731	-1.667	-3.017
H	-2.942	-5.002	-0.710
C	-3.413	-4.959	-1.688
H	-1.825	-3.793	-2.541
H	-5.129	-6.126	-1.096
C	-2.782	-4.269	-2.725
C	-4.639	-5.592	-1.905
O	-0.073	-3.303	-4.503
C	-3.369	-4.207	-3.998
C	-5.228	-5.539	-3.170
C	-2.907	-1.941	-5.125
O	1.806	-3.176	-7.252
S	-0.982	-4.043	-5.410
C	-4.594	-4.857	-4.210
C	-2.756	-3.448	-5.162
H	-6.179	-6.033	-3.353
H	-4.852	1.409	-6.900
O	-3.538	0.000	-6.307
O	-0.997	-5.518	-5.333
H	0.364	-5.429	-7.744

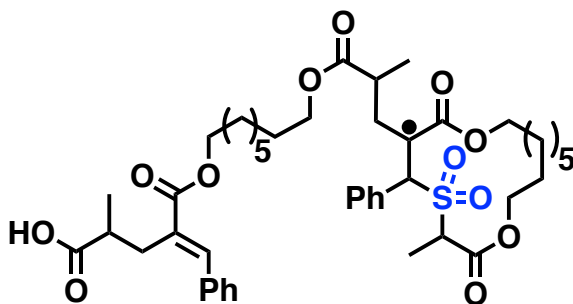
C	-3.347	-1.324	-6.408
C	0.688	-2.715	-7.166
C	-4.169	0.721	-7.405
C	-0.586	-3.554	-7.176
H	-5.056	-4.823	-5.194
H	-3.226	-3.797	-6.085
C	-0.460	-4.787	-8.063
H	1.070	0.440	-6.671
H	2.318	-0.820	-6.550
O	-3.553	-1.967	-7.432
H	-4.751	0.017	-8.005
H	-1.386	-5.367	-8.062
H	-2.416	1.935	-7.565
C	1.483	-0.449	-7.149
O	0.389	-1.411	-7.078
C	-3.158	1.497	-8.245
H	-0.266	-4.458	-9.090
H	-1.429	-2.932	-7.488
H	-3.697	2.342	-8.697
H	-0.186	1.555	-8.232
H	-2.076	-0.243	-8.961
C	1.912	-0.186	-8.592
C	-2.473	0.696	-9.363

H	2.619	0.654	-8.566
C	-0.001	1.424	-9.306
H	2.472	-1.056	-8.956
H	-3.237	0.412	-10.100
H	0.055	-0.732	-9.533
C	0.757	0.111	-9.562
C	-1.345	1.486	-10.057
H	0.637	2.267	-9.607
H	-1.661	2.532	-10.172
H	1.159	0.131	-10.584
H	-1.198	1.101	-11.076

	1	2	3
Frequencies --	-394.1616	7.3408	12.9425
Red. masses --	9.3587	5.6536	6.0465
Zero-point correction=			1.007368 (Hartree/Particle)
Thermal correction to Energy=			1.068412
Thermal correction to Enthalpy=			1.069356
Thermal correction to Gibbs Free Energy=			0.900541
Sum of electronic and zero-point Energies=			-3051.399306
Sum of electronic and thermal Energies=			-3051.338262
Sum of electronic and thermal Enthalpies=			-3051.337318
Sum of electronic and thermal Free Energies=			-3051.506133

	Item	Value	Threshold	Converged?
Maximum	Force	0.000006	0.000450	YES
RMS	Force	0.000001	0.000300	YES

**G<sub>4</sub>**



119

O	-3.059	-3.914	-3.302
H	-2.458	-0.638	-2.899
C	-3.512	-0.554	-3.142
H	-3.931	0.651	-1.412
C	-4.350	0.168	-2.290
C	-5.717	0.266	-2.559
C	-6.246	-0.372	-3.684
H	-6.366	0.830	-1.895
H	-7.310	-0.311	-3.899
H	3.447	-4.745	-7.581
H	2.298	-3.834	-5.548

H	2.277	-5.862	-6.886
C	2.372	-4.917	-7.434
O	0.473	-5.390	-4.817
C	1.862	-3.782	-6.549
H	2.076	-2.802	-6.978
C	-0.138	-4.631	-5.540
C	1.656	-5.044	-8.788
H	1.988	-5.973	-9.271
O	0.409	-3.792	-6.427
H	2.880	-3.954	-10.196
O	-0.937	-2.593	-3.768
H	-2.030	-6.290	-4.352
C	1.872	-3.877	-9.767
H	0.583	-5.174	-8.599
H	1.843	-2.916	-9.235
C	-1.660	-4.523	-5.566
C	-2.342	-5.862	-5.307
H	-2.060	-6.555	-6.107
S	-2.161	-3.257	-4.273
C	0.819	-3.857	-10.891
H	-1.984	-4.096	-6.517
H	0.670	-4.883	-11.255
H	-3.429	-5.757	-5.315

H 1.196 -3.284 -11.749  
H -0.761 -3.588 -9.424  
C -0.533 -3.261 -10.448  
C -3.194 -2.002 -5.254  
H 0.332 -1.296 -10.050  
C -2.356 -1.234 -6.228  
C -0.562 -1.728 -10.520  
C -4.035 -1.194 -4.276  
C -2.496 -1.635 -7.639  
H -3.859 -2.657 -5.822  
O -3.306 -2.471 -8.032  
O -1.639 -0.981 -8.446  
H -1.341 -3.652 -11.080  
H -0.535 -1.418 -11.574  
C -1.791 -1.083 -9.891  
C -5.412 -1.100 -4.532  
H -2.706 -1.634 -10.115  
H -1.903 -0.050 -10.230  
H -5.830 -1.602 -5.401  
C -1.580 1.268 -6.422  
C -2.964 1.838 -6.146  
O -3.228 2.649 -5.279  
O -3.875 1.334 -7.007

C	-5.240	1.821	-6.895
H	-5.466	2.005	-5.843
H	-5.857	0.995	-7.257
C	-5.442	3.074	-7.740
C	-6.886	3.588	-7.672
H	-7.147	3.799	-6.625
H	-7.573	2.797	-8.009
C	-7.112	4.850	-8.514
C	-8.545	5.390	-8.433
H	-8.792	5.607	-7.384
H	-9.248	4.609	-8.760
C	-8.764	6.652	-9.276
C	-10.196	7.196	-9.185
H	-10.441	7.434	-8.142
H	-10.908	6.431	-9.520
C	-10.380	8.450	-10.032
O	-11.717	8.998	-9.883
C	-12.680	8.517	-10.698
C	-14.016	9.131	-10.398
C	-14.075	10.337	-9.487
H	-15.113	10.593	-9.270
H	-13.590	10.110	-8.531
C	-13.386	11.608	-10.063

C -13.420 12.750 -9.038  
H -14.451 13.019 -8.786  
H -12.908 12.446 -8.119  
H -12.919 13.644 -9.426  
C -14.093 12.033 -11.339  
O -15.186 12.561 -11.396  
O -13.372 11.748 -12.447  
H -13.910 12.029 -13.216  
H -12.350 11.370 -10.311  
C -15.065 8.544 -11.019  
C -16.507 8.825 -10.924  
C -17.278 8.729 -12.100  
C -18.650 8.971 -12.081  
C -19.289 9.286 -10.878  
H -20.360 9.467 -10.859  
C -18.545 9.348 -9.697  
H -19.038 9.566 -8.753  
H -19.222 8.906 -13.002  
H -16.787 8.473 -13.036  
C -17.168 9.121 -9.717  
H -16.613 9.136 -8.785  
H -14.807 7.750 -11.718  
O -12.472 7.671 -11.553

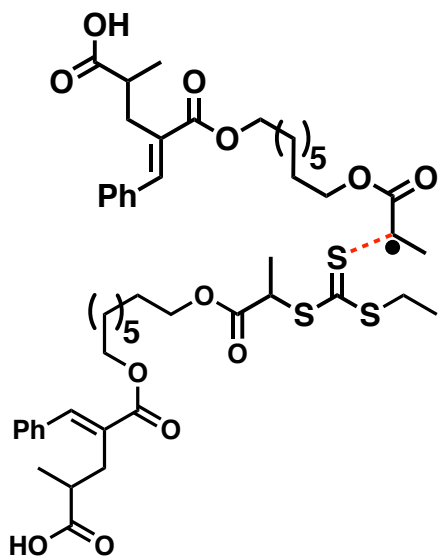
H	-9.719	9.253	-9.697
H	-10.195	8.251	-11.090
H	-8.058	7.431	-8.954
H	-8.524	6.434	-10.327
H	-6.411	5.632	-8.187
H	-6.863	4.634	-9.564
H	-4.754	3.854	-7.389
H	-5.172	2.849	-8.780
C	-0.491	2.202	-5.887
H	-0.565	2.319	-4.801
H	-0.573	3.197	-6.338
H	0.500	1.801	-6.125
H	-1.484	1.177	-7.506
C	-1.398	-0.158	-5.807
H	-1.403	-0.066	-4.720
H	-0.384	-0.475	-6.088

	1	2	3
Frequencies --	5.2755	10.4894	11.5789
Red. masses --	5.7363	5.7381	6.0856
Zero-point correction=			1.009946 (Hartree/Particle)
Thermal correction to Energy=			1.071063
Thermal correction to Enthalpy=			1.072007

Thermal correction to Gibbs Free Energy=	0.901122
Sum of electronic and zero-point Energies=	-3051.439091
Sum of electronic and thermal Energies=	-3051.377973
Sum of electronic and thermal Enthalpies=	-3051.377029
Sum of electronic and thermal Free Energies=	-3051.547915

	Item	Value	Threshold	Converged?
Maximum	Force	0.000006	0.000450	YES
RMS	Force	0.000001	0.000300	YES

TS<sub>5</sub>



137

H	7.119	1.312	-6.663
C	7.333	1.757	-7.642

H	7.710	3.748	-6.847
H	6.015	3.438	-7.290
H	8.379	1.549	-7.889
C	7.055	3.257	-7.570
H	6.695	1.259	-8.380
S	8.601	6.494	-10.183
S	7.397	3.988	-9.236
H	-6.160	12.009	-17.506
C	7.680	5.713	-9.036
H	-7.891	11.789	-17.191
C	-7.077	12.522	-17.197
O	4.378	6.592	-9.791
H	5.083	5.227	-7.781
S	7.090	6.610	-7.610
H	-4.819	13.608	-16.178
H	-4.308	10.777	-13.193
C	-6.889	13.150	-15.810
C	4.615	7.073	-8.699
C	5.249	6.281	-7.562
H	-6.688	12.366	-15.077
H	-2.204	9.885	-11.998
H	-0.097	9.001	-10.836
H	-2.074	11.798	-13.643

H	2.012	8.109	-9.687
C	-5.700	14.153	-15.820
H	0.040	10.878	-12.518
H	4.269	8.965	-10.342
H	-5.924	14.925	-16.558
H	2.149	9.947	-11.419
O	-4.580	12.693	-13.783
C	-4.048	11.764	-12.801
O	-8.782	14.654	-16.082
C	-8.158	13.872	-15.392
C	-1.948	10.903	-11.670
C	-2.539	11.920	-12.656
C	0.178	10.023	-10.537
C	-0.425	11.023	-11.532
C	2.303	9.133	-9.421
C	3.823	9.223	-9.378
O	4.384	8.349	-8.358
C	1.705	10.123	-10.429
C	4.735	6.628	-6.165
H	5.167	5.949	-5.424
H	-4.754	16.702	-16.758
H	-4.563	11.919	-11.851
C	-5.409	14.790	-14.478

O	-8.537	13.562	-14.131
H	3.646	6.514	-6.141
H	-2.416	11.037	-10.684
C	-4.944	13.919	-13.348
H	-5.408	18.678	-18.074
H	-2.315	12.939	-12.317
H	-0.269	10.183	-9.544
H	1.906	9.334	-8.417
H	-0.168	12.046	-11.219
C	-5.438	17.426	-16.327
H	4.155	10.222	-9.085
H	4.973	7.657	-5.883
H	1.985	11.147	-10.142
C	-5.795	18.553	-17.066
H	-9.340	14.090	-13.938
C	-5.555	16.098	-14.166
C	-5.916	17.246	-15.015
O	-4.870	14.263	-12.180
C	-6.636	19.523	-16.514
H	-6.914	20.400	-17.094
H	-5.399	16.348	-13.118
C	-6.733	18.251	-14.460
C	-7.101	19.369	-15.205

H	-7.087	18.142	-13.438
H	-7.743	20.125	-14.762
C	22.474	-5.609	-13.918
O	22.732	-5.488	-10.374
H	23.253	-6.021	-9.737
H	21.653	-4.491	-12.262
C	22.606	-6.232	-11.496
O	23.106	-7.334	-11.603
C	21.770	-5.535	-12.557
H	19.602	-1.867	-11.711
H	17.733	-0.112	-11.354
C	19.005	-2.543	-11.092
H	19.323	-2.448	-10.051
O	19.356	-3.869	-11.570
C	20.367	-6.204	-12.630
H	15.850	1.618	-10.968
C	17.150	-0.848	-10.782
H	19.796	-5.680	-13.405
H	17.444	-0.725	-9.729
H	20.509	-7.230	-12.972
C	17.515	-2.264	-11.248
H	11.328	7.308	-9.994
C	19.234	-4.891	-10.696

O	11.910	5.216	-11.410
H	13.946	3.331	-10.528
H	17.235	-2.397	-12.301
C	19.605	-6.203	-11.322
C	15.271	0.859	-10.421
H	15.562	0.953	-9.365
O	18.843	-4.746	-9.549
C	15.654	-0.537	-10.927
C	11.185	6.371	-9.466
C	11.575	5.190	-10.231
H	15.364	-0.636	-11.984
C	13.390	2.544	-10.003
H	12.072	6.282	-7.522
H	16.951	-3.002	-10.665
H	13.668	2.606	-8.942
C	19.239	-7.295	-10.612
C	13.774	1.167	-10.560
C	11.074	6.381	-7.981
H	13.486	1.105	-11.619
H	10.642	7.319	-7.623
C	19.361	-8.726	-10.933
O	11.524	4.057	-9.486
H	18.795	-7.090	-9.639

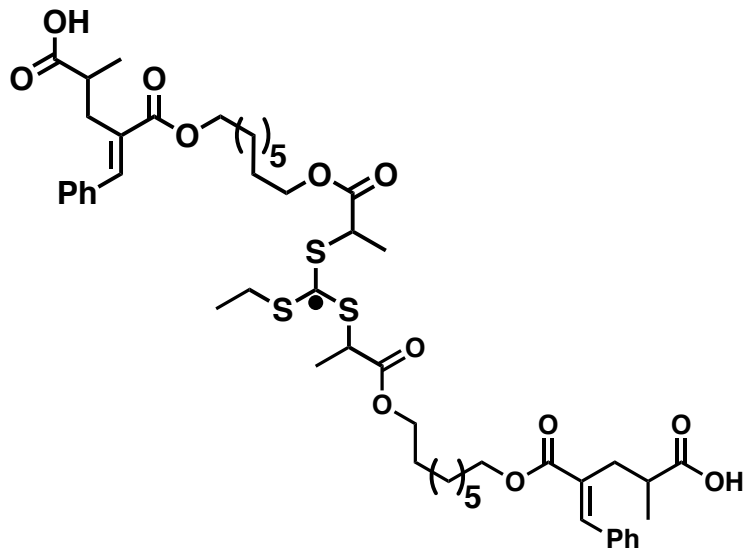
H 15.074 -1.293 -10.378  
 C 11.896 2.818 -10.134  
 H 18.867 -8.603 -13.036  
 C 19.149 -9.259 -12.219  
 H 11.587 2.855 -11.182  
 H 19.777 -9.230 -8.874  
 C 19.639 -9.621 -9.880  
 H 13.196 0.391 -10.037  
 C 19.249 -10.631 -12.447  
 H 10.475 5.543 -7.608  
 C 19.754 -10.990 -10.112  
 C 19.562 -11.501 -11.399  
 H 19.073 -11.022 -13.446  
 H 19.983 -11.659 -9.287  
 H 11.311 2.051 -9.617  
 H 19.641 -12.569 -11.581  
 H -7.314 13.287 -17.944  
 H 23.450 -5.112 -13.885  
 H 21.866 -5.113 -14.683  
 H 22.632 -6.649 -14.223

	1	2	3
Frequencies --	-143.3542	3.1684	6.4689

Red. masses --	10.6909	7.4162	6.3690
Zero-point correction=			1.154042 (Hartree/Particle)
Thermal correction to Energy=			1.229077
Thermal correction to Enthalpy=			1.230022
Thermal correction to Gibbs Free Energy=			1.019104
Sum of electronic and zero-point Energies=			-4082.392111
Sum of electronic and thermal Energies=			-4082.317076
Sum of electronic and thermal Enthalpies=			-4082.316132
Sum of electronic and thermal Free Energies=			-4082.527050

	Item	Value	Threshold	Converged?
Maximum	Force	0.000001	0.000450	YES
RMS	Force	0.000000	0.000300	YES

G<sub>5</sub>



137

H	7.640	1.605	-4.928
C	7.636	1.973	-5.961
H	8.529	3.895	-5.461
H	6.752	3.879	-5.420
H	8.523	1.574	-6.465
C	7.632	3.499	-5.945
H	6.745	1.570	-6.456
S	8.517	6.710	-8.900
S	7.612	4.123	-7.685
H	-5.251	11.103	-17.717
C	7.782	5.866	-7.543
H	-7.010	10.978	-17.536

C	-6.169	11.681	-17.569
O	4.618	6.722	-8.681
H	5.101	5.396	-6.561
S	7.063	6.803	-6.245
H	-3.968	12.847	-16.526
H	-3.802	10.443	-13.147
C	-6.076	12.495	-16.271
C	4.681	7.211	-7.568
C	5.213	6.462	-6.358
H	-5.963	11.818	-15.422
H	-1.827	9.670	-11.694
H	0.160	8.894	-10.272
H	-1.511	11.403	-13.490
H	2.169	8.105	-8.880
C	-4.853	13.457	-16.319
H	0.465	10.648	-12.049
H	4.452	9.073	-9.257
H	-4.992	14.124	-17.172
H	2.446	9.880	-10.643
O	-3.969	12.264	-14.009
C	-3.563	11.471	-12.862
O	-7.890	13.988	-16.907
C	-7.347	13.300	-16.065

C	-1.606	10.716	-11.436
C	-2.074	11.631	-12.576
C	0.380	9.939	-10.009
C	-0.109	10.859	-11.135
C	2.375	9.148	-8.609
C	3.870	9.312	-8.364
O	4.332	8.474	-7.269
C	1.880	10.082	-9.722
C	4.576	6.837	-5.023
H	4.962	6.196	-4.225
H	-3.749	15.818	-17.528
H	-4.172	11.755	-12.001
C	-4.646	14.268	-15.058
O	-7.829	13.187	-14.807
H	3.491	6.696	-5.079
H	-2.184	10.939	-10.527
C	-4.311	13.551	-13.782
H	-4.213	17.618	-19.142
H	-1.870	12.678	-12.321
H	-0.188	10.151	-9.091
H	1.834	9.355	-7.677
H	0.109	11.905	-10.871
C	-4.425	16.620	-17.250

H	4.109	10.329	-8.042
H	4.767	7.881	-4.757
H	2.101	11.124	-9.448
C	-4.675	17.649	-18.159
H	-8.625	13.757	-14.756
C	-4.760	15.611	-14.943
C	-5.002	16.641	-15.965
O	-4.316	14.055	-12.671
C	-5.503	18.718	-17.807
H	-5.697	19.516	-18.518
H	-4.677	15.998	-13.928
C	-5.804	17.745	-15.613
C	-6.064	18.764	-16.528
H	-6.232	17.791	-14.615
H	-6.697	19.599	-16.239
C	19.601	-5.660	-15.874
O	22.095	-4.821	-13.471
H	22.978	-5.204	-13.288
H	19.914	-4.239	-14.278
C	21.382	-5.771	-14.117
O	21.851	-6.858	-14.394
C	19.965	-5.319	-14.423
H	18.210	-1.595	-13.013

H	16.486	0.047	-12.027
C	18.165	-2.137	-12.064
H	18.955	-1.772	-11.405
O	18.449	-3.515	-12.421
C	18.977	-6.009	-13.436
H	14.737	1.661	-11.067
C	16.437	-0.549	-11.104
H	17.965	-5.698	-13.720
H	17.193	-0.130	-10.425
H	19.041	-7.085	-13.603
C	16.790	-2.008	-11.422
H	10.730	6.985	-9.594
C	19.057	-4.287	-11.495
O	10.445	4.528	-10.409
H	12.961	3.259	-10.149
H	16.040	-2.435	-12.102
C	19.228	-5.698	-11.977
C	14.681	1.058	-10.149
H	15.428	1.476	-9.459
O	19.394	-3.874	-10.397
C	15.046	-0.396	-10.474
C	10.354	6.331	-8.799
C	10.650	4.909	-9.273

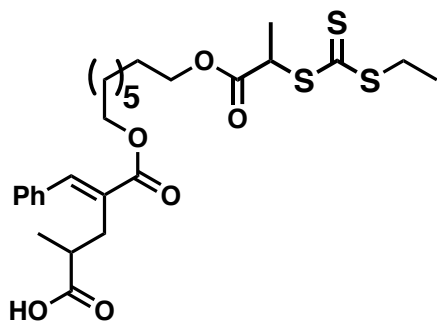
H	14.293	-0.815	-11.157
C	12.911	2.663	-9.229
H	12.039	6.576	-7.467
H	16.766	-2.604	-10.501
H	13.633	3.095	-8.523
C	19.631	-6.578	-11.032
C	13.283	1.206	-9.535
C	10.955	6.734	-7.458
H	12.538	0.779	-10.222
H	10.765	7.794	-7.266
C	19.838	-8.034	-11.110
O	11.182	4.151	-8.300
H	19.860	-6.145	-10.059
H	14.997	-0.998	-9.555
C	11.511	2.776	-8.637
H	18.116	-8.516	-12.331
C	18.988	-8.907	-11.816
H	10.752	2.391	-9.323
H	21.557	-7.933	-9.809
C	20.909	-8.590	-10.384
H	13.226	0.612	-8.611
C	19.227	-10.282	-11.823
H	10.534	6.149	-6.635

C	21.155	-9.962	-10.404
C	20.315	-10.813	-11.127
H	18.554	-10.939	-12.367
H	21.996	-10.367	-9.847
H	11.439	2.241	-7.687
H	20.500	-11.884	-11.136
H	-6.308	12.337	-18.434
H	20.278	-5.164	-16.578
H	18.581	-5.328	-16.094
H	19.658	-6.739	-16.051

	1	2	3
Frequencies --	2.6145	6.7761	8.7689
Red. masses --	7.3947	5.8420	5.8579
Zero-point correction=			1.156650 (Hartree/Particle)
Thermal correction to Energy=			1.231449
Thermal correction to Enthalpy=			1.232393
Thermal correction to Gibbs Free Energy=			1.022637
Sum of electronic and zero-point Energies=			-4082.410681
Sum of electronic and thermal Energies=			-4082.335882
Sum of electronic and thermal Enthalpies=			-4082.334938
Sum of electronic and thermal Free Energies=			-4082.544694

	Item	Value	Threshold	Converged?
Maximum	Force	0.000009	0.000450	YES
RMS	Force	0.000001	0.000300	YES

### G<sub>5</sub>\_CTA



74

H	6.959	1.336	-6.826
C	7.425	1.864	-7.666
H	7.028	3.856	-6.886
H	5.723	3.185	-7.897
H	8.504	1.916	-7.484
C	6.806	3.255	-7.772
H	7.251	1.269	-8.569
S	8.940	6.634	-9.745
S	7.524	4.120	-9.247
H	-6.247	12.003	-17.477
C	7.817	5.802	-8.846
H	-7.963	11.778	-17.091

C	-7.151	12.514	-17.129
O	4.424	6.550	-9.794
H	5.098	5.183	-7.778
S	7.051	6.632	-7.471
H	-4.850	13.597	-16.189
H	-4.292	10.809	-13.164
C	-6.906	13.139	-15.750
C	4.625	7.031	-8.696
C	5.225	6.237	-7.539
H	-6.669	12.354	-15.029
H	-2.191	9.903	-11.997
H	-0.087	8.992	-10.855
H	-2.052	11.807	-13.649
H	2.021	8.074	-9.712
C	-5.720	14.145	-15.811
H	0.063	10.868	-12.535
H	4.290	8.918	-10.341
H	-5.970	14.905	-16.553
H	2.170	9.912	-11.438
O	-4.551	12.718	-13.777
C	-4.018	11.798	-12.788
O	-8.830	14.618	-15.933
C	-8.155	13.857	-15.269

C -1.920 10.918 -11.674  
C -2.506 11.939 -12.659  
C 0.200 10.010 -10.554  
C -0.394 11.018 -11.545  
C 2.314 9.095 -9.440  
C 3.834 9.179 -9.383  
O 4.378 8.302 -8.355  
C 1.728 10.093 -10.448  
C 4.627 6.553 -6.168  
H 5.032 5.874 -5.412  
H -4.797 16.668 -16.828  
H -4.522 11.972 -11.835  
C -5.389 14.806 -14.490  
O -8.446 13.571 -13.980  
H 3.541 6.413 -6.208  
H -2.379 11.060 -10.685  
C -4.903 13.953 -13.355  
H -5.480 18.622 -18.162  
H -2.267 12.957 -12.326  
H -0.243 10.173 -9.560  
H 1.909 9.294 -8.439  
H -0.122 12.038 -11.234  
C -5.463 17.405 -16.390

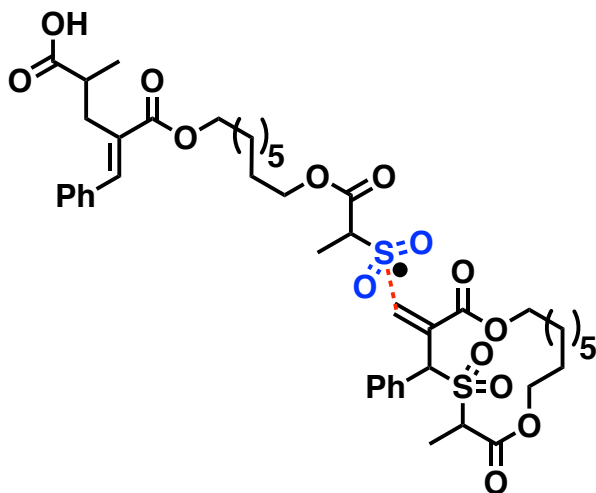
H	4.167	10.176	-9.085
H	4.824	7.584	-5.861
H	2.020	11.113	-10.161
C	-5.836	18.520	-17.140
H	-9.238	14.097	-13.743
C	-5.521	16.120	-14.200
C	-5.901	17.253	-15.060
O	-4.804	14.316	-12.195
C	-6.653	19.506	-16.581
H	-6.944	20.373	-17.169
H	-5.335	16.389	-13.161
C	-6.693	18.274	-14.500
C	-7.078	19.381	-15.255
H	-7.016	18.188	-13.465
H	-7.701	20.149	-14.806
H	-7.421	13.279	-17.864

	1	2	3
Frequencies --	10.5011	12.3606	13.8590
Red. masses --	5.9873	6.2147	6.5414
Zero-point correction=			0.617059 (Hartree/Particle)
Thermal correction to Energy=			0.658049
Thermal correction to Enthalpy=			0.658993

Thermal correction to Gibbs Free Energy=	0.533006
Sum of electronic and zero-point Energies=	-2697.129093
Sum of electronic and thermal Energies=	-2697.088103
Sum of electronic and thermal Enthalpies=	-2697.087159
Sum of electronic and thermal Free Energies=	-2697.213146

	Item	Value	Threshold	Converged?
Maximum	Force	0.000010	0.000450	YES
RMS	Force	0.000002	0.000300	YES

TS<sub>6</sub>



122

H	2.108	2.285	-5.385
O	0.516	0.091	-3.725
C	1.326	2.380	-6.143

S	-0.020	0.153	-5.110
H	1.287	3.426	-6.464
C	-0.038	1.990	-5.594
H	-0.814	2.051	-6.363
O	0.286	3.556	-3.779
H	-1.485	3.328	-2.135
C	-2.278	3.232	-2.881
H	-3.039	2.543	-2.508
H	-2.094	5.234	-3.645
C	-2.881	4.582	-3.245
C	-3.543	5.247	-2.030
H	-4.318	4.579	-1.628
H	-3.621	4.438	-4.043
H	-4.910	6.485	-3.159
H	-2.797	5.371	-1.232
H	-4.088	7.402	-0.347
H	-3.390	7.277	-2.760
C	-4.167	6.610	-2.358
C	-4.832	7.278	-1.148
H	-5.608	6.611	-0.745
H	-5.369	9.447	0.540
H	-4.680	9.308	-1.878
C	-5.455	8.641	-1.473

C	-6.112	9.308	-0.257
H	-6.900	8.659	0.145
H	-6.203	8.519	-2.270
H	-5.948	11.344	-0.994
H	-7.012	12.525	2.844
C	-6.712	10.662	-0.613
H	-5.949	14.742	2.500
O	-7.242	11.335	0.560
C	-8.020	12.915	2.666
H	-7.508	10.567	-1.355
C	-6.934	15.185	2.317
C	-8.525	11.082	0.899
H	-8.397	13.284	3.621
C	-8.923	11.818	2.145
H	-7.481	13.796	0.754
H	-7.325	15.565	3.266
H	-6.802	16.035	1.638
C	-7.878	14.138	1.712
O	-9.246	10.326	0.268
C	-10.107	11.439	2.676
H	-9.042	11.966	5.189
C	-10.114	12.119	5.122
H	-10.664	10.705	2.096

C	-10.784	11.879	3.907
C	-10.822	12.507	6.261
H	-10.287	12.678	7.191
C	-12.187	12.004	3.884
C	-9.247	14.746	1.465
C	-12.209	12.662	6.211
H	-12.723	11.794	2.962
C	-12.891	12.406	5.018
H	-12.757	12.966	7.099
O	-9.736	14.432	0.244
H	-13.972	12.509	4.974
O	-9.868	15.430	2.256
H	-10.627	14.833	0.182
C	-0.452	2.799	-4.373
O	-1.733	2.558	-4.054
H	1.583	1.764	-7.007
C	-2.329	-0.358	-5.117
O	0.689	-0.547	-6.205
H	-2.490	0.527	-5.721
H	-2.417	-0.220	-4.046
H	-3.347	-1.430	-0.379
C	-3.849	-1.819	-1.261
H	-2.046	-1.851	-2.429

H	-5.790	-1.901	-0.322
C	-3.113	-2.053	-2.424
C	-5.220	-2.086	-1.229
O	-0.357	-3.072	-4.173
C	-3.742	-2.561	-3.571
C	-5.851	-2.597	-2.364
C	-2.651	-1.587	-5.677
O	1.117	-5.540	-5.944
S	-1.514	-3.930	-4.506
C	-5.115	-2.838	-3.526
C	-3.002	-2.815	-4.872
H	-6.916	-2.813	-2.348
H	-3.179	0.599	-9.284
O	-2.497	-0.572	-7.793
O	-1.949	-4.946	-3.528
H	-1.205	-6.825	-5.348
C	-2.831	-1.701	-7.154
C	0.321	-4.734	-6.381
C	-2.799	-0.422	-9.213
C	-1.183	-4.799	-6.132
H	-5.611	-3.240	-4.406
H	-3.617	-3.458	-5.509
C	-1.715	-6.226	-6.104

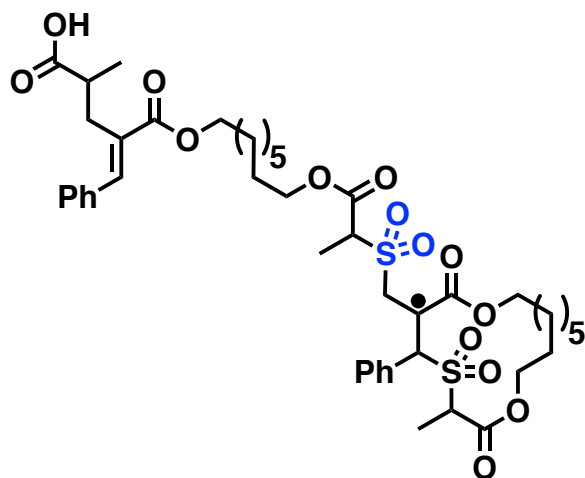
H	2.058	-2.338	-7.545
H	2.637	-3.771	-6.669
O	-3.265	-2.705	-7.705
H	-3.597	-1.119	-9.479
H	-2.790	-6.241	-5.906
H	-0.695	-0.192	-9.544
C	2.002	-3.425	-7.487
O	0.611	-3.679	-7.144
C	-1.558	-0.598	-10.087
H	-1.544	-6.681	-7.086
H	-1.700	-4.196	-6.880
H	-1.693	0.040	-10.970
H	1.188	-1.715	-9.557
H	-1.295	-2.718	-9.701
C	2.378	-4.098	-8.805
C	-1.289	-2.035	-10.559
H	3.382	-3.740	-9.073
C	1.263	-2.389	-10.421
H	2.466	-5.179	-8.638
H	-2.125	-2.345	-11.200
H	0.405	-4.224	-9.653
C	1.391	-3.849	-9.956
C	0.039	-2.172	-11.332

H 2.182 -2.101 -10.951  
H 0.186 -1.274 -11.948  
H 1.695 -4.464 -10.814  
H -0.028 -3.013 -12.036

	1	2	3
Frequencies --	-260.0869	4.0833	7.6738
Red. masses --	10.5793	6.0027	5.7919
Zero-point correction=			1.017890 (Hartree/Particle)
Thermal correction to Energy=			1.082567
Thermal correction to Enthalpy=			1.083511
Thermal correction to Gibbs Free Energy=			0.904098
Sum of electronic and zero-point Energies=			-3599.993797
Sum of electronic and thermal Energies=			-3599.929120
Sum of electronic and thermal Enthalpies=			-3599.928176
Sum of electronic and thermal Free Energies=			-3600.107589

	Item	Value	Threshold	Converged?
Maximum	Force	0.000017	0.000450	YES
RMS	Force	0.000001	0.000300	YES

G<sub>6</sub>



122

H	1.727	1.989	-5.329
O	0.190	-0.038	-3.448
C	0.912	2.048	-6.055
S	-0.373	-0.067	-4.815
H	0.865	3.074	-6.432
C	-0.429	1.697	-5.419
H	-1.233	1.716	-6.160
O	-0.019	3.440	-3.789
H	-1.673	3.406	-2.045
C	-2.518	3.188	-2.702
H	-3.210	2.516	-2.188
H	-2.507	5.083	-3.719
C	-3.219	4.457	-3.167

C	-3.799	5.243	-1.983
H	-4.479	4.593	-1.414
H	-4.022	4.184	-3.865
H	-5.369	6.233	-3.093
H	-2.986	5.517	-1.296
H	-4.306	7.581	-0.549
H	-3.876	7.158	-2.987
C	-4.552	6.510	-2.411
C	-5.125	7.296	-1.225
H	-5.789	6.641	-0.643
H	-5.662	9.624	0.233
H	-5.236	9.218	-2.216
C	-5.898	8.555	-1.641
C	-6.473	9.321	-0.442
H	-7.143	8.667	0.130
H	-6.717	8.271	-2.318
H	-6.598	11.265	-1.407
H	-7.368	12.678	2.359
C	-7.244	10.563	-0.874
H	-6.577	14.990	1.888
O	-7.723	11.315	0.272
C	-8.420	12.983	2.325
H	-8.096	10.307	-1.509

C	-7.613	15.326	1.767
C	-8.910	10.946	0.803
H	-8.672	13.358	3.319
C	-9.263	11.768	2.006
H	-8.136	13.790	0.340
H	-7.961	15.726	2.725
H	-7.622	16.140	1.034
C	-8.493	14.159	1.305
O	-9.588	10.038	0.351
C	-10.270	11.263	2.758
H	-11.260	9.673	4.603
C	-11.344	10.717	4.897
H	-10.677	10.320	2.398
C	-10.863	11.716	4.025
C	-11.910	11.043	6.128
H	-12.262	10.254	6.786
C	-11.014	13.062	4.413
C	-9.926	14.620	1.114
C	-12.033	12.383	6.507
H	-10.721	13.862	3.743
C	-11.592	13.386	5.641
H	-12.481	12.642	7.462
O	-10.496	14.080	0.015

H	-11.708	14.432	5.916
O	-10.531	15.381	1.847
H	-11.422	14.399	-0.013
C	-0.780	2.621	-4.257
O	-2.037	2.406	-3.835
H	1.127	1.380	-6.891
C	-2.176	-0.582	-4.670
O	0.296	-0.864	-5.857
H	-2.738	0.321	-4.924
H	-2.300	-0.770	-3.605
H	-3.860	-2.342	-0.313
C	-4.284	-2.510	-1.299
H	-2.359	-2.596	-2.249
H	-6.328	-2.477	-0.608
C	-3.434	-2.650	-2.398
C	-5.668	-2.589	-1.465
O	-0.565	-3.574	-3.990
C	-3.962	-2.875	-3.678
C	-6.201	-2.815	-2.736
C	-2.595	-1.733	-5.508
O	1.023	-5.650	-6.008
S	-1.721	-4.282	-4.581
C	-5.353	-2.962	-3.834

C	-3.102	-3.014	-4.923
H	-7.277	-2.883	-2.874
H	-2.981	1.088	-8.686
O	-2.420	-0.333	-7.375
O	-2.328	-5.399	-3.831
H	-1.331	-7.024	-5.816
C	-2.743	-1.572	-6.967
C	0.251	-4.815	-6.433
C	-2.650	0.051	-8.766
C	-1.266	-4.902	-6.289
H	-5.772	-3.142	-4.821
H	-3.681	-3.525	-5.697
C	-1.788	-6.317	-6.512
H	2.060	-2.353	-7.257
H	2.591	-3.923	-6.613
O	-3.148	-2.461	-7.709
H	-3.467	-0.554	-9.165
H	-2.874	-6.360	-6.405
H	-0.528	0.244	-9.004
C	1.980	-3.434	-7.375
O	0.578	-3.712	-7.108
C	-1.388	-0.046	-9.622
H	-1.535	-6.620	-7.534

H -1.736 -4.192 -6.974  
 H -1.473 0.720 -10.404  
 H 1.298 -1.367 -9.167  
 H -1.210 -2.208 -9.550  
 C 2.364 -3.898 -8.777  
 C -1.147 -1.407 -10.295  
 H 3.390 -3.551 -8.960  
 C 1.380 -1.899 -10.125  
 H 2.398 -4.996 -8.786  
 H -1.968 -1.586 -11.003  
 H 0.413 -3.786 -9.676  
 C 1.423 -3.418 -9.894  
 C 0.206 -1.480 -11.032  
 H 2.332 -1.579 -10.570  
 H 0.417 -0.502 -11.489  
 H 1.724 -3.905 -10.832  
 H 0.134 -2.192 -11.865

	1	2	3
Frequencies --	5.1527	10.1274	13.2199
Red. masses --	6.4312	5.7734	5.9699
Zero-point correction=			1.020096 (Hartree/Particle)
Thermal correction to Energy=			1.084650

Thermal correction to Enthalpy=	1.085595
Thermal correction to Gibbs Free Energy=	0.907406
Sum of electronic and zero-point Energies=	-3600.003741
Sum of electronic and thermal Energies=	-3599.939186
Sum of electronic and thermal Enthalpies=	-3599.938241
Sum of electronic and thermal Free Energies=	-3600.116430

	Item	Value	Threshold	Converged?
Maximum	Force	0.000005	0.000450	YES
RMS	Force	0.000001	0.000300	YES

## SO<sub>2</sub>

3

O 13.744 16.175 -1.961

S 12.963 14.984 -1.616

O 13.498 13.672 -1.987

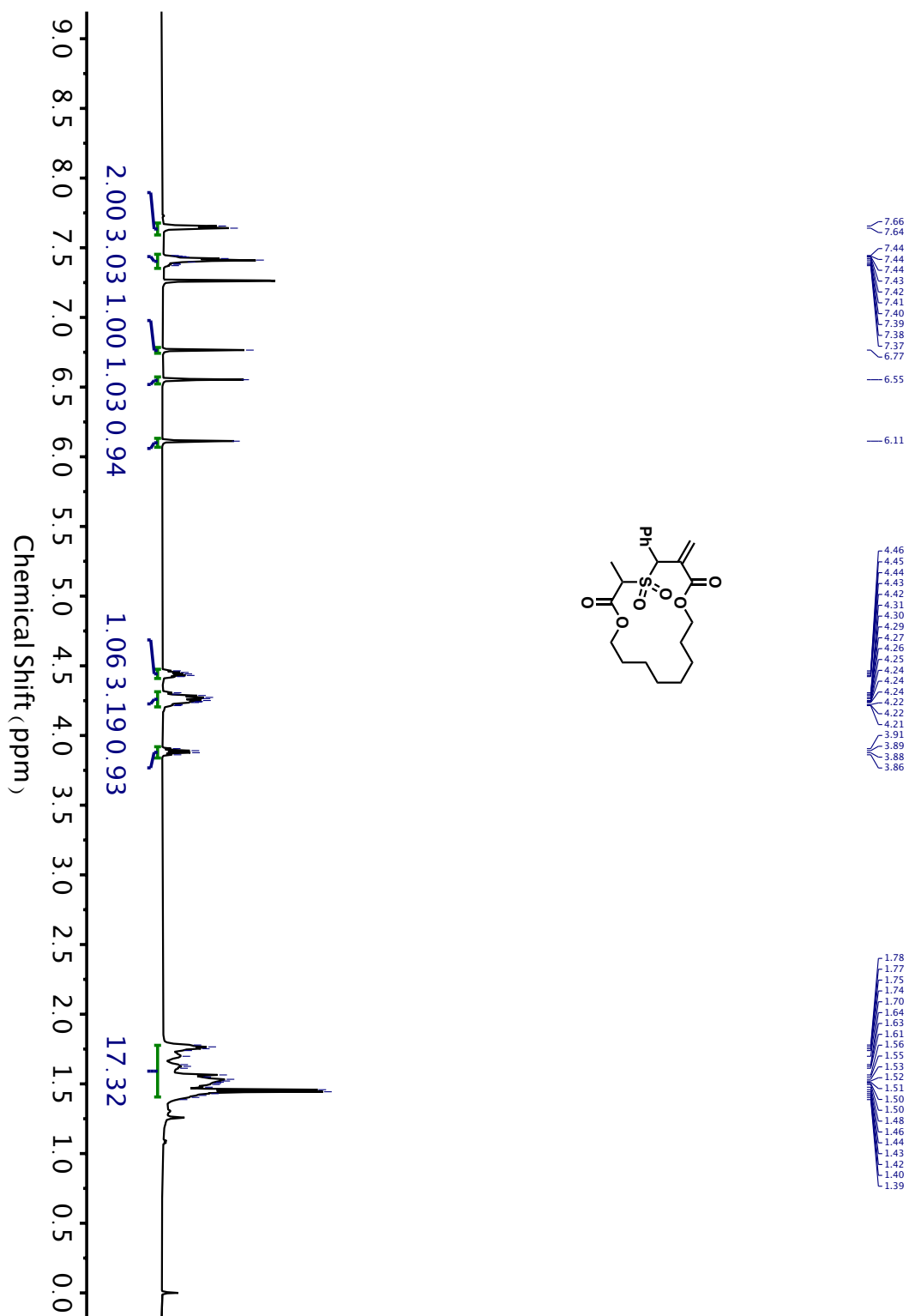
	1	2	3
Frequencies --	500.1737	1138.9015	1320.6621
Red. masses --	18.5441	18.0217	20.2989
Zero-point correction=	0.006743 (Hartree/Particle)		
Thermal correction to Energy=	0.009831		

Thermal correction to Enthalpy=	0.010775
Thermal correction to Gibbs Free Energy=	-0.018145
Sum of electronic and zero-point Energies=	-548.588930
Sum of electronic and thermal Energies=	-548.585842
Sum of electronic and thermal Enthalpies=	-548.584897
Sum of electronic and thermal Free Energies=	-548.613817

	Item	Value	Threshold	Converged?
Maximum	Force	0.000295	0.000450	YES
RMS	Force	0.000211	0.000300	YES

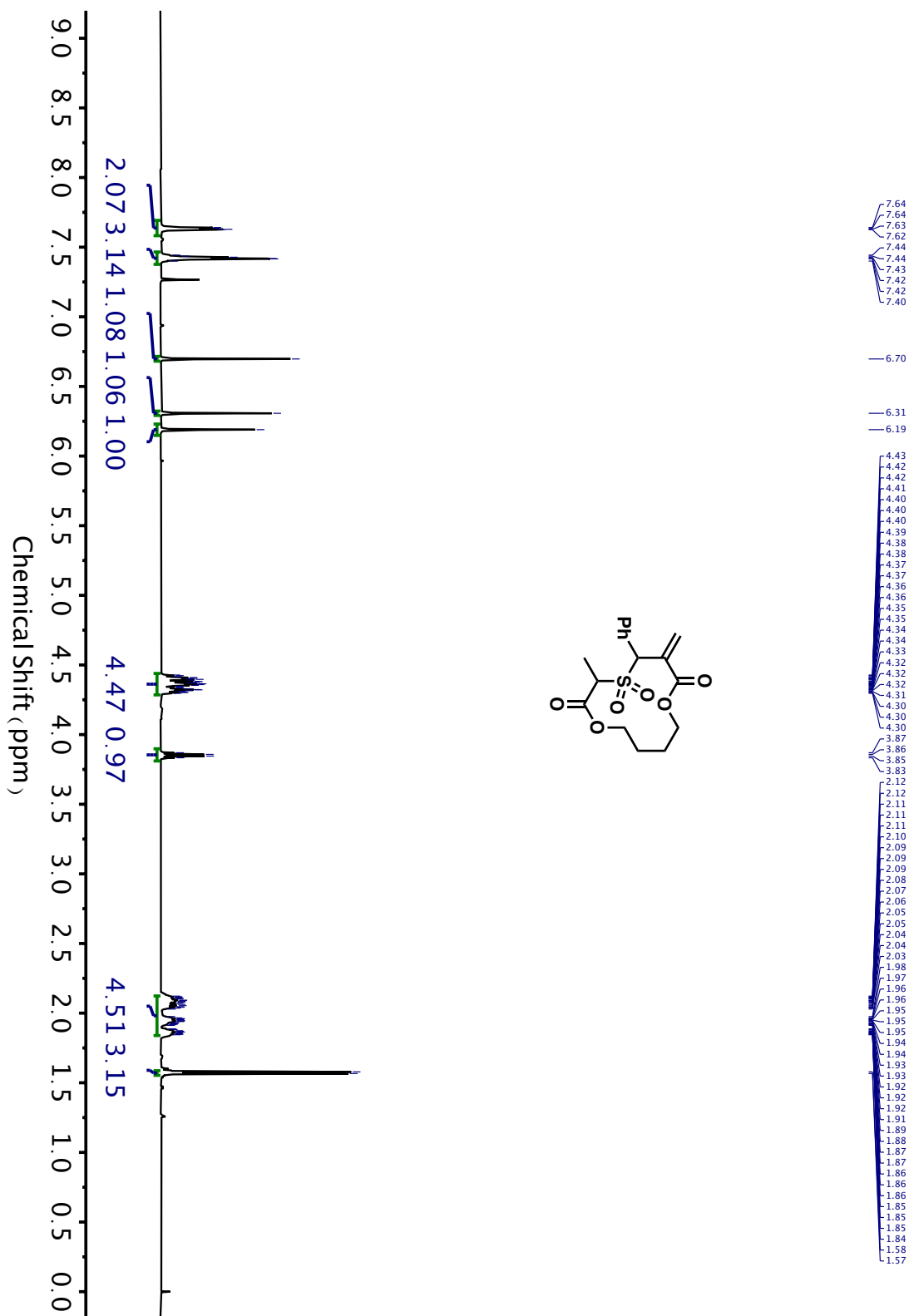
# NMR Spectra of Monomers and Polymers

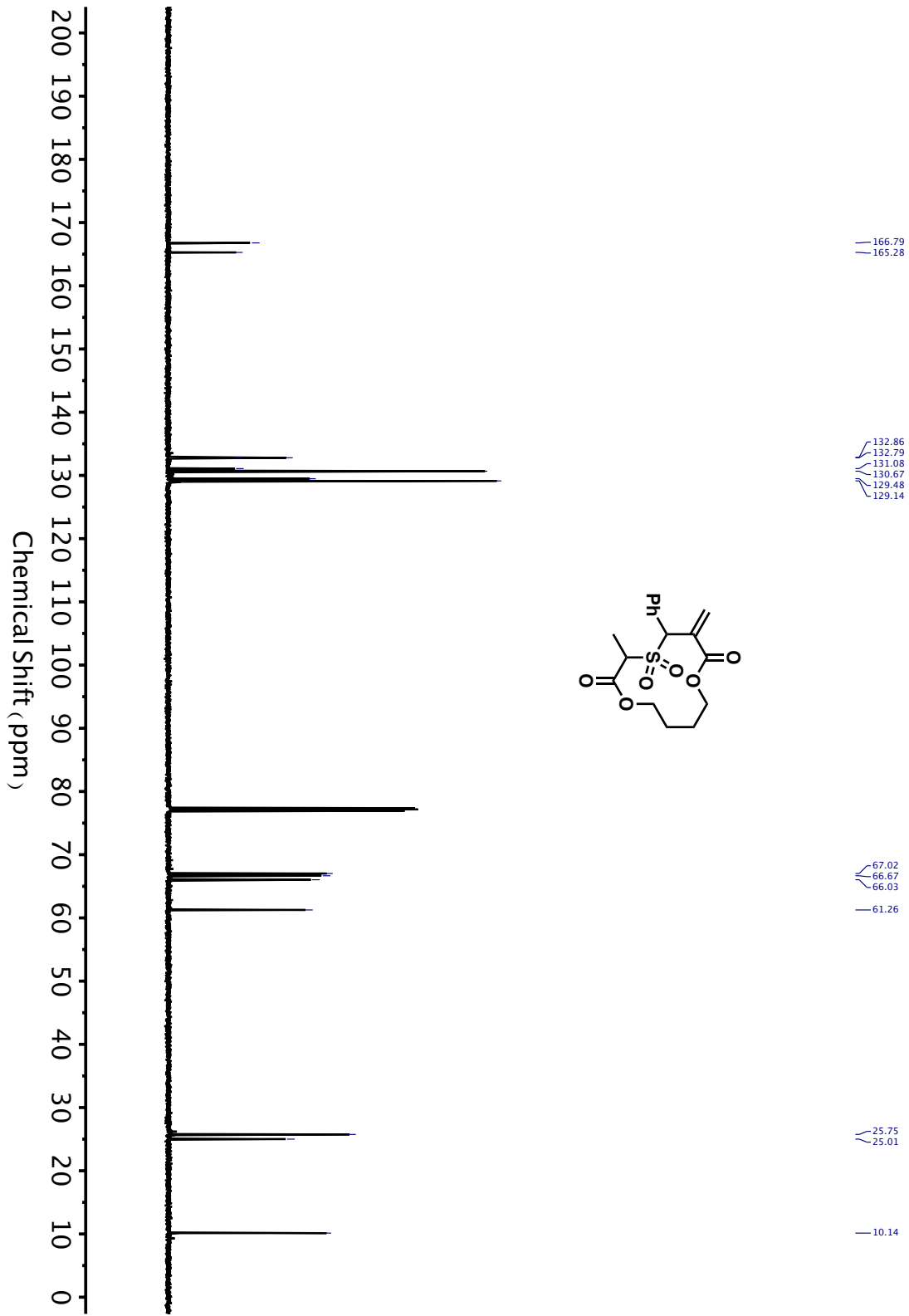
$^1\text{H}$  and  $^{13}\text{C}$  NMR spectra of **1**



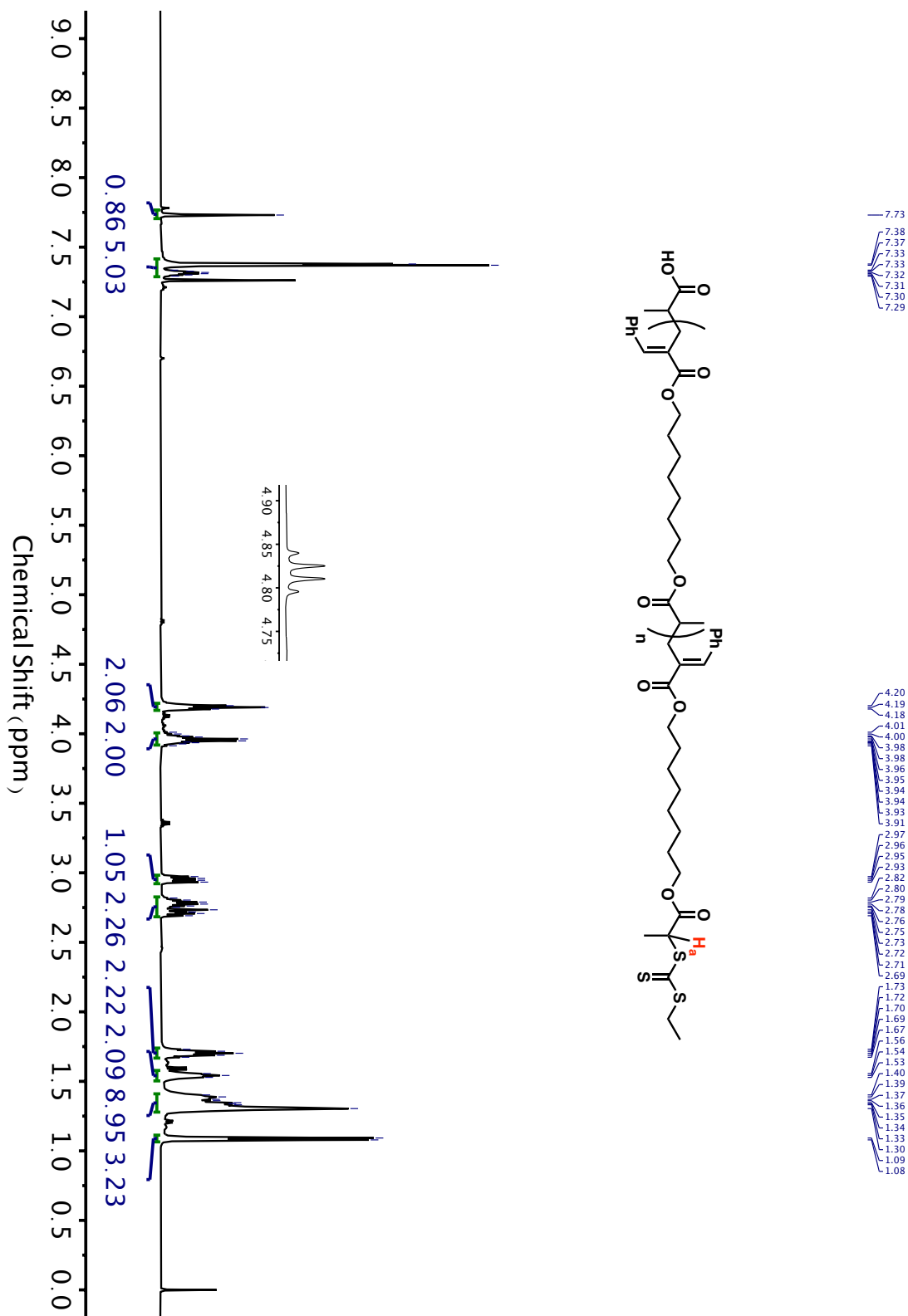


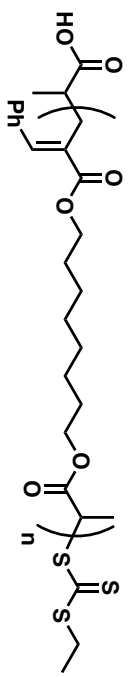
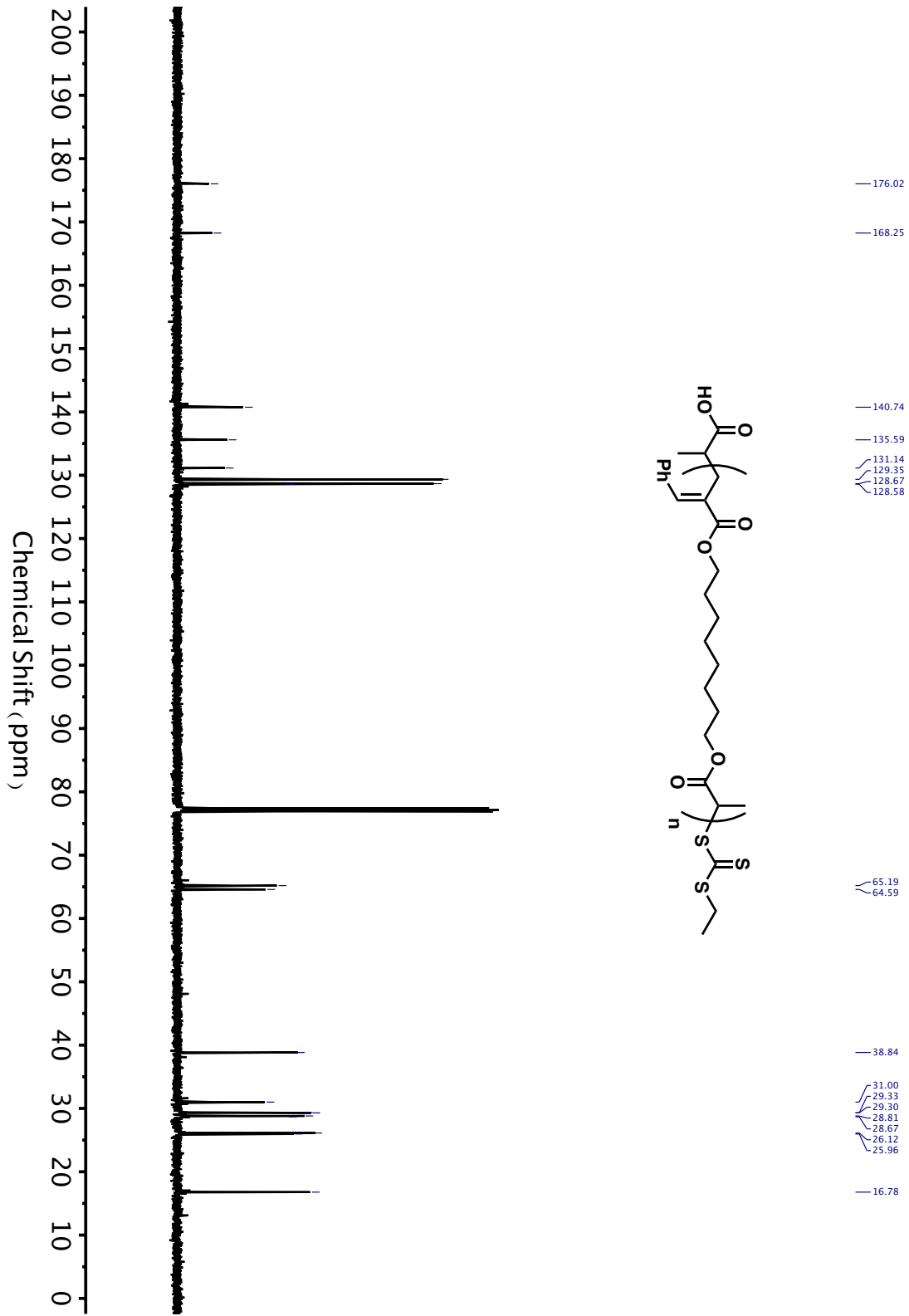
$^1\text{H}$  and  $^{13}\text{C}$  NMR spectra of 2



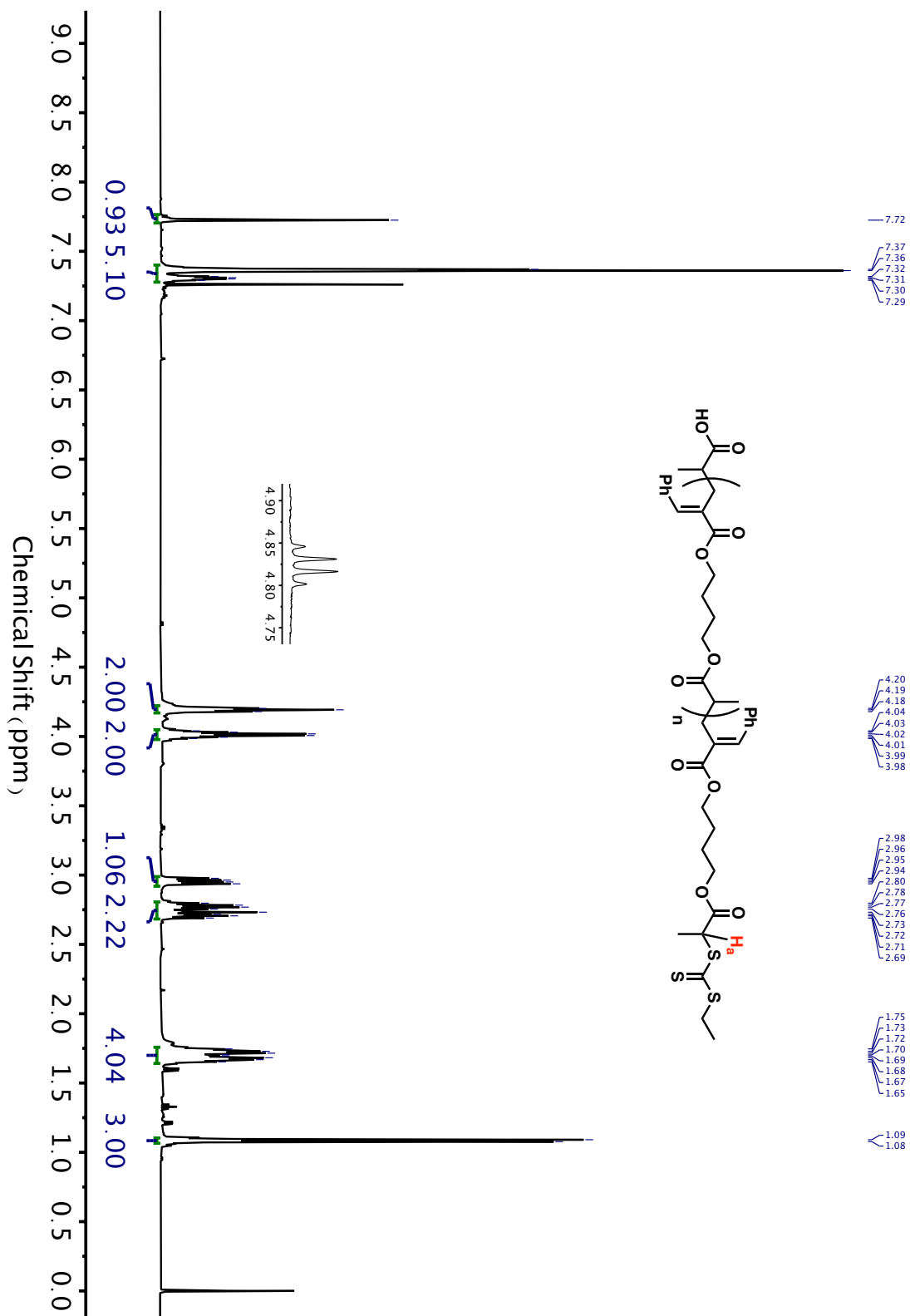


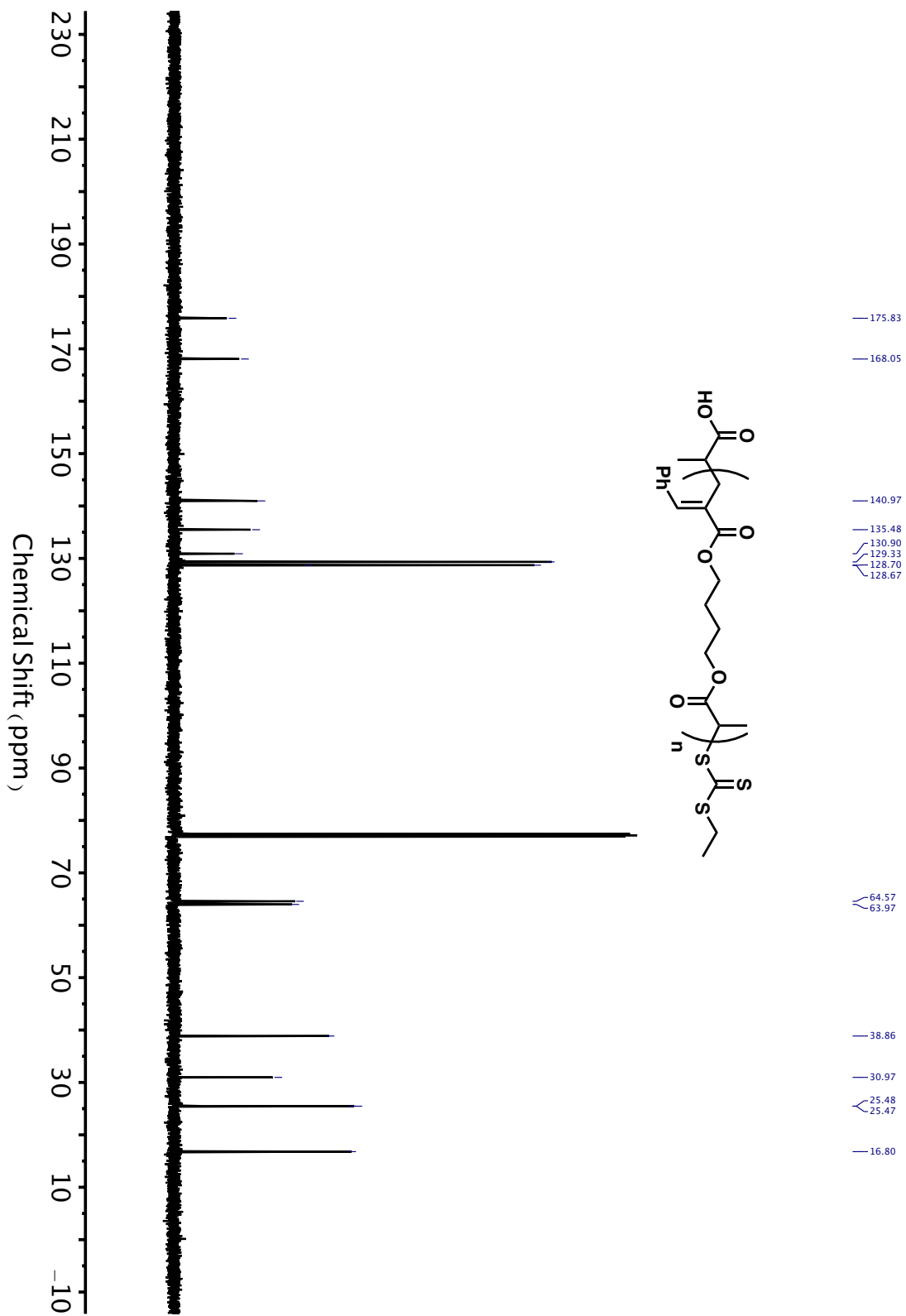
$^1\text{H}$  and  $^{13}\text{C}$  NMR spectra of **P-1**



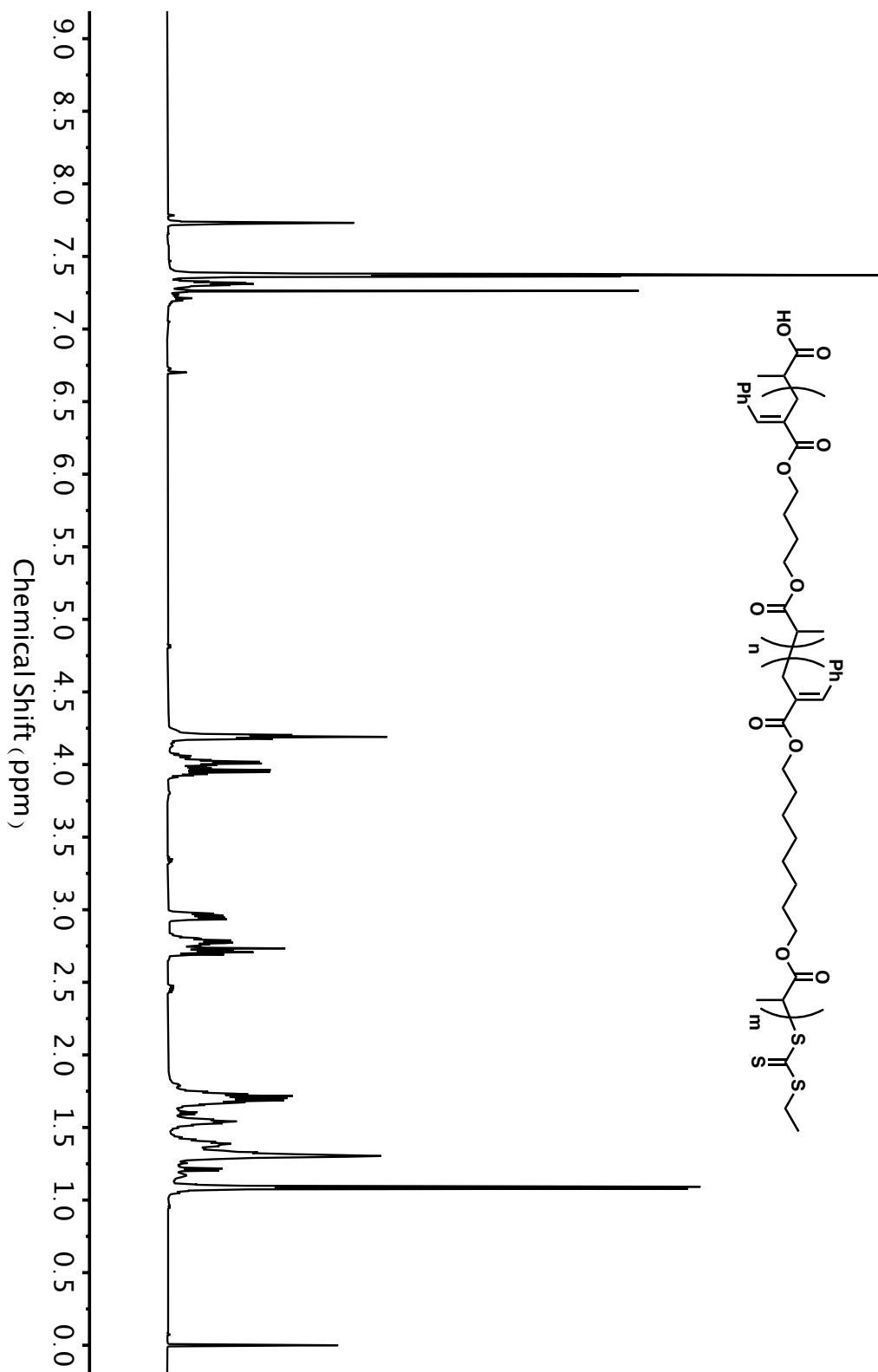


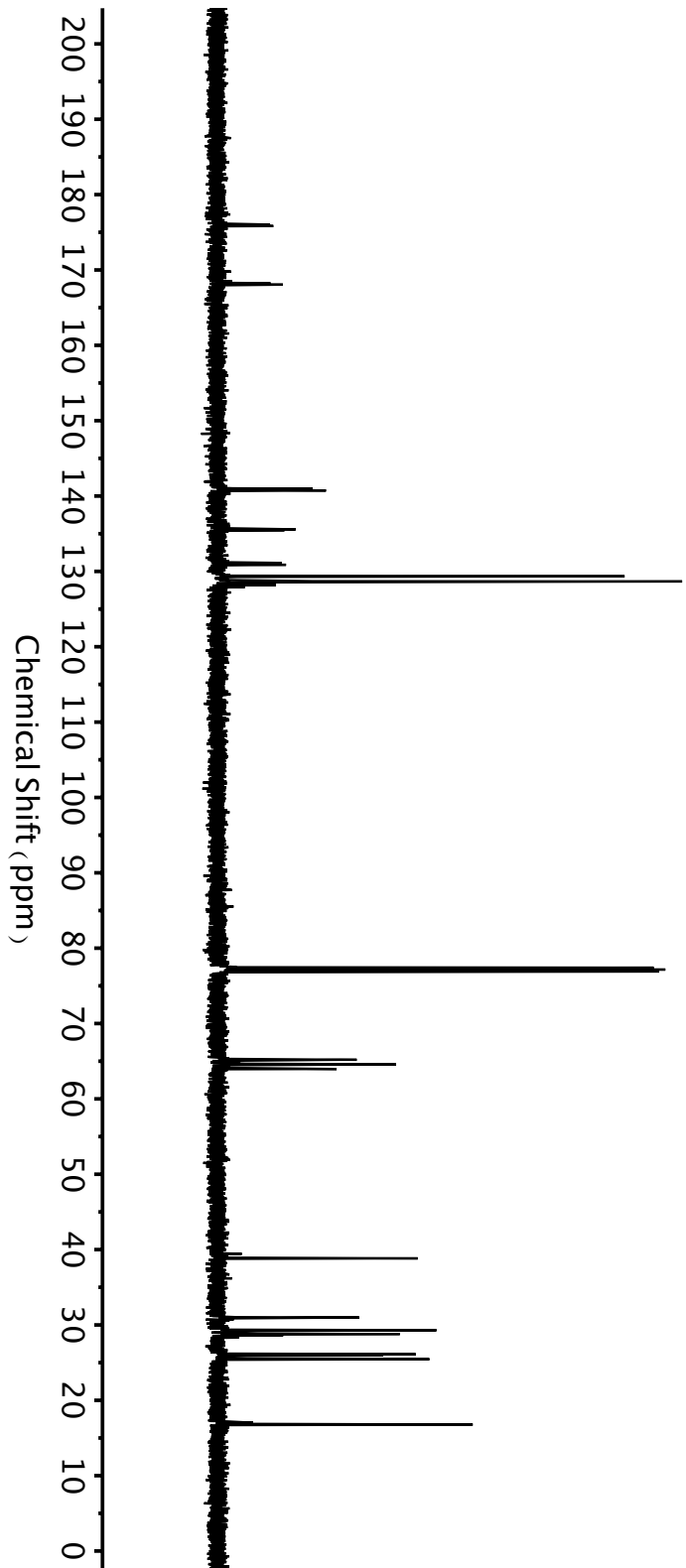
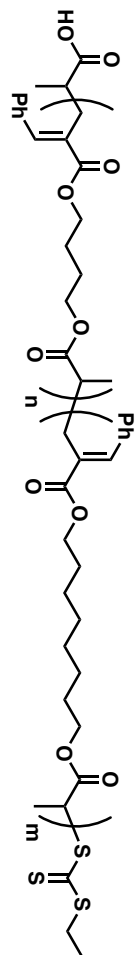
$^1\text{H}$  and  $^{13}\text{C}$  NMR spectra of P-2



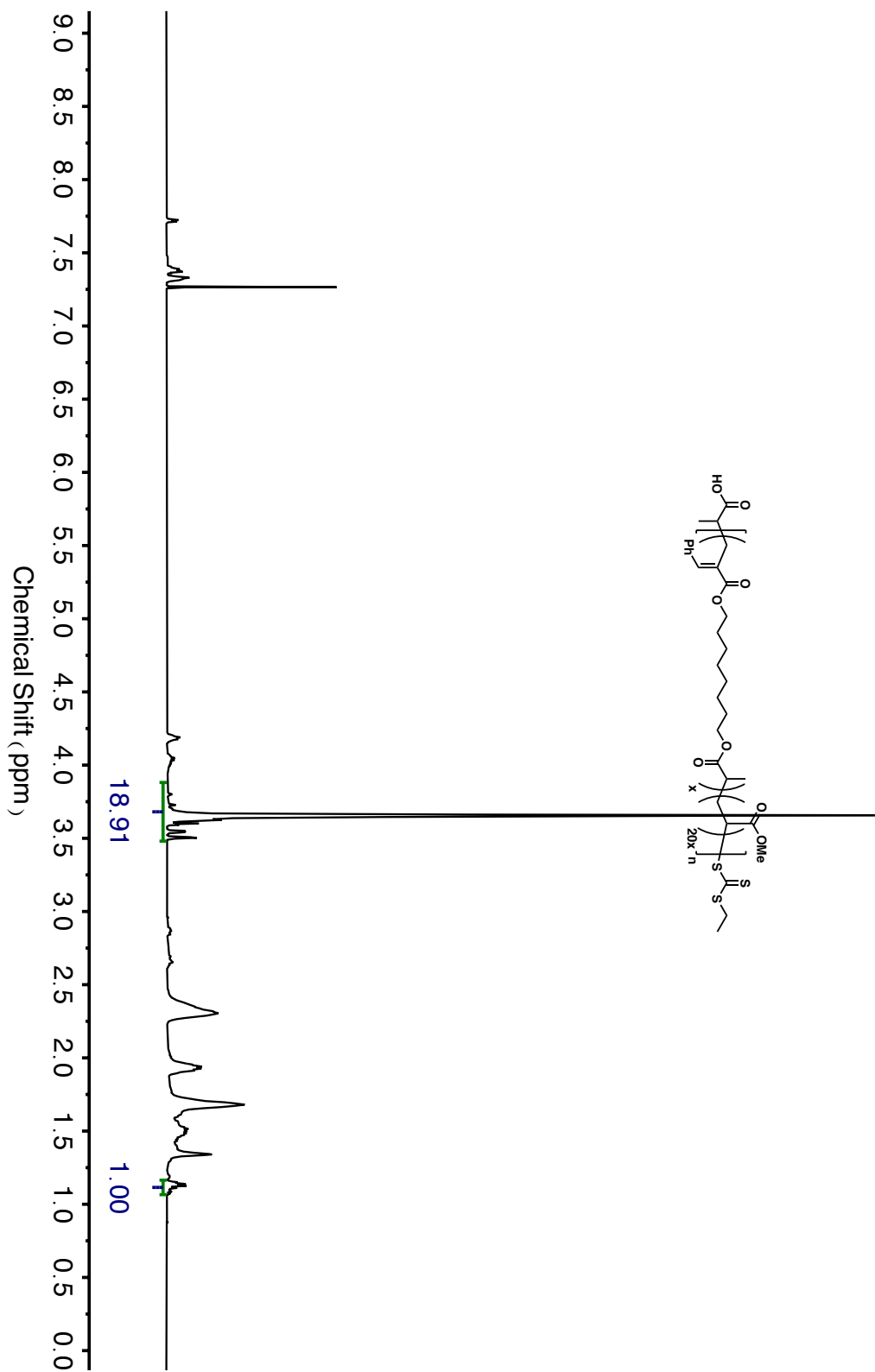


$^1\text{H}$  and  $^{13}\text{C}$  NMR spectra of P-2-*b*-P-1



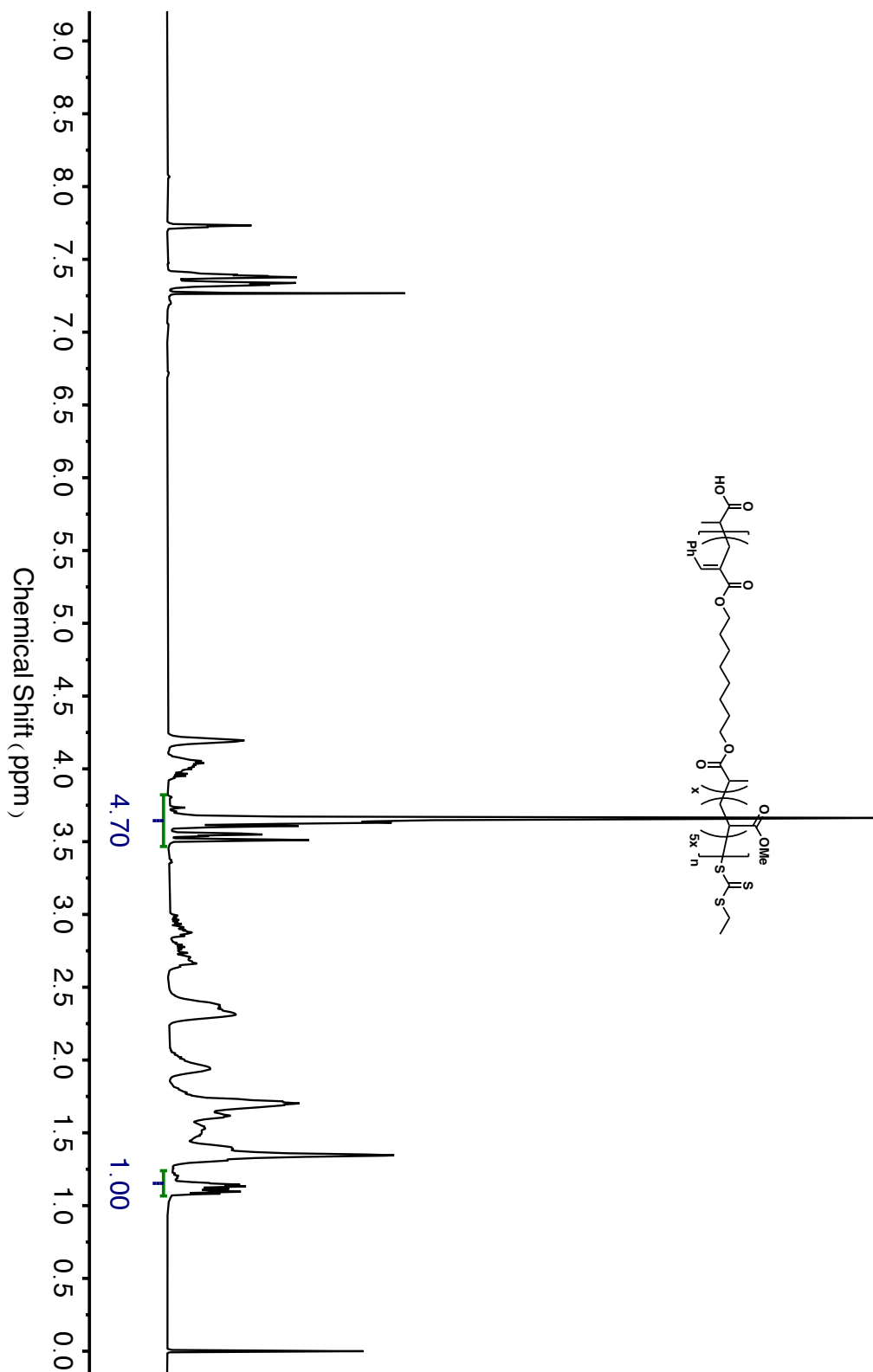


$^1\text{H}$  NMR spectrum of **P-1-co-MA** at  $f_1^0 = 0.05$ .

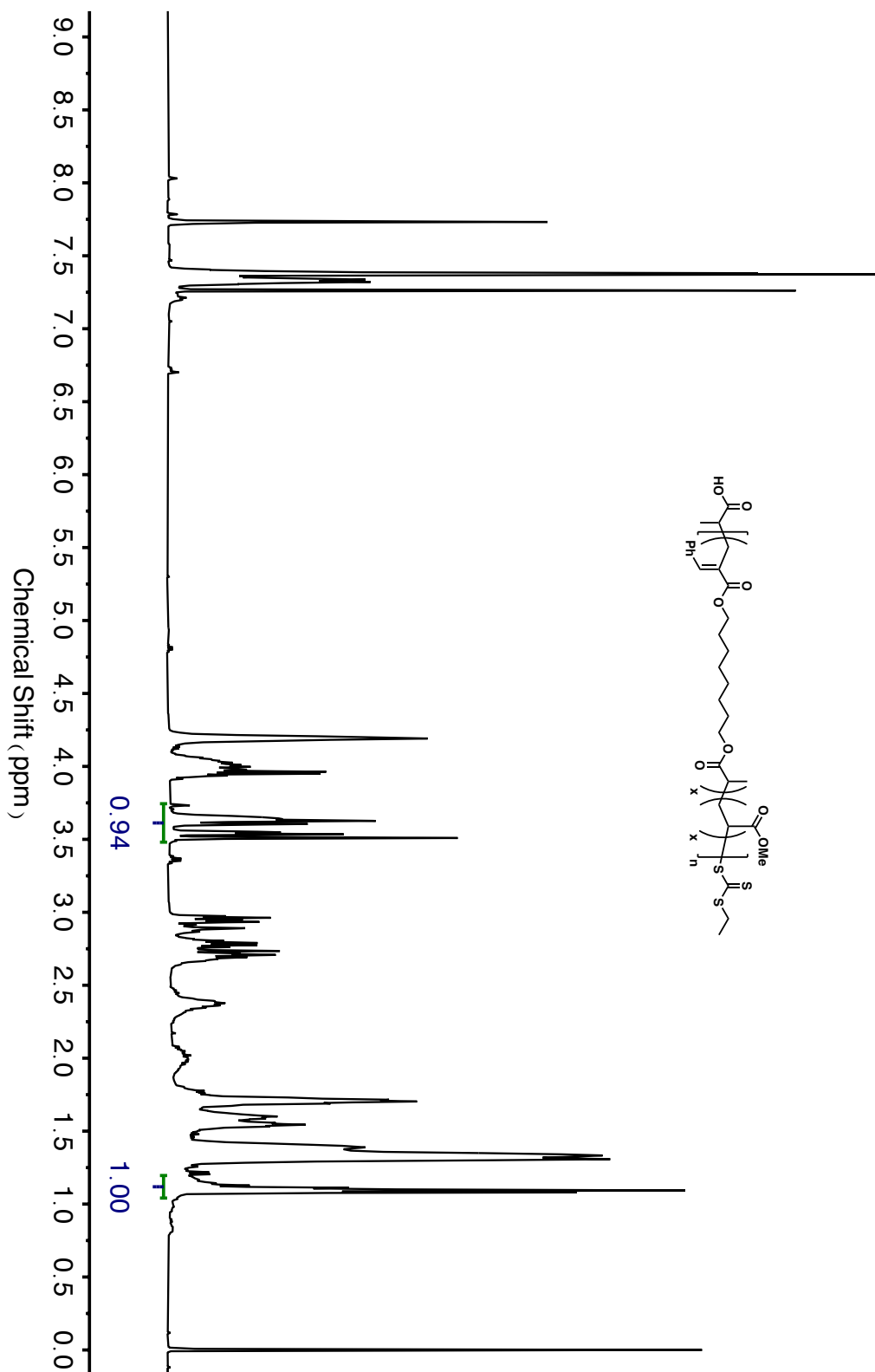




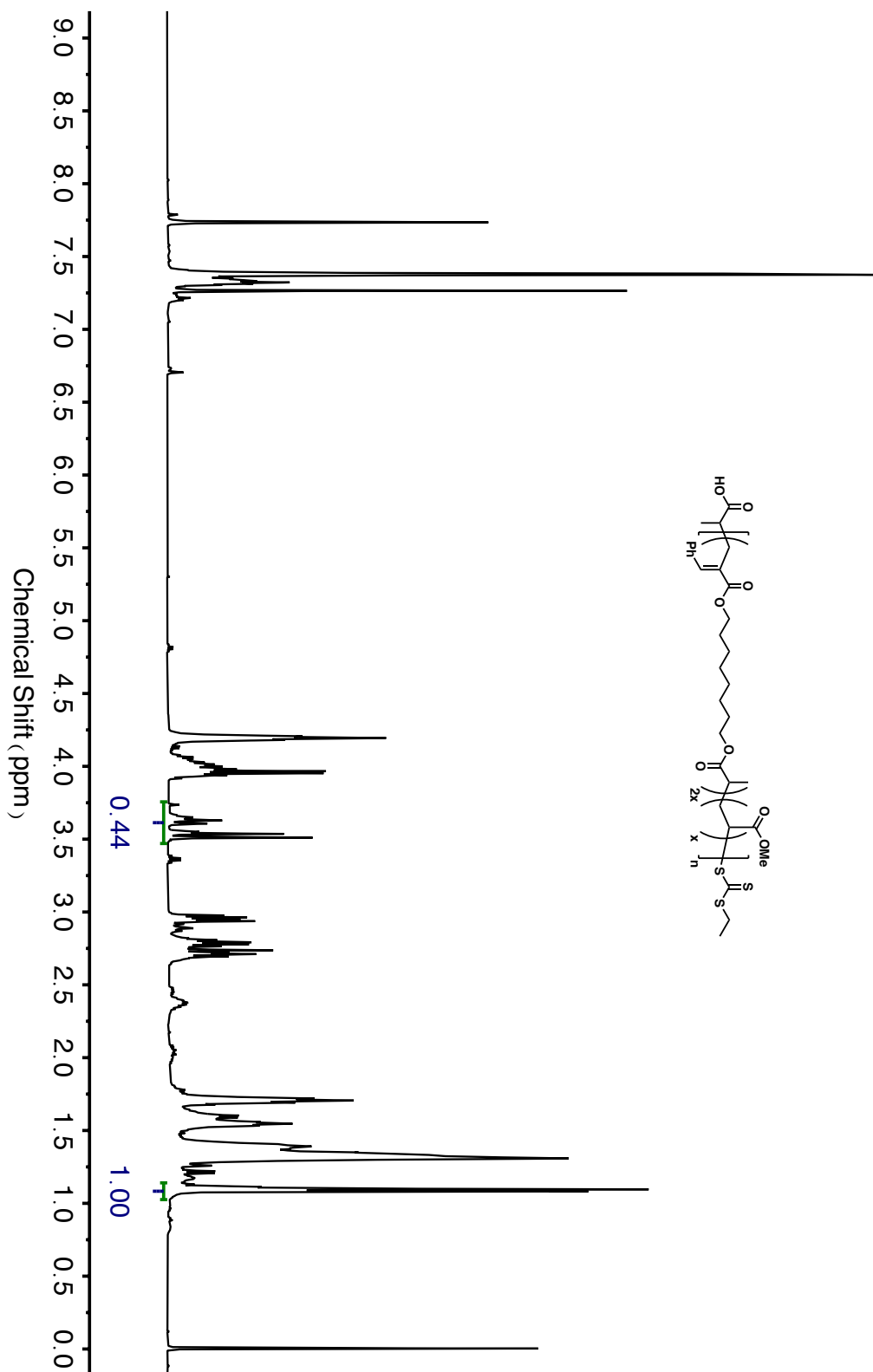
$^1\text{H}$  NMR spectrum of **P-1-co-MA** at  $f_1^0 = 0.17$ .



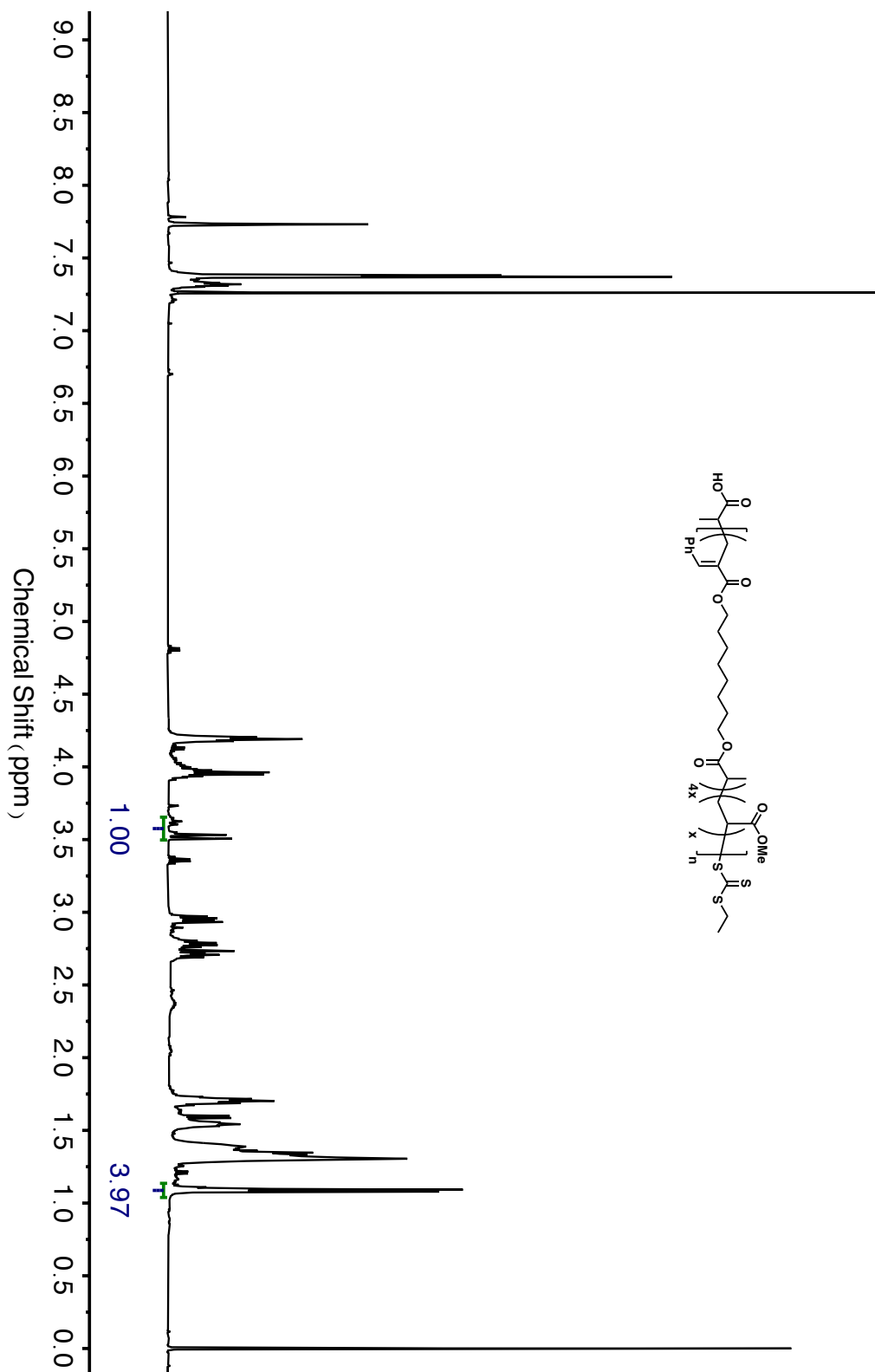
$^1\text{H}$  NMR spectrum of **P-1-co-MA** at  $f_1^0 = 0.50$ .



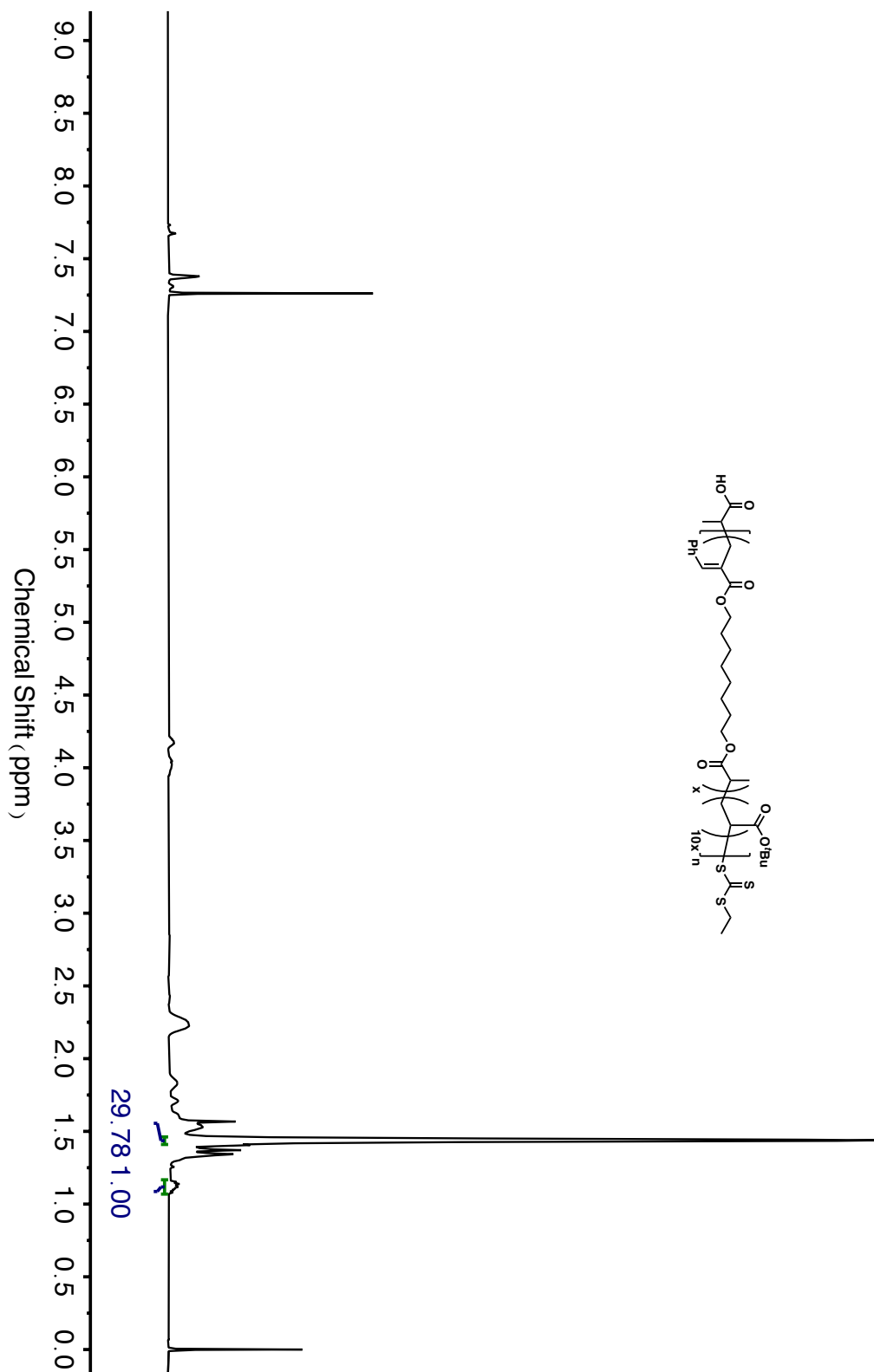
$^1\text{H}$  NMR spectrum of **P-1-co-MA** at  $f_1^0 = 0.67$ .



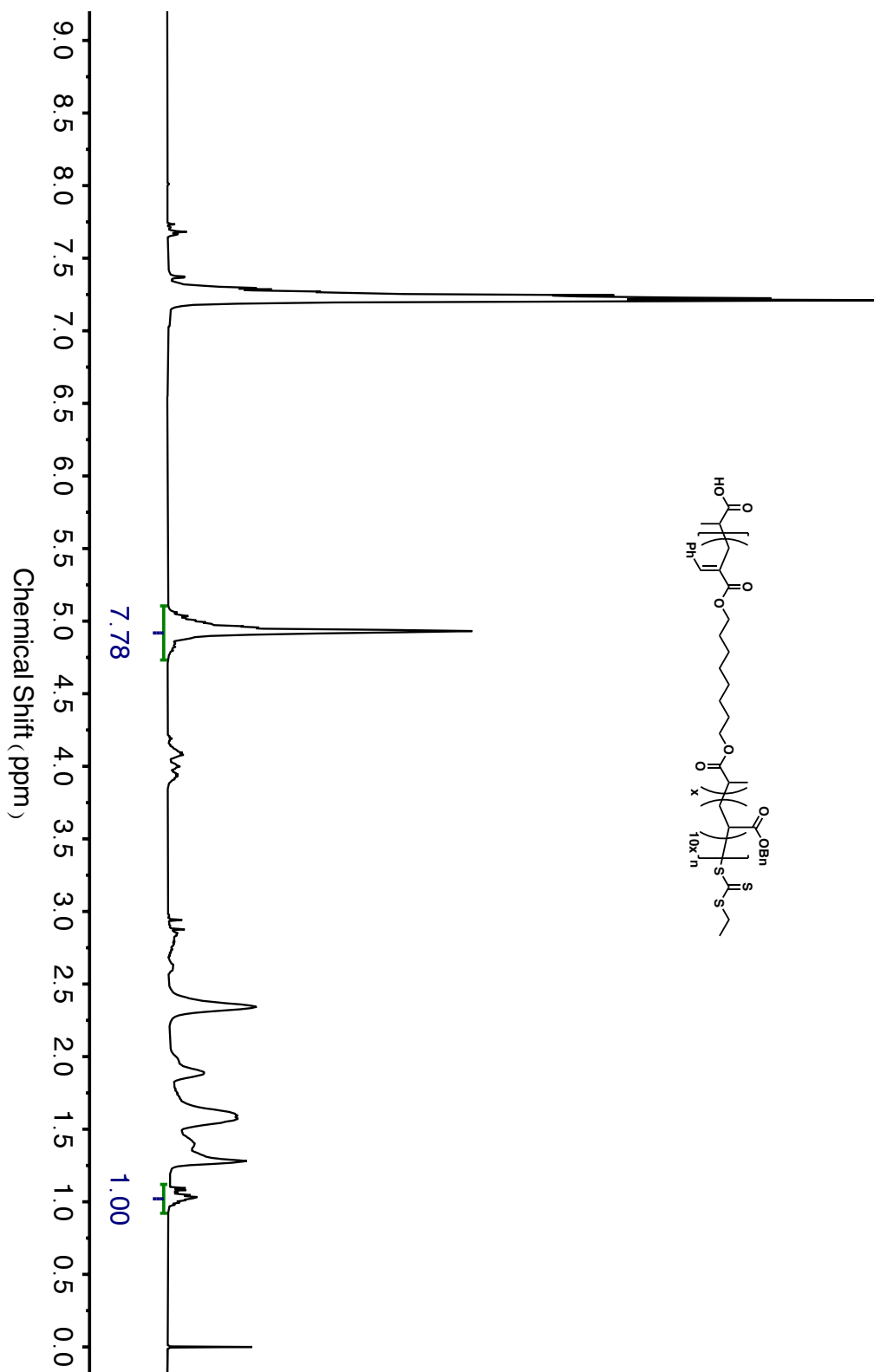
$^1\text{H}$  NMR spectrum of P-(1-co-MA) at  $f_1^0 = 0.80$ .



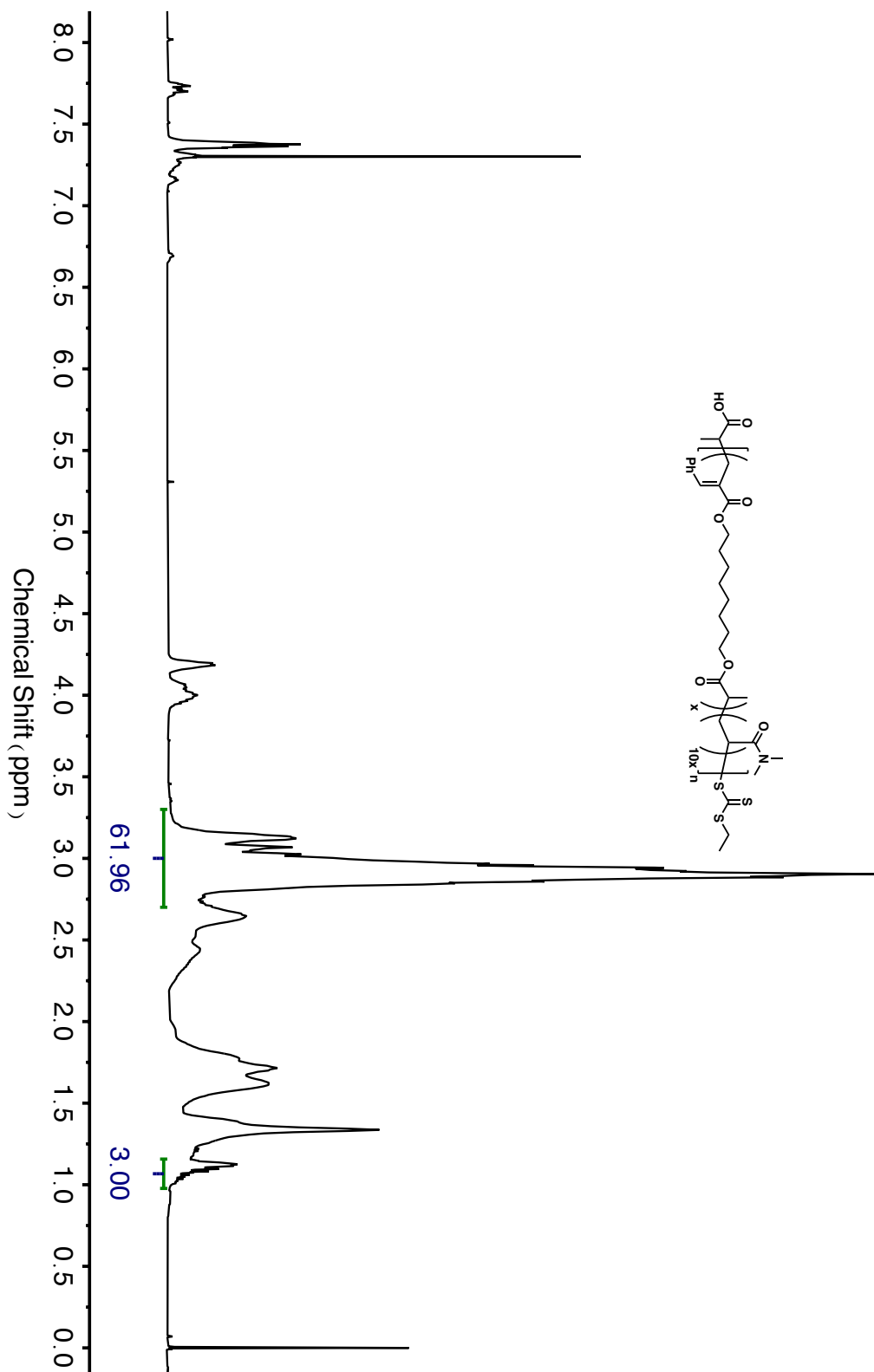
$^1\text{H}$  NMR spectrum of **P-1-co-tBA** at  $f_1^0 = 0.09$ .



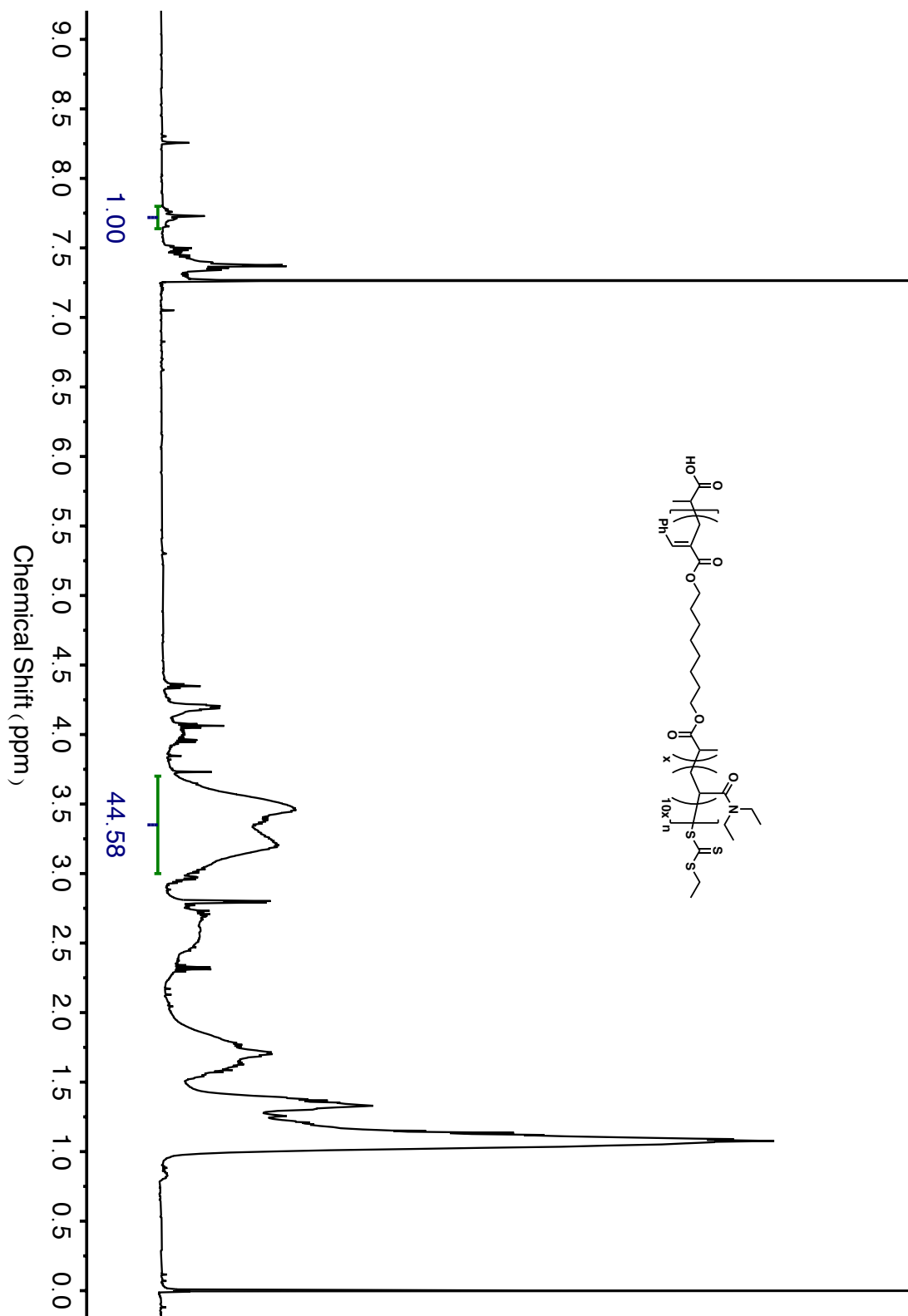
$^1\text{H}$  NMR spectrum of **P-1-co-BnA** at  $f_1^0 = 0.09$ .



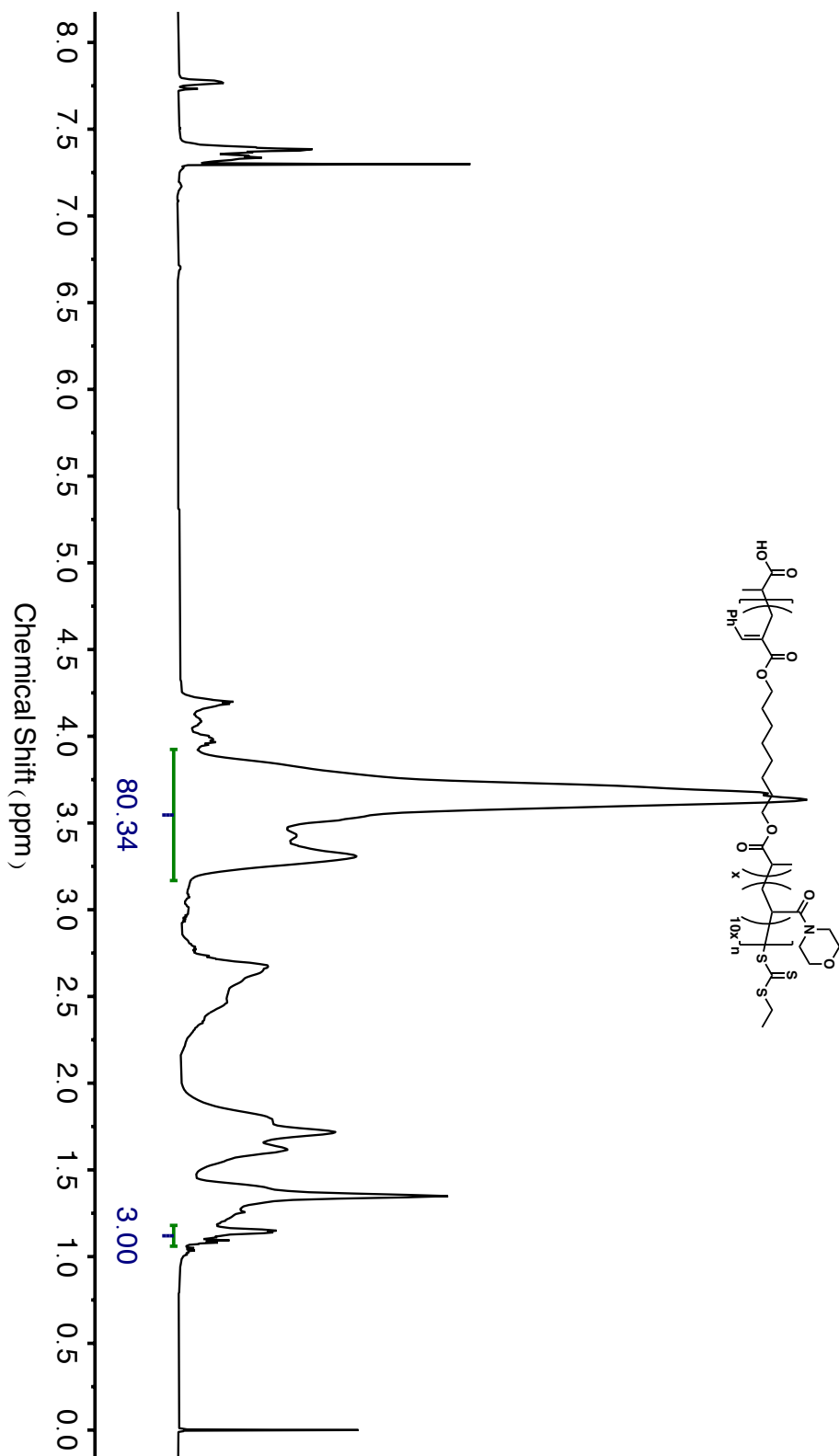
$^1\text{H}$  NMR spectrum of **P-1-co-DMA** at  $f_1^0 = 0.09$ .



$^1\text{H}$  NMR spectrum of **P-1-co-DEA** at  $f_1^0 = 0.09$ .



$^1\text{H}$  NMR spectrum of **P-1-co-NAM** at  $f_1^0 = 0.09$ .



## Reference

- (1) Geyer, R.; Jambeck, J. R.; Law, K. L. Production, use, and fate of all plastics ever made. *Sci. Adv.* **2017**, *3*, e1700782.
- (2) Seeley, M. E.; Song, B.; Passie, R.; Hale, R. C. Microplastics affect sedimentary microbial communities and nitrogen cycling. *Nat. Commun.* **2020**, *11*, 2372.
- (3) Delplace, V.; Nicolas, J. Degradable vinyl polymers for biomedical applications. *Nat. Chem.* **2015**, *7*, 771-784.
- (4) Mohadjer Beromi, M.; Kennedy, C. R.; Younker, J. M.; Carpenter, A. E.; Mattler, S. J.; Throckmorton, J. A.; Chirik, P. J. Iron-catalysed synthesis and chemical recycling of telechelic 1,3-enchaind oligocyclobutanes. *Nat. Chem.* **2021**, *13*, 156-162.
- (5) Bailey, W. J. Free Radical Ring-Opening Polymerization. *Polym. J.* **1985**, *17*, 85-95.
- (6) Tardy, A.; Nicolas, J.; Gigmès, D.; Lefay, C.; Guillauneuf, Y. Radical Ring-Opening Polymerization: Scope, Limitations, and Application to (Bio)Degradable Materials. *Chem. Rev.* **2017**, *117*, 1319-1406.
- (7) Pesenti, T.; Nicolas, J. 100th Anniversary of Macromolecular Science Viewpoint: Degradable Polymers from Radical Ring-Opening Polymerization: Latest Advances, New Directions, and Ongoing Challenges. *ACS Macro Lett.* **2020**, *9*, 1812-1835.
- (8) Corrigan, N.; Jung, K.; Moad, G.; Hawker, C. J.; Matyjaszewski, K.; Boyer, C. Reversible-deactivation radical polymerization (controlled/living radical polymerization): From discovery to materials design and applications. *Prog. Polym. Sci.* **2020**, *111*, 101311.

(9) Bailey, W. J.; Ni, Z.; Wu, S.-R. Synthesis of Poly- $\epsilon$ -Caprolactone via a Free Radical Mechanism. Free Radical Ring-Opening Polymerization of 2-Methylene-1,3-Dioxepane. *J. Polym. Sci., Polym. Chem. Ed.* **1982**, *20*, 3021-3030.

(10) Hedir, G. G.; Bell, C. A.; Jeong, N. S.; Chapman, E.; Collins, I. R.; O'Reilly, R. K.; Dove, A. P. Functional Degradable Polymers by Xanthate-Mediated Polymerization. *Macromolecules* **2014**, *47*, 2847-2852.

(11) Hedir, G. G.; Bell, C. A.; O'Reilly, R. K.; Dove, A. P. Functional Degradable Polymers by Radical Ring-Opening Copolymerization of MDO and Vinyl Bromobutanoate: Synthesis, Degradability and Post-Polymerization Modification. *Biomacromolecules* **2015**, *16*, 2049-2058.

(12) Bell, C. A.; Hedir, G. G.; O'Reilly, R. K.; Dove, A. P. Controlling the synthesis of degradable vinyl polymers by xanthate-mediated polymerization. *Polym. Chem.* **2015**, *6*, 7447-7454.

(13) Hedir, G. G.; Arno, M. C.; Langlais, M.; Husband, J. T.; O'Reilly, R. K.; Dove, A. P. Poly(oligo(ethylene glycol) vinyl acetate)s: A Versatile Class of Thermoresponsive and Biocompatible Polymers. *Angew. Chem., Int. Ed.* **2017**, *56*, 9178-9182.

(14) Hedir, G.; Stubbs, C.; Aston, P.; Dove, A. P.; Gibson, M. I. Synthesis of Degradable Poly(vinyl alcohol) by Radical Ring-Opening Copolymerization and Ice Recrystallization Inhibition Activity. *ACS Macro Lett.* **2017**, *6*, 1404-1408.

(15) Delplace, V.; Guegain, E.; Harrisson, S.; Gigmès, D.; Guillaneuf, Y.; Nicolas, J. A ring to rule them all: a cyclic ketene acetal comonomer controls the nitroxide-mediated polymerization of methacrylates and confers tunable degradability. *Chem. Commun.* **2015**, *51*, 12847-12850.

(16) Tran, J.; Guegain, E.; Ibrahim, N.; Harrisson, S.; Nicolas, J. Efficient synthesis of 2-methylene-4-phenyl-1,3-dioxolane, a cyclic ketene acetal for controlling the NMP of methyl methacrylate and conferring tunable degradability. *Polym. Chem.* **2016**, *7*, 4427-4435.

(17) Tardy, A.; Honore, J. C.; Tran, J.; Siri, D.; Delplace, V.; Bataille, I.; Letourneur, D.; Perrier, J.; Nicoletti, C.; Maresca, M.; Lefay, C.; Gigmes, D.; Nicolas, J.; Guillauneuf, Y. Radical Copolymerization of Vinyl Ethers and Cyclic Ketene Acetals as a Versatile Platform to Design Functional Polyesters. *Angew. Chem., Int. Ed.* **2017**, *56*, 16515-16520.

(18) Guegain, E.; Michel, J.-P.; Boissenot, T.; Nicolas, J. Tunable Degradation of Copolymers Prepared by Nitroxide-Mediated Radical Ring-Opening Polymerization and Point-by-Point Comparison with Traditional Polyesters. *Macromolecules* **2018**, *51*, 724-736.

(19) Guegain, E.; Tran, J.; Deguettes, Q.; Nicolas, J. Degradable polymer prodrugs with adjustable activity from drug-initiated radical ring-opening copolymerization. *Chem. Sci.* **2018**, *9*, 8291-8306.

(20) Guegain, E.; Zhu, C.; Giovanardi, E.; Nicolas, J. Radical Ring-Opening Copolymerization-Induced Self-Assembly (rROPISA). *Macromolecules* **2019**, *52*, 3612-3624.

(21) Hill, M. R.; Guegain, E.; Tran, J.; Figg, C. A.; Turner, A. C.; Nicolas, J.; Sumerlin, B. S. Radical Ring-Opening Copolymerization of Cyclic Ketene Acetals and Maleimides Affords Homogeneous Incorporation of Degradable Units. *ACS Macro Lett.* **2017**, *6*, 1071-1077.

(22) Hill, M. R.; Kubo, T.; Goodrich, S. L.; Figg, C. A.; Sumerlin, B. S. Alternating Radical Ring-Opening Polymerization of Cyclic Ketene Acetals: Access to Tunable and Functional Polyester Copolymers. *Macromolecules* **2018**, *51*, 5079-5084.

(23) Tardy, A.; Gil, N.; Plummer, C. M.; Siri, D.; Gimes, D.; Lefay, C.; Guillaneuf, Y. Polyesters by a Radical Pathway: Rationalization of the Cyclic Ketene Acetal Efficiency. *Angew. Chem., Int. Ed.* **2020**, *59*, 14517-14526.

(24) Evans, R. A.; Moad, G.; Rizzardo, E.; Thang, S. H. New Free-Radical Ring-Opening Acrylate Monomers. *Macromolecules* **1994**, *27*, 7935-7937.

(25) Paulusse, J. M. J.; Amir, R. J.; Evans, R. A.; Hawker, C. J. Free Radical Polymers with Tunable and Selective Bio- and Chemical Degradability. *J. Am. Chem. Soc.* **2009**, *131*, 9805-9812.

(26) Ratcliffe, L. P. D.; Couchon, C.; Armes, S. P.; Paulusse, J. M. J. Inducing an Order-Order Morphological Transition via Chemical Degradation of Amphiphilic Diblock Copolymer Nano-Objects. *Biomacromolecules* **2016**, *17*, 2277-2283.

(27) Du, J.; Choi, B.; Liu, Y.; Feng, A.; Thang, S. H. Degradable pH and redox dual responsive nanoparticles for efficient covalent drug delivery. *Polym. Chem.* **2019**, *10*, 1291-1298.

(28) Smith, R. A.; Fu, G.; McAteer, O.; Xu, M.; Gutekunst, W. R. Radical Approach to Thioester-Containing Polymers. *J. Am. Chem. Soc.* **2019**, *141*, 1446-1451.

(29) Bingham, N. M.; Roth, P. J. Degradable vinyl copolymers through thiocarbonyl addition-ring-opening (TARO) polymerization. *Chem. Commun.* **2019**, *55*, 55-58.

(30) Spick, M. P.; Bingham, N. M.; Li, Y.; de Jesus, J.; Costa, C.; Bailey, M. J.; Roth, P. J. Fully Degradable Thioester-Functional Homo- and Alternating Copolymers Prepared

through Thiocarbonyl Addition-Ring-Opening RAFT Radical Polymerization. *Macromolecules* **2020**, *53*, 539-547.

(31) Huang, H.; Sun, B.; Huang, Y.; Niu, J. Radical Cascade-Triggered Controlled Ring-Opening Polymerization of Macrocyclic Monomers. *J. Am. Chem. Soc.* **2018**, *140*, 10402-10406.

(32) Quiclet-Sire, B.; Zard, S. Z. New Radical Allylation Reaction. *J. Am. Chem. Soc.* **1996**, *118*, 1209-1210.

(33) Li, X.; Yin, X.; Wu, P.; Han, Z.; Zhu, Q. Effect of temperature on copolymerization parameters of hydroxyethyl acrylate and methyl methacrylate *Chin. J. Polym. Sci.* **1998**, *16*, 25-31.

(34) Fors, B. P.; Hawker, C. J. Control of a Living Radical Polymerization of Methacrylates by Light. *Angew. Chem., Int. Ed.* **2012**, *51*, 8850-8853.

(35) Zhou, H.; Johnson, J. A. Photo-controlled Growth of Telechelic Polymers and End-Linked Polymer Gels. *Angew. Chem., Int. Ed.* **2013**, *52*, 2235-2238.

(36) Anastasaki, A.; Nikolaou, V.; Zhang, Q.; Burns, J.; Samanta, S. R.; Waldron, C.; Haddleton, A. J.; McHale, R.; Fox, D.; Percec, V.; Wilson, P.; Haddleton, D. M. Copper(II)/Tertiary Amine Synergy in Photoinduced Living Radical Polymerization: Accelerated Synthesis of  $\omega$ -Functional and  $\alpha,\omega$ -Heterofunctional Poly(acrylates). *J. Am. Chem. Soc.* **2014**, *136*, 1141-1149.

(37) Treat, N. J.; Sprafke, H.; Kramer, J. W.; Clark, P. G.; Barton, B. E.; Read de Alaniz, J.; Fors, B. P.; Hawker, C. J. Metal-Free Atom Transfer Radical Polymerization. *J. Am. Chem. Soc.* **2014**, *136*, 16096-16101.

(38) Chen, M.; Zhong, M.; Johnson, J. A. Light-Controlled Radical Polymerization: Mechanisms, Methods, and Applications. *Chem. Rev.* **2016**, *116*, 10167-10211.

(39) Theriot, J. C.; Lim, C.-H.; Yang, H.; Ryan, M. D.; Musgrave, C. B.; Miyake, G. M. Organocatalyzed atom transfer radical polymerization driven by visible light. *Science* **2016**, *352*, 1082-1086.

(40) Stache, E. E.; Kottisch, V.; Fors, B. P. Photocontrolled Radical Polymerization from Hydridic C-H Bonds. *J. Am. Chem. Soc.* **2020**, *142*, 4581-4585.

(41) Jiang, K.; Han, S.; Ma, M.; Zhang, L.; Zhao, Y.; Chen, M. Photoorganocatalyzed Reversible-Deactivation Alternating Copolymerization of Chlorotrifluoroethylene and Vinyl Ethers under Ambient Conditions: Facile Access to Main-Chain Fluorinated Copolymers. *J. Am. Chem. Soc.* **2020**, *142*, 7108-7115.

(42) Quan, Q.; Ma, M.; Wang, Z.; Gu, Y.; Chen, M. Visible-Light-Enabled Organocatalyzed Controlled Alternating Terpolymerization of Perfluorinated Vinyl Ethers. *Angew. Chem., Int. Ed.* **2021**, *60*, 20443-20451.

(43) Perkowski, A. J.; You, W.; Nicewicz, D. A. Visible Light Photoinitiated Metal-Free Living Cationic Polymerization of 4-Methoxystyrene. *J. Am. Chem. Soc.* **2015**, *137*, 7580-7583.

(44) Messina, M. S.; Axtell, J. C.; Wang, Y.; Chong, P.; Wixtrom, A. I.; Kirlikovali, K. O.; Upton, B. M.; Hunter, B. M.; Shafaat, O. S.; Khan, S. I.; Winkler, J. R.; Gray, H. B.; Alexandrova, A. N.; Maynard, H. D.; Spokoyny, A. M. Visible-Light-Induced Olefin Activation Using 3D Aromatic Boron-Rich Cluster Photooxidants. *J. Am. Chem. Soc.* **2016**, *138*, 6952-6955.

(45) Kottisch, V.; Michaudel, Q.; Fors, B. P. Cationic Polymerization of Vinyl Ethers Controlled by Visible Light. *J. Am. Chem. Soc.* **2016**, *138*, 15535-15538.

(46) Michaudel, Q.; Chauvire, T.; Kottisch, V.; Supej, M. J.; Stawiasz, K. J.; Shen, L.; Zipfel, W. R.; Abruna, H. D.; Freed, J. H.; Fors, B. P. Mechanistic Insight into the Photocontrolled Cationic Polymerization of Vinyl Ethers. *J. Am. Chem. Soc.* **2017**, *139*, 15530-15538.

(47) Zhang, X.; Jiang, Y.; Ma, Q.; Hu, S.; Liao, S. Metal-Free Cationic Polymerization of Vinyl Ethers with Strict Temporal Control by Employing an Organophotocatalyst. *J. Am. Chem. Soc.* **2021**, *143*, 6357-6362.

(48) Ogawa, K. A.; Goetz, A. E.; Boydston, A. J. Metal-Free Ring-Opening Metathesis Polymerization. *J. Am. Chem. Soc.* **2015**, *137*, 1400-1403.

(49) Goetz, A. E.; Boydston, A. J. Metal-Free Preparation of Linear and Cross-Linked Polydicyclopentadiene. *J. Am. Chem. Soc.* **2015**, *137*, 7572-7575.

(50) Krappitz, T.; Jovic, K.; Feist, F.; Frisch, H.; Rigoglioso, V. P.; Blinco, J. P.; Boydston, A. J.; Barner-Kowollik, C. Hybrid Photo-induced Copolymerization of Ring-Strained and Vinyl Monomers Utilizing Metal-Free Ring-Opening Metathesis Polymerization Conditions. *J. Am. Chem. Soc.* **2019**, *141*, 16605-16609.

(51) Lai, H.; Zhang, J.; Xing, F.; Xiao, P. Recent advances in light-regulated non-radical polymerisations. *Chem. Soc. Rev.* **2020**, *49*, 1867-1886.

(52) Xu, J.; Jung, K.; Atme, A.; Shanmugam, S.; Boyer, C. A Robust and Versatile Photoinduced Living Polymerization of Conjugated and Unconjugated Monomers and Its Oxygen Tolerance. *J. Am. Chem. Soc.* **2014**, *136*, 5508-5519.

(53) Xu, J.; Jung, K.; Corrigan, N. A.; Boyer, C. Aqueous photoinduced living/controlled polymerization: tailoring for bioconjugation. *Chem. Sci.* **2014**, *5*, 3568-3575.

(54) Xu, J.; Shanmugam, S.; Duong, H. T.; Boyer, C. Organo-photocatalysts for photoinduced electron transfer-reversible addition-fragmentation chain transfer (PET-RAFT) polymerization. *Polym. Chem.* **2015**, *6*, 5615-5624.

(55) Shanmugam, S.; Xu, J.; Boyer, C. Exploiting Metalloporphyrins for Selective Living Radical Polymerization Tunable over Visible Wavelengths. *J. Am. Chem. Soc.* **2015**, *137*, 9174-9185.

(56) Corrigan, N.; Shanmugam, S.; Xu, J.; Boyer, C. Photocatalysis in organic and polymer synthesis. *Chem. Soc. Rev.* **2016**, *45*, 6165-6212.

(57) Yuan, J.; Wang, W.; Zhou, Z.; Niu, J. Cascade Reactions in Chain-Growth Polymerization. *Macromolecules* **2020**, *53*, 5655-5673.

(58) Peterson, G. I.; Choi, T.-L. Cascade polymerizations: recent developments in the formation of polymer repeat units by cascade reactions. *Chem. Sci.* **2020**, *11*, 4843-4854.

(59) Li, N.; Ding, D.; Pan, X.; Zhang, Z.; Zhu, J.; Boyer, C.; Zhu, X. Temperature programmed photo-induced RAFT polymerization of stereo-block copolymers of poly(vinyl acetate). *Polym. Chem.* **2017**, *8*, 6024-6027.

(60) Huang, H.; Wang, W.; Zhou, Z.; Sun, B.; An, M.; Haeffner, F.; Niu, J. Radical Ring-Closing/Ring-Opening Cascade Polymerization. *J. Am. Chem. Soc.* **2019**, *141*, 12493-12497.

(61) Lynd, N. A.; Ferrier, R. C.; Beckingham, B. S. Recommendation for Accurate Experimental Determination of Reactivity Ratios in Chain Copolymerization. *Macromolecules* **2019**, *52*, 2277-2285.

(62) Beckingham, B. S.; Sanoja, G. E.; Lynd, N. A. Simple and Accurate Determination of Reactivity Ratios Using a Nonterminal Model of Chain Copolymerization. *Macromolecules* **2015**, *48*, 6922-6930.

(63) Neugebauer, D.; Matyjaszewski, K. Copolymerization of *N,N*-Dimethylacrylamide with *n*-Butyl Acrylate via Atom Transfer Radical Polymerization *Macromolecules* **2003**, *36*, 2598-2603.

(64) O'Leary, K.; Paul, D. R. Copolymers of poly(*n*-alkyl acrylates): synthesis, characterization, and monomer reactivity ratios. *Polymer* **2004**, *45*, 6575-6585.

(65) Kamaly, N.; Yameen, B.; Wu, J.; Farokhzad, O. C. Degradable Controlled-Release Polymers and Polymeric Nanoparticles: Mechanisms of Controlling Drug Release. *Chem. Rev.* **2016**, *116*, 2602-2663.

(66) Penfold, N. J. W.; Yeow, J.; Boyer, C.; Armes, S. P. Emerging Trends in Polymerization-Induced Self-Assembly. *ACS Macro Lett.* **2019**, *8*, 1029-1054.

(67) Gao, C.; Zhou, H.; Qu, Y.; Wang, W.; Khan, H.; Zhang, W. *In Situ* Synthesis of Block Copolymer Nanoassemblies via Polymerization-Induced Self-Assembly in Poly(ethylene glycol). *Macromolecules* **2016**, *49*, 3789-3798.

(68) Florjańczyk, Z. On the reactivity of sulfur dioxide in chain polymerization reactions. *Prog. Polym. Sci.* **1991**, *16*, 509-560.

(69) Qiu, G.; Zhou, K.; Gao, L.; Wu, J. Insertion of sulfur dioxide via a radical process: an efficient route to sulfonyl compounds. *Org. Chem. Front.* **2018**, *5*, 691-705.

(70) Hofman, K.; Liu, N.-W.; Manolikakes, G. Radicals and Sulfur Dioxide: A Versatile Combination for the Construction of Sulfonyl-Containing Molecules. *Chem. Eur. J.* **2018**, *24*, 11852-11863.

(71) Marenich, A. V.; Cramer, C. J.; Truhlar, D. G. Universal Solvation Model Based on Solute Electron Density and on a Continuum Model of the Solvent Defined by the Bulk Dielectric Constant and Atomic Surface Tensions. *J. Phys. Chem. B* **2009**, *113*, 6378-6396.

(72) Hwang, J. S.; Tsonis, C. P. Radicals in the Synthesis of Sulphur Dioxide-Based Copolymers. *J. Polym. Sci., Part A: Polym. Chem.* **1993**, *31*, 1417-1421.

(73) Skey, J.; O'Reilly, R. K. Facile one pot synthesis of a range of reversible addition-fragmentation chain transfer (RAFT) agents. *Chem. Commun.* **2008**, *44*, 4183-4185.

(74) Gaussian 09, Revision A.02, M. J. Frisch, G. W. Trucks, H. B. Schlegel, G. E. Scuseria, M. A. Robb, J. R. Cheeseman, G. Scalmani, V. Barone, B. Mennucci, G. A. Petersson, H. Nakatsuji, M. Caricato, X. Li, H. P. Hratchian, A. F. Izmaylov, J. Bloino, G. Zheng, J. L. Sonnenberg, M. Hada, M. Ehara, K. Toyota, R. Fukuda, J. Hasegawa, M. Ishida, T. Nakajima, Y. Honda, O. Kitao, H. Nakai, T. Vreven, J. A. Montgomery, Jr., J. E. Peralta, F. Ogliaro, M. Bearpark, J. J. Heyd, E. Brothers, K. N. Kudin, V. N. Staroverov, R. Kobayashi, J. Normand, K. Raghavachari, A. Rendell, J. C. Burant, S. S. Iyengar, J. Tomasi, M. Cossi, N. Rega, J. M. Millam, M. Klene, J. E. Knox, J. B. Cross, V. Bakken, C. Adamo, J. Jaramillo, R. Gomperts, R. E. Stratmann, O. Yazyev, A. J. Austin, R. Cammi, C. Pomelli, J. W. Ochterski, R. L. Martin, K. Morokuma, V. G. Zakrzewski, G. A. Voth, P. Salvador, J. J. Dannenberg, S. Dapprich, A. D. Daniels, O. Farkas, J. B. Foresman, J. V. Ortiz, J. Cioslowski, and D. J. Fox, Gaussian, Inc., Wallingford CT, 2009.

## Chapter 3

### Organocatalyzed Photocontrolled Radical Copolymerization of Macrocyclic Allylic Sulfone with Vinyl Monomers

A significant portion of the work described in this chapter has been published in:

Wang, W.; Rondon, B.; Wang, Z.; Wang, J.; Niu, J. Macrocyclic Allylic Sulfone as A Universal Comonomer in Organocatalyzed Photocontrolled Radical Copolymerization with Vinyl Monomers. *Macromolecules* **2023**, *56*, 2052-2061.

### 3.1 Introduction

The global annual production of plastics has increased dramatically over the past four decades and is now approaching 400 million metric tons, approximately 70 percent of which are vinyl plastics.<sup>1</sup> Thanks to their low cost, high durability, and easy processability, vinyl plastics have been widely used in various types of applications, including packaging, construction materials, adhesives, coatings, and synthetic fibers. However, the half-lives of many types of commodity vinyl plastics are much longer than necessary for their applications, leading to the accumulation of plastic waste in the environment.<sup>2-6</sup> A potential solution to this challenge is to achieve polymer degradation at the end of their life cycle by incorporating labile functionalities into the main chain of vinyl polymers.

Since the first report in the 1960s,<sup>7</sup> radical ring-opening polymerization has emerged as a powerful approach to incorporating labile functionalities, such as ester, disulfide, or carbonate, into the backbone of vinyl polymers.<sup>8-11</sup> Pioneered by Bailey<sup>12</sup> and Endo,<sup>13</sup> cyclic ketene acetals<sup>14-17</sup> have been extensively investigated to copolymerize with various vinyl monomers but were often found to have non-optimal copolymerization reactivities and poor rates of incorporation. Recently reported by Roth<sup>18</sup> and Gutekunst<sup>19</sup> in 2019, dibenzo[*c,e*]oxepane-5-thiones (DOTs)<sup>20-24</sup> have shown successful copolymerization with acrylates, acrylamides, acrylonitrile, maleimide, and styrene to synthesize degradable linear copolymers and degradable polymer networks. However, copolymerization of DOTs and methacrylates remains challenging.

Polymerization regulated by light serves as a great alternative to thermally initiated polymerization due to its economic and ubiquitous nature.<sup>25-27</sup> Integrated with reversible deactivation radical polymerization,<sup>28-30</sup> photocontrolled radical polymerization could

produce macromolecular structures with defined molecular weight and architecture under mild conditions. Light-mediated polymerization at low temperatures (-20 to 50 °C) also enabled fine-tuning of polymer tacticity as well as composition.<sup>31-32</sup> In 2021, we reported that *fac*-Ir(ppy)<sub>3</sub>-mediated photocontrolled radical ring-opening cascade copolymerization (rROCCP) of the macrocyclic allylic sulfone and acrylic monomers produced degradable vinyl copolymers with favorable reactivities.<sup>33</sup> However, potential toxicity and challenges in the removal of transition-metal photocatalysts may preclude the use of these degradable vinyl copolymers in biomedical and electronic applications. Therefore, we explored organocatalyzed photocontrolled rROCCP.<sup>34-38</sup> We demonstrated that the macrocyclic allylic sulfone serves as a “universal” cyclic monomer in organocatalyzed photocontrolled rROCCP and can copolymerize with a variety of vinyl monomers, including acrylates, acrylamides, styrene, and methacrylate, incorporating degradability to otherwise nondegradable vinyl polymers (Figure 3.1).

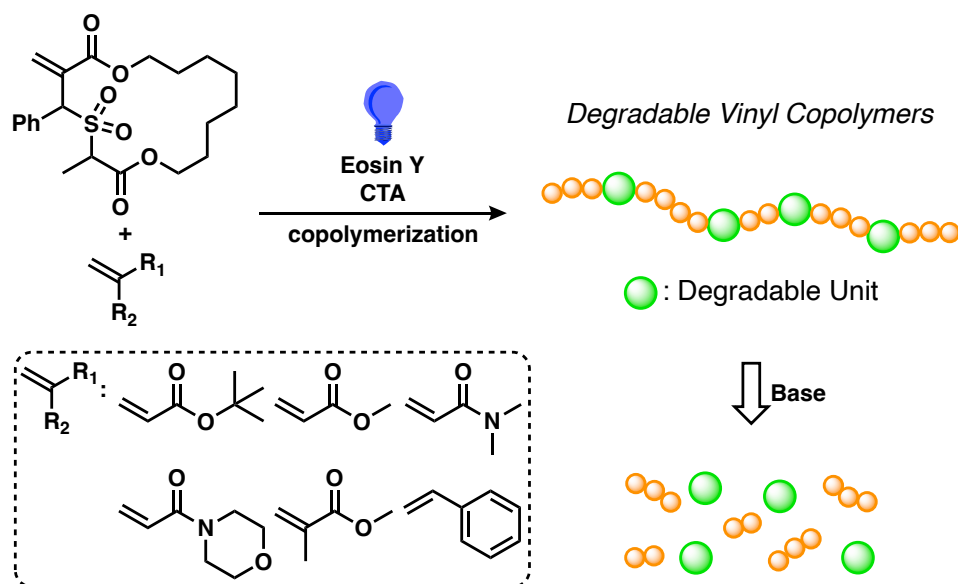


**Figure 3.1.** Organocatalyzed photocontrolled rROCCP of macrocyclic allylic sulfone and a variety of vinyl monomers generates degradable vinyl copolymers.

### 3.2 Organocatalyzed photocontrolled homopolymerization of macrocyclic allylic sulfone

Adopting the organocatalyzed photoinduced electron/energy transfer-radical addition/fragmentation chain transfer (PET-RAFT) method reported by Xu and Boyer,<sup>36</sup> the homopolymerization of macrocyclic allylic sulfone **1** was first investigated (Figure 3.2A). Polymerization of **1** ( $[M]_0 = 0.2 \text{ M}$ ) was initially attempted with control of Eosin Y (EY,  $[EY]_0/[M]_0 = 200 \text{ ppm}$ ) and chain transfer agent **CTA1** ( $[M]_0/[I]_0 = 50/1$ ) under  $\lambda_{\text{max}} = 450 \text{ nm}$  blue light irradiation (Figure 3.2A).

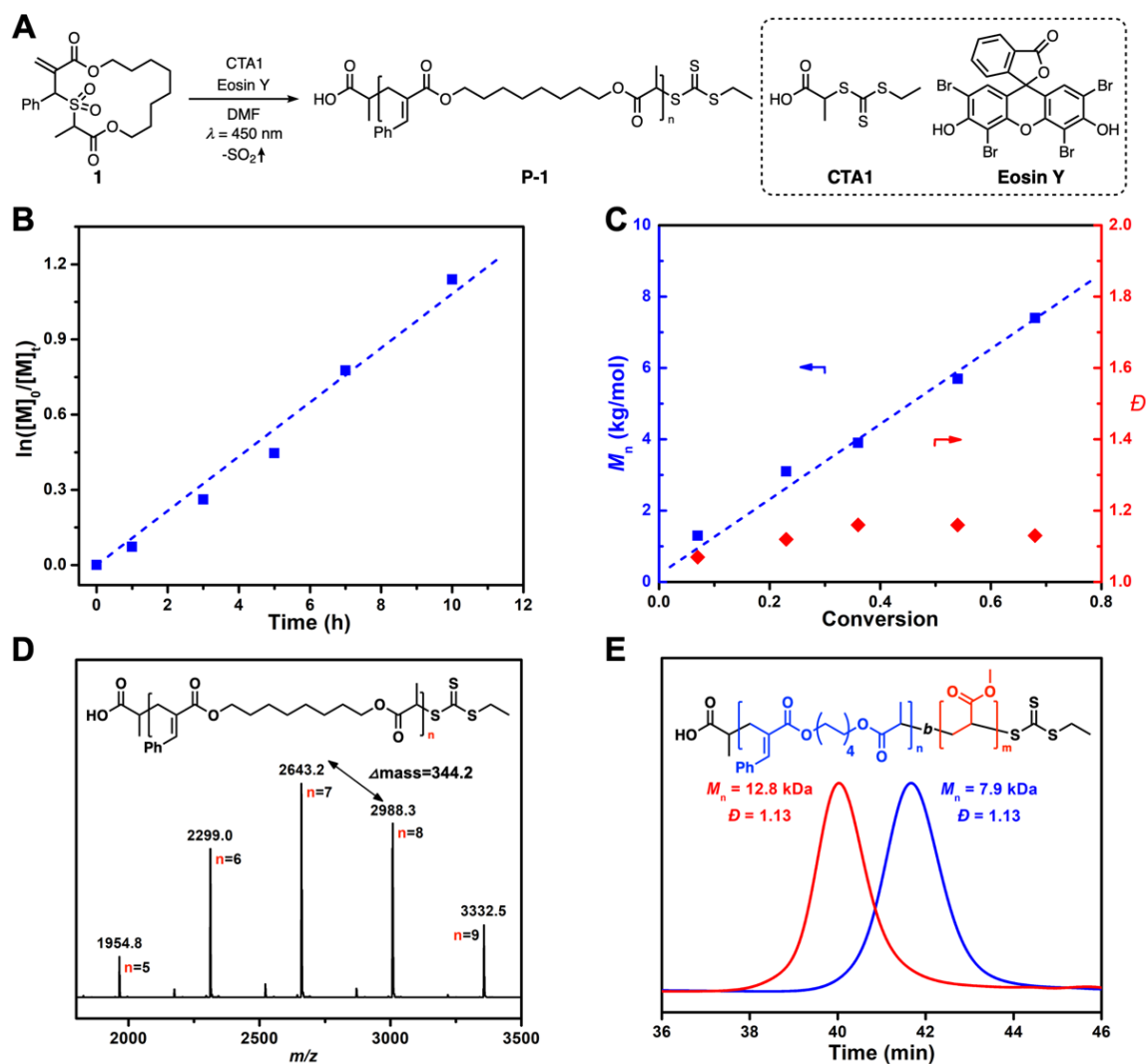
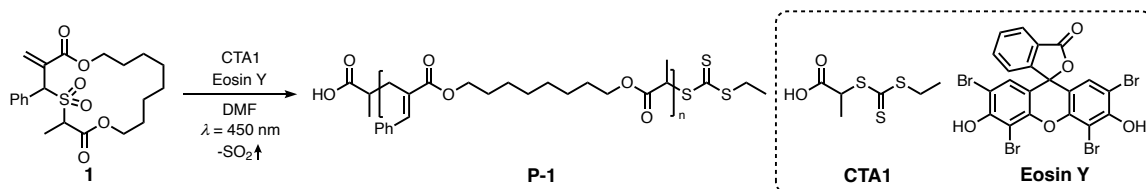


**Figure 3.2.** (A) Organocatalyzed photocontrolled homopolymerization of **1**. (B) Kinetic plot of  $\ln([M]_0/[M]_t)$  versus reaction time, where  $[M]_0$  is the initial monomer concentration and  $[M]_t$  is the monomer concentration at a given time  $t$ . (C) Plots of  $M_n$  and  $\bar{D}$  of **P-1** as a function of monomer conversion. (D) MALDI-TOF analysis of **P-1-3k**. Each peak corresponds to a discrete oligomer that consists of  $\alpha$ - and  $\omega$ -chain ends, the number of repeating units multiplied by its molar mass, and a sodium cation. A set of minor peaks was observed, which corresponded to the loss of the  $\omega$ -chain end of **P-1-3k** during MALDI-TOF measurement. (E) SEC analysis of the formation of diblock copolymer **P-1-*b*-PMA** from an extension of a macroinitiator **P-1-8k** by MA.

The reaction reached 20% conversion in 10 hours and yielded well-defined polymer **P-1** with a number average molecular weight ( $M_n^{(SEC)}$ ) of 3.0 kg mol<sup>-1</sup> and dispersity ( $\mathcal{D}$ ) of 1.08 by size-exclusion chromatography (SEC) (Table 3.1, entry 1). Further optimization of initial monomer concentration ( $[M]_0$ ) and photocatalyst loading ( $[EY]_0/[M]_0$ ) revealed that the polymerization reached 68% conversion with  $[M]_0 = 0.5$  M and  $[EY]_0/[M]_0 = 1000$  ppm, affording **P-1** with  $M_n^{(SEC)}$  of 7.7 kg mol<sup>-1</sup> and  $\mathcal{D}$  of 1.13 in 4 hours (Table 3.1, entry 5).

**Table 3.1.** Screening of photocatalyst loading and initial monomer concentration for organocatalyzed photoredox radical homopolymerization of **1**.



Entry <sup>a</sup>	$[EY]_0/[M]_0$	$[M]_0$	Conv. <sup>b</sup>	$M_n^{(SEC)}$ (kg mol <sup>-1</sup> ) <sup>c</sup>	$\mathcal{D}^c$
1	200 ppm	0.2 M	20 %	3.0	1.08
2	500 ppm	0.2 M	56 %	6.6	1.26
3	1000 ppm	0.2 M	69 %	7.2	1.37
4	1500 ppm	0.2 M	68 %	7.4	1.37
5 <sup>d</sup>	1000 ppm	0.5 M	68 %	7.7	1.13

<sup>a</sup>Reactions were performed at 25 °C under nitrogen with an 18 W blue LED light ( $\lambda_{max} = 450$  nm) for 10 hours. <sup>b</sup>Monomer conversion was determined by <sup>1</sup>H NMR spectroscopy. <sup>c</sup> $M_n$  and  $\mathcal{D}$  were determined by SEC analysis calibrated to polystyrene standards. <sup>d</sup>Reaction time: 4 hours.

Next, we examined the living/controlled characteristics of organocatalyzed radical homopolymerization of **1**. Kinetic study of the polymerization of **1** exhibited first-order kinetics (Figure 3.2B). The observed rate constant for **1** was calculated as  $k_1 = 0.11 \text{ h}^{-1}$ . At the feeding monomer/initiator ( $[M]_0/[I]_0$ ) ratio of 50/1, linear growth of  $M_n^{(\text{SEC})}$  of **P-1** with respect to monomer conversion was observed, and low dispersity ( $D < 1.2$ ) was maintained throughout the polymerization (Figure 3.2C), indicating an excellent control of the polymerization. Proton nuclear magnetic resonance ( $^1\text{H NMR}$ ) analysis of well-defined polymer **P-1-8k** showed an equal stoichiometry of the  $\alpha$ -chain end (1.21 ppm) and  $\omega$ -chain end (3.36 ppm), suggesting a high chain-end fidelity (Figure 3.3).

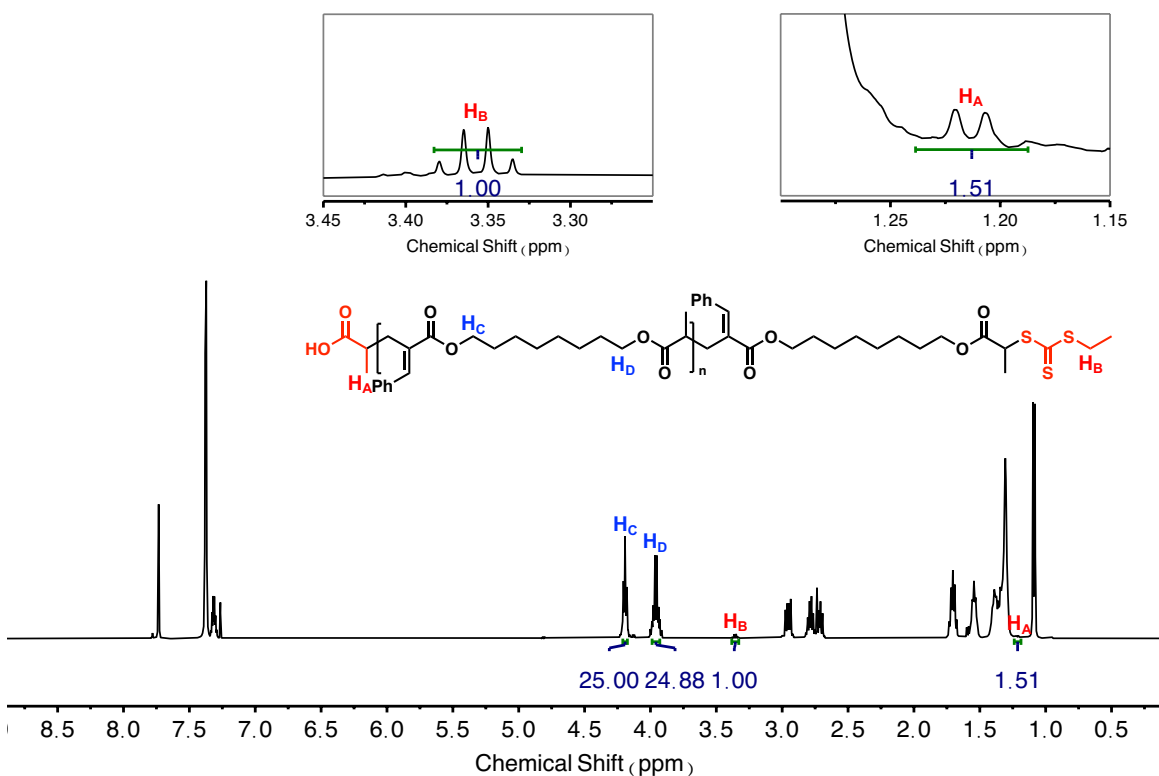


**Figure 3.3.**  $^1\text{H NMR}$  spectroscopy of **P-1-8k**.

The molecular weight of **P-1-8k** determined by  $^1\text{H}$  NMR integration ratio of the polymer backbone to  $\omega$ -chain end was  $8.9 \text{ kg mol}^{-1}$ , which was consistent with the theoretical value based on  $[\text{M}]_0/[\text{I}]_0$  ratio and monomer conversion ( $M_n^{\text{(theo)}} = 8.9 \text{ kg mol}^{-1}$ ) as well as the value obtained from SEC analysis ( $M_n^{\text{(SEC)}} = 8.3 \text{ kg mol}^{-1}$ ) (Figure 3.3). Matrix-assisted laser desorption/ionization time-of-flight (MALDI-TOF) mass spectrometry analysis of a lower molecular weight polymer **P-1-3k** showed discrete peaks spaced by  $344.2 \text{ g mol}^{-1}$ , which corresponds to the mass of the repeating unit (Figure 3.2D). These peaks were unambiguously assigned to discrete oligomers with a propionic acid group as  $\alpha$ -chain end and an ethyl trithiocarbonate group as  $\omega$ -chain end, respectively, consistent with the  $^1\text{H}$  NMR spectroscopy results. Encouraged by the excellent end-group fidelity, a block-copolymerization experiment was further conducted. First, organocatalyzed radical homopolymerization of **1** yielded a macroinitiator **P-1-8k** ( $M_n^{\text{(SEC)}} = 7.9 \text{ kg mol}^{-1}$ ,  $D = 1.13$ ), which was then used to polymerize methyl acrylate (MA) to generate a diblock copolymer **P-1-b-PMA** ( $M_n^{\text{(SEC)}} = 12.8 \text{ kg mol}^{-1}$ ,  $D = 1.13$ , Figure 3.2E). A clear shift of the original unimodal peak to a higher molecular weight region was observed on SEC after block copolymerization, suggesting the formation of a diblock copolymer. Taken together, these results supported that organocatalyzed photocontrolled homopolymerization of **1** maintained excellent control throughout polymerization.

### 3.3 Copolymerization of macrocyclic allylic sulfone with acrylic monomers

Encouraged by the homopolymerization results of **1**, we then investigated the copolymerization of **1** and acrylic monomers. First, **1** was copolymerized with *tert*-butyl



**Table 3.2.** Organocatalyzed Photocontrolled rROCCP of **1** and Vinyl Monomers.

Entry <sup>a</sup>	<b>B</b>	[ <b>B</b> ]:[ <b>1</b> ]:[CTA]	Conv. <sup>b</sup>	$f_1^0$	$F_1^{(\text{end})b}$	$M_n^{(\text{SEC})}$ (kg mol <sup>-1</sup> ) <sup>c</sup>	$\mathcal{D}^c$
1	<i>t</i> BA	100:10:1	90%	0.09	0.09	11.3	1.11
2	<i>t</i> BA	200:10:1	90%	0.05	0.05	22.5	1.15
3	<i>t</i> BA	200:20:1	92%	0.09	0.09	23.9	1.25
4	<i>t</i> BA	200:66:1	90%	0.25	0.25	24.4	1.26
5	DMA	100:10:1	92%	0.09	0.09	8.0	1.18
6	DMA	200:10:1	94%	0.05	0.05	15.7	1.29
7	DMA	200:20:1	95%	0.09	0.09	14.7	1.28
8	DMA	200:66:1	73%	0.25	0.25	13.6	1.31
9	MA	100:10:1	78%	0.09	0.09	7.8	1.10
10	MA	200:20:1	91%	0.09	0.09	17.9	1.24
11 <sup>d</sup>	NAM	100:10:1	83%	0.09	0.09	7.7	1.12
12 <sup>d</sup>	NAM	200:20:1	87%	0.09	0.09	19.2	1.22
13 <sup>e</sup>	St	100:10:1	44%	0.09	0.16	8.8	1.23
14 <sup>e</sup>	St	200:10:1	51%	0.05	0.07	13.0	1.35
15 <sup>e</sup>	St	200:20:1	41%	0.09	0.15	14.0	1.31
16 <sup>e</sup>	MMA	100:10:1	77%	0.09	0.01	11.5	1.36
17 <sup>e</sup>	MMA	50:50:1	62%	0.50	0.25	7.4	1.26

<sup>a</sup>Reactions were performed at 25 °C under nitrogen with an 18 W blue LED light ( $\lambda_{\text{max}} = 450$  nm) for 5 hours.  $[M]_0 = 0.5$  M;  $[EY]_0/[M]_0 = 1000$  ppm. <sup>b</sup>Monomer conversion and  $F_1^{(\text{end})}$  were determined by <sup>1</sup>H NMR spectroscopy. <sup>c</sup> $M_n$  and  $\mathcal{D}$  were determined by SEC analysis calibrated to polystyrene standards. <sup>d</sup>Reaction time: 75 minutes. <sup>e</sup>Reaction time: 50 hours.

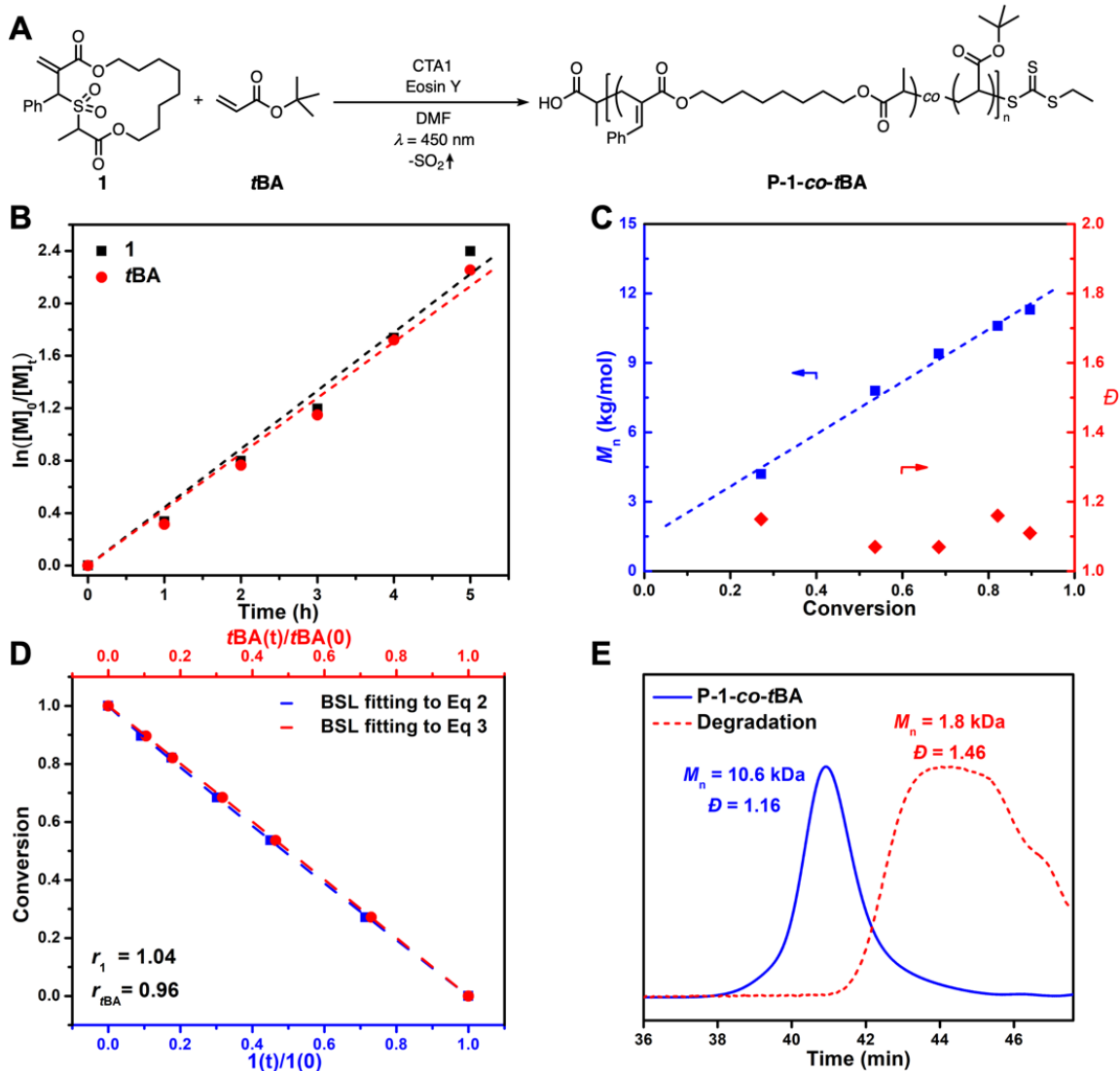


**Figure 3.4.** (A) Organocatalyzed photocontrolled rROCCP of **1** and *t*BA. (B) Kinetic plots of  $\ln([M]_0/[M]_t)$  versus reaction time of **1** and *t*BA. (C) Plots of  $M_n$  and  $\bar{D}$  of **P-1-co-tBA** as a function of total conversion. (D) Plots of total conversion with respect to  $[1(t)]/[1(0)]$  and  $[tBA(t)]/[tBA(0)]$  are fitted to Equations (2) and (3) of the BSL integrated model independently to derive the reactivity ratios of **1** and *t*BA. (E) Degradation of **P-1-co-tBA** exhibited a clear shift of the copolymer peak to a lower molecular weight region on SEC.

Kinetic analysis of the copolymerization of **1** and *t*BA monitored by <sup>1</sup>H NMR spectroscopy revealed that both **1** and *t*BA followed first-order kinetics throughout copolymerization (Figure 3.4B). Their observed rate constants were calculated for **1** and *t*BA as  $k_1 = 0.44 \text{ h}^{-1}$  and  $k_{t\text{BA}} = 0.43 \text{ h}^{-1}$ , respectively. The molecular weight of **P-1-co-tBA** increased linearly with the total conversion (Conv.) of the two monomers (Figure 3.4C), which is defined by Equation (1):

$$\text{conv.} = 1 - \frac{[\mathbf{1}(t)] + [\mathbf{B}(t)]}{[\mathbf{1}(0)] + [\mathbf{B}(0)]} \quad (1)$$

where  $[\mathbf{1}(t)]$  and  $[\mathbf{B}(t)]$  are the instantaneous concentrations of **1** and vinyl monomer **B** at time  $t$ , respectively, and  $[\mathbf{1}(0)]$  and  $[\mathbf{B}(0)]$  are the initial concentrations of **1** and vinyl monomer **B**, respectively. The dispersity of **P-1-co-tBA** remained low throughout copolymerization ( $\mathcal{D} < 1.2$ ) (Figure 3.4C). These results indicated excellent control throughout the copolymerization. By analyzing the <sup>1</sup>H NMR spectroscopy of the purified copolymers at different conversions, the molar fraction of **1** incorporated into the copolymer (denoted hereafter as  $F_1$ ) remained identical to the molar fraction of **1** in the initial comonomer mixture (denoted hereafter as  $f_1^0$ ) throughout copolymerization ( $F_1 = f_1^0 = 0.09$ ) (Figure 3.5).

**P-1-co-*t*BA with  $f_1^0 = 0.09$**

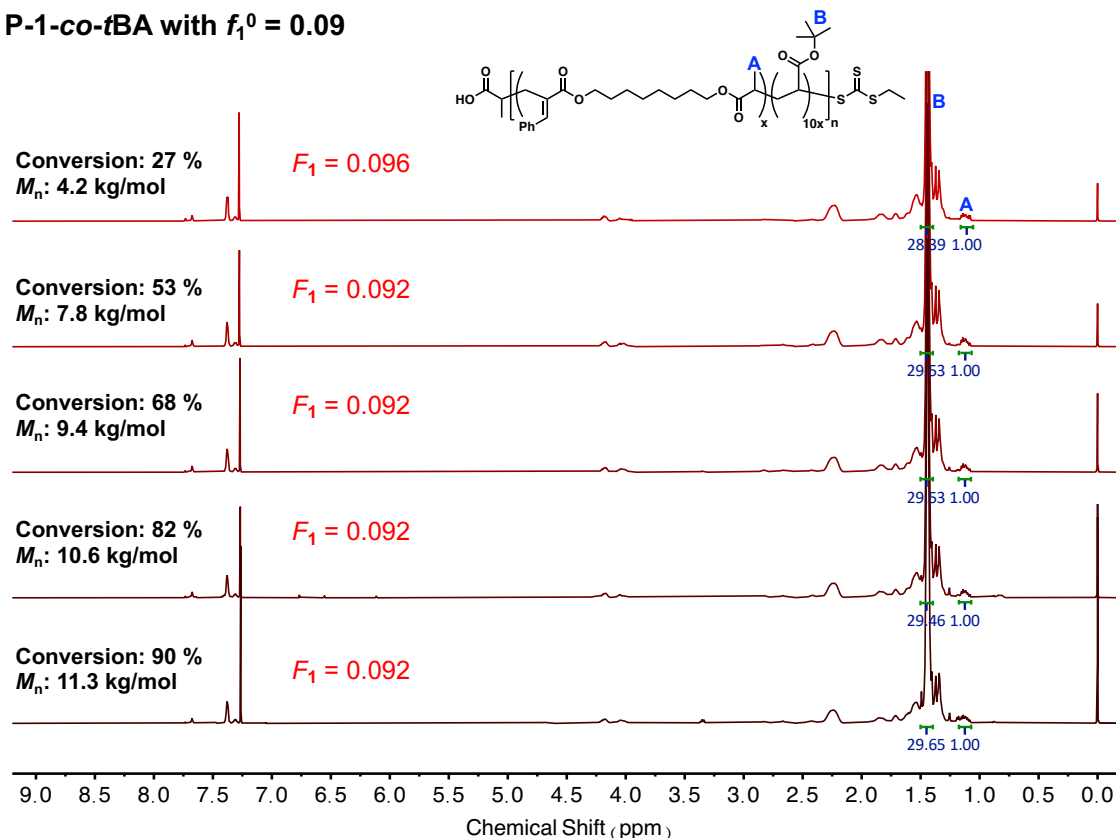


**Figure 3.5.** Compositional analysis of **P-1-co-*t*BA** at  $f_1^0 = 0.09$  at different time points of the copolymerization by  $^1\text{H}$  NMR spectroscopy.

These results suggested that the reactivities of **1** and *t*BA are similar during organocatalyzed photocontrolled rROCCP. We used reactivity ratios to quantitatively assess the reactivities of two comonomers in organocatalyzed photocontrolled rROCCP. To determine the reactivity ratios, the respective concentrations of **1** and *t*BA compared to the total conversions were fitted to the Beckingham-Sanoja-Lynd (BSL) integrated model, which is defined by Equations (2) and (3).<sup>39-40</sup>

$$\text{conv.} = 1 - f_1^0 \left[ \frac{\mathbf{1}(t)}{\mathbf{1}(0)} \right] - (1 - f_1^0) \left[ \frac{\mathbf{1}(t)}{\mathbf{1}(0)} \right]^{r_B} \quad (2)$$

$$conv. = 1 - f_1^0 \left[ \frac{\mathbf{B}(t)}{\mathbf{B}(0)} \right]^{r_1} - (1 - f_1^0) \left[ \frac{\mathbf{B}(t)}{\mathbf{B}(0)} \right] \quad (3)$$

The BSL integrated model is known to accurately determine the reactivity ratios of non-terminal copolymerization, where the rate of propagation completely depends on the reactivities of monomers with minimal dependence on the propagating species. Independent fitting of the respective instantaneous concentrations of **1** and *t*BA at various Conv. values to Equations (2) and (3) yielded reactivity ratios of **1** and *t*BA as  $r_1 = 1.04$  and  $r_{tBA} = 0.96$ , respectively (Table 3.3, entry 1 and Figure 3.4D).

**Table 3.3.** Reactivity Ratios of **1** and Vinyl Monomers and Degradation of Vinyl Copolymers.

Entry <sup>a</sup>	<b>B</b>	$r_1$	$r_B$	$f_1^0$	$F_1^{(end)b}$	$M_n^{(SEC)}$ (kg mol <sup>-1</sup> ) <sup>c</sup>	$\bar{D}^c$	Degraded $M_n^{(SEC)}$ (kg mol <sup>-1</sup> ) <sup>c</sup>	Degraded $\bar{D}^c$
1	<i>t</i> BA	1.04	0.96	0.09	0.09	11.3	1.11	1.8	1.46
2	MA	1.02	0.98	0.09	0.09	7.8	1.10	1.3	1.55
3	DMA	0.98	0.93	0.09	0.09	8.0	1.18	1.0	1.13
4	NAM	0.99	1.01	0.09	0.09	7.7	1.12	1.4	1.33
5	St	3.02	0.35	0.09	0.16	8.8	1.23	1.4	1.32
6	MMA	0.18	5.81	0.50	0.25	7.4	1.26	1.5	1.45

<sup>a</sup>Reactions were performed at 25 °C under nitrogen with an 18 W blue LED light ( $\lambda_{max} = 450$  nm).  $[M]_0 = 0.5$  M;  $[EY]_0/[M]_0 = 1000$  ppm. <sup>b</sup> $F_1^{(end)}$  was determined by <sup>1</sup>H NMR spectroscopy. <sup>c</sup> $M_n$  and  $\bar{D}$  were determined by SEC analysis calibrated to polystyrene standards.

The product of the two independently derived reactivity ratios equals unity ( $r_1 \times r_{tBA} = 1.002$ ), suggesting that the BSL integrated model can be applied to this copolymerization

system.<sup>39-40</sup> The close-to-unity reactivity ratios also suggest that the copolymerization of **1** and *t*BA formed random copolymers ( $r_a = r_b = 1$ ) with the main-chain diester motif statistically incorporated in the copolymer backbone. Organocatalyzed photocontrolled rROCCP of **1** and *t*BA at other feed ratios ( $f_1^0 = 0.05$  and  $0.25$ ) afforded copolymers **P-1-co-*t*BA** with predictable  $M_n^{(SEC)}$  and low  $D$  (Table 3.2, entry 2-4). Meanwhile, the  $F_1^{(end)}$  of the resulting copolymers all remained the same as their  $f_1^0$  (Table 3.2, entry 2-4). We further explored the copolymerization of **1** and other acrylic monomers, including MA, *N,N*-dimethylacrylamide (DMA), and *N*-acryloylmorpholine (NAM). All these copolymerization exhibited excellent control over polymerization and near-unity reactivity ratios ( $r_1 = 1.02$  and  $r_{MA} = 0.98$ ;  $r_1 = 0.98$  and  $r_{DMA} = 0.93$ ;  $r_1 = 0.99$  and  $r_{NAM} = 1.01$ ), suggesting that organocatalyzed photocontrolled rROCCP is generally applicable to acrylic monomers (Table 3.2, entry 5-12, Table 3.3, entry 2-4, and Figure 3.6-3.17).

**P-1-co-MA with  $f_1^0 = 0.09$**

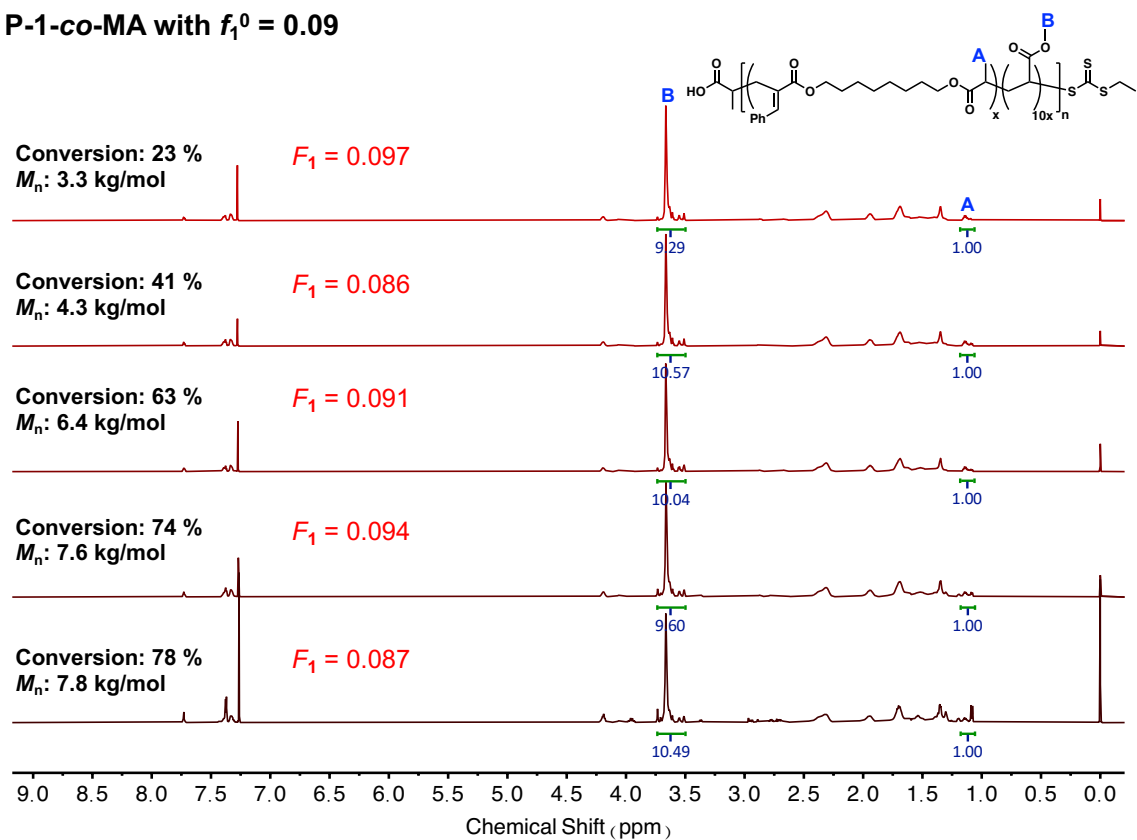


**Figure 3.6.** Compositional analysis of **P-1-co-MA** at  $f_1^0 = 0.09$  at different time points of the copolymerization by  $^1\text{H}$  NMR spectroscopy.

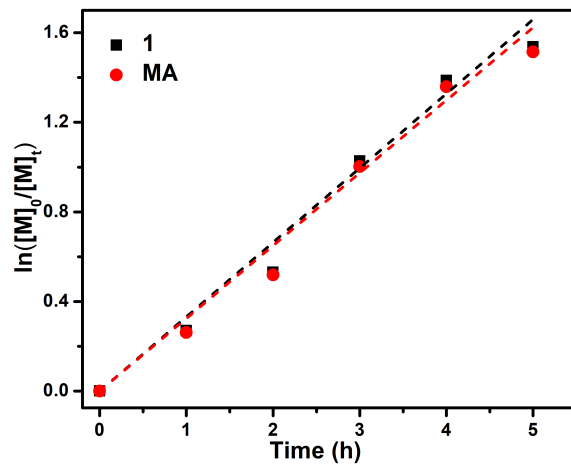


**Figure 3.7.** Kinetic plots of organocatalyzed photocontrolled radical ring-opening cascade copolymerization of **1** and MA at  $f_1^0 = 0.09$ .

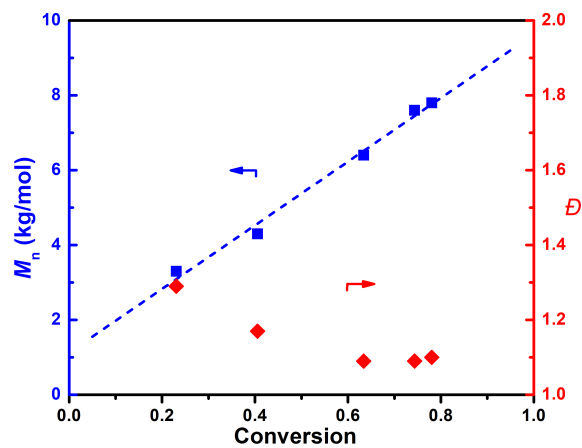


**Figure 3.8.** Plots of  $M_n$  and  $D$  of P-1-co-MA as a function of total conversion.

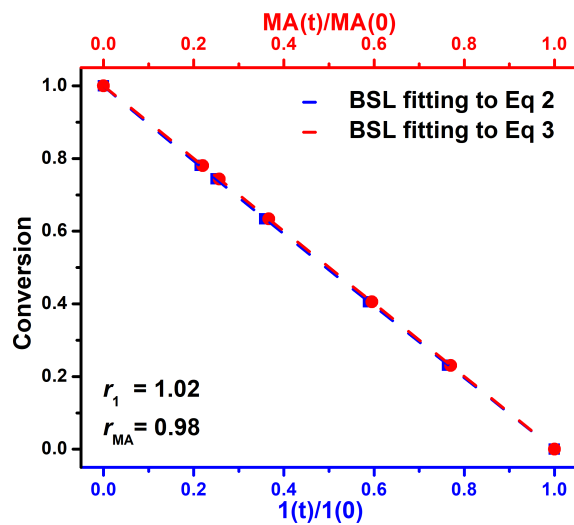


**Figure 3.9.** Plots of total conversion with respect to  $[1(t)]/[1(0)]$  and  $[MA(t)]/[MA(0)]$  are fitted to Equations (2) and (3) of the BSL integrated model independently to derive the comonomer reactivity ratios for the copolymerization of **1** and MA at  $f_1^0 = 0.09$ .

**P-1-co-DMA with  $f_1^0 = 0.09$**

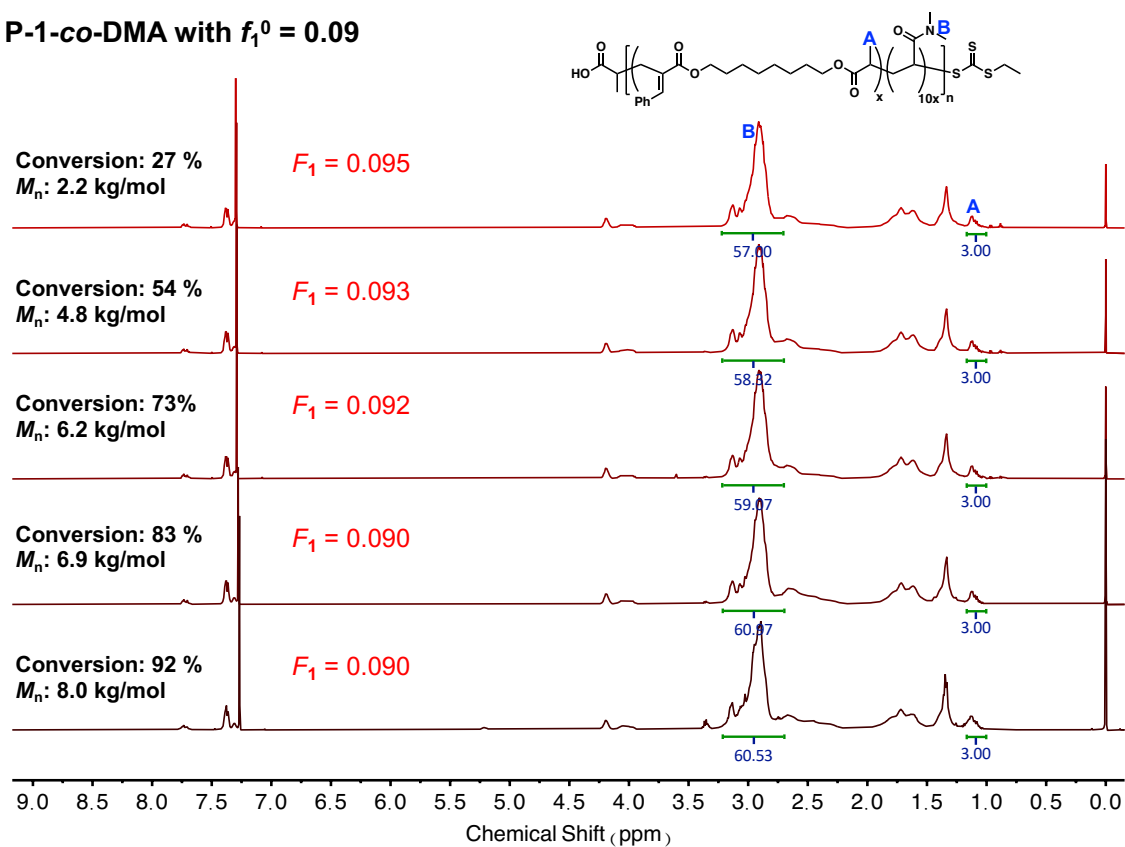


**Figure 3.10.** Compositional analysis of **P-1-co-DMA** at  $f_1^0 = 0.09$  at different time points of the copolymerization by  $^1\text{H}$  NMR spectroscopy.

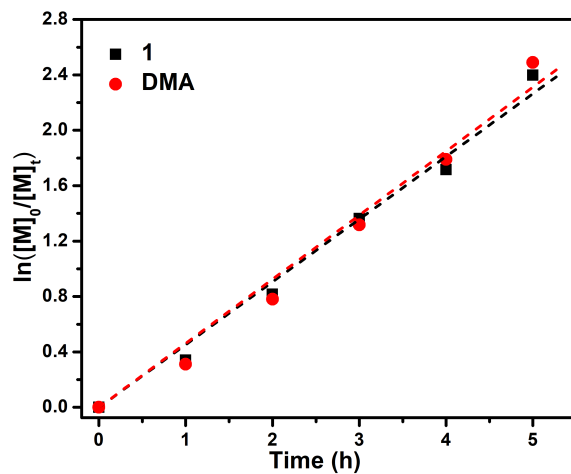


**Figure 3.11.** Kinetic Plots of organocatalyzed photocontrolled radical ring-opening cascade copolymerization of **1** and DMA at  $f_1^0 = 0.09$ .

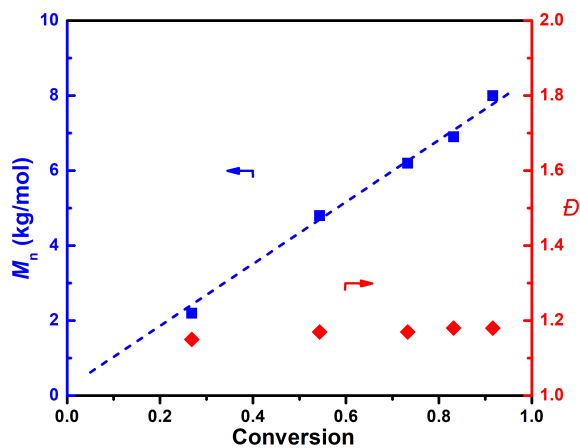


**Figure 3.12.** Plots of  $M_n$  and  $\bar{D}$  of **P-1-co-DMA** as a function of total conversion.

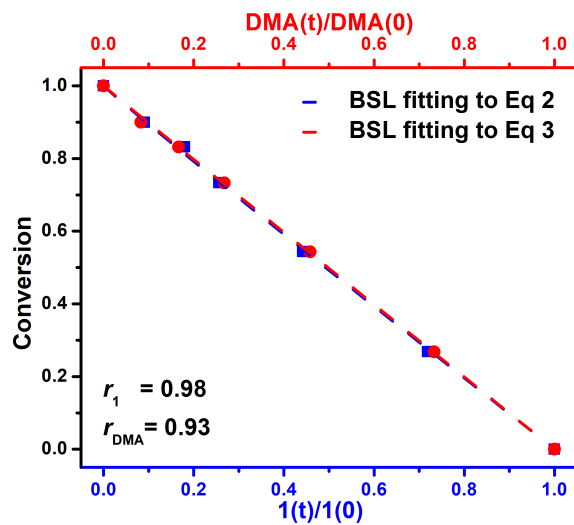


**Figure 3.13.** Plots of total conversion with respect to  $[1(t)]/[1(0)]$  and  $[DMA(t)]/[DMA(0)]$  are fitted to Equations (2) and (3) of the BSL integrated model independently to derive the comonomer reactivity ratios for the copolymerization of **1** and DMA at  $f_1^0 = 0.09$ .

**P-1-co-NAM with  $f_1^0 = 0.09$**

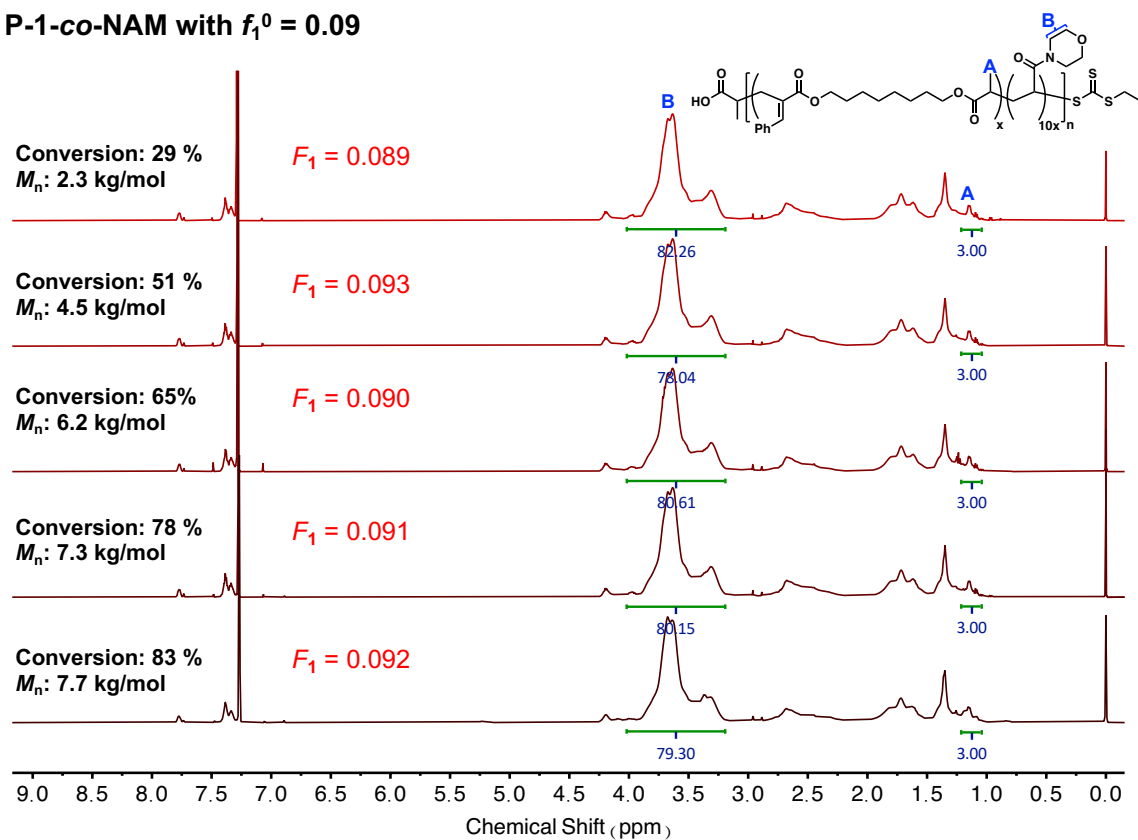


**Figure 3.14.** Compositional analysis of **P-1-co-NAM** at  $f_1^0 = 0.09$  at different time points of the copolymerization by  $^1\text{H}$  NMR spectroscopy.

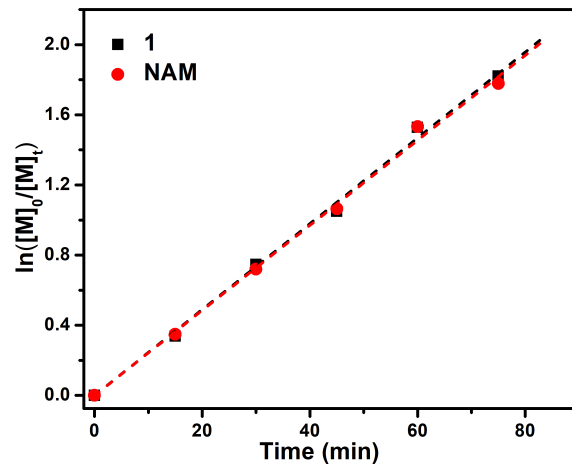


**Figure 3.15.** Kinetic plots of organocatalyzed photocontrolled radical ring-opening cascade copolymerization of **1** and NAM at  $f_1^0 = 0.09$ .

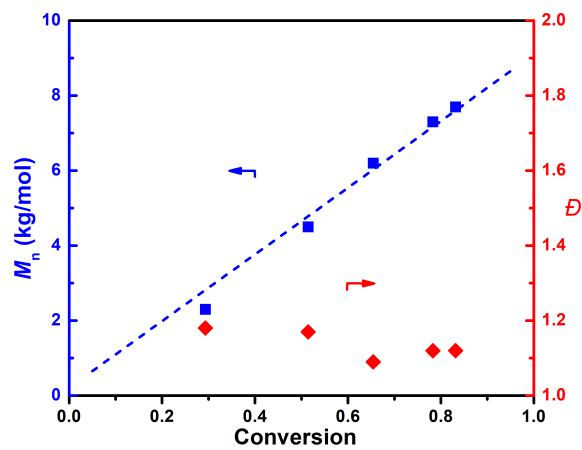


**Figure 3.16.** Plots of  $M_n$  and  $D$  of **P-1-co-NAM** as a function of total conversion.

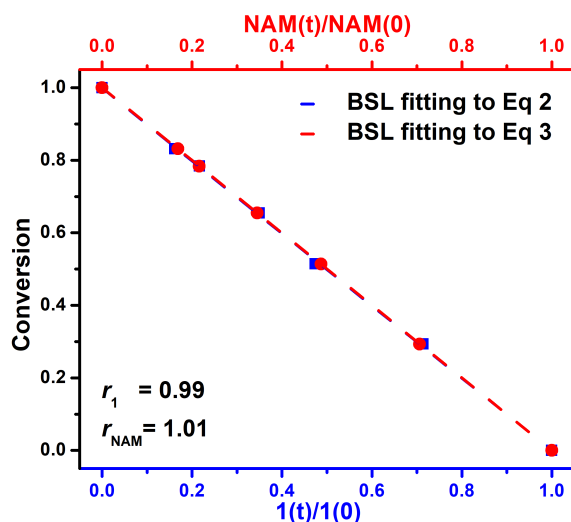


**Figure 3.17.** Plots of total conversion with respect to  $[1(t)]/[1(0)]$  and  $[NAM(t)]/[NAM(0)]$  are fitted to Equations (2) and (3) of the BSL integrated model independently to derive the comonomer reactivity ratios for the copolymerization of **1** and NAM at  $f_1^0 = 0.09$ .

To further confirm the statistical distribution of degradable building blocks in the copolymer backbone, the copolymers were treated with sodium methoxide (NaOMe) to cleave the main-chain diester motif. Taking **P-1-co-tBA** as an example, after incubating with 25 wt% NaOMe in methanol at 25 °C for 30 minutes, the  $M_n^{(SEC)}$  of the copolymer decreased from 10.6 kg mol<sup>-1</sup> to 1.8 kg mol<sup>-1</sup>, as evidenced by a clear shift of the original unimodal peak to a higher elution time region on SEC (Table 3.3, entry 1 and Figure 3.4E). Notably, <sup>1</sup>H NMR analysis revealed that the methylene groups adjacent to the main-chain esters (3.78 to 4.22 ppm) disappeared, while the *tert*-butyl group stayed untouched (1.44 ppm) after degradation (Figure 3.18). This result suggests that the ester linkages in the main chain of **P-1-co-tBA** were selectively cleaved, while the *tert*-butyl esters on the side chain remained intact.

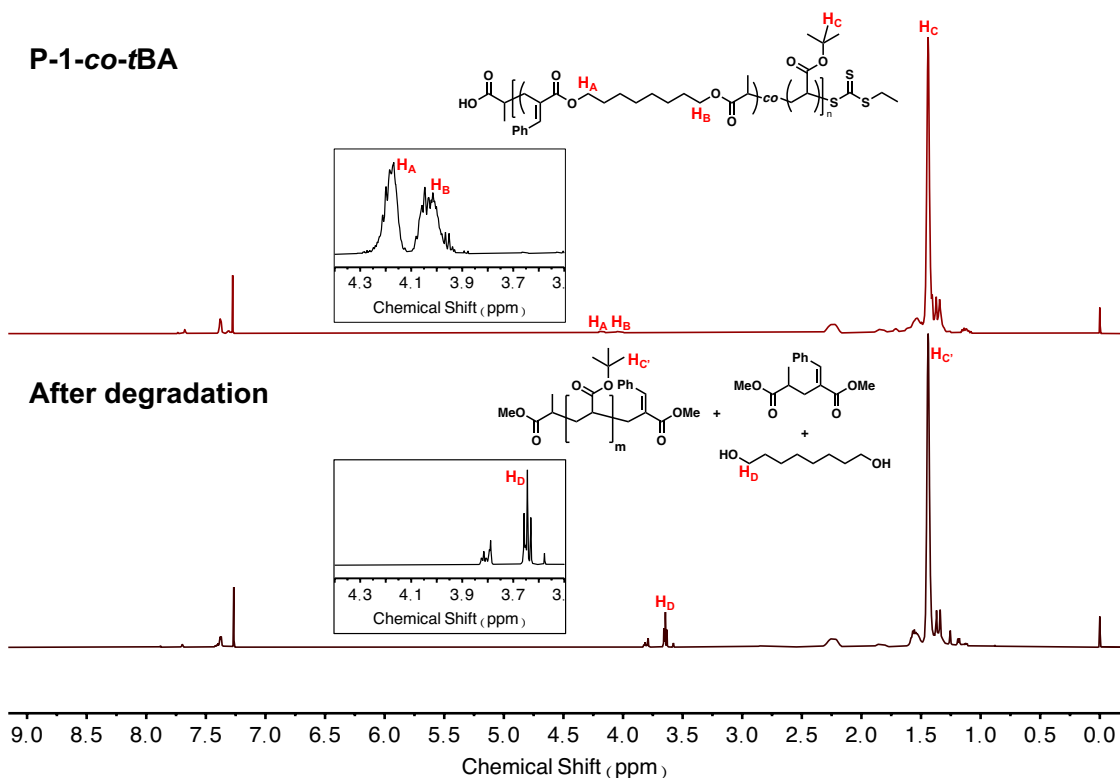


**Figure 3.18.**  $^1\text{H}$  NMR analysis of degradation of **P-1-co-*t*BA**.

Furthermore, the degradation of **P-1-co-MA**, **P-1-co-DMA**, and **P-1-co-NAM** all exhibited a similarly dramatic molecular weight reduction (degraded  $M_n^{(\text{SEC})} < 1.5 \text{ kg mol}^{-1}$ ), suggesting the statistical incorporation of degradable units in the copolymer backbone (Table 3.3, entry 2-4 and Figure 3.19-3.24).

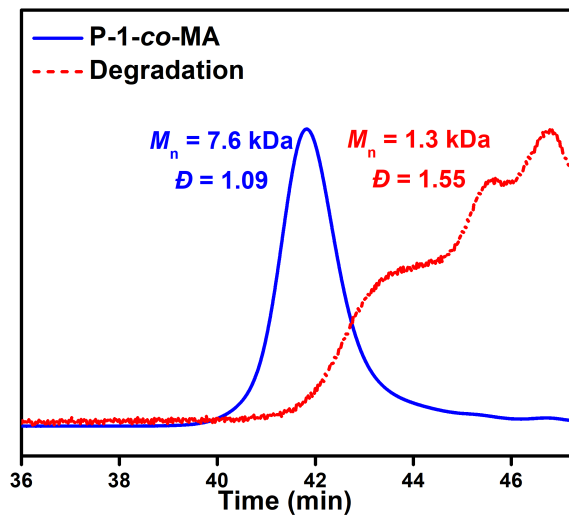


**Figure 3.19.** Degradation of P-1-co-MA exhibited a clear shift to a lower molecular region on SEC.

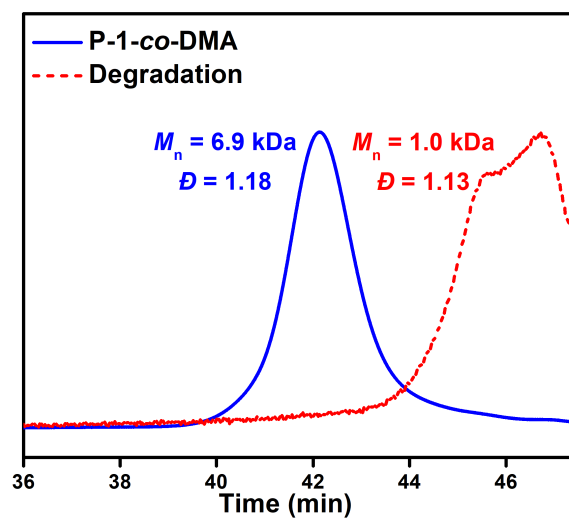


**Figure 3.20.** Degradation of P-1-co-DMA exhibited a clear shift to a lower molecular region on SEC.

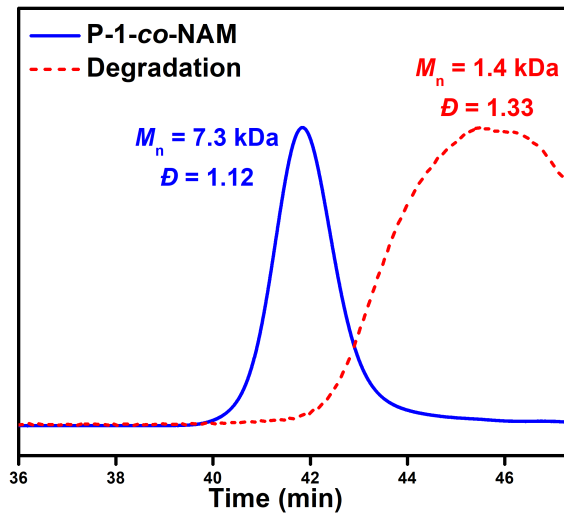


**Figure 3.21.** Degradation of **P-1-co-NAM** exhibited a clear shift to a lower molecular region on SEC.

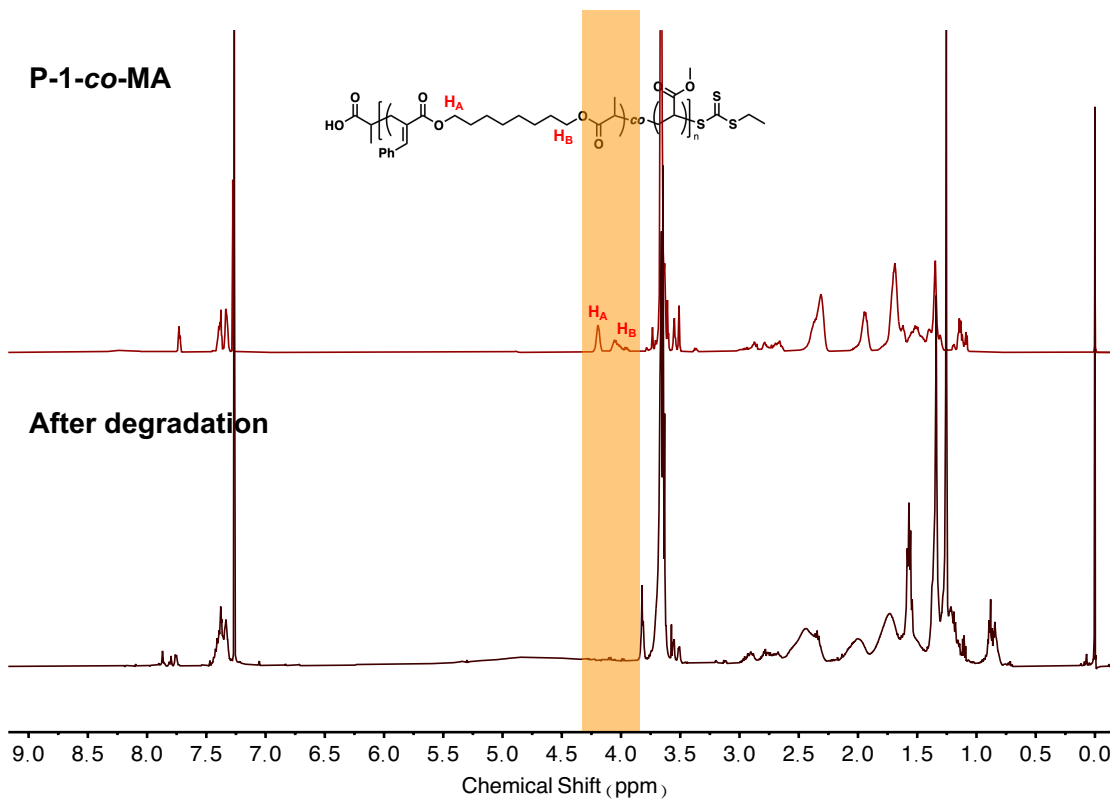


**Figure 3.22.**  $^1\text{H}$  NMR analysis of degradation of **P-1-co-MA**.

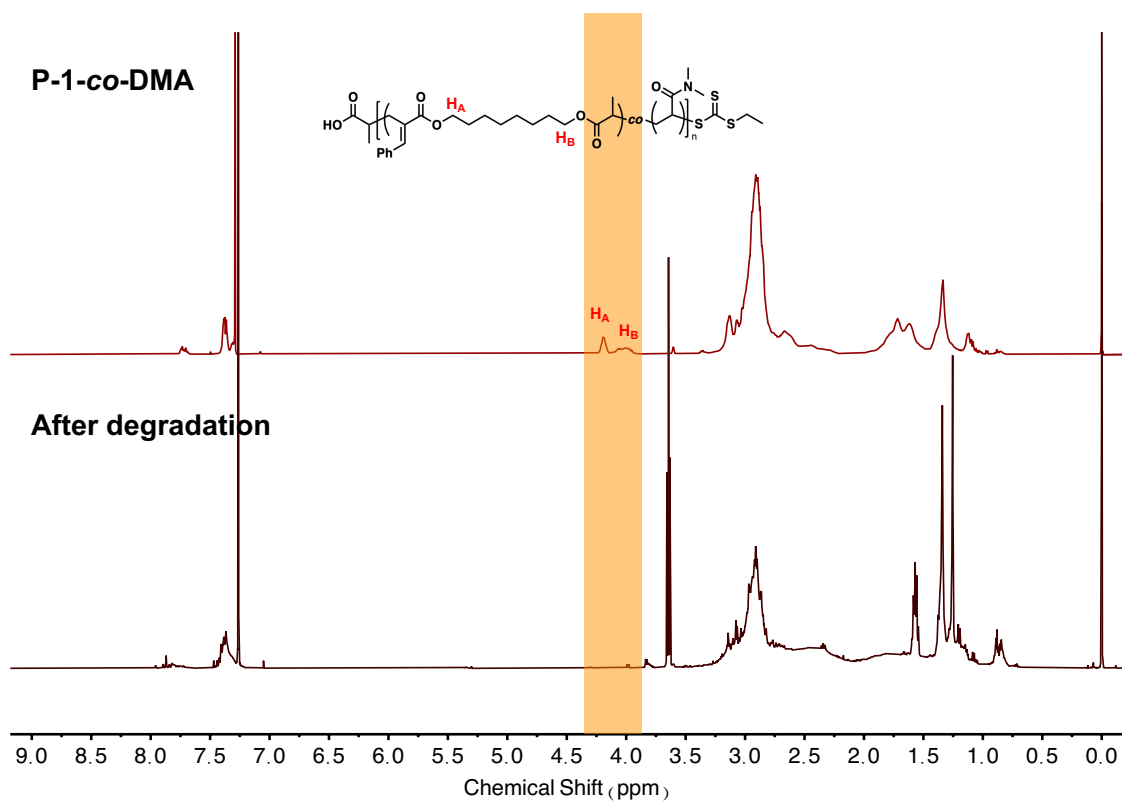


**Figure 3.23.**  $^1\text{H}$  NMR analysis of degradation of P-1-co-DMA.

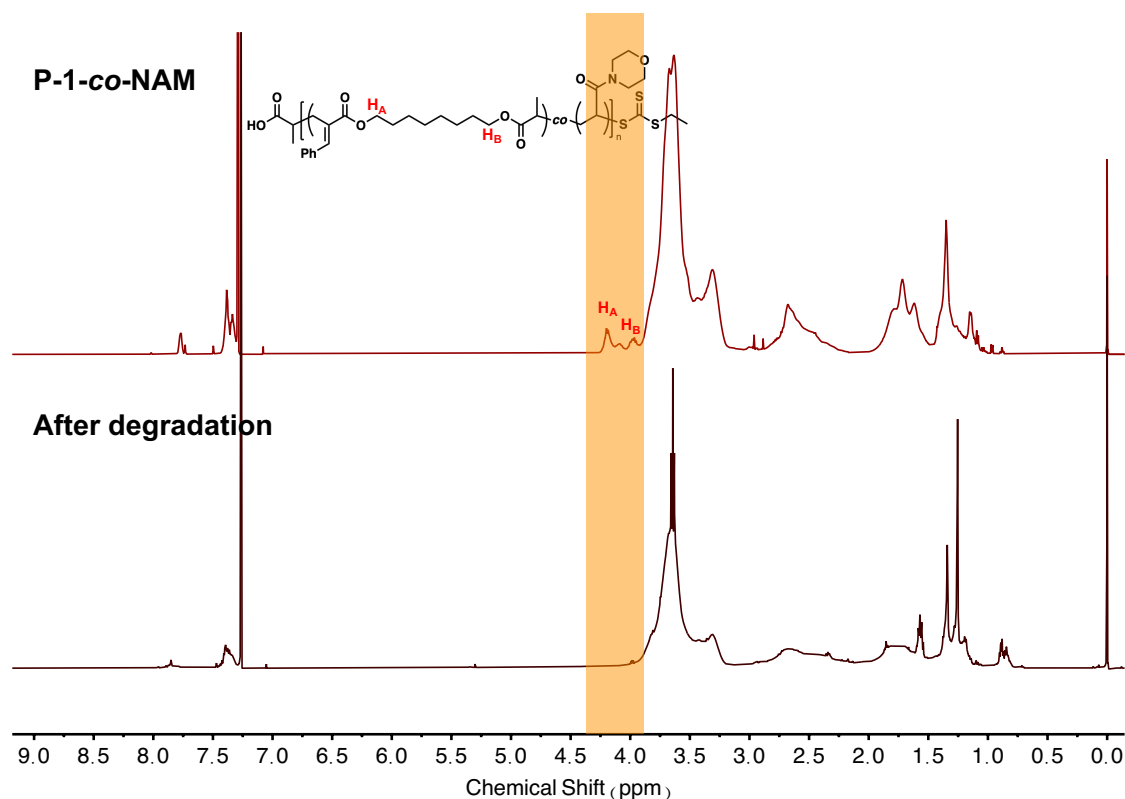


**Figure 3.24.**  $^1\text{H}$  NMR analysis of degradation of **P-1-co-NAM**.

### 3.4 Copolymerization of macrocyclic allylic sulfone with styrene

With a global annual production of more than 16 million metric tons, polystyrene is one of the major sources of synthetic plastics, and new approaches to degradable polystyrene have attracted much attention.<sup>21-22</sup> We explored organocatalyzed photocontrolled rROCCP of **1** and styrene (St) to incorporate degradable functionalities into the backbone of polystyrene. Regulated by Eosin Y and **CTA1** under  $\lambda_{\text{max}} = 450$  nm blue light irradiation, the copolymerization of **1** and St at  $[\text{St}]:[\mathbf{1}]:[\text{CTA1}] = 100:10:1$  yielded **P-1-co-St** with  $M_n^{\text{SEC}}$  of  $8.8 \text{ kg mol}^{-1}$  and  $D$  of 1.23 (Scheme 3.1, Table 3.2, entry 13, and Figure 3.25A).

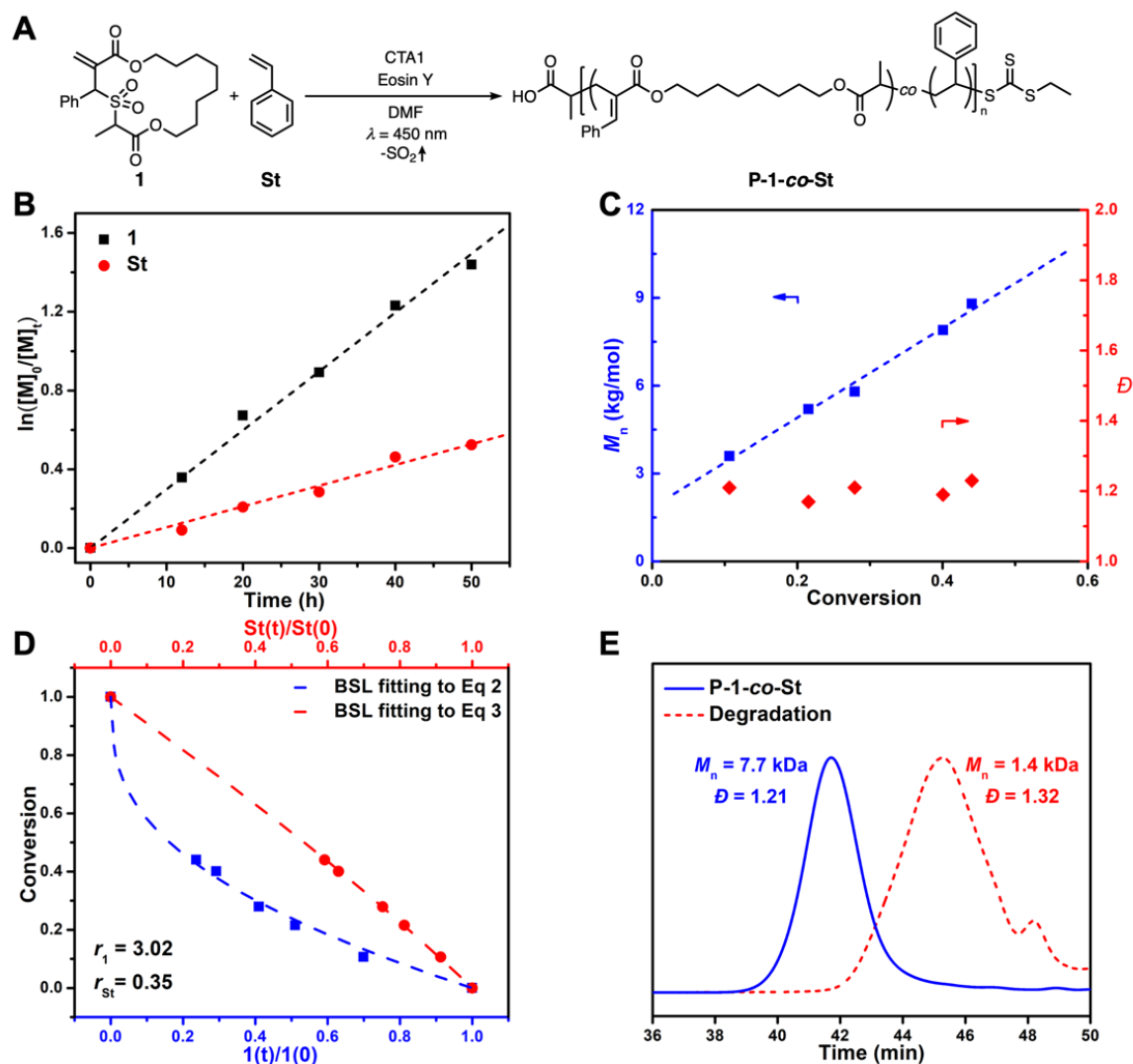


**Figure 3.25.** (A) Organocatalyzed photocontrolled rROCCP of **1** and St. (B) Kinetic plots of  $\ln([M]_0/[M]_t)$  versus reaction time of **1** and St. (C) Plots of  $M_n$  and  $\bar{D}$  of **P-1-co-St** as a function of total conversion. (D) Plots of total conversion with respect to  $[1(t)]/[1(0)]$  and  $[St(t)]/[St(0)]$  are fitted to Equations (2) and (3) of the BSL integrated model independently to derive the reactivity ratios of **1** and St. (E) Degradation of **P-1-co-St** exhibited a clear shift of the copolymer peak to a lower molecular weight region on SEC.

Degradable polystyrene with higher molecular weight (13.0 and 14.0 kg mol<sup>-1</sup>) was also obtained when [M]<sub>0</sub>/[I]<sub>0</sub> ratios were increased (Table 3.2, entry 14-15). Kinetic study of the copolymerization of **1** and St monitored by <sup>1</sup>H NMR spectroscopy displayed first-order kinetics of both **1** and St, despite a slower incorporation of St during the copolymerization ( $k_1 = 0.030 \text{ h}^{-1}$  and  $k_{\text{St}} = 0.011 \text{ h}^{-1}$ ) (Figure 3.25B). The copolymerization of **1** and St also exhibited slower kinetics compared to the copolymerization of **1** and acrylic monomers, which is attributed to the lower reactivity of St than acrylic monomers and reduced catalyst efficiency caused by the triplet quenching of St.<sup>38</sup> Despite lower polymerization rates, the  $M_n^{\text{SEC}}$  of **P-1-co-St** increased linearly with the total conversion of **1** and St, and low  $D$  was maintained throughout the copolymerization (Figure 3.25C), indicating a well-controlled copolymerization. By fitting the instantaneous concentrations of **1** and St at various Conv. values to the BSL integrated model, the reactivity ratios of **1** and St were determined as  $r_1 = 3.02$  and  $r_{\text{St}} = 0.35$ , respectively (Table 3.3, entry 5 and Figure 3.25D). The product of the two independently derived reactivity ratios approximately equals unity ( $r_1 \times r_{\text{St}} = 1.04$ ), supporting that the BSL integrated model is suitable to determine the reactivity ratios in the copolymerization of **1** and St. Higher incorporation of **1** (end-point copolymer composition  $F_1^{\text{(end)}} = 0.16$ ) in the copolymer than the feed composition ( $f_1^0 = 0.09$ ) was confirmed by <sup>1</sup>H NMR analysis of the purified **P-1-co-St** (Figure 3.26). <sup>1</sup>H NMR analysis of the purified copolymers at different conversions also suggested that the ratio of degradable units incorporated into **P-1-co-St** decreased as the total conversion increased (Figure 3.26).

**P-1-co-St with  $f_1^0 = 0.09$**

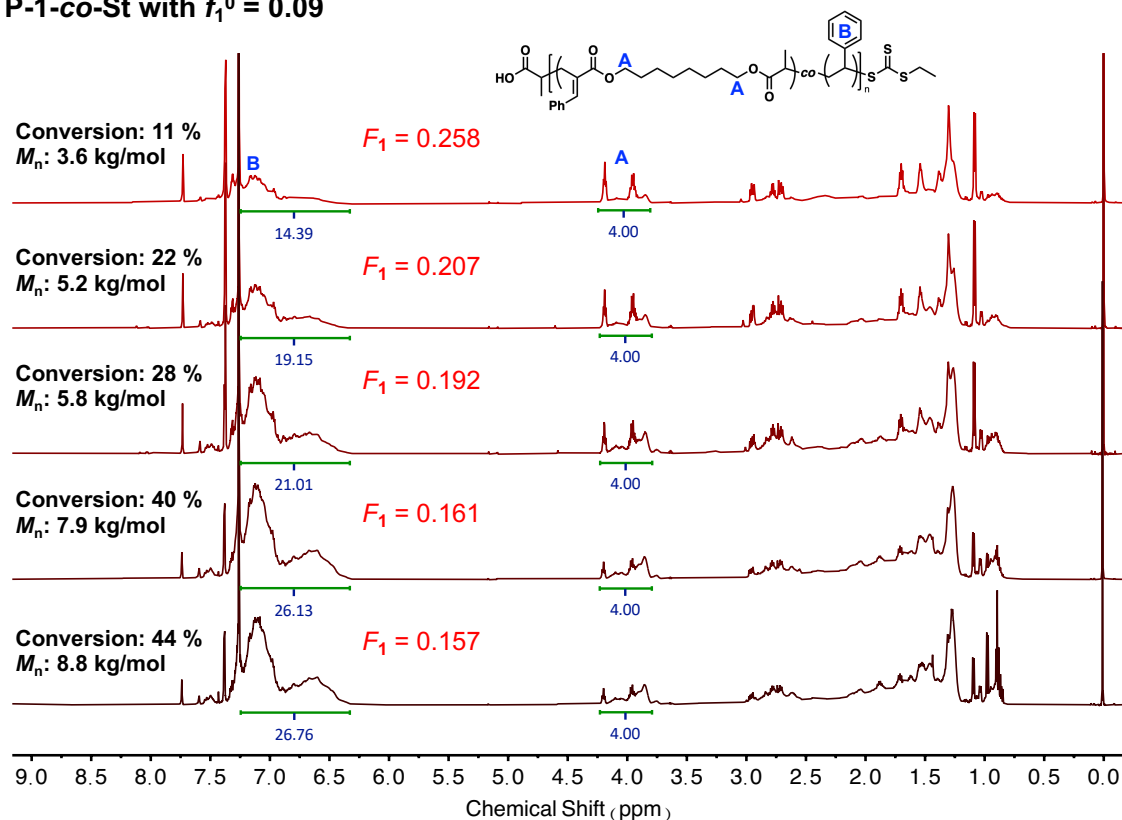


**Figure 3.26.** Compositional analysis of P-1-co-St at  $f_1^0 = 0.09$  at different time points of the copolymerization by  $^1\text{H}$  NMR spectroscopy.

$^1\text{H}$  NMR analysis of degraded P-1-co-St revealed successful cleavage of the main-chain ester groups in P-1-co-St (Figure 3.27).

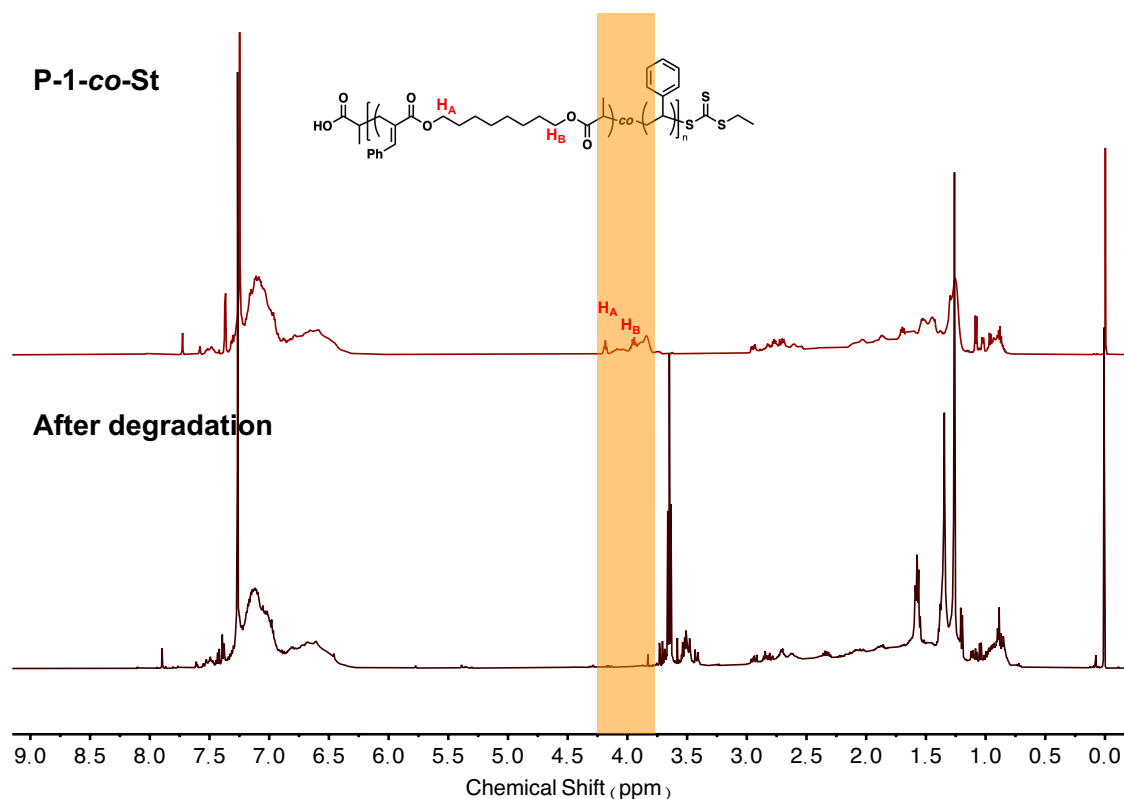


**Figure 3.27.**  $^1\text{H}$  NMR analysis of degradation of **P-1-co-St**.

SEC analysis of degraded **P-1-co-St** also exhibited a dramatic molecular weight reduction (degraded  $M_n^{\text{SEC}} = 1.4 \text{ kg mol}^{-1}$ ,  $D = 1.32$ ) (Table 3.3, entry 5 and Figure 3.25E), suggesting that **P-1-co-St** can be efficiently degraded.

### 3.5 Copolymerization of macrocyclic allylic sulfone with methyl methacrylate

We next turned our attention to the copolymerization of **1** and MMA. The initial attempt of organocatalyzed photocontrolled rROCCP of **1** and MMA at  $[\text{MMA}]:[\mathbf{1}]:[\text{CTA1}] = 100:10:1$  mediated by **CTA1** led to the loss of control. A dithiobenzoate chain transfer agent **CTA2** with an enhanced addition rate and reduced fragmentation rate has been reported to

facilitate better control over radical homopolymerization of MMA.<sup>41</sup> Consistent with the previous report, control over the copolymerization of **1** and MMA mediated by **CTA2** was improved, affording **P-1-co-MMA** with  $M_n^{\text{SEC}}$  of 11.5 kg mol<sup>-1</sup> and  $D$  of 1.36 (Table 3.2, entry 16, and Figure 3.28A).

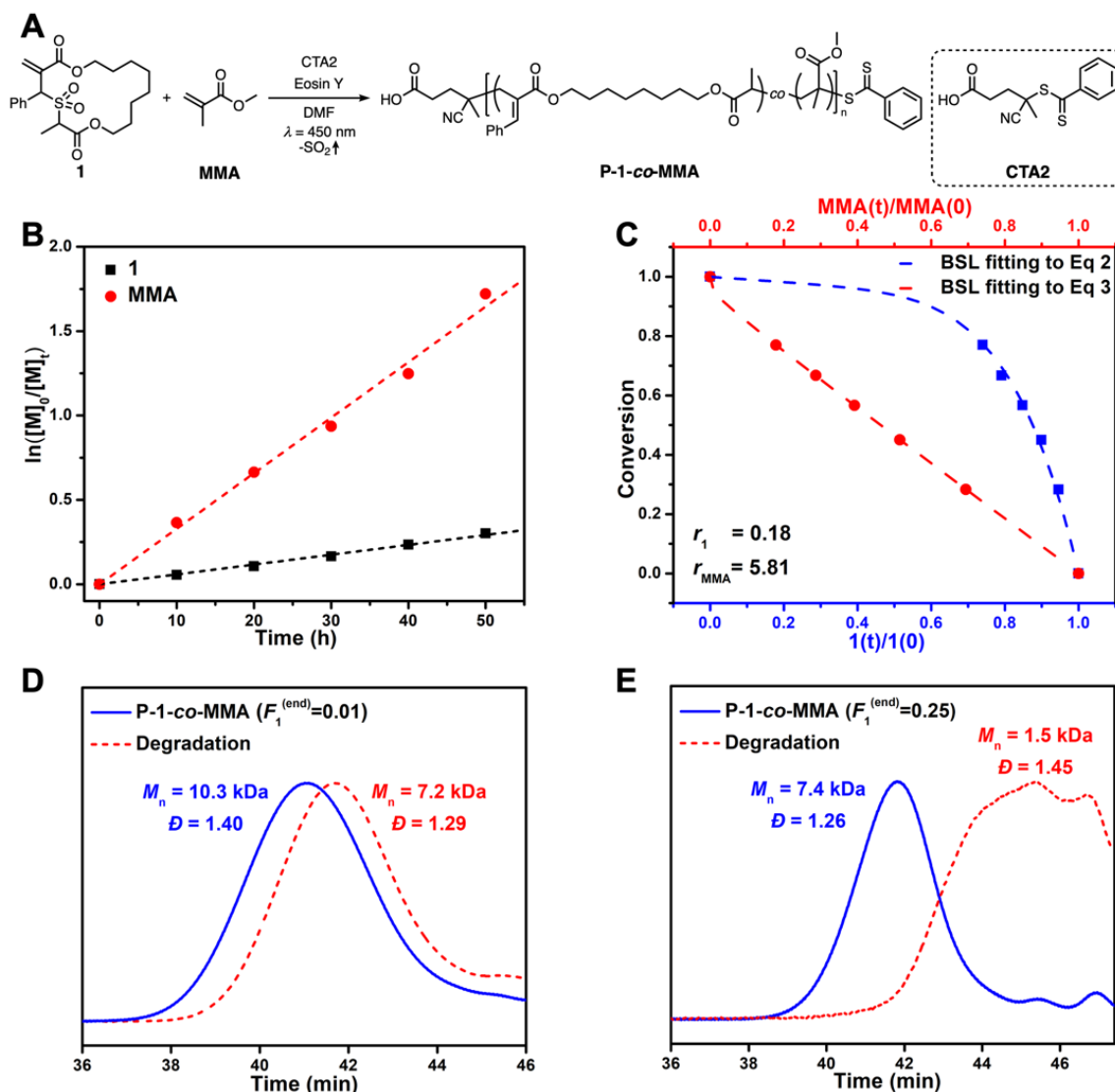


**Figure 3.28.** (A) Organocatalyzed photocontrolled rROCCP of **1** and MMA. (B) Kinetic plots of  $\ln([M]_0/[M]_t)$  versus reaction time of **1** and MMA. (C) Plots of total conversion with respect to  $[1(t)]/[1(0)]$  and  $[MMA(t)]/[MMA(0)]$  are fitted to Equations (2) and (3) of the BSL model independently to derive the reactivity ratios of **1** and MMA. (D) Degradation of **P-1-co-MMA** ( $F_1^{(end)} = 0.01$ ) exhibited a moderate shift to a lower molecular weight region on SEC. (E) Degradation of **P-1-co-MMA** ( $F_1^{(end)} = 0.25$ ) exhibited a clear shift to a lower molecular weight region on SEC.

Kinetic analysis of the copolymerization of **1** and MMA showed that both **1** and MMA followed first-order kinetics (Figure 3.28B). Control over the polymerization was further confirmed by a linear increase of  $M_n^{\text{SEC}}$  of **P-1-co-MMA** with respect to the total conversion of **1** and MMA (Figure 3.29).

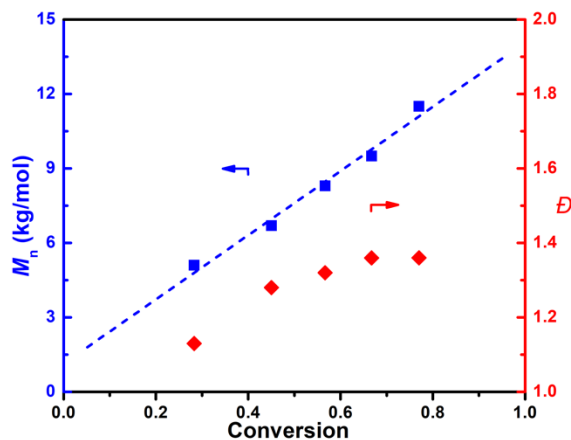


**Figure 3.29.** Plots of  $M_n$  and  $D$  of **P-1-co-MMA** as a function of total conversion.

However, the notably faster incorporation of MMA than **1** in the copolymerization ( $k_1 = 0.006 \text{ h}^{-1}$  and  $k_{\text{MMA}} = 0.033 \text{ h}^{-1}$ ) suggested that  $F_1$  was lower than  $f_1^0$ . Indeed,  $^1\text{H}$  NMR analysis of purified copolymers **P-1-co-MMA** revealed that less degradable main-chain diester motifs were incorporated in the backbone ( $F_1^{\text{(end)}} = 0.01$ ) compared to its feed ratio ( $f_1^0 = 0.09$ ) (Table 3.2, entry 16 and Figure 3.30).  $^1\text{H}$  NMR analysis of the purified copolymers at different conversions also suggested that, contrary to **P-1-co-St**, the ratio of degradable units incorporated into **P-1-co-MMA** increased with the total conversion (Figure 3.30).

### P-1-co-MMA with $f_1^0 = 0.09$

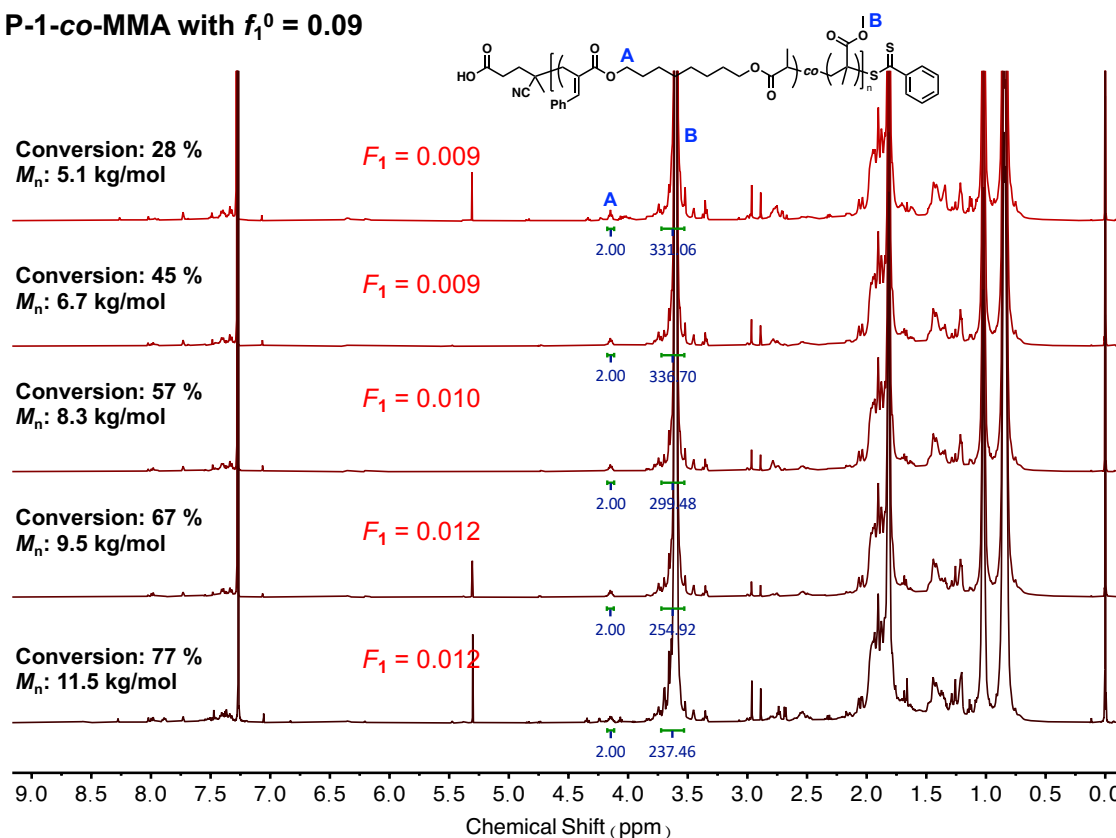


**Figure 3.30.** Compositional analysis of **P-1-co-MMA** at  $f_1^0 = 0.09$  at different time points of the copolymerization by  $^1\text{H}$  NMR spectroscopy.

Independently fitting the instantaneous concentrations of **1** and MMA of **P-1-co-MMA** at various Conv. values to the BSL integrated model yielded the reactivity ratios of **1** and MMA as  $r_1 = 0.18$  and  $r_{\text{MMA}} = 5.81$ , respectively (Table 3.3, entry 6 and Figure 3.28C). The product of  $r_1$  and  $r_{\text{MMA}}$  equals 1.04, suggesting that the BSL integrated model is suitable for determining the reactivity ratios in the copolymerization of **1** and MMA. SEC analysis of degradation of copolymer **P-1-co-MMA** with  $F_1^{(\text{end})} = 0.01$  only exhibited a moderate molecular weight reduction when treated with NaOMe, yielding oligomers with  $M_n^{\text{SEC}}$  of  $7.2 \text{ kg mol}^{-1}$  and  $D$  of 1.29 (Figure 3.28D). The poor degradability is likely caused

by the low incorporation of **1** in the copolymer. To improve the degradability of **P-1-co-MMA**,  $f_1^0$  was increased to 0.50, leading to an  $F_1^{(end)} = 0.25$  in the resulting copolymer (Table 3.2, entry 17). The degradability of the resulting **P-1-co-MMA** with  $F_1^{(end)} = 0.25$  was notably improved, producing fragments with lower molecular weight (degraded  $M_n^{SEC} = 1.5 \text{ kg mol}^{-1}$ ,  $D = 1.45$ ) after the NaOMe treatment (Table 3.3, entry 6, Figure 3.28E, and Figure 3.31).

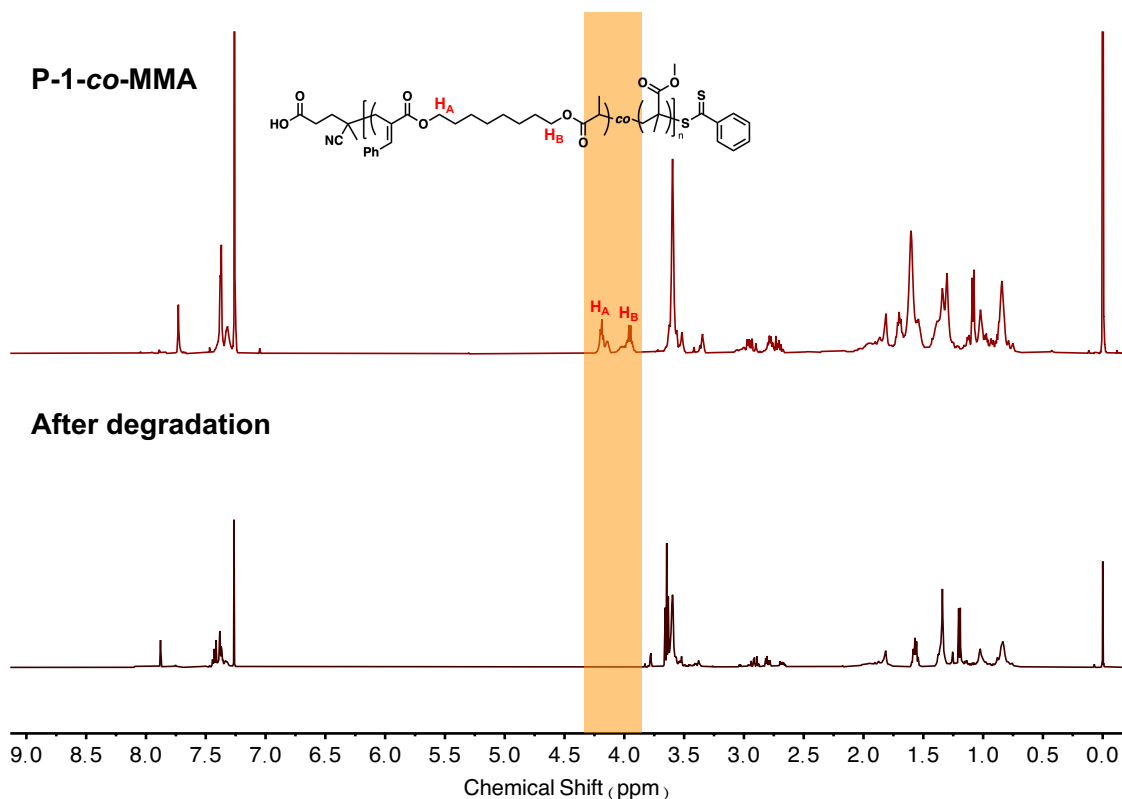


**Figure 3.31.**  $^1\text{H}$  NMR analysis of degradation of **P-1-co-MMA**.

### 3.6 Thermal properties of the degradable vinyl copolymers

The thermal properties of the degradable vinyl copolymers were analyzed by thermogravimetry (TG) and differential scanning calorimetry (DSC). The TG analysis revealed that the 5% weight loss decomposition temperature ( $T_d$ ) of **P-1-co-St** ( $T_d = 325$ - $347$  °C when  $F_1^{(end)} = 0.03$ - $0.15$ ) are higher than their corresponding homopolymers,  $T_d$  (polystyrene) =  $307$  °C (Figure 3.32A).

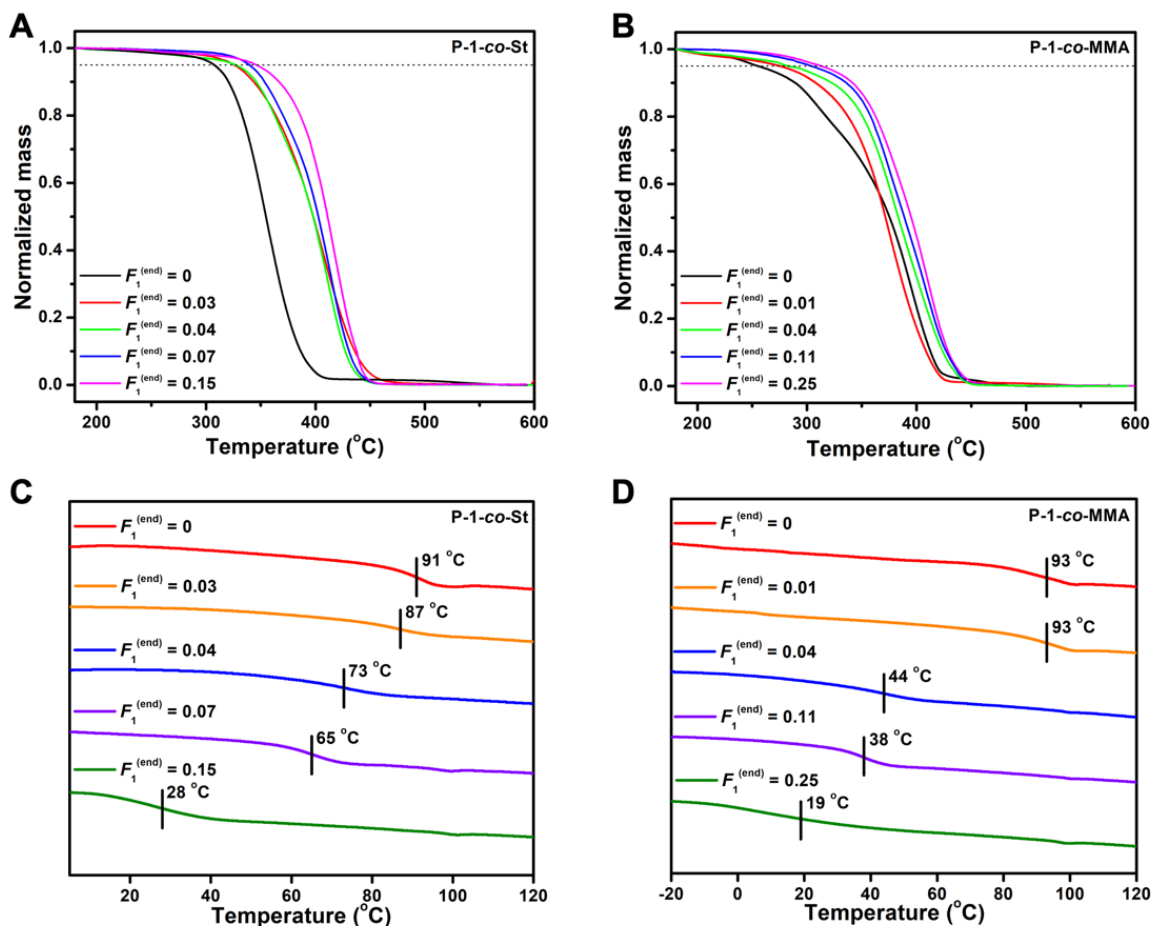


**Figure 3.32.** Thermal properties of the degradable vinyl copolymers in comparison to their corresponding homopolymers. (A)  $T_d$  of polystyrene and **P-1-co-St** at  $F_1^{(end)} = 0.03, 0.04, 0.07,$  and  $0.15$ . (B)  $T_d$  of PMMA and **P-1-co-MMA** at  $F_1^{(end)} = 0.01, 0.04, 0.11,$  and  $0.25$ . (C)  $T_g$  of polystyrene and **P-1-co-St** at  $F_1^{(end)} = 0.03, 0.04, 0.07,$  and  $0.15$ . (D)  $T_g$  of PMMA and **P-1-co-MMA** at  $F_1^{(end)} = 0.01, 0.04, 0.11,$  and  $0.25$ .

Similar results were also observed when **1** was copolymerized with MMA, where **P-1-co-MMA** ( $T_d = 275\text{-}313$  °C when  $F_1^{(end)} = 0.01\text{-}0.25$ ) demonstrated improved thermal stability compared to PMMA ( $T_d = 255$  °C) (Figure 3.32B). On the other hand, the glass transition temperatures ( $T_g$ s) of the degradable vinyl copolymers are dependent on the copolymer

compositions.  $T_g$ s of **P-1-co-St** ( $T_g = 87$  °C when  $F_1^{(end)} = 0.03$ ,  $T_g = 73$  °C when  $F_1^{(end)} = 0.04$ ,  $T_g = 65$  °C when  $F_1^{(end)} = 0.07$ , and  $T_g = 28$  °C when  $F_1^{(end)} = 0.15$ ) were reduced compared to the homopolymer,  $T_g$  (polystyrene) = 91 °C, when more degradable units were incorporated into the copolymer backbone (Figure 3.32C). While  $T_g$  of **P-1-co-MMA** remains the same as the corresponding homopolymer when the composition of the degradable motif is low ( $T_g = 93$  °C when  $F_1^{(end)} = 0.01$ ), it decreases at a higher incorporation ratio of the degradable motif ( $T_g = 44$  °C when  $F_1^{(end)} = 0.04$ ,  $T_g = 38$  °C when  $F_1^{(end)} = 0.11$ , and  $T_g = 19$  °C when  $F_1^{(end)} = 0.25$ ) (Figure 3.32D). The higher  $T_d$  and lower  $T_g$  values of the degradable vinyl copolymers can both be attributed to the incorporation of the main-chain diester motif from **1**, which has high thermal stability and contains a flexible octanediol spacer that reduces the rigidity of the copolymer chains. Therefore, the thermal properties of the copolymers are readily tunable by the incorporation of the degradable motif.

### 3.7 Conclusion

In summary, this work demonstrated that the macrocyclic allylic sulfone can serve as a universal comonomer to copolymerize with various conjugated vinyl monomers, including acrylates, acrylamides, styrene, and methacrylate, in organocatalyzed photocontrolled radical ring-opening cascade copolymerization. Fitting the copolymer compositions to the Beckingham-Sanoya-Lynd integrated model revealed unity reactivity ratios in the copolymerization of the macrocyclic allylic sulfone and acrylic monomers. While the macrocyclic allylic sulfone exhibited similar reactivity to acrylates and acrylamides in the copolymerization, its incorporation rate is higher than styrene but lower than methyl

methacrylate. As a result, a higher initial feed composition of the macrocyclic allylic sulfone is required to achieve appreciable incorporation in the copolymerization with methyl methacrylate. The approach described in this article represents a powerful method to incorporate degradability into mass-produced commodity vinyl plastics. Moving forward, improvement of the reactivity of macrocyclic allylic sulfones in the copolymerization with various vinyl monomers may benefit from further optimization of the structure of macrocyclic allylic sulfone and reaction conditions (e.g., solvent, temperature, and method of initiation).

## Experimental section

### Materials

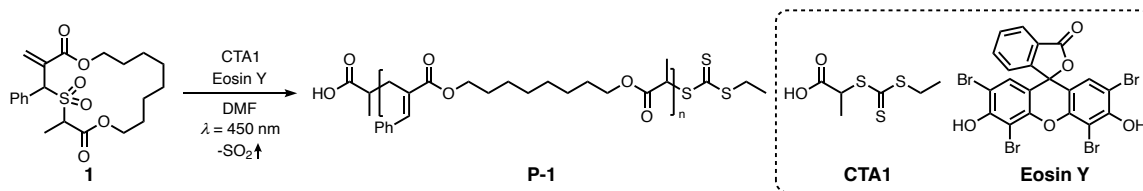
Organic solvents, including DMF, were bought from Fisher Scientific and purified by solvent purification systems (Pure Process Technology). Chain transfer agents were synthesized according to the reported procedures.<sup>42</sup> Chemicals were bought from Sigma-Aldrich, Strem Chemical, or Fisher Scientific and used without further purification.

### Instrumentation and Characterization

Photocontrolled polymerizations were performed in a HepatoChem EvoluChem PhotoRedOx Box TC with an EvoluChem LED spotlight (P201-18-2, 450 nm, 18W) and a recirculating chiller. Silica gel column chromatography was carried out using automated flash chromatography (Biotage). <sup>1</sup>H NMR spectra were recorded in CDCl<sub>3</sub> by a Varian 600 MHz spectrometer, a Varian 500 MHz spectrometer, and two Bruker AVANCE NEO 500 MHz spectrometers, one with a Prodigy and the other with a Helium CryoProbe, using residual chloroform ( $\delta = 7.26$  for <sup>1</sup>H NMR) as internal standard. The mass spectrum was obtained using a Bruker Auto Flex Max instrument (positive mode).  $\alpha$ -Cyano-4-hydroxycinnamic acid was used as the matrix, with NaI added as the cation source. SEC measurements were performed on Tosoh's high-performance SEC system HLC-8320GPC with TSKgel Alpha-M columns at 50 °C and a flow rate of 0.6 mL/min. HPLC grade DMF with 0.01 M LiBr was used as the eluent. Polystyrene standards (ReadyCal Kit, Sigma-Aldrich #81434) were used to determine the molecular weight and molecular weight distribution of polymers. The polymers were dissolved in the above DMF solution and filtered through a 0.20  $\mu$ m PTFE filter before being injected into the SEC system. DSC and

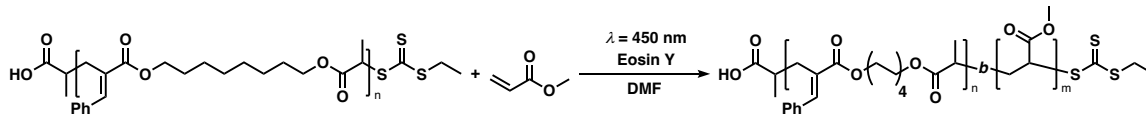
TGA measurements were performed on a Netzsch instrument STA 449 F1 Jupiter at a ramp of 10 °C/min.

**Scheme 3.2.** General procedure of organocatalyzed photocontrolled radical homopolymerization of the macrocyclic allylic sulfone.



Organocatalyzed photocontrolled radical homopolymerization of macrocyclic allylic sulfone **1** was performed under nitrogen in 4 mL glass vials equipped with TFE lined silicone SURE-LINK septa (Chemglass CG-4909-04) using a HepatoChem EvoluChem PhotoRedOx Box TC with an EvoluChem LED spotlight (P201-18-2, 450 nm, 18W) and a recirculating chiller. Macrocyclic allylic sulfone **1** was prepared following the reported procedures.<sup>33</sup> The stock solution of **1**, **CTA1**, and eosin Y was prepared and stored in the fridge (4 °C). A 4 mL glass vial equipped with a stir bar was charged with allylic sulfone macrocyclic monomer (0.1 mmol), CTA (2.00  $\mu\text{mol}$ ), eosin Y (0.1  $\mu\text{mol}$ ), and DMF (0.2 mL). The mixture was covered under aluminum foil and degassed with nitrogen for 20 minutes. The mixture was then irradiated by a blue LED spotlight (18 W,  $\lambda_{\text{max}} = 450 \text{ nm}$ ) at 25 °C. The vial was exposed to air to stop the polymerization. The reaction mixture was diluted with dichloromethane (DCM) and precipitated in hexane three times. The resulting polymers were analyzed by  $^1\text{H}$  NMR spectroscopy and SEC.  $^1\text{H}$  NMR data matches that in the literature.<sup>33</sup>

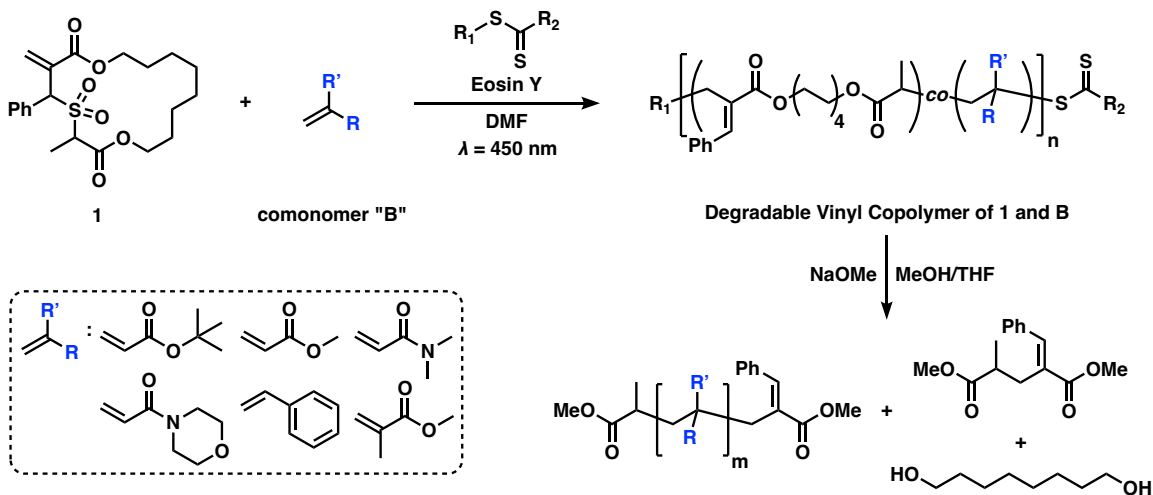
**Scheme 3.3.** Procedure for synthesis of diblock copolymers **P-1-*b*-PMA**.



A 4 mL glass vial equipped with a stir bar was charged with allylic sulfone macrocyclic monomer **1** (0.2 mmol), **CTA1** (5.0  $\mu\text{mol}$ ), eosin Y (0.2  $\mu\text{mol}$ ), and DMF (0.4 mL). The mixture was covered under aluminum foil and degassed with nitrogen for 20 minutes. The mixture was then irradiated by a blue LED spotlight (18 W,  $\lambda_{\text{max}} = 450 \text{ nm}$ ) at 25 °C for 4 hours. The monomer conversion was monitored by  $^1\text{H}$  NMR spectroscopy (64% conversion of **1**). The vial was then exposed to air to stop the polymerization. The reaction mixture was diluted with DCM and precipitated in hexane three times. The resulting polymers were analyzed by  $^1\text{H}$  NMR spectroscopy and SEC.

A 4 mL glass vial equipped with a stir bar was charged with methyl acrylate (MA) (0.4 mmol), macroinitiator **P-1** (2.0  $\mu\text{mol}$ ), eosin Y (0.4  $\mu\text{mol}$ ), and DMF (0.8 mL). The mixture was covered by aluminum foil and degassed with nitrogen at 0 °C for 20 minutes. The mixture was then irradiated by a blue LED spotlight (18 W,  $\lambda_{\text{max}} = 450 \text{ nm}$ ) at 25 °C for 4 hours. The monomer conversion was monitored by  $^1\text{H}$  NMR spectroscopy (69% conversion of MA). The vial was then exposed to air to stop the polymerization. The reaction mixture was diluted with DCM and precipitated in hexane three times. The resulting polymers were analyzed by  $^1\text{H}$  NMR spectroscopy and SEC.

**Scheme 3.4.** General procedure for synthesis and degradation of degradable vinyl copolymers from organocatalyzed photocontrolled radical ring-opening cascade copolymerization.



### Copolymerization of macrocyclic allylic sulfone and vinyl monomers

A 4 mL glass vial equipped with a stir bar was charged with allylic sulfone macrocyclic monomer (0.1 mmol), vinyl comonomer (1.0 mmol), CTA (10.0  $\mu\text{mol}$ ), EY (1.1  $\mu\text{mol}$ ), and DMF (0.2 mL). The mixture was covered under aluminum foil and degassed with nitrogen at 0 °C for 20 minutes. The mixture was then irradiated by a blue LED spotlight (18 W,  $\lambda_{\text{max}} = 450 \text{ nm}$ ) at 25 °C. The vial was exposed to air to stop the polymerization. The reaction mixture was diluted with DCM and precipitated in hexane three times. The resulting polymers were analyzed by <sup>1</sup>H NMR spectroscopy and SEC.

### Degradation of degradable vinyl copolymers

In a 4 mL glass vial equipped with a stir bar, 10 mg degradable vinyl copolymers were dissolved in 0.5 mL THF. A solution of sodium methoxide (100  $\mu\text{L}$  of a 25 wt% solution in

methanol) was added. After 30 minutes, the reaction was stopped by the addition of a 1 M aqueous hydrochloric acid. To collect the degraded products for  $^1\text{H}$  NMR spectroscopy and SEC analyses, the mixture was extracted with DCM. The organic phase was dried with  $\text{Na}_2\text{SO}_4$  and concentrated *in vacuo*.

### Determination of monomer conversion by $^1\text{H}$ NMR spectroscopy

The monomer conversion for the polymerization of macrocyclic allylic sulfone **1** was determined based on the assignment that the integral of the doublet at  $\delta = 1.09$  ppm (Peak *a*, Figure 3.33) corresponds to the methyl group of the polymer **P-1** (3H), and the integral of the singlet at  $\delta = 6.76$  ppm (Peak *b*, Figure 3.33) corresponds to terminal alkene of unreacted monomer (1H). When the integral of Peak *a* is normalized, the monomer conversion  $\theta$  is calculated based on the following equation, where  $I_b$  is the integral of Peak *b*.

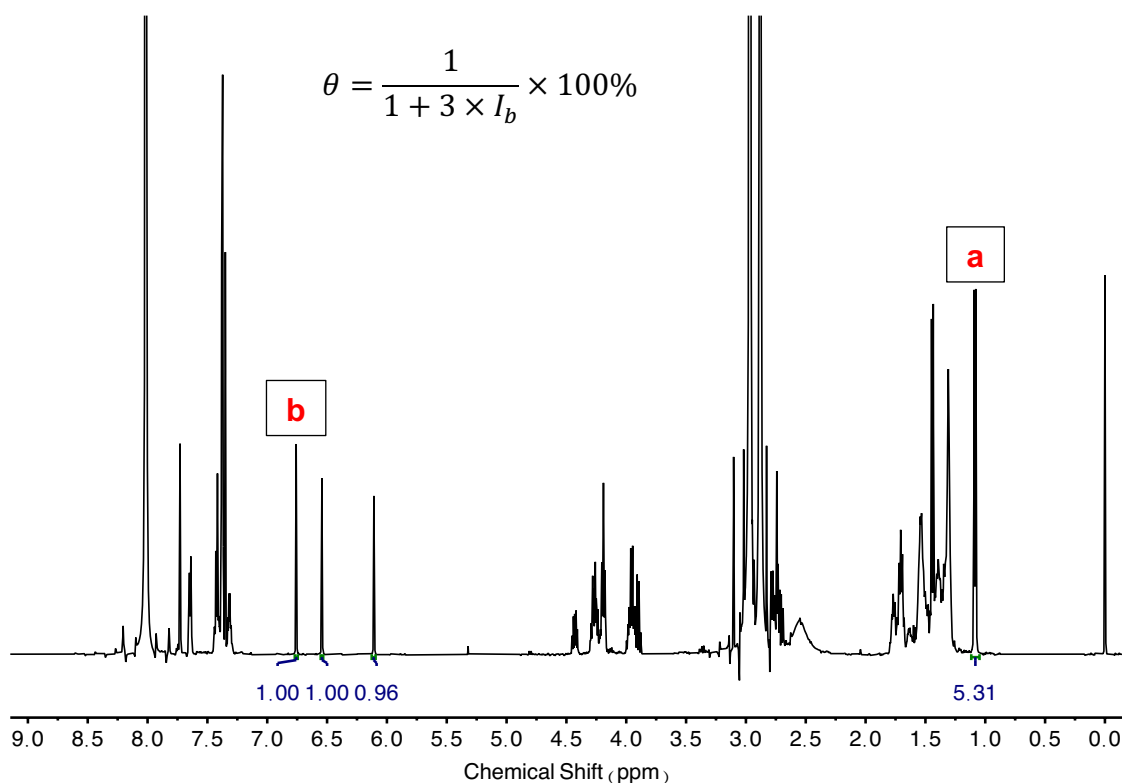


**Figure 3.33.** Determination of monomer conversion for organocatalyzed photoredox radical homopolymerization of macrocyclic allylic sulfone **1** by  $^1\text{H}$  NMR spectroscopy.

### Determination of comonomer conversions for the copolymerization of **1** and MA

The comonomer conversions for the copolymerization of **1** and MA were determined based on the assignments that the integral of the multiplet at  $\delta = 1.13$  ppm (Peak *a*, Figure 3.34) corresponds to the methyl group of **P-1** unit (3H); the integral of the singlet at  $\delta = 6.55$  ppm (Peak *b*, Figure 3.34) corresponds to the terminal alkene of unreacted allylic sulfone macrocyclic monomer **1** (1H); the integral of the singlet at  $\delta = 3.75$  ppm (Peak *c*, Figure 3.34) corresponds to the methyl group of unreacted MA (3H); and the integral of the singlet at  $\delta = 3.67$  ppm (Peak *d*, Figure 3.34) corresponds to the methyl group of PMA unit (3H). The monomer conversion  $\theta$  of **1** and MA is calculated based on the following equations, where  $I_a$  is the integral of Peak *a*,  $I_b$  is the integral of Peak *b*,  $I_c$  is the integral of Peak *c*, and  $I_d$  is the integral of Peak *d*.

$$\theta_{\mathbf{1}} = \frac{I_a}{I_a + 3 \times I_b} \times 100\%$$

$$\theta_{\text{MA}} = \frac{I_d}{I_c + I_d} \times 100\%$$

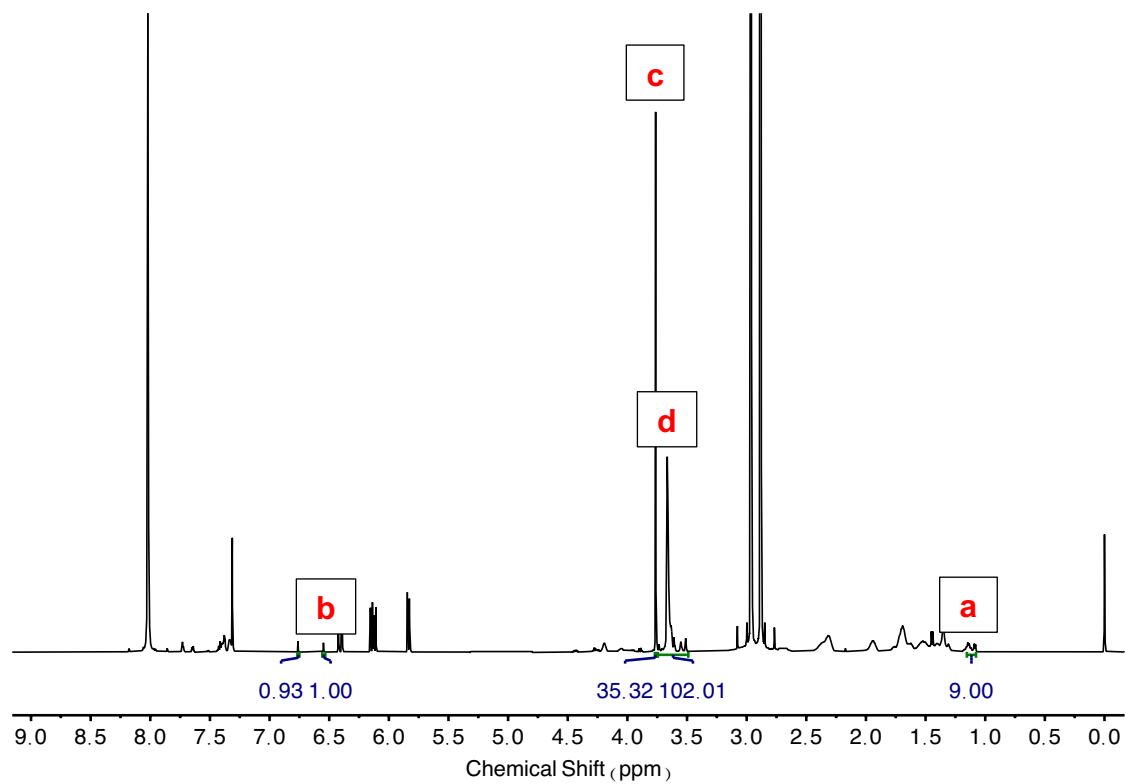


**Figure 3.34.**  $^1\text{H}$  NMR analysis of photocontrolled organocatalyzed radical ring-opening cascade copolymerization of allylic sulfone macrocyclic monomer **1** and MA.

Figure 3.35.  $^1\text{H}$  NMR spectrum of diblock copolymer P-1-*b*-PMA.

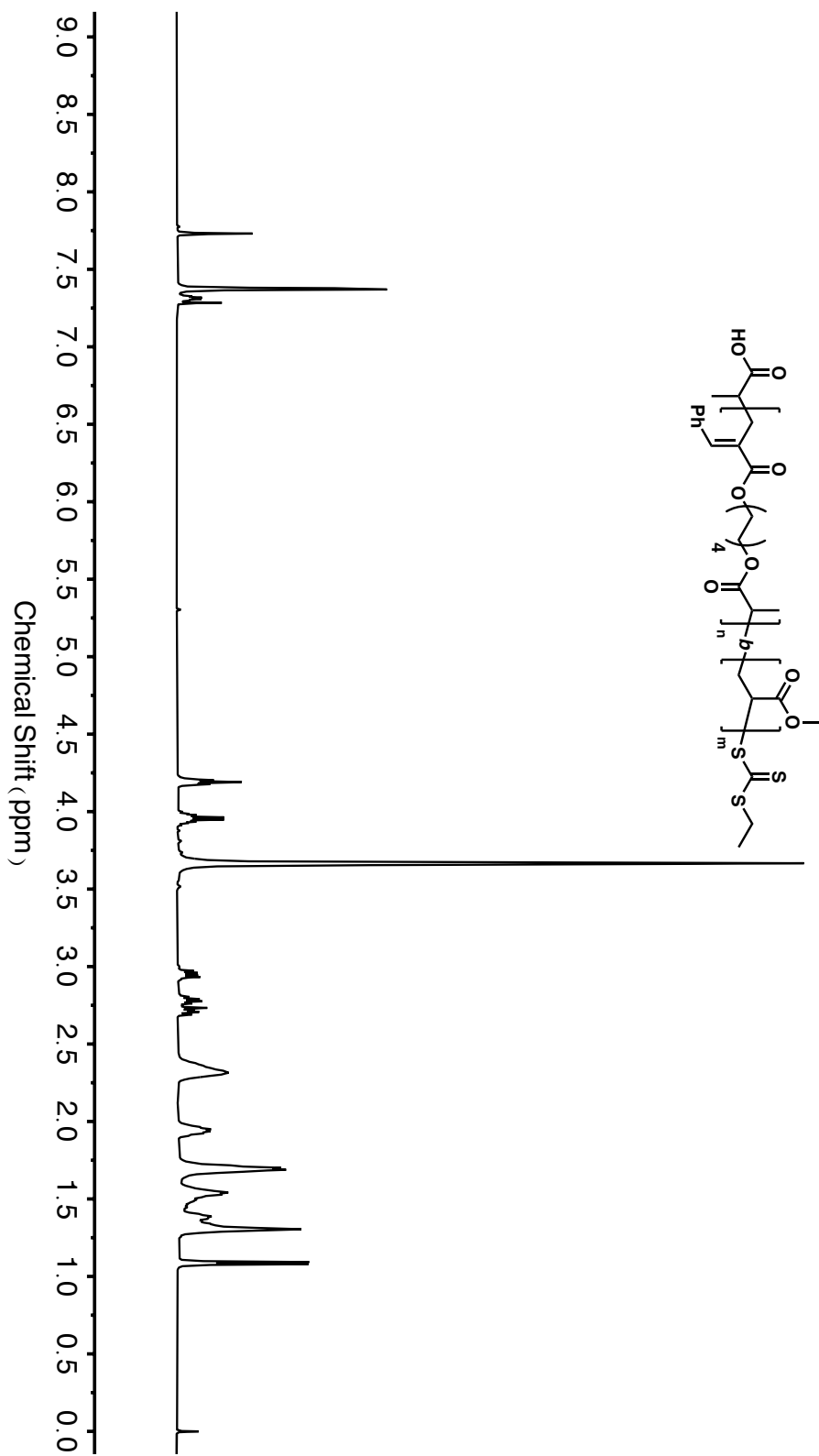
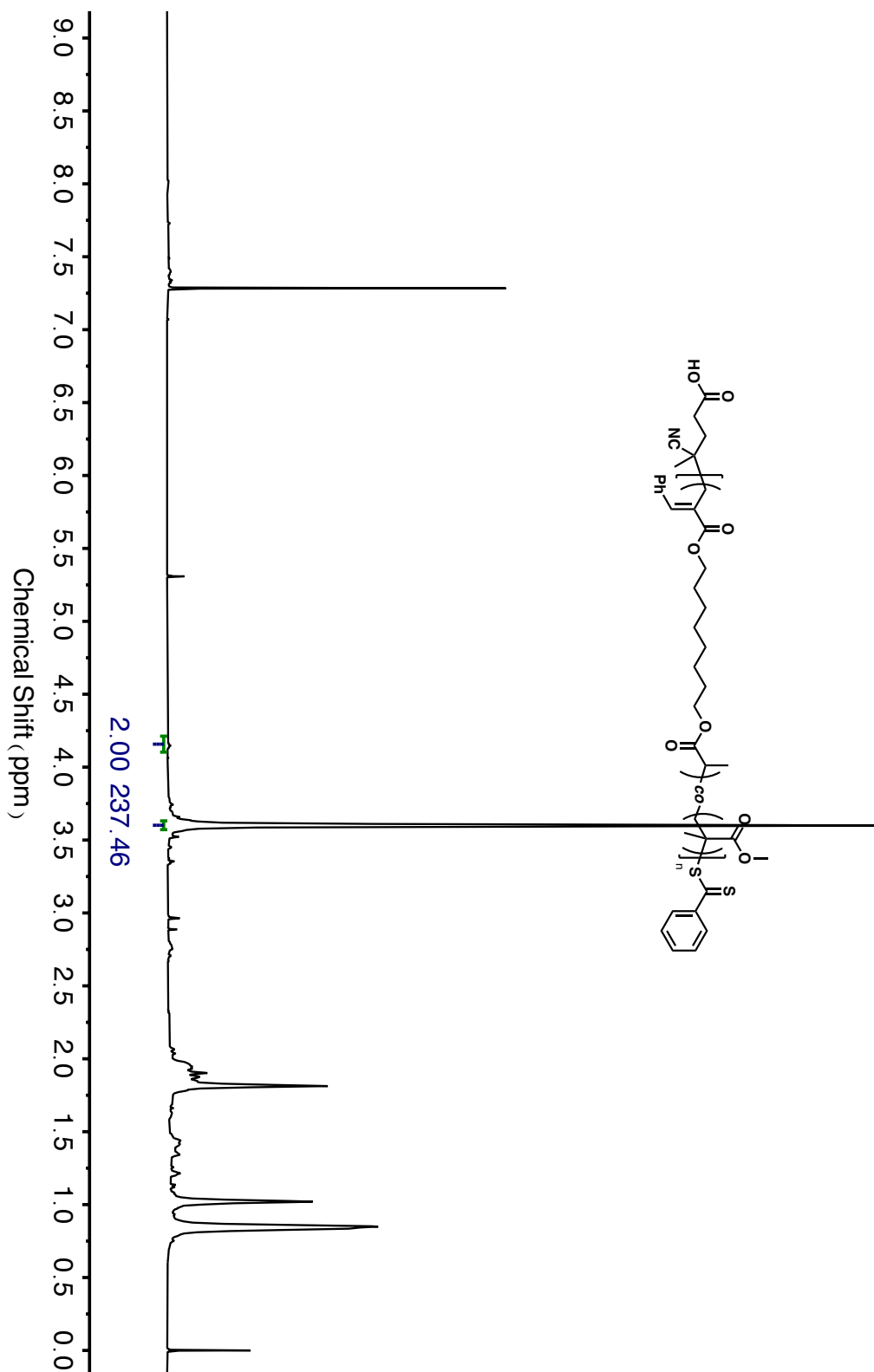




Figure 3.37.  $^1\text{H}$  NMR spectrum of degradable vinyl copolymer **P-1-co-MMA** at  $f_1^0 = 0.09$ .



## Reference

1. Geyer, R.; Jambeck, J. R.; Law, K. L. Production, use, and fate of all plastics ever made. *Sci. Adv.* **2017**, *3*, e1700782.
2. Chamas, A.; Moon, H.; Zheng, J.; Qiu, Y.; Tabassum, T.; Jang, J. H.; Abu-Omar, M.; Scott, S. L.; Suh, S. Degradation Rates of Plastics in the Environment. *ACS Sustainable Chem. Eng.* **2020**, *8*, 3494-3511.
3. Seeley, M. E.; Song, B.; Passie, R.; Hale, R. C. Microplastics affect sedimentary microbial communities and nitrogen cycling. *Nat. Commun.* **2020**, *11*, 2372.
4. Kakadellis, S.; Rosetto, G. Achieving a circular bioeconomy for plastics. *Science* **2021**, *373*, 49-50.
5. MacLeod, M.; Arp, H. P. H.; Tekman, M. B.; Jahnke, A. The global threat from plastic pollution. *Science* **2021**, *373*, 61-65.
6. Korley, L. T. J.; Epps, T. H.; Helms, B. A.; Ryan, A. J. Toward polymer upcycling—adding value and tackling circularity. *Science* **2021**, *373*, 66-69.
7. Errede, L. A. The Chemistry of Xylylenes. X. Some Polymers and Telomers of *Spiro-di-o-xylylene*. *J. Polym. Sci.* **1961**, *49*, 253-265.
8. Bailey, W. J. Free Radical Ring-Opening Polymerization. *Polym. J.* **1985**, *17*, 85-95.
9. Delplace, V.; Nicolas, J. Degradable vinyl polymers for biomedical applications. *Nat. Chem.* **2015**, *7*, 771-784.
10. Tardy, A.; Nicolas, J.; Gigmes, D.; Lefay, C.; Guillaneuf, Y. Radical Ring-Opening Polymerization: Scope, Limitations, and Application to (Bio)Degradable Materials. *Chem. Rev.* **2017**, *117*, 1319-1406.

11. Pesenti, T.; Nicolas, J. 100th Anniversary of Macromolecular Science Viewpoint: Degradable Polymers from Radical Ring-Opening Polymerization: Latest Advances, New Directions, and Ongoing Challenges. *ACS Macro Lett.* **2020**, *9*, 1812-1835.
12. Bailey, W. J.; Ni, Z.; Wu, S.-R. Synthesis of Poly- $\epsilon$ -Caprolactone via a Free Radical Mechanism. Free Radical Ring-Opening Polymerization of 2-Methylene-1,3-Dioxepane. *J. Polym. Sci., Polym. Chem. Ed.* **1982**, *20*, 3021-3030.
13. Endo, T.; Okawara, M.; Bailey, W. J.; Azuma, K.; Nate, K.; Yokono, H. Photoinitiated Ring-Opening Polymerization of 2-Methylene-1,3-Dioxepane. *J. Polym. Sci., Polym. Lett. Ed.* **1983**, *21*, 373-380.
14. Hedir, G. G.; Bell, C. A.; Jeong, N. S.; Chapman, E.; Collins, I. R.; O'Reilly, R. K.; Dove, A. P. Functional Degradable Polymers by Xanthate-Mediated Polymerization. *Macromolecules* **2014**, *47*, 2847-2852.
15. Delplace, V.; Guégain, E.; Harrisson, S.; Gigmes, D.; Guillaneuf, Y.; Nicolas, J. A ring to rule them all: a cyclic ketene acetal comonomer controls the nitroxide-mediated polymerization of methacrylates and confers tunable degradability. *Chem. Commun.* **2015**, *51*, 12847-12850.
16. Hill, M. R.; Guégain, E.; Tran, J.; Figg, C. A.; Turner, A. C.; Nicolas, J.; Sumerlin, B. S. Radical Ring-Opening Copolymerization of Cyclic Ketene Acetals and Maleimides Affords Homogeneous Incorporation of Degradable Units. *ACS Macro Lett.* **2017**, *6*, 1071-1077.
17. Tardy, A.; Honoré, J.-C.; Tran, J.; Siri, D.; Delplace, V.; Bataille, I.; Letourneur, D.; Perrier, J.; Nicoletti, C.; Maresca, M.; Lefay, C.; Gigmes, D.; Nicolas, J.; Guillaneuf,

- Y. Radical Copolymerization of Vinyl Ethers and Cyclic Ketene Acetals as a Versatile Platform to Design Functional Polyesters. *Angew. Chem., Int. Ed.* **2017**, *56*, 16515-16520.
18. Bingham, N. M.; Roth, P. J. Degradable vinyl copolymers through thiocarbonyl addition-ring-opening (TARO) polymerization. *Chem. Commun.* **2019**, *55*, 55-58.
19. Smith, R. A.; Fu, G.; McAteer, O.; Xu, M.; Gutekunst, W. R. Radical Approach to Thioester-Containing Polymers. *J. Am. Chem. Soc.* **2019**, *141*, 1446-1451.
20. Spick, M. P.; Bingham, N. M.; Li, Y.; de Jesus, J.; Costa, C.; Bailey, M. J.; Roth, P. J. Fully Degradable Thioester-Functional Homo- and Alternating Copolymers Prepared through Thiocarbonyl Addition-Ring-Opening RAFT Radical Polymerization. *Macromolecules* **2020**, *53*, 539-547.
21. Kiel, G. R.; Lundberg, D. J.; Prince, E.; Husted, K. E. L.; Johnson, A. M.; Lensch, V.; Li, S.; Shieh, P.; Johnson, J. A. Cleavable Comonomers for Chemically Recyclable Polystyrene: A General Approach to Vinyl Polymer Circularity. *J. Am. Chem. Soc.* **2022**, *144*, 12979-12988.
22. Gil, N.; Caron, B.; Siri, D.; Roche, J.; Hadiouch, S.; Khedaioui, D.; Ranque, S.; Cassagne, C.; Montarnal, D.; Gigmes, D.; Lefay, C.; Guillaneuf, Y. Degradable Polystyrene via the Cleavable Comonomer Approach. *Macromolecules* **2022**, *55*, 6680-6694.
23. Elliss, H.; Dawson, F.; Nisa, Q. u.; Bingham, N. M.; Roth, P. J.; Kopeć, M. Fully Degradable Polyacrylate Networks from Conventional Radical Polymerization Enabled by Thionolactone Addition. *Macromolecules*, **2022**, *55*, 6695-6702.

24. Nisa, Q. u.; Theobald, W.; Hepburn, K. S.; Riddlestone, I.; Bingham, N. M.; Kopeć, M.; Roth, P. J. Degradable Linear and Bottlebrush Thioester-Functional Copolymers through Atom-Transfer Radical Ring-Opening Copolymerization of a Thionolactone. *Macromolecules* **2022**, *55*, 7392-7400.
25. Chen, M.; Zhong, M.; Johnson, J. A. Light-Controlled Radical Polymerization: Mechanisms, Methods, and Applications. *Chem. Rev.* **2016**, *116*, 10167-10211.
26. Lai, H.; Zhang, J.; Xing, F.; Xiao, P. Recent advances in light-regulated non-radical polymerisations. *Chem. Soc. Rev.* **2020**, *49*, 1867-1886.
27. Wu, C.; Corrigan, N.; Lim, C.-H.; Liu, W.; Miyake, G.; Boyer, C. Rational Design of Photocatalysts for Controlled Polymerization: Effect of Structures on Photocatalytic Activities. *Chem. Rev.* **2022**, *122*, 5476-5518.
28. Parkatzidis, K.; Wang, H. S.; Truong, N. P.; Anastasaki, A. Recent Developments and Future Challenges in Controlled Radical Polymerization: A 2020 Update. *Chem.* **2020**, *6*, 1575-1588.
29. Corrigan, N.; Jung, K.; Moad, G.; Hawker, C. J.; Matyjaszewski, K.; Boyer, C. Reversible-deactivation radical polymerization (Controlled/living radical polymerization): From discovery to materials design and applications. *Prog. Polym. Sci.* **2020**, *111*, 101311.
30. Truong, N. P.; Jones, G. R.; Bradford, K. G. E.; Konkolewicz, D.; Anastasaki, A. A comparison of RAFT and ATRP methods for controlled radical polymerization. *Nat. Rev. Chem.* **2021**, *5*, 859-869.

31. Li, N.; Ding, D.; Pan, X.; Zhang, Z.; Zhu, J.; Boyer, C.; Zhu, X. Temperature programmed photo-induced RAFT polymerization of stereo-block copolymers of poly(vinyl acetate). *Polym. Chem.* **2017**, *8*, 6024-6027.
32. Chen, D.-F.; Boyle, B. M.; McCarthy, B. G.; Lim, C.-H.; Miyake, G. M. Controlling Polymer Composition in Organocatalyzed Photoredox Radical Ring-Opening Polymerization of Vinylcyclopropanes. *J. Am. Chem. Soc.* **2019**, *141*, 13268-13277.
33. Wang, W.; Zhou, Z.; Sathe, D.; Tang, X.; Moran, S.; Jin, J.; Haeffner, F.; Wang, J.; Niu, J. Degradable Vinyl Random Copolymers via Photocontrolled Radical Ring-Opening Cascade Copolymerization. *Angew. Chem., Int. Ed.* **2022**, *61*, e202113302.
34. Treat, N. J.; Sprafke, H.; Kramer, J. W.; Clark, P. G.; Barton, B. E.; Read de Alaniz, J.; Fors, B. P.; Hawker, C. J. Metal-Free Atom Transfer Radical Polymerization. *J. Am. Chem. Soc.* **2014**, *136*, 16096-16101.
35. Miyake, G. M.; Theriot, J. C. Perylene as an Organic Photocatalyst for the Radical Polymerization of Functionalized Vinyl Monomers through Oxidative Quenching with Alkyl Bromides and Visible Light. *Macromolecules* **2014**, *47*, 8255-8261.
36. Xu, J.; Shanmugam, S.; Duong, H. T.; Boyer, C. Organo-photocatalysts for photoinduced electron transfer-reversible addition-fragmentation chain transfer (PET-RAFT) polymerization. *Polym. Chem.* **2015**, *6*, 5615-5624.
37. Theriot, J. C.; Lim, C.-H.; Yang, H.; Ryan, M. D.; Musgrave, C. B.; Miyake, G. M. Organocatalyzed atom transfer radical polymerization driven by visible light. *Science* **2016**, *352*, 1082-1086.

38. Corbin, D. A.; Miyake, G. M. Photoinduced Organocatalyzed Atom Transfer Radical Polymerization (O-ATRP): Precision Polymer Synthesis Using Organic Photoredox Catalysis. *Chem. Rev.* **2022**, *122*, 1830-1874.
39. Beckingham, B. S.; Sanoja, G. E.; Lynd, N. A. Simple and Accurate Determination of Reactivity Ratios Using a Nonterminal Model of Chain Copolymerization. *Macromolecules* **2015**, *48*, 6922-6930.
40. Lynd, N. A.; Ferrier, R. C.; Beckingham, B. S. Recommendation for Accurate Experimental Determination of Reactivity Ratios in Chain Copolymerization. *Macromolecules* **2019**, *52*, 2277-2285.
41. Perrier, S. 50th Anniversary Perspective: RAFT Polymerization-A User Guide. *Macromolecules* **2017**, *50*, 7433-7447.
42. Skey, J.; O'Reilly, R. K. Facile one pot synthesis of a range of reversible addition-fragmentation chain transfer (RAFT) agents. *Chem. Commun.* **2008**, *44*, 4183-4185.